Crystal Chemistry of Cadmium Oxysalt and associated Minerals from Broken Hill, New South Wales

Peter Elliott, B.Sc. (Hons)

Geology and Geophysics
School of Earth and Environmental Sciences
The University of Adelaide

This thesis is submitted to The University of Adelaide in fulfilment of the requirements for the degree of Doctor of Philosophy

September 2010

Table of contents

Abstract

Secondary minerals, formed at low temperature, are the product of the oxidation of primary sulphide ore bodies. The formation and mineralogy of oxidized zones, which phases are stable and which are not, and how toxic heavy metals become incorporated into the crystal structures of the constituent minerals have implications for the heavy metal mobility in the environment and in the disposal of heavy metal and the remediation of contaminated sites

This thesis presents an inverstigation of the the crystal chemistry of a suite of Cd, Pb, Zn, Cu, Se and As oxysalt minerals from Broken Hill, NSW; the new mineral species plimerite, nyholmite, liversidgeite and edwardsite, as well as gartrellite, munakataite, osakaite and cadmian serpierite. Crystal structures were studied using single-crystal X-ray diffraction data, in conjunction with the results from electron microprobe analysis, powder X-ray diffraction, infrared absorption spectroscopy, Raman spectroscopy and Mössbauer spectroscopy. The crystal structures are classified according to the mode of polymerization of strongly bonded coordination polyhedra: chains, sheets or frameworks. The chemical compositions of the minerals and their stabilities are discussed in terms of a combinination of hierarchical ordering, bond-valence theory and the valence-matching principle.

For the first time in natural minerals, extensive solid solutions involving cadmium have been observed. Solid solutions between Cd and Zn (in nyholmite), Cd and Ca (in serpierite), and Cd and (Pb+Ca) (in sampleite-lavendulan-zdenekite and conichalcite-duftite) are examined.

The minerals examined in this study have implications for the mobility of heavy metals in the environment and in remediation of heavy metal contaminated sites.

Declaration

This work contains no material which has been accepted for the award of any other degree or diploma in any university or other tertiary institution and, to the best of my knowledge and belief, contains no material previously published or written by another person, except where due reference has been made in the text.

I give consent to this copy of my thesis when deposited in the University Library, being made available for loan and photocopying, subject to the provisions of the Copyright Act 1968.

I also give permission for the digital version of my thesis to be made available on the web, via the University's digital research repository, the Library catalogue, the Australasian Digital Theses Program (ADTP) and also through web search engines, unless permission has been granted by the University to restrict access for a period of time.

The author acknowledges that copyright of published works contained within this thesis resides with the copyright holder(s) of those works.

Signed Date

Acknowledgements

First of all I would like to thank my principal supervisors Allan Pring and Joël Brugger for encouraging me to pursue this research and for providing support and encouragement throughout. I would also like to thank my co-supervisor, John Foden, for his encouragement, support and invaluable help.

I am indebted to a number of persons for making available facilities at various stages of the research. Dr. Anthony Willis of the Research School of Chemistry, The Australian National University, Canberra is thanked for obtaining single crystal X-ray data for several samples, and for processing the data. My research gave me the opportunity to travel to Vienna, Austria. I would like to thank Professor Ekkehart Tillmanns for hosting me at the Institut für Mineralogie und Kristallographie, Universität Wien for six weeks in 2007. I am grateful to everyone in the Institute who provided assistance and support. Special thanks go to Gerald Giester for access to the CCD diffractometers and for assistance with single crystal X-ray data collection and data processing, Uwe Kolitsch for assistance with single crystal X-ray data collection, data processing and with interpretation of the data, and Eugen Libowitzky for provided assistance with the collection of Raman data.

I am grateful to Peter Turner and Paul Jensen for obtaining single-crystal x-ray data for nyholmite under the Australian Synchrotron Research Program. I appreciate the assistance of Catherine McCammon, who provided Mössbauer data for plimerite, which was essential in understanding the crystal chemistry of the mineral. I am also indebted to Angus Netting and John Terlet of Adelaide Microscopy for their assistance with the electron microprobe analysis. Thanks are also due to Paul Pigou and Hayley Brown of the Forensic Science Centre, Adelaide, who provided access to the infrared spectrometer and assistance in obtaining infrared spectra.

Three of the suite of Broken Hill samples that made this study possible were generously provided by Glyn Francis, Steve Taylor and John Toma.

I would also like to acknowledge the funding provided by the Federal government under an Australian Postgraduate Award.

Finally, I wish to thank my family for their support and encouragement throughout my study.

List of published papers

Elliott, P., Kolitsch, U., Giester, G., Libowitzky, E., McCammon, C., Pring, A. Birch, W.D. (2009) Description and crystal structure of a new mineral – plimerite, $ZnFe^{3+}_4(PO_4)_3(OH)_5$ – the Zn-analogue of rockbridgeite and frondelite, from Broken Hill, New South Wales, Australia. Mineralogical Magazine, 73, 131–148.

Elliott, P., Turner, P., Jensen, P., Kolitsch, U., and Pring. (2009) Description and crystal structure of nyholmite, a new mineral related to hureaulite, from Broken Hill, New South Wales, Australia, Mineralogical Magazine, 2009, 73, 521–533.

Elliott, P., Giester, G., Libowitzky, E., Kolitsch, U. (2010) Description and crystal structure of liversidgeite, $Zn_6(PO_4)_4 \cdot 7H_2O$, a new mineral from Broken Hill, New South Wales, Australia. American Mineralogist, 95, 397–404.

Elliott, P., Brugger, J., and Caradoc-Davies, T. (2010) Description and crystal structure of a new mineral, edwardsite, $Cu_3Cd_2(SO_4)_2(OH)_6 \cdot 4H_2O$, from Broken Hill, New South Wales, Australia. Mineralogical Magazine, 74, 39–53.

Chapter 1. Introduction

1.1 General Introduction

The oxidized zone of the Broken Hill Ag-Pb-Zn deposit has had a long and complex history which is reflected in the complexity of its mineralogy, a mix of sulphates, carbonates, oxides, phosphates, arsenates, halides, silicates and native metals (Birch 1999). This diversity arises from the vast bulk and chemical complexity of the primary sulphides plus the long weathering history. Primary sulphides are rich in Pb, Zn, Ag, Mn and Cu and contain significant amounts of As, Sb, Co, Ni, Se and Cd, and small amounts of Sn, Bi, Hg, and U. Very few deposits offer such an opportunity for the study of the crystal chemisty of such a wide variety of seconday minerals.

Heavy metal mobility in the oxidized zones of ore deposits is governed largely by the formation of the secondary minerals such as carbonates, sulphates, phosphates, arsenates etc. Low-temperature minerals are also important for the transportation of heavy metals from sites of heavy metal contamination to the biosphere. Geochemical weathering processes acting upon mining and metallurgical wastes initiate the process of transporting heavy metals from contaminated areas and redistributing them to surrounding soils, streams, and groundwater (Fuge *et al.* 1993; Paulson 1997).

The crystal structures of complex oxysalt minerals are related to the stability, occurence and distribution of the minerals. Knowledge of their crystal structures is thus important for understanding the transport and re-deposition of heavy metals during weathering and can lead to effective approaches to remediation of heavy metal contamination in the environment, and aid in the development of reliable methods for the disposal of heavy metal waste. A study of the behaviour of heavy metals in the environment and the formulation of solutions to the environmental problems also requires knowledge of the thermodynamic stability of the possible precipitating phases, which can be estimated from their structural data (e.g., Chen *et al.* 1999).

In recent years, low-temperature minerals have received considerable attention because of their importance to the environment. Recent research of the crystal chemistry of heavy metals such as lead and uranium (e.g. Burns 1999; Krivovichev and Burns 2000a; Li *et al.* 2000; Li *et al.* 2001; Brugger *et al.* 2003) has involved investigation of the mechanisms of formation and the crystal chemistry of both

naturally occuring minerals and synthetically prepared compounds. The research has in large part been driven by the role these elements play in the environmental problems associated with the disposal of heavy metal and radioactive wastes and in the remediation of contaminated sites. The crystal chemistries of heavy metals like Cd, Cr, Se and As and their speciation in geochemical systems are however, less well known. This may be due to their low concentration in the earths crust and the resulting relative rarity of their minerals.

Oxysalt minerals found in the oxidized zones of ore deposits and in contaminated sites are commonly found in complex parageneses that contain a large number of complex minerals of several different chemical types. The factors that control the relative stabilities of the minerals remain largly unknown, however, the paragenetic sequences of minerals in such complex environments and their stabilities should be related to the crystal structures of the constituent minerals (Hawthorne 1992 1998).

Structural investigations of secondary heavy metal bearing phases are important in their own right and will also lead to a better understanding of the crystal chemistry of these elements, and thereby may help to elucidate the mechanisms for their release, transport and precipitation under natural conditions.

This study concentrates on the crystal chemistry of eight oxysalt minerals of Pb, Cd, Cu, Zn, Se and As from the secondary zone of the Broken Hill deposit.

1.2 Crystal Chemistry

Evans (1966) defined crystal chemistry as "the study of the relationship of the internal structure of a body to its physical and chemical properties. It aims at interpreting the properties of any substance in terms of its crystal structure, and, conversely, at associating with any structural characteristic a corresponding set of physical and chemical properties." The early development of crystal chemistry was empirical in nature and resulted from the development of crystal structure analysis by X-ray diffraction techniques by Max von Laue and W.H. and W.L. Bragg and in the 1920's and the work of V.M. Goldschmidt who analysed crystal structures in terms of the stoichiometry of the compound, the observed interatomic distances, the relative sizes of the component atoms and their polarization. Later in the 1930's, Pauling introduced the concept of electronegativity to help account for varying degrees of covalence in chemical bonds and showed the importance of chemical valence.

Although there has been recent substantial progress in applying quantum mechanical techniques to minerals (e.g. Gibbs 1982; Gibbs *et al*. 1987; Gibbs *et al*. 2008), this approach is sometimes difficult to apply to mineral structures, which are relatively complex and are composed of infinite periodic arrays of ions rather than of molecules. The empirical approach, based on the concept of periodic structures containing ions of specific size, charge, and coordination number, is still used by invesigators. Pauling's five rules, despite criticism as being an unrealistic model for bonding in most solids (Pauling 1929, 1960), are, in various modifications, are still being used today.

1.2.1 Characteristics of Cadmium

Cadmium, element 48, is the 49th most abundant element in the earths crust and exists in nature as seven stable isotopes and one radioactive isotope (Table 1) (Leland and Nier 1958). The ground electronic configuration of the Cd atom is [Kr]4d^{10}5s^2. Cadmium is a typical chalcophile element and thus has a strong affinity for sulphide liquid phases and tends to accumulate in magmatic sulphides (Goldschmidt 1958). Cadmium is found mainly as the sulphide mineral greenockite, however Cd does frequently substitute for other heavy metals, like Zn and Pb, in sulphide minerals. Small concentrations of Cd are frequently found in galena (PbS), the most common Pb sulphide mineral and the most important lead ore, and in sphalerite, ZnS, the most important zinc ore (Berry *et al.* 1983). Typically, this substitution occurs by isomorphic replacement (replacement of a particular metal within the crystal lattice)., Sphalerite, and a lesser extent galena, readily absorb Cd through isomorphous exchange (Tauson *et al.*, 2004, Tauson *et al.* 2005).

In minerals, Cd usually appears in the formal valence state Cd^{2+}, which results from the formal loss of the two 5*s* electrons, giving a 4d^{10} closed shell configuration. There have been 20 minerals described with essential Cd since the element was first discovered in 1817. Six are sulphides and one is a selenide. Cadmium secondary minerals are rare and result mainly from the weathering of Cd-bearing zinc minerals. The secondary minerals comprise four oxides, four carbonates, four sulphates, four phosphates and four arsenates and, apart from the carbonate otavite, all are each restricted to one or two worldwide occurrences. Volcanic activity is a major natural

source of environmental cadmium release (Nriagu 1979) and volcanic sublimates contain numerous rare phases with unusual chemical compositions, for example Pb-As-Bi sulphosalts, Pb-As and Bi sulphohalides and As-, Cd-, Tl- and I-bearing sulphosalts from the active Mutnovsky volcano in southern Kamchatka, Russia (Zelenski and Bortnikova 2005). Four of the known Cd minerals were described from volcanic sublimates [burnsite, $KCdCu_7O_2(SeO_3)_2Cl_9$, cadmoindite, $CdIn_2S_4$, kudriavite, $(Cd,Pb)Bi_2S_4$, tazieffite, $Pb_{20}Cd_2(As,Bi)_{22}S_{50}Cl_{10}$] and a number of others await characterization.

1.2.2 Characteristics of Lead

Lead, the 36th most abundant element in the earth's crust (average concentration = 13 ppm), is a widely distributed lithophile element that is enriched (relative to the mantle) in the continental crust (Rose *et al*. 1979). Lead has electronic configuration $[Xe]4f^{14}5d^{10}6s^26p^2$ and exists in three oxidation states in nature, Pb(0), Pb(II) and Pb(IV), Pb(II) being the most common. Lead is found as a major element in a wide variety of minerals.

The crystal chemistry and the relative stability Pb(II) minerals in the environment is controlled largely by the stereoactivity of a lone $6s^2$ electron pair (Krivovichev 2003). In most Pb(II) mineral structures, the lone-electron pair is stereoactive and the distribution of chemical bonds within the coordination sphere of the Pb(II) ion becomes highly asymmetric in order to minimize the repulsive interactions between lone-electron pair and bonding electron pairs (Sidgewick and Powell 1940). A stereochemically active lone pair plays the role of an additional ligand and occupies a volume approximately equal to the volume of an O^{2-} anion. Gillespie and Nyholm (1957) suggested that a lone pair of electrons occupies more space than a bond pair thus leading to distortions of coordination polyhedra from regular shape, and the general rule is that lone-pair-lone-pair repulsion > lone-pair-bond-pair repulsion > bond-pair-bond-pair repulsion. Cooper and Hawthorne (1994) have suggested that the presence or absence of stereoactive lone-pair behavior is to a large extent dictated by the local bond-valence requirements of the surrounding anions. Shimoni-Livny *et al*. (1998) found that lone-electron pairs were stereoactive for Pb(II) coordination numbers 2 to 5, but not for coordination numbers 9 and 10. For coordination numbers 6-8, the lone-electron pair may or may not be stereoactive. This was attributed to

ligands of higher coordination number compounds crowding the pair of electrons and lessening their effect. The stereoactivity of the lone-electron pair is controlled by the Lewis basicity of anions present in the structure (Krivovichev 2003). When Lewis strength of coordinating anions is low (e.g. in carbonates and sulfates), coordination of Pb(II) is more symmetrical and such phases tend to be less stable in the environment. The greater presence of strong Lewis bases such as O and OH induces high stereoactive behaviour of the lone-electron pair and such phases are usually more stable in the environment. It is likely that there are limits on the range of Lewis base strengths for which the lone pair is stereoactive, as has been found for Tl^{+} (Brown and Faggiani 1990). Density functional theory calculations on PbO and PbS, which have litharge and rocksalt type structures respectively, show that the formation of the asymmetric electron density associated with the stereoactive lone pair is chemically dependent on both the cation and anion (Walsh and Watson 2005).

1.2.3 Characteristics of Selenium

Selenium is the 66th most abundant crustal element (average concentration = 0.05 ppm). Selenium exists in four oxidation states in the natural environment; selenide (Se^{2-}), elemental selenium (Se^{0}), selenite (Se^{4+}) and selenate (Se^{6+}). The electronic structure of selenium in the ground state is $[Ar]3d^{10}4s^{2}4p^{4}$. Selenium resembles sulphur in many of its properties and small concentrations of selenium are common replacing S in ore minerals such as pyrite, pyrrhotite, chalcopyrite, bornite, galena (Edwards and Carlos 1954) and sulphate minerals such as barite and jarosite.

There are 129 minerals known that contain essential selenium (Back and Mandarino 2008). Twenty-eight are selenium oxysalts, of which thirteen are pure selenites and three contain two anionic groups; the selenate sulphate, olsacherite, $Pb_2(Se^{6+}O_4)(SO_4)$, the selenate selenite, schmeiderite, $Pb_2Cu_2(Se^{4+}O_3)(Se^{6+}O_4)(OH)_4$, and the sulphate selenite, munakataite, $Pb_2Cu_2(Se^{4+}O_3)(SO_4)(OH)_4$.

1.2.4 Characteristics of zinc

Zinc is a relatively common element in the earths crust; its crustal abundance is ~80 ppm. Approximately 185 Zn minerals have been described (Back and Mandarino

2008). Zinc has electronic configuration [Ar]$3d^{10}4s^2$. Zn^{2+} has a complex crystal chemistry, a result of its lack of a crystal-field stabilization, high polarizability, chalcophilicity, and a tendency towards highly covalent, hybridized sp^3 bonds. In minerals, Zn^{2+} is found in 4-, 5- (trigonal bipyramidal and square pyramidal) and 6-coordination and occurs in mixed coordination in a number of minerals. The Zn^{2+} cation has a strong tendency to adopt a tetrahedral coordination as the filling of the *d* orbitals leaves the 4*s* orbital and the three 4*p* orbitals available for hybridization to form four tetrahedral bond orbitals. Since the d^{10} configuration affords no crystal field stabilization energy, Zn^{2+} exhibits few of the characteristic properties of the transition metals and instead displays crystal-chemical tendencies similar to smaller [4]-coordinated cations such as Si, Al, Be, Li and Fe^{3+}.

1.2.5 Characteristics of copper

Copper, element 29, is the 20th most abundant element in the earths crust and exists in nature as two stable isotopes, ^{63}Cu and ^{65}C, and numerous radioisotopes. Copper has electronic configuration [Ar]$3d^{10}4s^1$. Divalent copper commonly occurs in a variety of coordinations; six-coordinated octahedral and trigonal-prismatic, five-coordinated square-pyramidal and triangular-bipyramidal, and four-coordinated square-planar geometries (Eby and Hawthorne 1993). The most common coordination for Cu^{2+} in mineral structures is octahedral. Unlike most other octahedrally coordinated small- and medium-sized (0.53–0.83 Å) divalent and trivalent cations, nearly all $Cu\phi_6$ (ϕ: O^{2-}, OH, H_2O) octahedra in minerals and synthetic inorganic solids are stongly distorted away from holosymmetric symmetry. This distortion, in which one axis of the octahedron is either elongated or compressed, is due to due to the electonic instability of the d^9 configuration of Cu^{2+} in an octahedral ligand-field, as indicated by the Jahn-Teller theorem (Jahn and Teller 1937) which states that

"*any non-linear molecular system in a degenerate electronic state will be unstable and will undergo distortion to form a system of lower symmetry and lower energy thereby removing the degeneracy*".

Eby and Hawthorne (1993) have shown that there is a very strong bimodal distribution of Cu-ϕ (ϕ: O^{2-}, OH, H_2O) distances in Cu^{2+} oxysalt minerals with maxima at 1.97 and 2.44 Å and populations near the ratio 2:1. This may reflect an

ideal stable axially elongated [4+2]-distorted geometry, with an equatorial bond length of 1.97 Å and an axial bond length of 2.44 Å. Bond valence arrangements will perturb these values such that the mean equatorial bond length will decrease and the mean axial bond length will increase so that the sum of bond valences around each ion will equal the magnitude of the ions formal valence (Brown 1981). The dispersion of axial bond lengths is greater than equatorial bond lengths due to the "softer" interaction at longer bond distances (Dunitz and Orgel 1960).

1.2.6 Characteristics of Arsenic

Arsenic is the 35th most abundant element in the earth's crust. It occurs primarily as the anion, dianion As_2^{2-} or sulfarsenide anion AsS^{2-} in sulfur-containing minerals such as arsenopyrite, FeAsS, lollingite, $FeAs_2$, realgar, AsS, and orpiment, As_2S_3 (Vaughan 2006). It can also occur as a minor component in pyrite (FeS_2). Oxidation of primary As bearing sulphides results in a large number of secondary arsenic minerals.

Arsenic has electronic configuration [Ar]$3d^{10}4s^24p^3$. The five valence electrons allow As to exist in four different oxidation states: (-III), (0), (III), and (V), however, oxidized As(III) and As(V) are the most widespread forms in nature. Arsenic shows a diverse chemical behavior and will bond readily to a wide variety of ligands. More than 300 arsenic minerals are known to occur in nature (Back and Mandarino 2008). Base-metal arsenates are exceptionally widespread in the oxidized zones of sulphide orebodies and are derived from the common mineral arsenopyrite (FeAsS) or from less common species such as lollingite (FeAs2) and arsenic-containing sulphosalts. Secondary As minerals display a wide range of stoichiometries and are frequenly being involved in complex solid solution series (Gaines *et al*. 1997).

A large number of secondary As minerals have been found in highly contaminated soils, stream sediments, industrial sites and mine tailings (Drahota and Filippi 2009), in particular oxides, arsenates, sulphoarsenates, sulphoarsenites. (e.g. arsenolite, claudetite, scorodite, arseniosiderite, pharmacosiderite, yukonite, kaňkite, symplesite, amorphous ferric arsenate/pitticite, beudantite, mimetite, schultenite, haidingerite, hörnesite, pharmacolite, picropharmacolite and weilite). Structural data is available for most of the environmentally important secondary As minerals, and solubility and thermodynamic data have been reported for many.

1.3 Solid solution in Minerals

An important factor in understanding the crystal chemistry of minerals is the nature of atomic substitution or replacement. Natural minerals are rarely pure stoichiometric compounds and frequently exhibit replacement of one of more cations or anions by other ions. In many cases these substitutions can be quite extensive and the mineral may be considered a solid solution.

A solid solution is a set of solid mixtures having the same two (or more) components, which crystallize in the same structural arrangement, but in which the composition and lattice parameters progressively change in a systematic manner (Galwey 1967). In binary solid solution systems, the composition varies from the pure substance A through all possible compositional ratios A:B to the pure substance B. The atoms in an ideal solid solution are randomly dispersed over the available lattice positions (disordered); however they may undergo a crystallographic transformation known as an order-disorder transition and display a regular arrangement with respect to each other (ie. become ordered).

A distinction is usually drawn between convergent and nonconvergent ordering (Thompson 1969). In the former, two or more crystallographic sites can become related by symmetry when their average occupancy by different atoms becomes the same (Putnis 1992). The ordering characteristically gives rise to a reduction in symmetry at a discrete phase transition. In contrast, the sites over which nonconvergent ordering occurs can never become related by symmetry even if their occupancies are identical-a degree of site preference by different atoms is retained at all temperatures and pressures because of some fundamental differences in local coordination or bonding.

1.4 The Stability of Minerals

The stability and solubilities of secondary oxysalt minerals are of considerable importance for understanding the mobility of heavy metals in the environment and their concentration in groundwaters. Since the discovery of X-ray diffraction, crystallographers have attempted to elucidate the fundamental factors that determine why a crystalline compound adopts a particular structure rather that another. That the behaviour of crystals of minerals and inorganic compounds is governed by some

empirical rules was known from the early work on crystal chemistry by W.L. Bragg, V.M. Goldschmidt and others. The most rigorous constraint on possible chemical variations in crystals is the rule of electroneutrality, which states that:

"*the sum of the formal charges of all the ions in a crystal is zero*".

Early ideas on the size of atoms, their coordination and polymerization into coordination polyhedra were refined by Pauling, who proposed five rules, based on the electroneutrality principal, governing the geometries of ionic crystals (Pauling 1929, 1960).

The strength of the bonds formed by a cation was defined by Pauling (1929) as

"*the strength of an electrostatic bond in an ionic crystal is the formal valence of the cation divided by its coordination number*".

Byström and Wilhelmi (1951) and Zachariasen (1954) and others applied the concept to vanadates, borates, uranates and silicates and showed that the bond strengths are inversely related to the bond lengths. Donnay and Allmann (1970) developed these ideas into the concept of bond valence. Deviations from Paulings second rule led Baur (1970) to observe that an effective charge balance is achieved by adjustments in the cation-anion bond distances, that is, by distortion of the cation-centred polyhedra. By correlating bond lengths to bond strengths, Baur's extended electostatic valence rule allowed prediction of bond lengths more accurately from empirically derived parameters.

This approach did not work well for very distorted environments, which led Brown and Shannon (1973) to model the length of a bond to its strength with the expression

$$s = (R_0/R)^{-N}$$

(where s is the strength of a given bonded interaction with length R) and to develop a set of empirical bond-strength bond-length curves. The regression constants R_0 and N were determined for the individual bond lengths observed for a large number of crystal structures with the constraint that the sum of the strengths of the bonded interactions reaching each cation and anion in a structure is equal to its formal valence. Brown and Shannon (1973) found the expression to be capable of modeling bonded interactions for a wide range of materials, ranging from predominately ionic to predominately covalent, and found a correlation between bond valence and the covalent character of a bond.

The most widely used expressions for the dependence of bond valence on bond lengths is:

$$s = \exp\left[(R_0 - R) / B\right] \qquad \text{(Brown and Altermatt 1985)}$$

where s is the bond-valence in *vu* (valence units), R is the observed bond-length, and R_0, and B are constants characteristic of specific cation-anion bonds. Empirical paratameters have been calculated for a large number of cation-anion pairs by Brown and Altermatt (1985) and (Brese and O'Keeffe 1991). The concept of bond valence has found wide applicability in solid-state chemistry and provides a powerful method for the prediction and interpretation of bond lengths in crystals.

Paragenetic studies (e.g., Bandy 1938, Fisher 1958) have shown that there are well-defined relations between chemical compositions of hydroxy-hydrated minerals and their position in paragenetic sequences. Common rocks consist of a small number of rock-forming minerals that are stable over a wide range of conditions (pressure, temperature, pH, etc.) (*cf.* Hawthorne 1992). In response to changing external conditions these minerals adjust their chemistry but retain their structural integrity ie. the topological details of their bond networks do not change very frequently. The non-rock-forming minerals commonly occur as constituents of complex geological environments; highly fractionated pegmatites, weathering zones of sulphide ore-bodies, etc. These are characterized by the presence of a large number of complex minerals, often of several different chemical types (e.g. arsenates, phosphates, silicates, oxides and sulphates), which are stable over a very limited range of external conditions. In response to even small changes in ambient conditions, rather than change their chemistry, many adjust their structure ie. break down to form new minerals, often closely related in structure. Hence Moore (1973) and Hawthorne (1979) have suggested that the crystal structures of minerals in complex geochemical environments should be related to the paragenetic sequences of the minerals. Little however is known about the factors that control the atomic arrangement, chemical composition and stability of these minerals.

Hierarchies of mineral structures, based upon structural connectivity, are a means to organize complex and diverse structures into a cohesive framework. They can be the basis for understanding the linkages between the paragenetic sequences of minerals and the crystal structures of the constituent minerals. Bragg (1930) classified

the silicate minerals based on polymerization (SiO_4) tetrahedra and this scheme was generalized to polymerized tetrahedral structures by Zoltai (1960) and Liebau (1985). Similar hierarchical classifications were developed for the aluminium hexafluoride minerals (Pabst 1950; Hawthorne 1984) and the borate minerals (Christ 1960; Christ and Clark 1977).

A classification based on chemical-structural criteria developed by Moore (1984) for the phosphate minerals was based on the polymerization of divalent and trivalent cation octahedra, a scheme that was also able to encompass some sulphates, arsenates, vanadates etc. However, this scheme has the disadvantage that it focuses on specific chemical classes of compounds. More adequate classifications of phosphate minerals, based on the polymerizations of octahedral-tetrahedral coordination polyhedra, were developed by Hawthorne (1979) and Moore (1980).

Based on Pauling's second rule (Pauling 1929) which states that the sum of the bond strengths around an anion is approximately equal to the magnitude of the valence of that anion, Hawthorne (1983) proposed that that structures of oxide and oxysalt minerals may be classified based on general stoichiometries that are written in terms of the strongly bonded coordination polyhedra, thus defining structural elements by bond-valences rather than by chemistry. Hawthorne (1985) used this hypothesis to develop a hierarchical classification and description of minerals structually based on octahedra and tetrahedra. The possible classes of cluster polymerization are (1) unconnected polyhedra; (2) finite clusters; (3) infinite chains; (4) infinite sheets and (5) infinite frameworks. This approach has been used to produce a hierarchical scheme for a large group of oxide and oxysalt structures (Hawthorne 1985, 1986, 1990, 1994; Eby and Hawthorne 1993).

A combination of a binary representation of structure and bond-valence theory has been used to interpret the relationships between structure stereochemistry, chemical composition, occurrence and stability of complex hydroxyhydrated oxysalt minerals, which crystallize from low-temperature aqueous solutions (Schindler and Hawthorne 2001 and references therein). An oxysalt mineral structure can be divided into two parts, a structural unit and an interstitial complex (Hawthorne 1985). The structural unit is an (usually anionic) array of strongly bonded polyhedra and the interstitial complex is an array of weakly bonded (usually cationic or neutral) species. The structural unit and the interstitial complex are characterized by their Lewis basicity

and Lewis acidity respectively ie. the affinity of each component to donate or to accept electrons (Brown 1981). The Lewis-acid strength of a cation can be defined as:

the characteristic bond-valence = atomic (formal) valance/mean coordination-number

where the mean coordination number is derived from a large number of crystal structures containing the relevant cation. The Lewis-base strength of an anion can be defined as the characteristic strength of the bonds formed by the anion.

The interaction between these two components can be examined using the valence-matching principle (Brown 1981):

Stable structures will form when the Lewis-acid strength of the cation closely matches the Lewis-base strength of the anion.

For a structural arrangement to be stable, the Lewis acidity and basicity of the constituent parts must match. This approach gives an insight into mineral stability, as it is the weak interstitial bonds that will control the breakdown of the structure. The valence-matching principle can also be used to examine the controls on the nature of interstitial cation chemistry in minerals. Minerals with different structural units often have contrasting interstitial-cation chemistry, a result of the matching of the acid and base strengths of the interstitial cations and the structural unit.

The roles of H_2O groups are of particular importance in understanding the interaction of the interstitial complex with the structural unit, and H_2O groups play a key role in moderating the Lewis acidity of the interstitial complex such that it matches with the Lewis basicity of a specific structural unit (Schindler and Hawthorne 2001).

1.5 References

Back, M. and Mandarino, J.A. (2008) Fleischer's Glossary of Mineral Species 2008. Mineralogical Record Inc., Tuscon, 346 p.

Birch, W.D. (1999) The Minerals. In Minerals of Broken Hill. W.D. Birch, ed., Broken Hill Council, Broken Hill, p. 88–256.

Bragg, W.L (1930) The structure of silicates. Zeitschrift für Kristallographie, 74, 237–305.

Brown, I.D. (1981) The bond-valence method: an empirical approach to chemical structure and bonding. In M. O'Keefe and A. Navrotsky, Eds., Structure and Bonding in Crystals. Academic Press, London, p. 1–30.

Brown, I.D. and Altermatt, D. (1985) Bond-valence parameters obtained from a systematic analysis of the inorganic crystal structure database. Acta Crystallographica, B41, 244–247.

Brown, I.D. and Shannon R.D. (1973) Empirical bond-strength–bond-length curves for oxides. Acta Crystallographica, A29, 266–282.

Burns, P.C. (1999) The crystal chemistry of uranium. In Uranium: Mineralogy, Geochemistry and the Environment. P.C. Burns and R. Finch, Eds. Reviews in Mineralogy and Geochemistry 38, Mineralogical Society of America, Washington, D.C. p 23-90.

Byström, A. and Wilhelmi, K.A. (1951) The Crystal Structure of $(NH_4)_2Cr_2O_7$. With a Discussion of the Relation between Bond Number and Interatomic Distances. Acta Chemica Scandinavica, 5, 1003–1010.

Chen, F.R., Ewing, R.C. and Clark, S.B. (1999) The Gibbs free energies and enthalpies of formation of U^{6+} phases: An empirical method of prediction. American Mineralogist, 84, 650–664.

Christ, C.L. (1960) Crystal chemistry and systematic classification of hydrated borate minerals. American Mineralogist, 45, 334–340.

Christ, C.L. and Clark, J.R. (1977) A crystal-chemistry classification of borate structures with emphasis on hydrated borates. Physics and Chemistry of Minerals, 2, 59–87.

Donnay, G., and Allmann, R. (1970) How to recognize O^{2-}, OH^{-}, and H_2O in crystal structures determined by X-rays. American Mineralogist, 55, 1003–1015.

Eby, R.K. and Hawthorne, F.C. (1993) Structural relationships in copper oxysalt minerals. I. Structural hierarchy. Acta Crystallographica, B49, 28–56.

Edwards, A.B. and Carlos, G.C. (1954) The selenium content of some Australian sulphide deposits. Proceedngs of the Australasian Institute of Mining and Mellallurgy, 172, 31–63.

Evans, R.C. (1966) An Introduction to Crystal Chemistry. Cambridge University Press. 410 p.

Faure, G. (1991) Principles and Applications of Inorganic Geochemistry. MacMillian Publishing Company, New York, 626 p.

Fisher, D. J. (1958) Pegmatite phosphates and problems. American Mineralogist, 43, 181–207.

Fuge, R., Pearce, F.M., Pearce, N.J.G. and Perkins, W.T. (1993) Geochemistry of Cd in the secondary environment near abandoned metalliferous mines, Wales. Applied Geochemistry, Supplement 2, 29–35.

Gaines, R.W., Skinner, H.C.W., Foord, E.E., Mason, B. and Rosenzweig, A. (1997) Dana's New Mineralogy, John Wiley and Sons, New York, 1819 p.

Galwey, A.K. (1967) Chemistry of solids. Chapmann and Hall, London, 210 p.

Gibbs, G.V, Downs, R.T., Cox, D.F., Ross, N.L., Prewitt, C.T., Rosso K.M., Lippmann, T. and Kirfel, A. (2008) Bonded interactions and the crystal chemistry of minerals: a review. Zeitschrift für Kristallographie, 223, 1–40.

Gibbs, G.V., Finger, L,W. and Boisen, M.B. (1987) Molecular mimicry of the bond-length–bond-strength variations in oxide crystals. Physics and Chemistry of Minerals, 14, 327–331.

Gibbs, G.V. (1982) Molecules as model for bonding in silicates. American Mineralogist, 67, 421–450.

Hawthorne, F.C. (1979) The crystal structure of morinite. Canadian Mineralogist, 17, 93–102.

Hawthorne (1990) Structural hierarchy in $M^{[6]}T^{[4]}\phi_n$ minerals. Zeitschrift für Kristallographie, 192, 1–52.

Hawthorne, F. C. (1986) Structural hierarchy in $^{VI}M_x^{III}T_y\phi_z$ minerals. Canadian Mineralogist, 24, 625–642.

Hawthorne, F.C. (1985) Towards a structural classification of minerals: the $^{VI}M^{IV}T_2\phi_n$ minerals. American Mineralogist, 70, 455–473.

Hawthorne, F.C. (1992) Bond topology, bond-valence and structure stability. In G.D. Price and N.L. Ross, Eds., The Stability of Minerals. Chapman and Hall, London, pp. 25–87.

Hawthorne, F.C. (1994) Structural aspects of oxide and oxysalt crystals. Acta Crystalographica, B50, 481–510.

Hawthorne, F.C. (1998) Structure and chemistry of phosphate minerals. Mineralogical Magazine, 62, 141–164.

Krivovichev, S.V. (2003) Structural Chemistry of Basic Pb(II) Oxysalt Minerals and Inorganic Compounds. Geophysical Research Abstracts, 5, 10517.

Krivovichev, S.Y., and Burns, P.C. (2000) Crystal chemistry of basic lead carbonates. I. The crystal structure of synthetic shannonite, $Pb_2O(CO_3)$. Mineralogical Magazine, 64, 1063–1068.

Li, Yaping, Krivovichev, S.V. and Burns, P.C. (2000) Crystal Chemistry of Lead Oxide Hydroxide Nitrates I. The Crystal Structure of $[Pb_6O_4](OH)(NO_3)(CO_3)$ Journal of Solid State Chemistry, 153, 365–370.

Li, Yaping, Krivovichev, S.V. and Burns, P.C. (2001) Crystal chemistry of lead oxide hydroxide nitratres. II. The crystal structure of $Pb_{13}O_8(OH)_6(NO_3)_4$. Journal of Solid State Chemistry, 158, 74-77.

Liebau, F. (1985) Structural chemistry of silicates: Structure, bonding, and classification. Springer-Verlag, Berlin, 347 p.

Moore, P.B. (1973) Pegmatite phosphates: Mineralogy and crystal chemistry. Mineralogical Record, 4, 103–130.

Moore, P.B. (1984) Crystallochemical aspects of the phosphate minerals. In J.O. Niagru and P.B. Moore, Eds., Phosphate Minerals. Springer-Verlag, Berlin, 155–170.

Pabst, A. (1950) A structural classification of fluoaluminates. American Mineralogist, 35, 149–165.

Pauling, L. (1929) The principles determining the structure of complex ionic crystals. Journal of the American Chemical Society, 51, 1010–1026.

Pauling, L. (1947) Atomic and interatomic distances in metals. Journal of the American Chemical Society, 69, 542–553.

Pauling, L (1960) The nature of the chemical bond, 3rd Ed. Cornell University Press, Ithaca, New York, 644 p.

Paulson, A.J. (1997) The transport and fate of Fe, Mn, Cu, Zn, Cd, Pb, and SO_4 in a groundwater plume and in downstream surface water in the Coeur d'Alene mining district. Idaho, USA. Applied Geochemistry, 12, 447–464.

Putnis, A. (1992) Introduction to Mineral Sciences. Cambridge University Press, Cambridge, 456p.

Schindler, M. and Hawthorne, F.C. (2001) A bond-valence approach to the structure, chemistry and paragenesis of hydroxy-hydrated oxysalt minerals. I. Theory. Canadian Mineralogist, 39, 1225–1242.

Shimoni-Livny, L., Glusker, J.P. and Bock, C.B. (1998) Lone Pair Functionality in Divalent Lead Compounds. Inorganic Chemistry, 37, 1853–1867.

Sidgwick, N.V., and Powell, H.M. (1940) Bakerian Lecture. Stereochemical Types and Valency Groups. Proceedings of the Royal Society of London. Series A, Mathematical and Physical Sciences, 176, 153–180.

Thompson, J.B., Jr. (1969) Chemical reactions in crystals. American Mineralogist, 54, 341–375.

Walsh, A. and Watson, G.W. (2005) The origin of the stereochemically active Pb(II) lone pair: DFT calculations on PbO and PbS. Journal of Solid State Chemistry, 178, 1422–1428.

Zachariasen, W.H. (1954) Crystal chemical studies of the 5*f*-Series of elements XXII. On the crystal chemistry of uranyl compounds and of related compounds of transuranic elements. Acta Crystallographica, 7, 795–799.

Zoltai, T. (1960) Classification of silicates and other minerals with tetrahedral structures. American Mineralogist, 45, 960–973.

Chapter 2 Experimental

2.1 Sample acquisition

This study is based on natural mineral specimens from the Kintore and Block 14 Opencuts, Broken Hill collected between 1986 and 2001. All specimens were obtained from private collections. The studied specimens (type specimens) of plimerite, nyholmite, liversidgeite and edwardsite have now been deposited in the collection of the South Australian Museum.

2.2 Single-crystal X-ray Diffraction

The technique of single-crystal X-ray diffraction was used as the method of crystal structure analysis in this research. A recent text on the method is Blake et al. (2009). To be suitable for single crystal X-ray diffraction data collection a crystal must be of suitable size and quality. Potentially suitable crystals for X-ray data collection were examined using a polarizing microscope. Those considered to be most suitable were mounted on glass fibres, using oil or grease, and data were collected using one of four CCD (charge-coupled device) diffractometers (Burns 1998):

1. A Nonius KappaCCD diffractometer at the Research School of Chemistry, The Australian National University, Australian Capital Territory. Data reduction and unit cell refinement were carried out using the Denzo and Scalepack and HKL Scalepack programs (Otwinowski and Minor 1997, Otwinowski *et al*. 2003) Gaussian integration absorption correction, based on the crystal size and indexing of faces, was applied (Coppens 1970).

2. A Nonius KappaCCD diffractometer at the Institut für Mineralogie und Kristallographie, Universität Wien, Wien, Austria. The intensity data were processed and corrected for absorption with the Nonius program suite DENZO-SMN (Otwinowski and Minor 1997, Otwinowski et al. 2003).

3. A Bruker APEX II KappaCCD diffractometer at the Institut für Mineralogie und Kristallographie, Universität Wien, Wien, Austria. The data were reduced and corrected for Lorentz, polarization, and absorption effects and the unit cell was refined using the Bruker program SADABS (Bruker 2006).

4. An ADSC Quantum 210r detector using synchrotron X-ray radiation at the PX1 Beamline, Australian Synchrotron, Clayton, Victoria. The data reduction was carried out with the imosflm (Leslie 1992) program.

Normalized structure factors (E) were calculated from the intensity data. These are distributed differently in centrosymmetric and noncentrosymmetric structures. A mean $|E^2-1|$ close to 0.968 may indicate a centre of symmetry, and a value close to 0.736 the absence of a centre of symmetry (Wilson 1949; Howells *et al*. 1950; Karle *et al*. 1965). The use of statistical values is, however, not always reliable and if based only on the stronger intensities may be strongly biased toward a noncentrosymmetric indication (Marsh 1981). Also, the contribution of one or more heavy atoms in a centrosymmetric structure to the overall scattering may result in an acentric distribution of values of $|E^2-1|$ (Hargreaves 1955; Snow and Tiekink 1988). Determination of the Laue symmetry and space group was completed using the programs XPREP (Bruker 1997) or WinGx (Farrugia 1999). The space group was considered to be conclusively determined when the structure model both agreed with the X-ray diffraction data and was chemically reasonable. Structure solution, by direct methods (Giacovazzo 1980; Woolfson 1987) or Patterson methods (Patterson 1934), and refinement, by full-matrix least-squares techniques, were carried out with the SHELX97 program package (Sheldrick 1997a, 1997b) using atomic scattering factors for neutral atoms taken from the International Tables for Crystallography (Wilson 1992).

The bond valence concept (Brown 1981) and the parameters of Brown and Altermat 1985) and Brese and O'Keeffe (1991) were used for the identification of OH^- and H_2O groups in the crystal structures and to support the validity of the refined structural models.

2.3 Electron-microprobe analysis

The chemical analyses in this study were obtained on a CAMECA SX51 electron microprobe, operating in the wavelength-dispersion mode, at Adelaide Microscopy, The University of Adelaide. Data were reduced using the $\phi(\rho Z)$ method of Pouchou and Pichoir (1985). Accelerating voltage, specimen current and beam diameter were selected based on the stability of each mineral under the electron beam.

2.4 X-ray powder diffraction

Powder X-ray diffraction was used for refinement of the unit cell parameters. Powder X-ray diffraction data were obtained using a 100 mm Guinier-Hägg camera using Cr $K\alpha$ radiation (λ 2.28970 Å) and silicon (NBS SRM 640a) as an internal standard. The Guinier-Hägg films were scanned using an Epson film scanner, and the powder-diffraction profile over the 2θ range 10 to 90° were extracted using the program SCION IMAGE (Palmer 1997) and Universal-Si-Calibration, a macro function based on IGOR PRO 4.0 (WaveMetrics Inc., 2000). The unit-cell parameters were refined by treating the whole powder pattern with the Le Bail profile-fitting method (Le Bail et al. 1988; Hunter 1998).

2.5 Other instrumental techniques

Other instrumental techniques that were used in this research were Fourier Transform (FTIR) infrared spectroscopy and Raman spectroscopy for the verification of molecular water content and identification of chemical groups such as PO_4, AsO_4 etc. Mössbauer spectroscopy was used for determination of the Fe^{2+}/Fe^{3+} ratio in plimerite.

2.6 References

Blake, A.J., Cole, J.M., Clegg, W., Evans, J.S.O., Main, P., Parsons, S. and Watkin, D.J. (2009) Crystal structure analysis: principles and practice. 2nd ed. (W. Clegg, editor). IUCr Texts on Crystallography 13, Oxford University Press, Oxford. 387 p.

Brese, N.E. and O'Keeffe, M. (1991) Bond-valence parameters for solids. Acta Crystallographica, B47, 192–197.

Brown, I.D. (1981) The bond-valence method: an empirical approach to chemical structure and bonding. In M. O'Keefe and A. Navrotsky, Eds., Structure and Bonding in Crystals. Academic Press, London.

Brown, I.D. and Altermatt, D. (1985) Bond-valence parameters obtained from a systematic analysis of the inorganic crystal structure database. Acta Crystallographica, B41, 244–247.

Bruker (1997) SMART, SAINT and XPREP. Area detector control, data integration and reduction software. Bruker Analytical X-ray Instruments Inc., Madison, Wisconsin, USA.

Bruker (2006) SADABS. Bruker AXS Inc., Madison, Wisconsin, USA.

Burns, P.C. (1998) CCD area detectors of X-rays applied to the analysis of mineral structures. Canadian Mineralogist, 36, 847–853.

Coppens, P. (1970) Crystallographic Computing. F.R. Ahmed, S.R. Hall and C.P. Huber, Eds., p. 255–270. Munksgaard, Copenhagen.

Farrugia, L.J. (1999) WinGX Suite for Single Crystal Small Molecule Crystallography. Journal of Applied Crystalography, 32, 837–838.

Giacovazzo, C. (1980) Direct methods in crystallography. Academic Press, London. 432 p.

Howells, E.R., Phillips, D.C. and Rogers, D. (1950) The probability distribution of X-ray intensity. II. Experimental investigation on the X-ray detection of center of symmetry. Acta Crystallographica, 3, 210–214.

Hunter, B.A. (1998) Rietica - A Visual Rietveld Program. Commission on Powder Diffraction Newsletter, 20, 21.

Karle, I.L. Dragonette, K.S. and Brenner, S.A. (1965) The crystal and molecular structure of the serotonin-creatinine sulphate complex. Acta Crystallographica, 19, 713–716.

Le Bail, A., Duroy, H. and Fourquet, J.L. (1988) Ab-initio structure determination of $LiSbWO_6$ by X-ray powder diffraction. Materials Research Bulletin, 23, 447–452.

Leslie, A.G.W. (1992) Recent changes to the MOSFLM package for processing film and image plate data. Joint CCP4 + ESF-EAMCB Newsletter on Protein Crystallography, No. 26.

Otwinowski, Z. and Minor, W. (1997) Processing X-ray diffraction data collected in oscillation mode. In Macromolecular Crystallography, C.W. Carter Jr. and R.M. Sweet, Eds., Vol. 276, p. 307–326. Academic Press, New York.

Otwinowski, Z., Borek, D., Majewski, W. and Minor, W. (2003) Multiparametric scaling of diffraction intensities. Acta Crystallographica, **A59**, 228–234.

Palmer, D.C. (1997) Digital analysis of X-ray films. Mineralogical Magazine, 61, 453–461.

Patterson, A.L. (1934) A Fourier series method for the determination of the components of interatomic distances in crystals. Physical Review, 46, 372–376.

Pouchou, J.L. and Pichoir, F. (1985) "PAP" ϕ (ρZ) procedure for improved quantitative microanalysis. In J.T. Armstrong, Ed., Microbeam Analysis, 104–106. San Francisco Press, California.

Sheldrick, G.M. 1997a. SHELXS–97, a Program for the Solution of Crystal Structures. University of Göttingen, Göttingen, Germany.

Sheldrick, G.M. 1997b. SHELXL–97, a Program for Crystal Structure Refinement. University of Göttingen, Göttingen, Germany.

Snow, M.R., and Tiekink, E.R.T. (1988) Practical resolution of the centrosymmetric/noncentrosymmetric ambiguity with the use of E statistics. Acta Crystallographica, B44, 676–677.

Wavemetrics, Inc. (2000) IGOR PRO version 4.0. WaveMetrics Inc., Lake Oswego, Oregon.

Wilson, A.J.C., Ed. (1992) International Tables for Crystallography, vol. C, 883 p. Kluwer Academic, Dordrecht, The Netherlands.

Wilson, A.J.C. (1949) The probability distribution of X-ray intensities. Acta Crystallographica, 2, 318–321.

Woolfson, M.M. (1987) Direct methods - from birth to maturity. Acta Crystallographica, A43, 593–612.

CHAPTER 3

The crystal structure of munakataite

Peter Elliott[1,2] and Anthony C. Willis[3]

[1]School of Earth and Environmental Sciences, The University of Adelaide, Adelaide, South Australia 5005, Australia.

[2]South Australian Museum, North Terrace, Adelaide, South Australia 5000, Australia.

[3]Research School of Chemistry, The Australian National University, Australian Capital Territory 0200, Australia.

STATEMENT OF AUTHORSHIP

The crystal structure of munakataite from the Block 14 Opencut, Broken Hill, New South Wales

Peter Elliott (Candidate)

Performed analysis on all samples, interpreted data and wrote manuscript.

I hereby certify that the statement of contribution is accurate.

Signed .....*Date*.....23/8/2010

Anthony Willis

Single-crystal X-ray data collection and data reduction.

I hereby certify that the statement of contribution is accurate and I give permission for the inclusion of the paper in the thesis.

Signed .....*Date*.....12/7/2010

CHAPTER 3

The crystal structure of munakataite

Peter Elliott[1,2] and Anthony C. Willis[3]

[1]School of Earth and Environmental Sciences, The University of Adelaide, Adelaide, South Australia 5005, Australia

[2]South Australian Museum, North Terrace, Adelaide, South Australia 5000, Australia

[3]Research School of Chemistry, The Australian National University, Australian Capital Territory 0200, Australia

ABSTRACT

The crystal structure of munakataite, $Pb_2Cu_2Se^{4+}O_3SO_4(OH)_4$, monoclinic, $P2_1/m$, a = 9.790(2), b = 5.6668(11), c = 9.2933(19) Å, β = 102.34(3)º, V = 503.67(18) Å^3, Z = 2, has been solved by Patterson methods and refined to $R1$ = 12.27% based on 1385 reflections with $F_o > 4\sigma(F_o)$ measured with Mo$K\alpha$ X-radiation. There are two symmetrically independent Pb positions, one Cu, one Se and one S position in the structure. The coordination polyhedron of Pb1 is strongly distorted due to the effect of a stereoactive s^2 lone-electron pair on the Pb^{2+} cation. The structure is based on chains of composition $Cu_2(SO_4)(SeO_3)\phi_4$ which extend along [010]. Parallel chains are linked by interstitial Pb^{2+} cations and hydrogen bonds. The structural model is of low quality due to the poor quality of the crystal used for data collection, however, munakataite is shown to be isostructral with schmiederite and structurally related to linarite.

INTRODUCTION

Munakataite, $Pb_2Cu_2(Se^{4+}O_3)(SO_4)(OH)_4$ is a recently described mineral from the Kato mine, Munakata City, Fukuoka Prefecture, Japan (Matsubara *et al*. 2008) where it was found as aggregates of pale blue, fibrous crystals to 30 μm in length associated with malachite. The mineral formed in a quartz vein containing Cu-Zn-Pb-Ag-Au ore minerals. Matsubara *et al*. (2008) considered the mineral to be the (SO_4)-dominant

analogue of schmiederite, $Pb_2Cu_2(Se^{4+}O_3)(Se^{6+}O_4)(OH)_4$, a member of the linarite-chenite group, based on the presence of a selenite group, $(Se^{4+}O_3)^{2-}$, and a sulphate group, $(S^{6+}O_4)^{2-}$ detected by FT-IR analysis, and also by the similarity of the powder X-ray diffraction pattern to those of linarite and schmiederite. The refined unit cell parameters were a = 9.922(3), b = 5.712(2), c = 9.291(10) Å, β = 101.98(3)° and V = 520.8 Å^3. By analogy to schmiederite, the mineral was considered to be monoclinic with space group $P2_1/m$. No crystals suitable for a single-crystal X-ray-diffraction study could be found. Matsubara *et al*. (2008) also noted a second occurrence of munakataite at the Akita Prefecture, Tohuko Region, Honshu Island, Japan and the mineral has more recently been identified from Otto Mountain, Baker, San Bernardino Co., California, USA and on a specimen from the Mammoth-Saint Anthony Mine, Tiger, Pinal Co., Arizona, USA. (Ralph and Chau 2009).

Munakataite has been identified on specimens collected in the late 1980s from the Kintore Opencut, Broken Hill, New South Wales. The mineral forms aggregates of purplish-blue, fibrous crystals to 2 mm across and rare, elongated, individual bladed crystals to 0.25 mm in length associated with malachite in a matrix comprising cerussite, goethite, coronadite and garnet. Munakataite is the first mineral containing essential selenium to be reported from Broken Hill. It has likely formed as a result of the weathering of Se-bearing galena. In a study of trace element chemistry of sphalerite and galena in the Broken Hill lode, Both (1973) found selenium content of up to 250 ppm in galena from the Zinc Lode lenses. Analyses of arsenopyrite, chalcopyrite, galena, lollingite, pyrrhotite and sphalerite from the Broken Hill show selenium contents of ~49 ppm in lollingite and ~30 ppm in chalcopyrite and pyrrhotite (Edwards and Carlos 1954).

A determination of the crystal structure of munakataite has been undertaken by single-crystal X-ray methods in order to clarify the crystal chemistry and its relationship to schmiederite.

CHEMICAL COMPOSITION

Chemical analyses of munakataite were performed using a Cameca SX51 electron microprobe operating in the wavelength-dispersion mode at the following conditions: accelerating voltage 20 kV, specimen current 20 mA, peak count-time 20 s, background count-time 10 s and beam diameter 20 μm. The standards used were chalcopyrite (Cu *K*α), sphalerite (Zn *K*α), galena (Pb *M*α), almandine (Fe *K*α), almandine (Al *K*α), bismuth selenide (Se *L*α) and marcasite (S *K*α). Data were reduced using the φ(ρZ) method of Pouchou and Pichoir (1985). The mineral was very difficult to polish due to the soft fibrous nature of the crysral aggregates, resulting in variable analysis totals. The mean chemical composition for ten points analysed and unit formula are given in Table 1. Elements detected in amounts < 0.05 wt.% were Fe, Mn, Ba, Zn and Si.

TABLE 1. Compositional data for munakataite.

	Average (10 points)	Range	Stand. Dev.	Ideal**	Number of ions	
SO_3	8.99	8.29–9.78	0.46	9.12	S	0.93
SeO_3	0.96	0.10–1.36	0.43		Se^{6+}	0.06
SeO_2	13.21	12.88–15.14	1.06	13.97	Se^{4+}	0.99
CuO	18.96	17.37–20.53	1.13	19.07	Cu	1.98
Al_2O_3	0.13	0.10–0.18	0.02		Al	0.02
PbO	53.70	52.72–54.96	0.81	53.52	Pb	1.99
H_2O (calc)*	4.33			4.33	OH	4.00
Sum	100.28					

*H_2O was calculated from the ideal formula based on structure determination.
**number of ions based on 11 oxygen atoms.

INFRARED SPECTROSCOPY

The infrared spectrum of munakataite (Figure 1) was recorded in the range 4000–650 cm^{-1} using a Nicolet 5700 FTIR spectrometer equipped with a Nicolet Continuum IR microscope and a diamond-anvil cell. A broad band from 3580–3170 cm^{-1} centred on 3328 cm^{-1} and with shoulders at 3490 and 3328 cm^{-1} is due to O–H stretching. A strong split band at 1095 and 1058 cm^{-1} is due to the SO^{4-} asymmetric stretch, ν_3 and a weak band at 665 cm^{-1} is due to the SO_4 asymmetric bend, ν_4. Weak bands at 792 and 728 cm^{-1} are assigned to selenite Se–O stretching and at 962 cm^{-1} to the SO_4 symmetric stretch, ν_1. Bands at 868 cm^{-1} and 818 cm^{-1} are possibly due to OH δ bending.

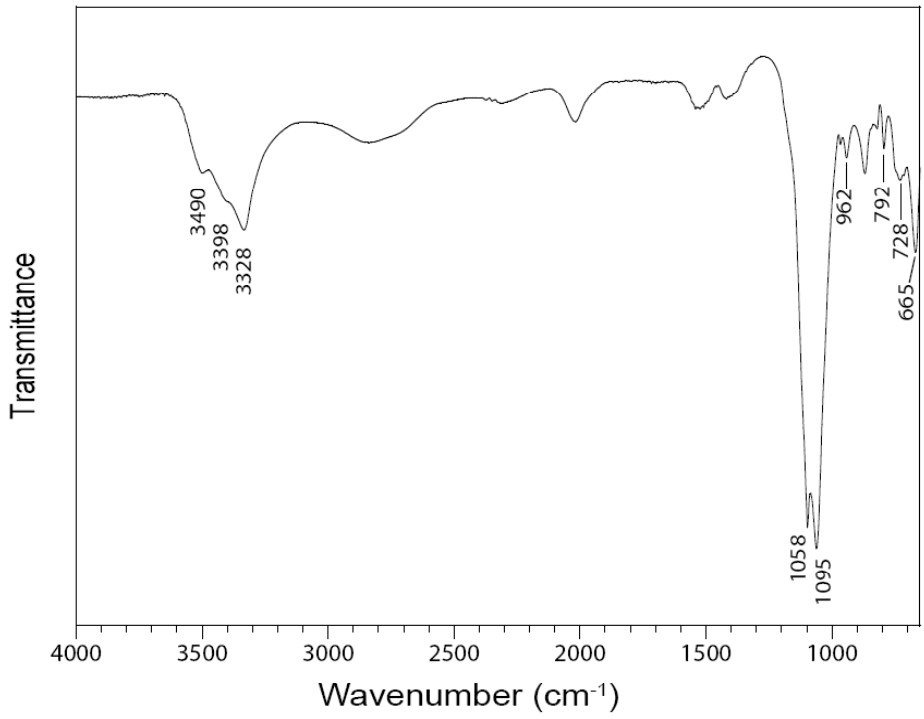

Figure 1. FT-IR spectrum of powdered munakataite.

STRUCTURE DETERMINATION

A bladed crystal of munakataite of dimensions 0.23 × 0.07 × 0.02 mm was mounted on a glass fiber and X-ray intensity data were collected at room temperature using a Nonius KappaCCD diffractometer. The 12284 measured intensities were corrected for Lorentz and polarization effects (Otwinowski and Minor 1997, Otwinowski *et al*. 2003). An absorption correction was applied using the Gaussian integration method (Coppens, 1970), with minumum and maximum transmission-coefficients of 0.035 and 0.356 rspectively. The unit cell-parameters, refined with the program HKL-SCALEPACK, are a = 9.790(2), b = 5.6668(11), c = 9.2933(19) Å, β = 102.34(3)º, V = 503.67(18) Å^3. Conditions for the data collection and subsequent refinement are summarized in Table 2.

Scattering curves for neutral atoms, together with coefficients of anomalous dispersion, were taken from the International Tables for X-ray Crystallography (Wilson 1992). Intensity statistics did not provide a conclusive indication of the presence of a center of symmetry ($|E^2-1| = 0.831$; predicted values: 0.968, centrosymmetric, 0.736, non-centrosymmetric). The Laue symmetry was found to be 2/*m* and the systematic absence condition 0*k*0: *k*=2n+1 was consistent with space groups $P2_1$ and $P2_1/m$. The structure was successfully solved in $P2_1/m$ by Patterson methods (SHELXS-97, Sheldrick, 1997a) and full-matrix least-squares refinement on F^2 (SHELXL-97, Sheldrick, 1997b) resulted in $R1$ index of ~ 19.37% for an isotropic displacement model. An omission of about 70 reflections with F_{obs} considerably larger than F_{calc} reduced $R1$ to 14.20%. Conversion to anisotropic displacement parameters resulted in the OH3 and O22 atoms becoming 'non-positive definitive' and in physically unrealistic atom shapes for most of the remaining O atoms. Also, anisotropic led to an only very small improvement of the R-values, hence isotropic refinement was retained for the anions.

Possible twinned models were investigated using the programs ROTAX (Cooper *et al*. 2002) and TwinRotMat (Spek 2003), but none led to an improvement in the refined model. It was not possible to locate the H atoms in difference Fourier maps. The final $R1$ index was 12.33% calculated for 1385 unique observed reflections, $F_o > 4\sigma(F_o)$.

Table 2. Crystal data, data collection and refinement details.

Crystal data	
Formula (idealized)	$Pb_2Cu_2(Se^{4+}O_3)(SO_4)(OH)_4$
Space group	$P2_1/m$
a,b,c (Å)	9.790(2), 5.6668(11), 9.2933(19)
β (º)	102.34(3)
V (Å^3), Z	503.67(18), 2
F(000)	720
μ (mm^{-1})	41.36
Absorption correction	Gaussian integration
Crystal dimensions (mm)	0.23×0.07× 0.02
Data collection	
Diffractometer	Nonius KappaCCD
Temperature (K)	293
Wavelength	λ = 0.71073 Å
θ range (°)	2.74 to 30.05
h,k,l ranges	-13 → 13, -7 → 7, -13 → 13,
Total reflections measured	12284
Data completeness (%)	93.2
Unique reflections	1496 (R_{int} = 10.71%)
Refinement	
Refinement on	F^2
$R1^*$ for $F_o > 4\sigma(F_o)$	12.33%
w$R2^\dagger$ for all F_o^2	31.97%
Reflections used $F_o > 4\sigma(F_o)$	1385
Number of parameters refined	68
Extinction factor	0.0000(8)
$\Delta\rho_{min}$, $\Delta\rho_{max}$ (e/Å^3)	23.745, -7.876
GooF	1.057

$^*R1 = \Sigma||F_O|-|F_C|| / \Sigma|F_O|$

$^\dagger wR2 = \Sigma w(|F_O|^2-|F_C|^2)^2 / \Sigma w|F_O|^2)^{1/2}$; $w = 1/[\sigma^2(F_O^2) + (0.042\ P)^2 + 12.60\ P]$;
$P = ([\text{max of } (0 \text{ or } F_0^2)] + 2F_C^2)/ 3$

The high *R*1 value and problems with anisotropic refinement can likely be attributed to the poor quality of the crystal used for data collection. Munakataite crystals from Broken Hill invariably have a fibrous nature. All available crystals were checked by examination in transmitted light microscope. Of those large enough for data collection, all except one, which was used for data collection, were apparently composed of several individuals.

The minimum and maximum peaks in the final difference Fourier maps were -7.876 and 23.745 e/Å^3 located located 0.80 and 0.93 Å from the Pb2 and OH3 atoms respectively. Next highest peaks of 17.98 and 11.21 e/Å^3 were located 0.88 and 0.87 Å from the Pb1 and S atoms respectively. These values are very high, but such "ghost" peaks (positive electron density close to heavy atoms) are a typical symptom of absorption, particularly in structures determined from less-than ideal crystals. Absorbtion is due to the inelastic interaction of the X-rays with the atoms in the crystal and is related to the path length (τ) the X-rays travel through the material and the nature of the atoms in the crystal. It is expressed by the equation.

$$I_{hkl} = I_0 e^{-\mu\tau}$$

where μ is the linear absorbtion coefficient. The ideal shape for a crystal is spherical as the path lengths of the X-rays through a plate-shaped or needle shaped crystal will be very different for the different (*hkl*) values. The value for the absorption coefficient, μ, for the munakataite crystal used for data collection was 41.36 mm^{-1}, the highest of any of the minerals in this study, which reflects the presence of the heavy atoms Pb and Se. The "ghost" peaks are likely due to a combination of the poor crystal quality, the presence of heavy atoms and absorption correction that was not entirely adequate. Final atomic coordinates and anisotropic displacement parameters are given in Table 3, and selected interatomic distances are in Table 4. Table 5 provides a bond-valence analysis using the parameters taken from Krivovichev and Brown (2001) for the Pb^{2+}–O bonds and from Brown and Altermatt (1985) and Brese and O'Keeffe (1991) for other bonds.

Table 3. Fractional coordinates and displacement parameters (Å2) for atoms for munakataite.

	x	y	z	Ueq	U11	U22	U33	U12	U13	U23
Pb1	0.8200(2)	0.75	0.4186(2)	0.0251(6)	0.0282(9)	0.0234(8)	0.0218(8)	0	0.0009(5)	0
Pb2	0.1655(2)	0.25	0.0279(3)	0.0412(8)	0.0257(10)	0.0349(11)	0.0589(15)	0	0.0000(8)	0
Cu	0.4904(4)	0.4998(5)	0.2452(4)	0.0202(13)	0.032(2)	0.010(2)	0.0171(18)	0.0012(11)	0.0018(12)	-0.0001(13)
S	0.1637(9)	0.75	0.3103(9)	0.023(3)	0.027(4)	0.021(4)	0.022(4)	0	0.003(3)	0
Se	0.8566(5)	0.25	0.2218(5)	0.0254(14)	0.033(2)	0.019(2)	0.025(2)	0	0.0074(16)	0
O11	0.884(4)	0.25	0.050(5)	0.040(9)	0.024(16)	0.04(2)	0.04(2)	0	-0.009(14)	0
O12	0.750(2)	0.479(4)	0.212(2)	0.023(4)	0.014(8)	0.024(10)	0.028(10)	-0.001(8)	-0.006(7)	0.000(7)
O21	0.008(3)	0.75	0.247(4)	0.037(9)	0.026(16)	0.06(3)	0.019(15)	0	-0.004(12)	0
O22	0.183(5)	0.75	0.472(6)	0.055(12)						
O23	0.235(3)	0.537(4)	0.273(3)	0.031(5)	0.040(12)	0.022(10)	0.036(12)	-0.004(9)	0.016(10)	0.002(10)
OH1	0.535(4)	0.25	0.407(4)	0.036(9)	0.035(17)	0.021(15)	0.034(18)	0	-0.030(15)	0
OH2	0.581(3)	0.75	0.378(3)	0.017(5)	0.027(13)	0.003(10)	0.026(13)	0	0.016(11)	0
OH3	0.451(2)	0.75	0.102(2)	0.009(4)						
OH4	0.408(3)	0.25	0.107(3)	0.022(6)	0.025(13)	0.010(11)	0.025(14)	0	-0.007(11)	0

Table 4. Selected interatomic distances (Å), angles (°) and suggested hydrogen-bonds for munakataite.

Pb1	–OH2	2.29(3)	Cu	–OH3	1.92(2)
	–O12	2.44(2)		–OH2	1.96(2)
	–O12	2.44(2)		–OH4	1.97(2)
	–O21	2.69(4)		–OH1	2.04(3)
	–O22	3.01(3)		–O23	2.57(2)
	–O22	3.01(3)		–O12	2.63(2)
	<Pb-O>	2.65		<Cu-O>	2.18
Pb2	–OH4	2.33(3)	S	–O22	1.47(5)
	–O23	2.76(2)		–O23	1.48(2)
	–O23	2.76(2)		–O23	1.48(2)
	–O21	2.75(3)		–O21	1.51(3)
	–O11	2.81(3)		<S-O>	1.49
	–O11	2.94(3)			
	–O11	2.94(3)	Se	–O12	1.65(2)
	–O12	2.97(3)		–O12	1.65(2)
	–O12	2.97(3)		–O11	1.67(4)
	<Pb-O>	2.80		<Se-O>	1.66
OH3–Cu–OH2		84.3(8)	O22–S2–O23		106.1(15)
OH3–Cu–OH4		94.9(8)	O22–S2–O23		106.1(15)
OH2–Cu–OH1		92.3(9)	O23–S2–O23		110(2)
OH4–Cu–OH1		88.6(9)	O22–S2–O21		107(2)
OH3–Cu–O23		87.2(9)	O23–S2–O21		113.5(12)
OH2–Cu–O23		101.2(9)	O23–S2–O21		113.5(12)
OH4–Cu–O23		81.5(11)	<O–S–O>		109.4
OH1–Cu–O23		92.5(13)			
OH3–Cu–O12		90.6(8)	O12–Se1–O12		103.3(15)
OH2–Cu–O12		77.9(9)	O12–Se1–O11		100.0(11)
OH4–Cu–O12		99.3(10)	O12–Se1–O11		100.0(11)
OH1–Cu–O12		89.6(13)	<O–Se–O>		101.1
<O–Cu–O>		90.0			

Atomic separations corresponding to possible hydrogen-bonds

OH2–OH(1)	2.50	OH4–OH3	2.61
OH(1)–(22)	2.75		

STRUCTURE DESCRIPTION

Cation coordination

The crystal structure of munakataite contains five cation sites. The Pb1, Pb2, Se and S atoms are each located on special positions (Wyckoff position *e*; site symmetry *m*) and the Cu atom is located on a general position (Wyckoff position *f*; site symmetry 1).

The Pb1 site is coordinated by five O^{2-} anions and one OH^{-} group forming "strong" bonds, with Pb–O distances in the range 2.29(3)–3.01(3) Å (Figure 2). The Pb^{2+} cation is also weakly bonded to three anions, with Pb–O distances of 3.44(3)–3.48(3) Å, on the side opposite to the short bonds, and with a large solid angle not occupied by any anion. Such an arrangement is typical of Pb^{2+} with a stereoactive $6s^2$ lone-pair of electrons, with space for the lone pair to project into the space between the long bonds emanating from the central cation.

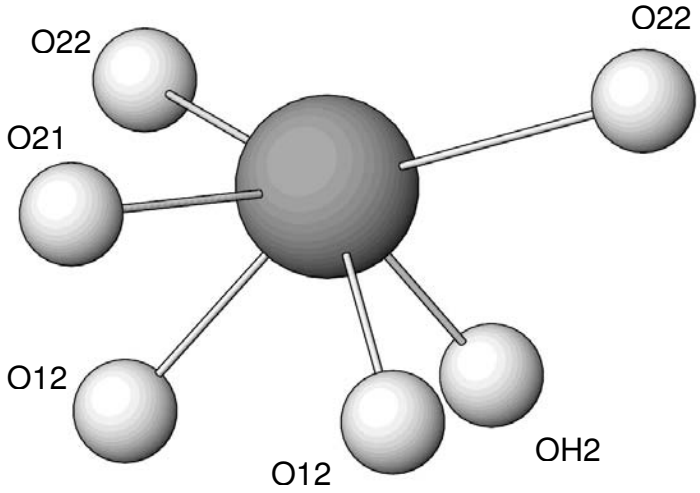

Figure 2. Coordination of the Pb(1) site in the structure of munakataite. All structure drawings were completed using ATOMS (Shape Software 1997).

The Pb2 site is coordinated by nine O^{2-} anions with Pb–O distances in the range 2.33(3)–2.97(3) Å (mean 2.80 Å) (Figure 3). The arrangement of the anions around Pb2 shows no obvious one-sided nature, which suggests that the Pb^{2+} cation is not significantly lone-pair stereoactive. The coordination of the Pb sites in munakataite is

in accord with the findings of Shimoni-Livny *et al*. (1998) who found that for the Pb(II) compounds investigated, Pb(II) coordination numbers 2 to 5 exhibited a one sided geometry, while all coordination number 9 and 10 compounds did not. For coordination numbers 6–8, both types of geometry are found.

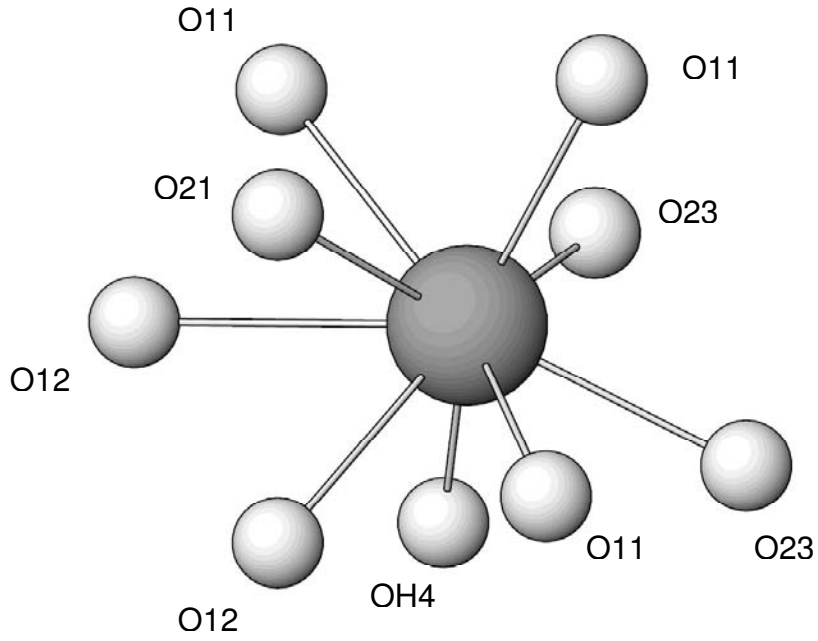

Figure 3. Coordination of the Pb(2) site in the structure of munakataite.

The bond valence sums for the Pb1 and Pb2 sites, calculated using the parameters of Brown and Altermatt (1985), are somewhat lower than the expected 2.00 *vu*. Examination of a wide range of crystal structures has found that bond valences around a specific cation lie within ~20% of the mean value which is characteristic of that particular cation (Brown 1981), however the bond valence sum for Pb1, 1.66 *vu*, is anomalously low. Calculation of bond-valence sums using the bond-valence parameters of Krivovichev and Brown (2001) (see below) gave a result closer to the ideal of 2.00 *vu* for Pb2 but a lower sum for Pb1, however both are still underbonded (Table 5).

The Pb1 site (1.69 *vu*) in the structure of schmeiderite is also underbonded (Effenberger 1987). Similar underbonding of Pb^{2+} cations with a stereochemically inactive s^2 lone pair has been observed for Pb sites in the structures of other Pb

minerals [eg. parakhinite (1.49 *vu*), Burns *et al*. (1995), and anglesite (1.76 *vu*) Miyake *et al*. (1978)]. Li *et al*. (2001) noted that it is not clear whether this underbonding is due to structural steric constraints, or is simply a consequence of incorrect bond valence parameters. The microprobe analyses and refined site-occupancies indicate that the Pb1 and Pb2 sites are completely occupied by Pb.

The crystal structure of munakataite contains one Cu position coordinated by two O^{2-} anions and four OH^{-} groups. As is usual for most octahedrally coordinated Cu^{2+} cations in minerals, the $Cu\phi_6$ octahedon is distorted due to the Jahn-Teller effect (Jahn and Teller 1937; Burns and Hawthorne 1995), with four short equatorial [1.924(15), 1.96(2), 1.97(2) and 2.04(3) Å] and two longer apical Cu-ϕ bonds [2.57(2) and 2.63(2) Å].

The structure contains one *S* site, coordinated by four O atoms in a tetrahedral arrangement with S–O distances between 1.48(5) and 1.50(3) Å (Table 4). The O–S–O angles of the sulphate group range from 105.8(15) to 113.7(12)°, which compare to the ideal O–S–O angle for a tetrahedron of 109.47°. The <S–O> distance of 1.49 Å is greater than the average <S–O> length of 1.473 Å typical for a sulphate ion (Baur 1981; Hawthorne *et al*. 2000). The occupancy factor for the site, refined using the S scattering factor, was 1.26, suggesting substitution of S by a heavier atom. Refinement of the S:Se ratio gave 0.828:0.172. The S:Se ratio obtained from the results of the microprobe analysis is 0.94:1.06, which results in an occupancy of the *S* site of $S_{0.94}Se^{6+}_{0.06}$. Reasons for this discrepency could be a variation between the composition of the crystal used for data collection and the grain used for the electron microprobe analysis or the refined S:Se ratio may differ somewhat from the true ratio due to the poor quality of the structure refinement. The bond-valence sum for the S site (5.93 *vu*) agrees with the complete occupancy of the position by hexavalent cations.

The structure contains one symmetrically distinct Se^{4+} site, which is coordinated by three O atoms arranged at the vertices of a trigonal pyramid (Figure 4). The electronic configuration of Se^{4+} is $[Ar]3d^{10}4s^2$, which results in a stereochemically active s^2 lone pair of electrons in the outer shell. The electron lone pair is positioned

on the opposite side of the Se^{4+} cation, so the cation can be considered to have a tetrahedral configuration. The O– Se–O angles of 100.4(10), 100.4(11) and 103.2(15)º are significantly smaller than the ideal angle within a tetrahedron due to the lone pair-bond pair interaction (Andersson and Aström, 1972). The mean angle of 101.3º compares well to that in selenite groups from inorganic crystal structures [mean 100.2º; Hawthorne *et al*., (1987)].

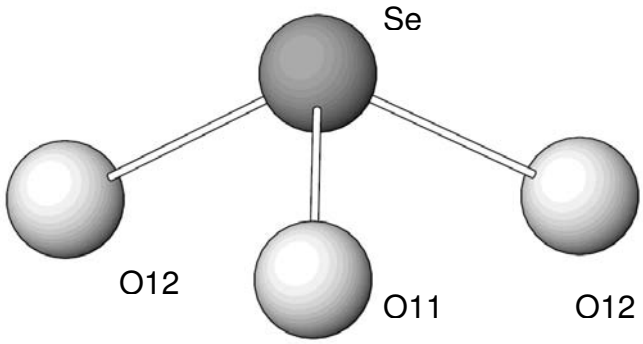

Figure 4. Coordination of the Se site in the structure of munakataite.

The Se–O bond lengths of 1.65(2), 1.65(2) and 1.67(4) Å are within the range observed in selenite groups in inorganic crystal structures (eg. Fischer and Zemann 1974). The mean distance of 1.66 Å is however less than the mean of 1.709 Å observed in selenite groups (Hawthorne *et al*., 1987). This could be interpreted as being due to patrial occupancy of the site by a lighter atom (e.g. S), although the refined occupancy of the site indicated full occupancy by Se. The precision of the bond-lengths is however lacking, and the standard uncertainties are high, a result of the less than ideal quality of the structure refinement. The bond-valence sum for the Se site (Table 5) of 4.47 *vu* is greater than the ideal value expected for Se^{4+}, and can also be attributed to the low precision of the bond-lengths.

Structure topology

The results of the structure refinement confirm that munakataite is isostructural with schmiederite, $Pb_2Cu_2Se^{4+}O_3SO_4(OH)_4$ (Effenberger 1987). $Cu\phi_6$ octahedra share *trans* edges producing infinite chains of composition $Cu_2(SO_4)(SeO_3)\phi_4$ which extend

along [010] (Figure 5). The chains are decorated by SO_4 tetrahedra and SeO_3 trigonal pyramids which assume a staggered arrangement, each sharing two vertices with the chain and linking across the apical anions of two adjoining octahedra. The result is a chain of composition $Cu_2(SO_4)(SeO_3)\phi_4$.

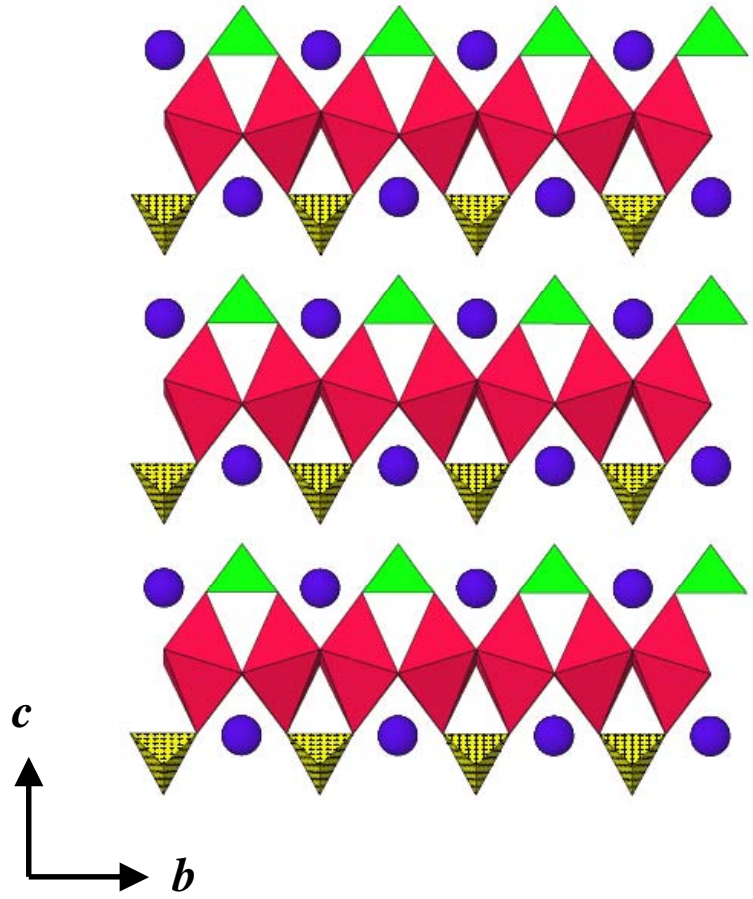

Figure 5. The crystal structure of munakataite projected onto a plane close to (100). $Cu\phi_6$ octahedra are shaded red, SO_4 tetrahedra are yellow and marked with crosses, SeO_3 trigonal pyramids are green and Pb atoms are blue spheres.

The edges of the SO_4 tetrahedra and SeO_3 trigonal pyramids are less than the separation of adjacent octahedral vertices for an $[M\phi_4]$ chain of maximal symmetry and consequently there is a cooperative tilting of octahedra along the chain such that the shortening of alternate vertex separations on one side of the chain spontaneously produces an offset distortion on the other side of the chain. The chains are crosslinked by the [9]-coordinated Pb^{2+} cations and by hydrogen bonds (Figure 6).

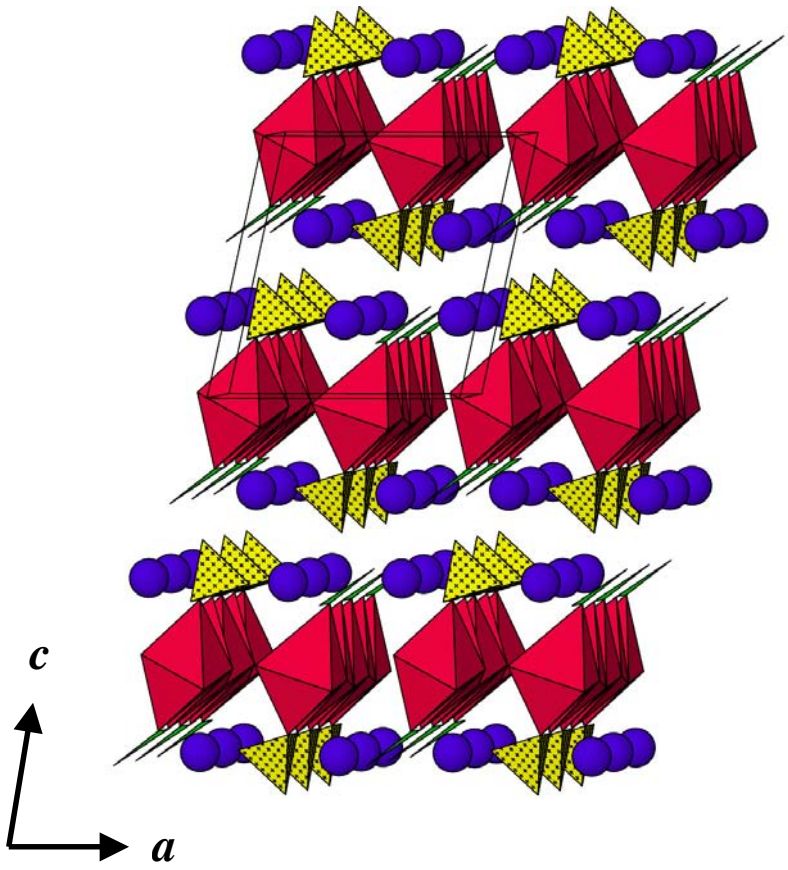

Figure 6. The crystal structure of munakataite viewed in a direction close to [010]; legend as in Figure 5.

Eby and Hawthorne (1993) classified this type of copper oxysalt mineral structure as being based on infinite $M = M–T$ chains where M denotes octahedrally coordinated cations and the double hyphen denotes edge sharing.

BOND VALENCE CALCULATIONS AND HYDROGEN BONDING

Bond-valence sums incident upon the cation and anion sites were calculated (Brese and O'Keeffe 1991; Brown 1996) using the parameters of Brown and Altermatt (1985). The resulting sums for OH2, OH3 and OH4 of 2.23, 2.27 and 2.25 *vu* respectively, are significantly higher than the expected ideal value of 2.00 *vu*.

Krivovichev and Brown (2001) found that large bond-valence sums for O^{2-} encapsulated in a tetrahedral [OPb_4] cluster are the result of inappropriate bond-valence parameters for Pb^{2+}. Hence they determined new parameters (b = 0.49 Å; r_0 = 1.963 Å) for Pb^{2+}–O bonds, based on the examination of 140 crystal structures containing Pb^{2+}. The new parameters are independent of the type of coordination and of the stereoactivity of s^2 lone-pair electrons around Pb^{2+}. Recalculation of bond-valences for the Pb–O bonds using the bond-valence parameters of Krivovichev and Brown (2001) resulted in closer to ideal sums for OH2 and OH4, which are coordinated to the Pb^{2+} cations, of 2.12 and 2.16 *vu* respectively (Table 5).

Difference-Fourier maps did not reveal the locations of the H atoms, which was not unexpected considering the imperfect quality of the crystal used for data collection. However the bond-valence analysis (Table 5) indicates that four of the nine anion positions in the asymmetric unit are hydroxyl groups, and probable hydrogen bonds were identified on the basis of stereochemical and bond valence criteria. The calculated bond valence sums demonstrate that the O11, O21, O22 and O23 atoms are somewhat undersaturated (1.89, 1.82, 1.76 and 1.80 *vu* respectively). Only O22 however is an acceptor of a likely hydrogen bond, donated by the OH1 group, to provide the necessary increase in bond valence. The nearest oxygen neighbour to O23 is OH3 at 3.00 Å, but this distance forms an edge on the coordination polyhedron around Cu, and hydrogen bonding almost never occurs along the edge of an octahedron occupied by a divalent or trivalent cation (Baur 1972; 1973). The same holds for an OH4 neighbour at 3.14 Å. The O21 anion has no nearby oxygen neighbours. The OH2 group likely provides a hydrogen bond accepted by OH1 and the OH4 group likely donates a hydrogen bond accepted by OH3. An additional hydrogen bond, OH3 to O11, was proposed for schmeiderite, with an O…O distance of 3.10 Å (Effenberger 1987). The equivalent distance in munakataite is 3.28 Å, which seems too large for H bonding to occur. The proposed hydrogen bonds would represent moderately strong links, with O…O distances of 2.50, 2.61 and 2.75 Å, and reinforce the structure along the *c*-axis.

Table 5. Bond-valence analysis for munakataite.

	Pb1	Pb2	Cu	S	Se	H1	H2	H3	H4	Sum (excluding H)	Sum (including H)
O11		0.18 0.14^{x2}			1.43					1.89	1.89
O12	0.38↓→ 0.38↓	0.13 ^{x2}	0.08		1.52↓→ 1.52↓					2.11	2.11
O21	0.23	0.20↓		1.39						1.82	1.82
O22	0.12 ^{x2}			1.52		0.19				1.76	1.95
O23		0.20↓→ 0.20↓	0.09	1.51↓→ 1.51↓						1.80	1.80
OH1			0.38↓→ 0.38 →			0.81	0.31			0.76	1.88
OH2	0.51		0.46↓→ 0.46 →				0.69			1.43	2.12
OH3			0.52↓→ 0.52 →					1.00	0.23	1.04	2.27
OH4		0.47	0.46↓→ 0.46 →						0.77	1.39	2.16
	1.74	1.79	1.99	5.93	4.47	1.00	1.00	1.00	1.00		

STRUCTURAL RELATIONS

The structures of munakataite and schmiederite are closely related to that of linarite (Bachmann and Zemann, 1961; Araki, 1962; Effenberger 1987; Schofield *et al*. 2009), but their unit cell volumes are doubled (the *c*-axis is doubled) relative to that of linarite due to the ordering of S and Se into distinct positions in the structure. Munakataite, schmiederite and linarite are examples of structures based on isolated $[MT\phi_4]$ chains of edge-sharing octahedra. The chains are decorated by alternate SO_4 tetrahedra (linarite), alternate SO_4 tetrahedra and SeO_3 trigonal pyramids (munakataite) or alternate SeO_4 tetrahedra and SeO_3 trigonal pyramids (schmiederite) to give chains of general stoichiometry $M(TO_4)\phi_2$ or $M_2(TO_4)(TO_3)\phi_4$ respectively. Isolated $[MT\phi_4]$ chains flanked by pairs of tetrahedra along the length of the chain, with stoichiometry of $[M(TO_4)_2\phi]$ are found in the structures of the brackebuschite-group, the fornacite-group minerals and the vauquelinite-group minerals.

ACKNOWLEDGEMENTS

We thank Angus Netting and John Terlet of Adelaide Microscopy, The University of Adelaide for their assistance with the microprobe analysis. We are grateful to Hayley Brown and Paul Pigou for assistance with collection of the infrared spectrum.

REFERENCES

Andersson, S. and Aström, A. (1972) The stereochemistry of the inert iodates pair in some solid oxides or oxide fluorides of Sb^{3+}, Bi^{3+} and Pb^{2+}. National Bureau of Standards Special Publication, 364, Proceedings of the Fifth Materials Research Symposium, 3–14.

Araki, T. (1962) The crystal structure of linarite, reexamined. Mineralogical Journal, 3, 282–295.

Bachmann, H.G. and Zemann, J. (1961) Die Kristallstruktur von Linarit, $PbCuSO_4(OH)_2$. Acta Crystallographica, 14, 747–753.

Baur, W.H. (1972) Prediction of hydrogen-bonds and hydrogen atom positions in crystalline solids. Acta Crystallographica, B28, 1456–1465.

Baur, W.H. (1973) Criteria for hydrogen bonding. II. A hydrogen bond in the edge of a coordination polyhedron around a cation. Acta Crystallographica, B29, 139–140.

Baur, W.H. (1981) Interatomic distance predictions for computer simulation of crystal structures. In M. O'Keeffe and A. Navrotsky, Eds., Structure and Bonding in Crystals Vol. II, p. 31–52. Academic Press, New York.

Both, R. A. (1973) Minor element geochemistry of sulphide minerals in the Broken Hill lode (N.S.W.) in relation to the origin of the ore. Mineralium Deposita, 8, 349–369.

Brese, N.E. and O'Keeffe, M. (1991) Bond-valence parameters for solids. Acta Crystallographica, B47, 192–197.

Brown, I.D. (1981) The bond-valence method: an empirical approach to chemical structure and bonding. In M. O'Keefe and A. Navrotsky, Eds., Structure and Bonding in Crystals. Academic Press, London, 1–30.

Brown, I.D. (1996) VALENCE: a program for calculating bond-valences. Journal of Applied Crystallography, 29, 479–480.

Brown, I.D., and Altermatt, D. (1985) Bond-valence parameters obtained from a systematic analysis of the inorganic crystal structure database. Acta Crystallographica, B41, 244–247.

Burns, P.C., and Hawthorne, F.C. (1995) Coordination-geometry structural pathways in Cu^{2+} oxysalt minerals. Canadian Mineralogist, 33, 889–905.

Burns, P.C., Cooper, M.A. and Hawthorne, F.C. (1995) Parakhinite, $Cu^{2+}{}_3PbTe^{6+}O_6(OH)_2$: Crystal structure and revision of chemical formula. Canadian Mineralogist, 33, 33–40.

Cooper, R.I., Gould, R.O., Parsons, S. and Watkin, D.J. (2002) The derivation of non-merohedral twin laws during refinement by analysis of poorly fitting intensity data and the refinement of non-merohedrally twinned crystal structures in the program CRYSTALS. Journal of Applied Crystallography, 35, 168–174.

Coppens, P. (1970) Crystallographic Computing. F.R. Ahmed, S.R. Hall and C.P.Huber, Eds., p. 255–270. Munksgaard, Copenhagen.

Eby, R.K., and Hawthorne, F.C. (1993) Structural relations in copper oxysalt minerals. I. Structural hierarchy. Acta Crystallographica, B49, 28–56.

Edwards, A.B. and Carlos, G.C. (1954) The selenium content of some Australian sulphide deposits. Proceedngs of the Australasian Institute of Mining and Mellallurgy, 172, 31–63.

Effenberger, H. (1987) Crystal structure and chemical formula of schmiederite, $Pb_2Cu_2(OH)_4(SeO_3)(SeO_4)$, with a comparison to linarite, $PbCu(OH)_2(SO_4)$. Mineralogy and Petrology, 36, 3–12.

Fischer, R. and Zemann, J. (1974) Selenium. 34-A. Crystal chemistry. In K.H. Wedepohl, Ed., Handbook of geochemistry II-3. Springer, Berlin Heidelberg New York

Hawthorne, F.C., Groat, L.A. and Ercit, T.S. (1987) Structure of cobalt diselenite. Acta Crystallographica, C43, 2042–2044.

Hawthorne, F.C., Krivovichev, S.V., and Burns, P.C. (2000) Crystal chemistry of sulfate minerals. In C.N. Alpers, J.L. Jambor, and D.K. Nordstrom, Eds., Sulfate Minerals, Crystallography, Geochemistry, and Environmental Significance, 40, p. 1–112. Reviews in Mineralogy and Geochemistry, Mineralogical Society of America, Chantilly, Virginia.

Jahn, H.A. and Teller, E. (1937) Stability of polyatomic molecules in degenerate electronic states. Proceedings of the Royal Society, Series A, 161, 220–236.

Krivovichev, S.V. and Brown, I.D. (2001) Are the compressive effects of encapsulation an artifact of bond valence parameters? Zeitschrift für Kristallographie, 216, 245–247.

Matsubara, S., Mouri, T., Miyawaki, R., Yokoyama, K. and Nakahara, M. (2008) Munakataite, a new mineral from the Kato mine, Fukuoka, Japan. Journal of Mineralogical and Petrological Sciences, 103, 327–332.

Miyake, M., Minato, I., Morikawa, H. and Iwai, S. (1978) Crystal structures and sulphate constants of barite, celestite, and anglesite. American Mineralogist, 63, 506–510.

Otwinowski, Z., and Minor, W. (1997) Processing X-ray diffraction data collected in oscillation mode. In Macromolecular Crystallography, C.W. Carter Jr. and R.M. Sweet, Eds., Vol. 276, p. 307–326. Academic Press, New York.

Otwinowski, Z., Borek, D., Majewski, W. and Minor, W. (2003) Multiparametric scaling of diffraction intensities. Acta Crystallographica, **A59**, 228–234.

Pouchou, J.L. and Pichoir, F. (1985) "PAP" ϕ (ρZ) procedure for improved quantitative microanalysis. In J.T. Armstrong, Ed., Microbeam Analysis, 104–106.

Ralph, J. and Chau, I. (2009) mindat.org—the mineral and location database (http://www.mindat.org/index.php).

Schofield, P.F., Wilson, C.C., Knight, K.S. and Kirk, C.A. (2009) Proton location and hydrogen bonding in the hydrous lead copper sulfates linarite, $PbCu(SO_4)(OH)_2$, and caledonite, $Pb_5Cu_2(SO_4)_3CO_3(OH)_6$. Canadian Mineralogist, 47, 649–662.

Shape Software (1997) ATOMS for Windows and Macintosh V 4.0, Kingsport, Tennessee, U.S.A.

Sheldrick, G.M. (1997a) SHELXS-97, a Program for the Solution of Crystal Structures. University of Göttingen, Göttingen, Germany.

Sheldrick, G.M. (1997b) SHELXL-97, a Program for Crystal Structure Refinement. University of Göttingen, Göttingen, Germany.

Shimoni-Livny, L., Glusker, J.P. and Bock, C.W. (1998) Lone pair functionality in divalent lead compounds. Inorganic Chemistry, 37, 1853–1867.

Spek, A.L. (2003) Single-crystal structure validation with the program PLATON. Journal of Applied Crystallography, 36, 7–13.

Wilson, A.J.C., Ed. (1992) International Tables for Crystallography, vol. C, 883 p. Kluwer Academic, Dordrecht, The Netherlands.

CHAPTER 4

Description and crystal structure of a new mineral, edwardsite, $Cu_3Cd_2(SO_4)_2(OH)_6{\cdot}4H_2O$, from Broken Hill, New South Wales, Australia

Peter Elliott[1,2], Joël Brugger[1,2], Tom Caradoc-Davies[3]

[1]School of Earth and Environmental Sciences, The University of Adelaide, Adelaide, South Australia 5005, Australia

[2]South Australian Museum, North Terrace, Adelaide, South Australia 5000, Australia

[3]Australian Synchrotron, 800 Blackburn Road, Clayton, Victoria 3168, Australia

Mineralogical Magazine, 2010, 74, 39–53

STATEMENT OF AUTHORSHIP

Description and crystal structure of a new mineral, edwardsite, $Cu_3Cd_2(SO_4)_2(OH)_6{\cdot}4H_2O$, from Broken Hill, New South Wales, Australia, *Mineralogical Magazine*, 2010, 74(1), 29–43

Peter Elliott (Candidate)

Obtained X-ray data, performed analysis on all samples, interpreted data, wrote manuscript and acted as corresponding author. I hereby certify that the statement of contribution is accurate

Signed .....*Date*.....23/8/2010

Joël Brugger

Assistance with X-ray data collection, manuscript evaluation

I hereby certify that the statement of contribution is accurate and I give permission for the inclusion of the paper in the thesis

Signed .....*Date*.....24/8/10

Tom Caradoc-Davies

Assistance with X-ray data collection, manuscript evaluation

I hereby certify that the statement of contribution is accurate and I give permission for the inclusion of the paper in the thesis

Signed .....*Date*.....9/8/10

Elliott, P., Brugger, J., & Caradoc-Davies, T. (2010) Description and crystal structure of a new mineral, edwardsite, $Cu_3Cd_2(SO_4)_2(OH)_6 \cdot 4H_2O$, from Broken Hill, New South Wales, Australia. *Mineralogical Magazine, v. 74(1), pp. 39 -53.*

CHAPTER 5

The crystal structure of cadmian serpierite from the Block 14 Opencut, Broken Hill, New South Wales

Peter Elliott[1,2] and Anthony C. Willis[3]

[1]School of Earth and Environmental Sciences, The University of Adelaide, Adelaide, South Australia 5005, Australia.

[2]South Australian Museum, North Terrace, Adelaide, South Australia 5000, Australia.

[3]Research School of Chemistry, The Australian National University, Australian Capital Territory 0200, Australia.

STATEMENT OF AUTHORSHIP

The crystal structure of cadmian serpierite from the Block 14 Opencut, Broken Hill, New South Wales

Peter Elliott (Candidate)

Performed analysis on all samples, interpreted data and wrote manuscript.

I hereby certify that the statement of contribution is accurate.

Signed .....*Date*.....23/8/2010

Anthony Willis

Single-crystal X-ray data collection and data reduction.

I hereby certify that the statement of contribution is accurate and I give permission for the inclusion of the paper in the thesis.

Signed .....*Date*.....12/7/2010

The crystal structure of cadmian serpierite from the Block 14 Opencut, Broken Hill, New South Wales

Peter Elliott[1,2] and Anthony C. Willis[3]

[1]School of Earth and Environmental Sciences, The University of Adelaide, Adelaide, South Australia 5005, Australia.

[2]South Australian Museum, North Terrace, Adelaide, South Australia 5000, Australia.

[3]Research School of Chemistry, The Australian National University, Australian Capital Territory 0200, Australia.

ABSTRACT

The crystal chemistry of a cadmian serpierite from an occurrence at Broken Hill, New South Wales is described. Microprobe analysis gave the following range of compositions: CaO 2.21–5.83, CdO 7.50–13.41, CuO 30.56–44.96 and ZnO 5.41–15.12 Wt.%. The crystal structure has been determined using single-crystal X-ray diffraction data (Mo-$K\alpha$, CCD area detector) and has been refined in space group $C2/c$, with a = 22.0607(14), b = 6.2147(3), c = 21.8598(13), β = 113.212(3)°, V = 2781.60(3) and Z = 8 to $R1$ = 6.28% for 1803 observed reflections with $F_o > 4\sigma(F_o)$. The structure contains of one unique X site occupied by Ca and Cd and [7]-coordinated by O atoms with a <X–O> distance of 2.399 Å. There are five distinct [6]-coordinated Cu sites occupied by Cu and Zn. There are two distinct S positions each coordinated by a tetrahedral arrangement of O anions. The structure consists of a sheet of edge-sharing (Cu,Zn) octahedra parallel to (100), decorated on both sides by SO_4 tetrahedra. The sheets are link along the a-direction via the Ca^{2+} cations, with additional linkage provided by hydrogen bonding.

INTRODUCTION

Serpierite, $Ca(Cu,Zn)_4(SO_4)_2(OH)_6{\cdot}3H_2O$, a common secondary mineral in the oxidized zones of Cu-Zn deposits, was first found at the Serpieri Mine, Kamareza Mines, Lavrion, Attikí Prefecture, Greece (Bertrand 1881) and described by Des Cloizeaux (1881). The unit-cell parameters were determined by Faraone *et al*., (1967)

from Weissenberg photographs and the crystal structure of serpierite was determined by Sabelli and Zanazzi (1968). The mineral is monoclinic, space group, $C2/c$ with a = 22.186(2), b = 6.250(2), c = 21.853(2) Å, β = 113.36(1)°, V = 2781.60(3) Å^3, and Z = 8. The structure was only refined isotropically and although the positions of the oxygen atoms corresponding to the water and hydroxyl groups were reported, the hydrogen atom coordinates were not determined. The precision of the refinement ($R1$ ~ 10%) was low due to the diffusion of intensity of reflections with $k+l = 2n+1$, which was attributed to multiple twinning. Standard deviations for the interatomic distances and angles were not reported. Serpierite is dimorphous with orthoserpierite which crystallizes in space group $Pca2_1$ with a = 22.10(2), b = 6.20(2), c = 20.39(2) and Z = 8 (Sarp 1985).

The crystal structure of a cadmium bearing serpierite has been determined using samples from the Block 14 Opencut, Broken Hill, NSW. Serpierite is a relatively common mineral in the oxidized zone of the Broken Hill deposit (Birch 1999) where it occurs as sprays and aggregates of radiating acicular, pale blue crystals associated with niedermayrite (Figure 1).

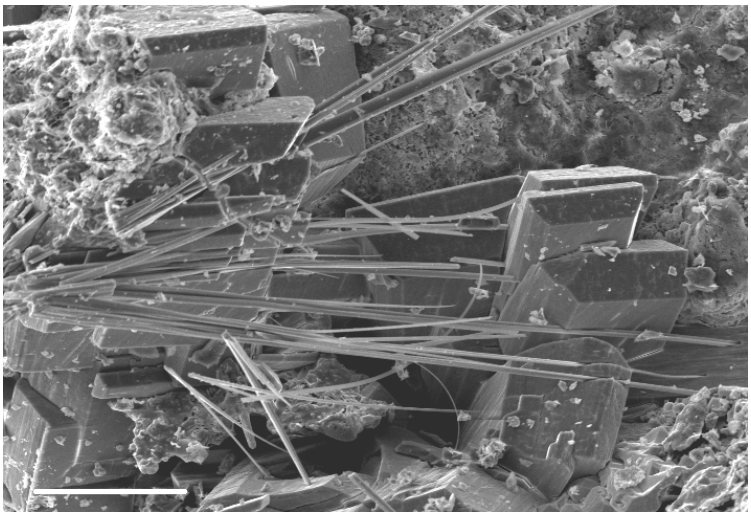

Figure 1. SEM photomicrograph showing pale blue, acicular crystals of cadmian serpierite with greenish blue crystals of niedermayrite. The scale bar is 50 μm in length.

The present refinement confirms the cation polyhedra and structural connectivities proposed by Sabelli and Zanazzi (1968), but refinement with modern data collected for a higher-quality crystal using a CCD-based area detector has improved the

precision of the structure. Ten of the twelve hydrogen atoms in the structure were located and shed additional light on the hydrogen-bonding scheme proposed by Sabelli and Zanazzi (1968). The results also show that Cd^{2+} is incorporated into the serpierite structure by replacement of Ca in the large intersheet cation site.

INFRARED SPECTROSCOPY

The infrared spectrum of cadmian serpierite (Figure 2) was recorded in the range 4000–650 cm^{-1} using a Nicolet 5700 FTIR spectrometer equipped with a Nicolet Continuum IR microscope and a diamond-anvil cell. A broad band from ~3640 to ~2805 cm^{-1} centred on 3358 cm^{-1} is due to O–H stretching. The absorption band at 1652 cm^{-1} is assigned to H–O–H bending. A strong band at 1120 cm^{-1} is due to the SO^{4-} asymmetric stretch, ν_3 and a weak band at 985 cm^{-1} to the SO_4 symmetric stretch, ν_1. Bands at 834 and 716 cm^{-1} are possibly due to OH δ bending.

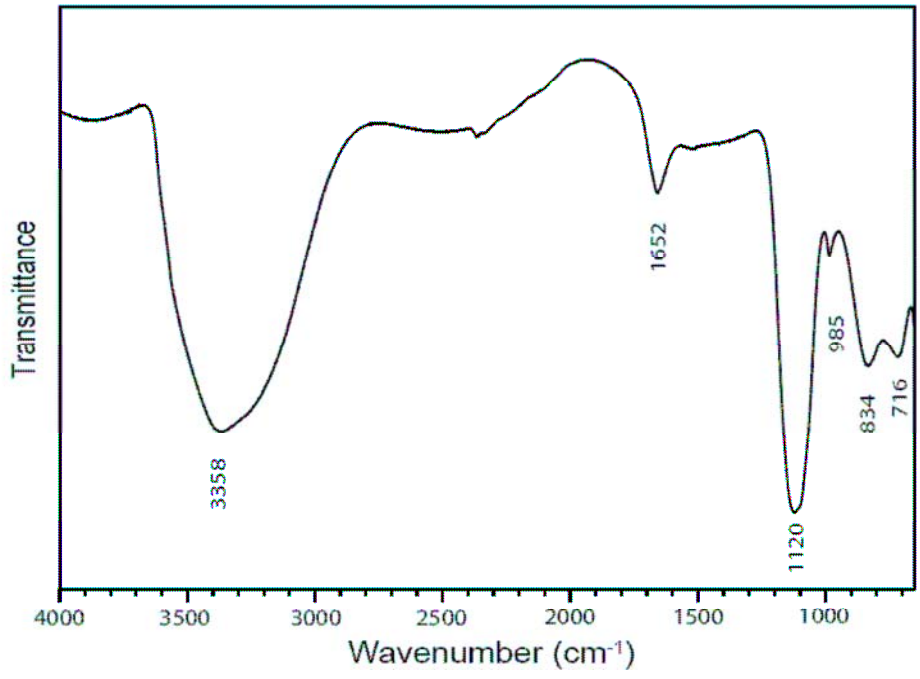

c

Figure 2. FT-IR spectrum of powdered cadmian serpierite.

CHEMICAL COMPOSITION

Crystal aggregates from two specimens of cadmian serpierite were analyzed with a Cameca SX-51 electron microprobe operating in wavelength-dispersion mode with an accelerating voltage of 15 kV, a specimen current of 10 nA, a beam size of 20 μm and

counting times on peak and background of 20 and 10 s, respectively. The following standards were used: cadmium metal (Cd *L*α), hydroxylapatite (Ca *K*α) chalcopyrite (Cu *K*α, S *K*α), sphalerite (Zn *K*α) and galena (Pb *M*α). Data were reduced using the ϕ(ρZ) procedure of Pouchou and Pichoir (1985). Cation totals are higher than ideal due to the instability of the mineral under the electron beam. The results (Table 1) show that contents of Ca, Cd, Cu and Zn are variable: CaO 2.21–5.83, CdO 7.50–13.41, CuO 30.56–44.96 and ZnO 5.41–15.12 Wt.% (Table 1). Cadmian serpierite

Table 1. Chemical composition (Wt.%) and unit formula† (*apfu*) of cadmian serpierite.

Sample number	1	2	Min.	Max.
No. of analyses	15	16		
SO_3	24.01	23.46	21.70	27.08
CaO	4.98	3.43	2.21	5.83
CdO	9.25	12.22	7.50	13.41
PbO	0.04	0.11	0.00	0.45
CuO	40.49	33.96	30.56	44.96
ZnO	8.48	13.25	5.41	15.12
H_2O (calc)*	16.59	16.06	15.22	18.05
Sum	103.83	102.50	96.78	111.87
S	1.95	1.97	1.82	2.22
Ca	0.58	0.41	0.27	0.68
Cd^{2+}	0.47	0.64	0.35	0.69
Pb^{2+}	0.00	0.00	0.00	0.00
∑	1.05	1.05	0.95	1.14
Cu^{2+}	3.32	2.87	2.65	3.53
Zn	0.68	1.10	0.46	1.26
∑	4.00	3.97	3.78	4.12
OH*	6.18	6.10	5.11	6.71
H_2O*	2.91	2.95	2.64	3.44

†The analyses are normalized on the basis of 7 cations.
*The H_2O and OH contents are calculated to obtain to obtain a total of 12 H *pfu* and charge balance.

crystals vary in habit from thin prismatic to very fine acicular, with the finest crystals having the greatest Cd content.

A plot of atoms of atoms of Ca vs. atoms of Cd *pfu* (per formula unit) (Figure 3) for all analyses shows a distinct negative linear correlation, with $R^2 = 0.782$ and a slope close to –1 indicating a simple replacement of Ca by Cd in the structure.

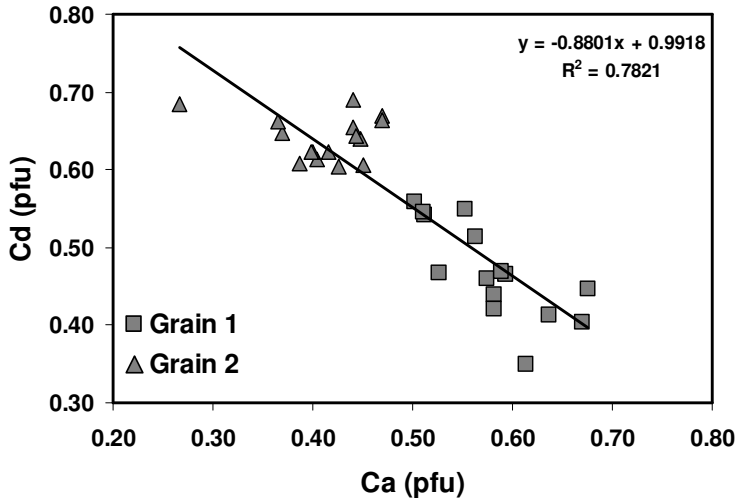

Figure 3. Bivariate plot illustrating the negative correlation between Ca and Cd in cadmian serpierite.

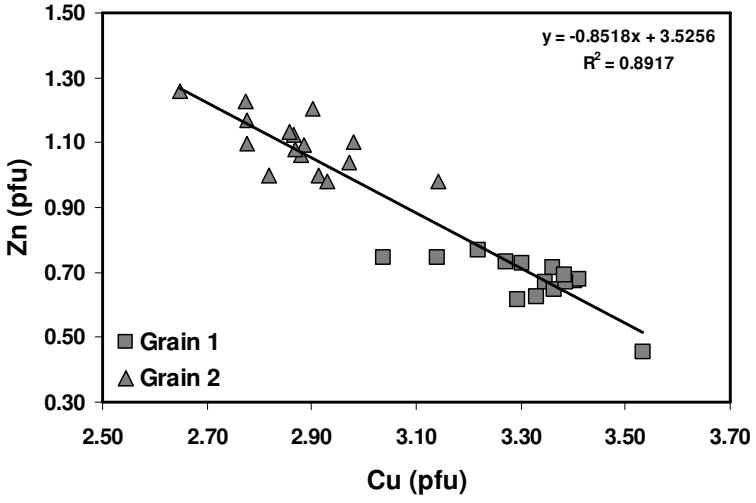

Figure 4. Bivariate plot illustrating the negative correlation between Cu and Zn in cadmian serpierite.

A plot of atoms of Cu atoms vs. atoms of Zn *pfu* (Figure 4) also shows a strong negative linear correlation, with $R^2 = 0.892$ and a slope close to –1 indicating a simple replacement of Cu by Zn.

SINGLE-CRYSTAL X-RAY DIFFRACTION

The unit-cell parameters and X-ray diffraction intensity data were measured at room temperature, using a Nonius KappaCCD diffractometer. The data were reduced for Lorentz, polarization, and background effects using the Denzo and Scalepak programs (Otwinowski and Minor 1997; Otwinowski *et al*. 2003) and a multi-scan absorption correction was applied (Blessing 1995). The unit cell parameters, refined by least squares methods of $a = 22.0607(14)$, $b = 6.2147(3)$, $c = 21.8598(13)$, $\beta = 113.212(3)°$, $V = 2754.4(3)$ Å^3 are very simiar to those determined for serpierite (Sabelli and Zanazzi 1968) [$a = 22.186(2)$, $b = 6.250(2)$, $c = 21.853(2)$, $\beta = 113.36(1)$, $V = 2781.60(3)$]. The small difference in unit cell volume is expected due to the similarities in ionic radii of $^{[6]}Ca^{2+}$ (1.00 Å) and $^{[6]}Cd^{2+}$ (0.95 Å) (Shannon 1976). The crystallographic data, data collection parameters, and refinement parameters are summarized in Table 2.

Scattering curves for neutral atoms were taken from the International Tables for Crystallography (Wilson 1992). The systematic absences, *h*00, *h*=2*n*+1; 0k0, *k*=2*n*+1; 00*l*, *l*=2*n*+1; 0*kl*, *k*=2*n*+1; *h*0*l*, *h*=2*n*+1; *h*0*l*, *l*=2*n*+1; *hk*0, *h*+*k*=2*n*+1; *hkl*, *h*+*k*=2*n*+1, were consistent with space groups *Cc* (non centrosymmetric) and *C*2/*c* (centrosymmetric). However, the mean value of $|E^2–1|$ of 0.816 did not give a conclusive indication of the presence of a centre of symmetry (predicted values: 0.968, centrosymmetric, 0.736, non-centrosymmetric).

The structure proved impossible to solve in either space groups *Cc* or *C*2/*c*, using both the programs SHELXS-97 (Sheldrick, 1997a) and SIR92 (Altomare *et al*. 1994). Difficulties in solving mineral structures can be due to twinning (Herbst-Irmer and Sheldrick 1998) and all serpierite crystals from Lavrion, Greece examined by Sabelli and Zanazzi (1968) proved to be twinned on (100), which was shown by diffuse reflections with $k + l = 2n + 1$ along the a^* reciprocal axis. The possibility that the

crystals from Broken Hill were also twinned was checked using the programs ROTAX (Cooper *et al*. 2002) and TwinRotMat (Spek 2003) but no twin law was found.

The structure refinement was then initiated in space group *C*2/*c,* starting with the atomic coordinates for serpierite of Sabelli and Zanazzi (1968) using SHELXL-97 (Sheldrick, 1997b). The refinement converged to $R1 = 9.49\%$ with anisotropic displacement parameters for all atoms. The positions of ten hydrogen atoms were subsaquently located in difference-Fourier maps and were added to the refinement.

As is usual for the refinement of hydrogen positions using X-ray intensity data, anomalously short O–H bond-lengths resulted (H–O distances of 0.75 to 0.83), as the center of gravity of the electron density associated with the H atom is moved significantly toward the donor O atom by chemical bonding. Neutron diffraction (Baur 1972) and *ab initio* density fuctional modelling (Milman and Winkler 2001) have shown that *D*-H distances obtained from X-ray diffraction data can be underestimated by up to 44%. Accordingly, O–H distances were constrained to 0.95 Å, with the H position free to seek its optimal position around the O atom.

The final difference-Fourier map showed a strong peak at (0.2414, 0.5857, 0.1455) with a height of 10.36 e/Å^3. This peak was located 2.04 Å from the *X* site and 1.27 Å from $H_2O(9)$. The next highest peak was 2.87 e/Å^3 located 0.89 Å from S1. A significant residual of electron density located close to $H_2O(9)$ could indicate positional disorder. However occupancy refinement of the $H_2O(9)$ site showed full occupancy by O. In addition, a positional disordered atom could be expected to have anomalously large atomic displacement parameters, and those of $H_2O(9)$ are comparible to the displacement parameters of the other H_2O groups. Also, the distance of the peak from the *X* site of 2.04 Å seems to be somewhat short for a Ca–O bond. Unexplained electron density could indicate the presence of a light cation (e.g. Na), however, no elements with $Z > 8$ other that those reported were detected during the chemical analysis. The unexplained electron density can likely be attributed to the crystal used for X-ray data collection not being single ie. a subparallel intergrowth of the presence of twinning that was not detected.

Table 2. Crystal data, data collection and refinement details for cadmian serpierite.

Crystal data	
Formula	$(Ca_{0.34},Cd_{0.66})(Cu,Zn)_4(SO_4)_2(OH)_6\ 3H_2O$
Space group	*C*2/*c*
a,*b*,*c* (Å)	22.0607(14), 6.2147(3), 21.8598(13)
V (Å^3), Z	2754.4(3), 8
D (calc.) (g/cm^3)	3.647
F(000)	2576
μ (mm^{-1})	7.05
Absorption correction	Gaussian integration
Crystal dimensions (mm)	0.18 x 0.02 x 0.01
Data collection	
Diffractometer	Nonius Kappa CCD
Temperature (K)	293
Radiation	Mo$K\alpha$, λ = 0.71073 Å
θ range (°)	3.37 – 27.71
Detector distance (mm)	28
Rotation axes, width (°)	ϕ, ω, 2
Total no. of frames	307
Collection time per frame (s)	200
h,*k*,*l* ranges	-28 → 28, -8 → 8, -28 → 28
Total reflections measured	30227
Data completeness (%)	98.1
Unique reflections	3158 (R_{int} = 11.29%)
Refinement	
Refinement on	F^2
$R1^*$ for $F_o > 4\sigma(F_o)$	6.28%
w$R2^\dagger$ for all F_0^2	19.06%
Reflections used $F_o^2 > 4\sigma(F_o^2)$	1803
Number of parameters refined	259
$(\Delta/\sigma)_{max}$	0.0001
$\Delta\rho_{min}$, $\Delta\rho_{max}$ (e/Å^3)	10.363, -1.407
GooF	0.995

$^*R1 = \Sigma||F_O|-|F_C|| / \Sigma|F_O|$

$^\dagger wR2 = \Sigma w(|F_O|^2-|F_C|^2)^2 / \Sigma w|F_O|^2)^{1/2}$; $w = 1/[\sigma^2(F_o^2) + (0.042\ P)^2 + 12.60\ P]$;
$P = ([\text{max of } (0 \text{ or } F_0^2)] + 2F_c^2)/ 3$

Table 3. Fractional atomic coordinates and isotropic displacement parameters ($Å^2$) for cadmian serpierite.

	x	y	z	U_{eq}
*X*1	0.24183(6)	0.9152(2)	0.14635(6)	0.0191(5)
Cu(1)	0.00106(6)	0.24961(17)	0.00269(5)	0.0124(3)
Cu(2)	0.99512(6)	0.00567(18)	0.12376(5)	0.0146(3)
Cu(3)	0.99641(6)	0.50770(18)	0.12398(5)	0.0147(3)
Cu(4)	0	0.7572(2)	0.25	0.0133(4)
Cu(5)	0	0.2571(3)	0.25	0.0152(4)
S1	0.15155(13)	0.1938(5)	0.22687(13)	0.0266(7)
S2	0.35092(13)	0.2969(5)	0.00999(13)	0.0272(7)
O(1)	0.1700(4)	0.1224(15)	0.2965(4)	0.041(2)
O(2)	0.1629(4)	0.0204(15)	0.1872(5)	0.047(2)
O(3)	0.0814(3)	0.2532(11)	0.1978(4)	0.0204(16)
O(4)	0.1942(5)	0.3767(15)	0.2303(4)	0.048(2)
O(5)	0.4234(3)	0.2644(11)	0.0422(3)	0.0189(15)
O(6)	0.3367(4)	0.4365(16)	-0.0484(4)	0.047(2)
O(7)	0.3193(4)	0.0922(15)	-0.0098(4)	0.043(2)
O(8)	0.3300(4)	0.4057(14)	0.0587(4)	0.039(2)
H_2O(9)	0.1787(4)	0.5987(14)	0.1184(4)	0.0348(19)
H_2O(10)	0.2962(5)	0.8212(16)	0.0769(5)	0.051(3)
H3	0.285(6)	0.676(9)	0.064(5)	0.034(12)
H4	0.308(6)	0.888(14)	0.045(4)	0.034(12)
H_2O(11)	0.3091(5)	1.2085(16)	0.1590(4)	0.048(2)
H5	0.322(6)	1.221(16)	0.123(4)	0.034(12)
H6	0.304(6)	1.348(10)	0.171(5)	0.034(12)
OH(12)	0.0405(3)	-0.0028(11)	0.0626(3)	0.0193(15)
H7	0.086(3)	-0.015(19)	0.086(5)	0.034(12)
OH(13)	1.0413(3)	0.5140(10)	0.0621(3)	0.0156(14)
H8	1.089(2)	0.528(19)	0.079(6)	0.034(12)
OH(14)	1.0421(3)	0.7562(11)	0.1769(3)	0.0195(15)
H9	1.088(3)	0.779(19)	0.194(6)	0.034(12)
OH(15)	0.9500(3)	0.2596(10)	0.0730(3)	0.0184(15)
H10	0.905(3)	0.257(18)	0.063(6)	0.034(12)
OH(16)	0.9540(3)	0.0208(11)	0.1889(3)	0.0175(15)
H11	0.909(3)	0.047(19)	0.175(6)	0.034(12)
OH(17)	0.9541(3)	0.4941(11)	0.1885(3)	0.0188(15)
H12	0.915(4)	0.452(19)	0.192(6)	0.034(12)

Table 4. Anisotropic displacement parameters (Å^2) for cadmian serpierite.

	U_{11}	U_{22}	U_{33}	U_{12}	U_{13}	U_{23}
*X*1	0.0189(7)	0.0187(7)	0.0193(7)	0.0018(5)	0.0071(5)	0.0005(5)
Cu(1)	0.0192(6)	0.0093(6)	0.0099(6)	0.0011(4)	0.0070(5)	0.0005(4)
Cu(2)	0.0218(7)	0.0114(6)	0.0113(6)	0.0010(4)	0.0071(5)	-0.0012(5)
Cu(3)	0.0202(7)	0.0124(6)	0.0126(6)	-0.0016(4)	0.0076(5)	-0.0011(5)
Cu(4)	0.0262(9)	0.0074(8)	0.0092(8)	0	0.0101(7)	0
Cu(5)	0.0217(9)	0.0123(9)	0.0126(8)	0	0.0078(7)	0
S1	0.0207(14)	0.0422(17)	0.0168(13)	-0.0006(11)	0.0073(11)	-0.0019(12)
S2	0.0175(13)	0.0444(17)	0.0187(13)	0.0012(12)	0.0060(11)	0.0001(12)
O(1)	0.043(5)	0.059(6)	0.017(4)	0.008(4)	0.007(4)	0.010(4)
O(2)	0.040(5)	0.056(6)	0.045(5)	-0.025(4)	0.017(4)	0.008(4)
O(3)	0.017(4)	0.019(4)	0.024(4)	0.001(3)	0.007(3)	0.004(3)
O(4)	0.060(6)	0.045(6)	0.032(5)	-0.006(4)	0.013(4)	-0.016(5)
O(5)	0.014(3)	0.022(4)	0.020(4)	0.001(3)	0.007(3)	0.002(3)
O(6)	0.031(5)	0.070(6)	0.035(5)	0.031(5)	0.007(4)	0.004(4)
O(7)	0.047(5)	0.041(5)	0.040(5)	0.000(4)	0.016(4)	-0.008(5)
O(8)	0.043(5)	0.039(5)	0.042(5)	-0.003(4)	0.023(4)	0.005(4)
H_2O(9)	0.022(4)	0.041(5)	0.036(5)	-0.003(4)	0.005(4)	-0.006(4)
H_2O(10)	0.084(8)	0.043(5)	0.043(6)	0.007(5)	0.043(6)	0.013(5)
H_2O(11)	0.060(6)	0.054(6)	0.032(5)	-0.005(4)	0.020(5)	-0.013(5)
OH(12)	0.019(4)	0.024(4)	0.015(4)	-0.002(3)	0.007(3)	-0.002(3)
OH(13)	0.017(3)	0.022(4)	0.010(3)	0.002(3)	0.007(3)	0.003(3)
OH(14)	0.020(4)	0.020(4)	0.018(4)	0.002(3)	0.006(3)	-0.002(3)
OH(15)	0.019(4)	0.015(4)	0.017(3)	0.004(3)	0.003(3)	0.007(3)
OH(16)	0.017(3)	0.023(4)	0.013(3)	0.000(3)	0.006(3)	0.001(3)
OH(17)	0.022(4)	0.018(4)	0.019(4)	0.002(3)	0.011(3)	0.002(3)

Table 5. Selected interatomic distances (Å) for cadmian serpierite.

*X*1	–H_2O(11)	2.297(10)	Cu(1)	–OH(13)	1.999(6)
	–H_2O(10)	2.349(9)		–OH(12)	2.009(7)
	–O6	2.348(8)		–OH(12)	2.049(7)
	–O2	2.342(8)		–OH(13)	2.066(7)
	–H_2O(9)	2.347(8)		–OH(15)	2.236(7)
	–O4	2.514(9)		–O5	2.243(7)
	–O1	2.596(9)		<Cu-O>	2.100
	<*X*-O>	2.399			
Cu(2)	–OH(15)	1.960(6)	Cu(3)	–OH(15)	1.942(7)
	–OH(12)	1.962(7)		–OH(14)	1.955(7)
	–OH(16)	1.968(7)		–OH(13)	1.967(6)
	–OH(14)	1.969(7)		–OH17	1.975(7)
	–O5	2.389(7)		–O5	2.462(7)
	–O3	2.486(7)		–O3	2.497(7)
	<Cu-O>	2.122		<Cu-O>	2.133
Cu(4)	–OH(16)	2.105(7)	Cu(5)	–OH(16)	1.976(7)
	–OH(16)	2.105(7)		–OH(16)	1.976(7)
	–OH17	2.106(7)		–OH17	1.982(7)
	–OH17	2.106(7)		–OH17	1.982(7)
	–OH(14)	2.142(7)		–O3	2.478(7)
	–OH(14)	2.142(7)		–O3	2.478(7)
	<Cu-O>	2.118		<Cu-O>	2.145
S1	–O4	1.459(9)	S2	–O7	1.433(9)
	–O2	1.465(8)		–O6	1.471(8)
	–O3	1.470(7)		–O8	1.479(8)
	–O1	1.481(8)		–O5	1.486(7)
	<S-O>	1.469		<S-O>	1.467

The final refinement converged to an agreement index (R1) of 6.28%, calculated for the 1803 observed reflections Fo > 4s(Fo). Positional and isotropic-displacement parameters are given in Table 3 and anisotropic-displacement parameters in Table 4. Selected interatomic distances are listed in Table 5 and interatomic angles in Table 6.

Table 6. Selected interatomic angles (°) for cadmian serpierite.

OH(13)–Cu(1)–OH(12)	95.8(3)	OH(15)–Cu(2)–OH(12)	85.3(3)
OH(12)–Cu(1)–OH(12)	80.2(3)	OH(15)–Cu(2)–OH(16)	95.5(3)
OH(13)–Cu(1)–OH(13)	80.0(3)	OH(12)–Cu(2)–OH(14)	95.1(3)
OH(12)–Cu(1)–OH(13)	104.1(3)	OH(16)–Cu(2)–OH(14)	84.0(3)
OH(13)–Cu(1)–OH(15)	104.2(2)	OH(15)–Cu(2)–O5	92.5(3)
OH(12)–Cu(1)–OH(15)	77.3(2)	OH(12)–Cu(2)–O5	80.8(3)
OH(12)–Cu(1)–OH(15)	106.9(3)	OH(16)–Cu(2)–O5	102.2(3)
OH(13)–Cu(1)–OH(15)	75.8(2)	OH(14)–Cu(2)–O5	89.2(2)
OH(13)–Cu(1)–O5	86.5(2)	OH(12)–Cu(2)–O3	89.7(3)
OH(12)–Cu(1)–O5	92.8(3)	OH(14)–Cu(2)–O3	90.8(3)
OH(12)–Cu(1)–O5	82.6(3)	OH(15)–Cu(2)–O3	87.6(3)
OH(13)–Cu(1)–O5	95.5(2)	OH(16)–Cu(2)–O3	87.3(3)
<O–Cu(1)–O>	90.14	<O–Cu(2)–O>	90.0
OH(15)–Cu(3)–OH(13)	85.2(3)	OH(16)–Cu(4)–OH(16)	77.8(4)
OH(14)–Cu(3)–OH(13)	96.3(3)	OH(16)–Cu(4)–OH17	102.0(3)
OH(15)–Cu(3)–OH17	94.9(3)	OH(16)–Cu(4)–OH17	102.0(3)
OH(14)–Cu(3)–OH17	83.7(3)	OH17–Cu(4)–OH17	78.1(4)
OH(13)–Cu(3)–O3	90.2(3)	OH(16)–Cu(4)–OH(14)	103.5(3)
OH(14)–Cu(3)–O3	92.1(3)	OH(16)–Cu(4)–OH(14)	76.7(3)
OH(15)–Cu(3)–O3	87.7(3)	OH17–Cu(4)–OH(14)	76.2(3)
OH17–Cu(3)–O3	87.5(3)	OH17–Cu(4)–OH(14)	103.5(3)
OH(13)–Cu(3)–O5	81.4(3)	OH(16)–Cu(4)–OH(14)	76.7(3)
OH(14)–Cu(3)–O5	87.4(3)	OH(16)–Cu(4)–OH(14)	103.5(3)
OH(15)–Cu(3)–O5	93(3)	OH17–Cu(4)–OH(14)	103.5(3)
OH17–Cu(3)–O5	100.8(3)	OH17–Cu(4)–OH(14)	76.2(3)
<O–Cu(3)–O>	90.0	<O–Cu(4)–O>	91.08
OH(16)–Cu(5)–OH(16)	84.0(4)	O4–S1–O2	110.2(6)
OH(16)–Cu(5)–OH17	96.0(3)	O4–S1–O3	112.0(5)
OH(16)–Cu(5)–OH(16)	83.90(3)	O2–S1–O3	109.0(5)
OH(16)–Cu(5)–OH17	96.00(3)	O4–S1–O1	105.7(5)
OH(16)–Cu(5)–O3	87.4(3)	O2–S1–O1	110.2(6)
OH(16)–Cu(5)–O3	91.8(3)	O3–S1–O1	109.6(5)
OH17–Cu(5)–O3	87.9(3)	<O-S1-O>	109.45
OH17–Cu(5)–O3	92.9(3)		
OH(16)–Cu(5)–O3	91.8(3)	O7–S2–O6	110.5(6)
OH(16)–Cu(5)–O3	87.4(3)	O7–S2–O8	111.7(5)
OH17–Cu(5)–O3	92.9(3)	O6–S2–O8	109.5(6)
OH17–Cu(5)–O3	87.9(3)	O7–S2–O5	109.1(5)
<O–Cu(5)–O>	90.0	O6–S2–O5	108.2(4)
		O8–S2–O5	107.7(5)
		<O-S2-O>	109.45

STUCTURE DESCRIPTION

Cation coordination

The structure contains one *X* site occupied by Ca and Cd and coordinated by four O^{2-} anions and three H_2O groups in an augmented octahedral arrangement (Figure 5) with a <Ca–O> distance of 2.399 A° [range: 2.297–2.596 Å] (Table 5). The $^{[7]}Ca^{2+}$ and $^{[7]}Cd^{2+}$ ions have similar ionic radii of 1.06 and 1.02 Å respectively (Shannon 1976) hence their coordination polyhedra would be expected to have similar observed bond lengths. Summing the constituent ionic radii (Shannon 1976) gives 1.354 + 1.02 = 2.374 Å for Ca^{2+} and 1.354 + 1.06 = 2.414 Å and for Cd^{2+}, which compare well with the observed value of 2.410 Å. The *X*–O distances are very similar to those observed in the structure of serpierite (Sabelli and Zanazzi 1968), with Ca–O bond lengths in the range 2.30–2.54 Å and a <Ca–O> distance of 2.41 Å.

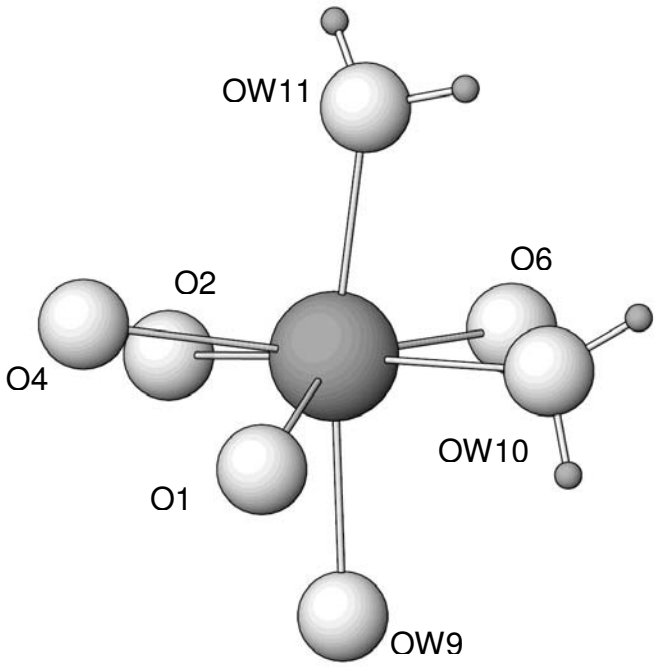

Figure 5. The coordination environment of the *X* site in cadmian serpierite. All structure drawings were completed using ATOMS (Shape Software 1997).

Site-occupancy refinement for the *X* site, using the Ca scattering factor, provided an occupancy factor of 1.20(2), indicating partial incorporation of a heavier cation at the site. The Ca^{2+} and Cd^{2+} cations can be distinguished by their difference in scattering power (Ca: [Ar] $4s^2$, 20 electrons; Cd: [Kr] $4d^{10}5s^2$, 48 electrons), and

refinement of the Ca:Cd occupancy of the site gave a ratio of 0.341(7):0.659(7). The crystal used for X-ray data collection was not analysed, however, this ratio falls within the range of compositions for cadmian serpierite determined from the microprobe analyses.

The structure contains five Cu sites, each coordinated by six O atoms in a distorted octahedral arrangement. The Cu(4) and Cu(5) atoms are located on special positions (Wyckoff position *e*; site symmetry 2) and the Cu(1), Cu(2) and Cu(3) atoms are located in general positions (Wyckoff position 8*f*). Occupancy refinement of each of the Cu sites gave values near 1.00, which did not give any indication of the presence of any heavier atoms (eg. Cd).

The $Cu\phi_6$ octahedra exhibit differing degrees of distortion, with the Cu(2), Cu(3) and Cu(5) sites in particular showing a distorted, [4 + 2] coordination, with the lengthening of the two axial bonds relative to the four equatorial bonds. Unlike most other octahedrally coordinated small- and medium-sized (0.535–0.83 Å) divalent and trivalent cations, nearly all $Cu\phi_6$ (ϕ: O^{2-}, OH, H_2O) octahedra in minerals and synthetic inorganic solids are similarly strongly distorted away from holosymmetric symmetry (Jahn and Teller, 1937), although both (2 + 4)-distorted and holosymmetric octahedra have been reported in mineral structures (Burns and Hawthorne, 1996). There are also a significant number of instances where the $Cu^{2+}\phi6$ octahedron have two short bonds, two intermediate-length bonds, and two long bonds in a [2 + 2 + 2] coordination (Burns and Hawthorne 1996). As shown by *ab initio* MO (molecular orbital) calculations, extension of the axial bonds (a [4 + 2] distortion) is energetically favored over contraction of the axial bonds (a [2 + 4] distortion) (Burns and Hawthorne 1995).

A parameter ($\Delta = 1/6\sum[(l_i - l_o)/ l_o]^2$) used to describe the polyhedral distortion for Cu^{2+} octahedra was introduced by Eby and Hawthorne (1993) who found a linear relationship between bond-length distortion and mean bond length. Values of Δ calculated for Cu^{2+} octahedra in cadmian serpierite (Table 7) fall within the range quoted by Eby and Hawthorne (1993) for a number of copper oxysalt minerals with octahedrally coordinated Cu^{2+} ions.

The Cu^{2+} and Zn^{2+} cations have both very similar ionic radii (0.73 and 0.74 Å for [6]-coordination) and scattering power (Cu [Ar] $3d^{10}4s$, 29 electrons; Zn [Ar] $3d^{10}4s^2$, 30 electrons) so it is not possible to distinguish between these two cations unambiguously on the basis of observed bond lengths or occupation factors. However, progressive replacement of Zn by Cu should result in less regular octahedra due to Jahn-Teller distortion.

A means of calculating the relative occupancy by Cu and Zn in the sites in continuous sheets of edge sharing octahedra was developed by Mellini and Merlino (1978). A linear correlation between the Cu content and ΔL, where ΔL is the difference between the average values of axial and equatorial bond distances in the octahedra, is assumed, with a ΔL-value of 0.0 for 100% Zn of 0.57 for 100% Cu (the maximum value of distortion for the Cu(l)-site in veszelyite). The value of ΔL can be used as a basis for the calculation of the Cu content. Mellini and Merlino (1978) found a good agreement between the calculated Cu and Zn occupancies and the chemical analyses for ktenasite and serpierite, as did Adiwidjaja *et al*. (1996) for christelite. However Mellini and Merlino (1978) pointed out that as $Cu\phi_6$ octahedra show different degrees of distortion in crystal different structures, their approach has its weakness and the results must be considered only an rough approximation of the actual Cu:Zn occupancy.

Table 7. Cu contents calculated from distotion of the octahedra.

Site	ΔL	Cu atoms
Cu(1)	0.22	0.37
Cu(2)	0.47	0.83
Cu(3)	0.52	0.91
Cu(4)	0.04	0.03
Cu(5)	0.50	0.44

The calculation of the relative number of Cu and Zn atoms in each of the Cu(1)-Cu(5) sites, based on ΔL for cadmian serpierite (Table 7), suggest that the Cu(2) and Cu(3) sites have the grearest occupancy by Cu and Cu(4) site would be expected to be almost fully occupied by Zn. The resultant formula for the crystal used for X-ray data collection is $(Ca,Cd)(Cu_{2.67}Zn_{1.33})_4(SO_4)_2(OH)_6{\cdot}3(H_2O)$.

There are two symmetrically distinct S positions in the structure; each S atom is coordinated by four O^{2-} anions in a tetrahedral arrangement. The mean S–O distances for the S(1) and S(2) tetrahedra are 1.469 and 1.467 Å respectively, which is in agreeance with the mean <S-O> length of 1.473 Å typical for a sulphate ion (Baur 1981; Hawthorne *et al*. 2000). Differences between the two polyhedra however, are apparent from the analysis of their distortions. The different distortion modes are defined in Table 8 and the individual values for the S(1) and S(2) tetrahedra are listed. The ELD parameter, which shows the degree of deviation from a regular tetrahedron, is less for the S(2) than for the S(1) site, whereas the BLD parameter, which measures the tetrahedral cation off-center shift, is greater for the S(2) than for the S(1) site.

Calculated bond valences (Brown and Altermatt 1985; Brese and O'Keeffe 1991; Brown 1996) for the Pb, Cu, and S atoms are all close to expected values (Table 9).

Table 8. Selected tetrahedral distortion parameters for cadmian serpierite.

Tetrahedral site	S(1)	S(2)
<S–O>	1.469	1.467
<O–O>	2.398	2.396
BLD* (%)	0.4596	1.1671
ELD** (%)	0.8944	0.424
TAV§ (°)	4.38	2.18

* Bond length distortion (BLD) = $(100/n)\sum^{n}_{i=1}\{[(X–O)_i – (<X –O>)]/(<X –O>)\}$, with n = number of bonds, $(X–O)_i$ = central cation±oxygen bond length and $(<X –O>)$ = average cation-oxygen bond length (Renner and Lehmann, 1986). ** Edge length distortion (ELD) = $(100/n)\sum^{n}_{i=1}\{[(O–O)_i – (<O–O>)]/(< O–O>)\}$, with n = number of edges, $(O–O)_i$ = polyhedron edge length and <O–O> = average polyhedron edge length (Renner and Lehmann, 1986). §Tetrahedral angle variance (TAV) = $\sum^{n}_{i=1}(\theta_i – 109.47)^2/5$ (Robinson *et al*., 1971).

The S(1) tetrahedron displays greater angular distortion ($TAV_{S(1)}$ = 4.38°; $TAV_{S(2)}$ 2.18°), with O–S–O angles ranging from 105.7(9) to 112.0(8)° and 107.7(9) to 111.7(7)° for S(1) and S(2) respectively (Table 6). The narrowest angle (105.7°) is associated with the S(1) tetrahedron edge shared with the $X\phi_7$ polyhedron.

Stucture topology

Each (Cu,Zn)ϕ_6 (ϕ: unspecified ligand) octahedron shares four edges with adjacent octahedra to form a continuous sheet parallel to (100) (Figure 6). The sheets are decorated on both sides by SO_4 tetrahedra, which link via the O3 and O5 anions, resulting in a sheet of composition $[(Cu,Zn)_4(SO_4)_2(OH)_6]^{2-}$.

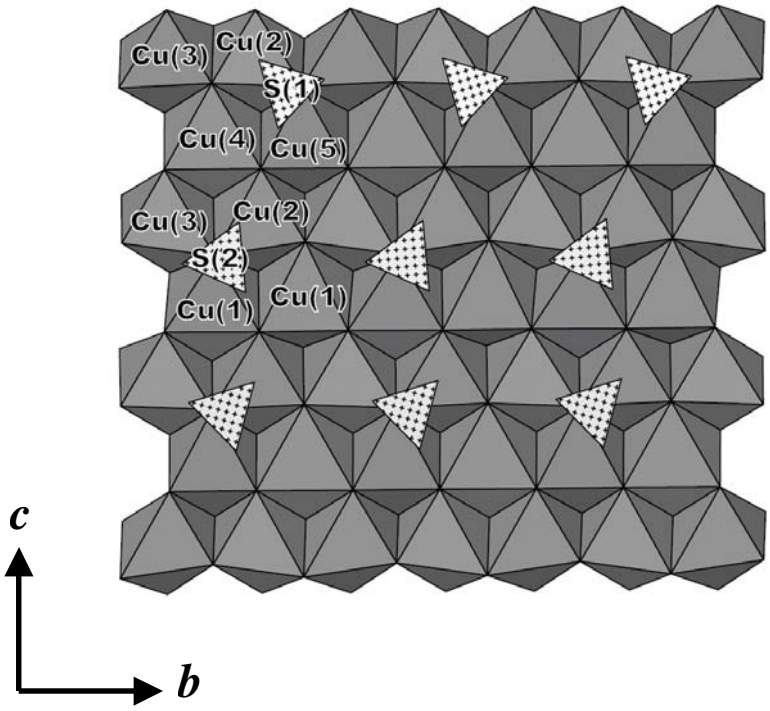

Figure 6. The crystal structure of cadmian serpierite projected onto (001).

Each anion within the sheet of edge-sharing octahedra is coordinated to three (Cu,Zn) cations. The linking O3 and O5 anions are thus [4]-coordinated, and each receives ~1.5 *vu* (valence units) from an S^{6+} cation, and so require an additional 0.50 *vu* from the three (Cu,Zn)–O bonds to satisfy their bond-valence requirements. $Cu^{2+}\phi_6$ octahedra are invariably [4 + 2]-distorted, with mean equatorial and apical bond lengths of 1.97 and 2.44 Å, respectively (Eby and Hawthorne, 1993) which correspond to bond valences of 0.40 and 0.10 *vu*, respectively. Hence, as is the case with other $[Cu^{2+}\phi_6]_N$ sheets in mineral structures, to satisfy local bond valence requirements, three apical $Cu^{2+}\phi$ bonds must meet at the the O3 and O5 anions (Hawthorne and Schindler 2000). The same condition holds for an $(H_2O)^0$ group

linked to an $[M\phi_2]_N$ sheet; the the H_2O group must be involved in a Cu^{2+}–O(apical) bond in all three constituent octahedra.

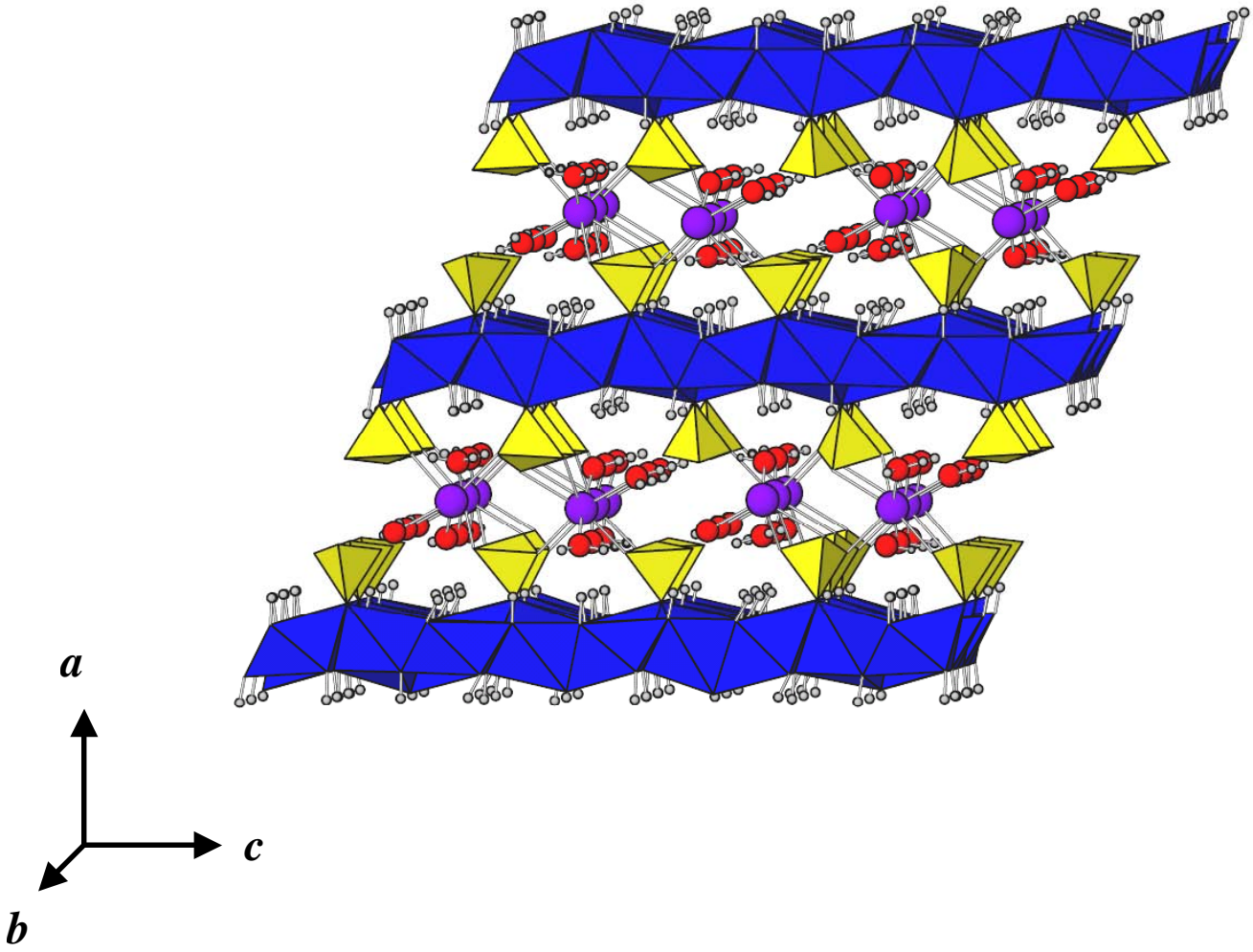

Figure 7. The crystal structure of cadmian serpierite viewed in a direction close to [010]. Cu,Znϕ_6 octahedra are blue; SO_4 tetrahedra are yellow; Pb atoms are purple spheres; H_2O molecules are red spheres; hydrogen atoms are small grey spheres.

Linkage between the sheets in the *a*-direction is provided via the Ca^{2+} cations which link to two anions of the S(1) tetrahedra and one anion of the S(2) tetrahedra (Figure 7). Additional linkage is provided by hydrogen bonding.

H_2O and OH groups and hydrogen bonding

The bond-valence incident at the various anions (Table 9) show that six oxygen atoms are OH groups and three are H_2O groups. The crystal-structure refinement indicates that all OH and H_2O groups are fully occupied. All H atoms belonging to the OH and H_2O groups were located in the refinement except H1 and H2 associated with $H_2O(9)$. The hydrogen-bonding scheme proposed by Sabelli and Zanazzi (1968) is confirmed with the addition of a hydrogen bond accepted by the O2 anion from the H7 atom.

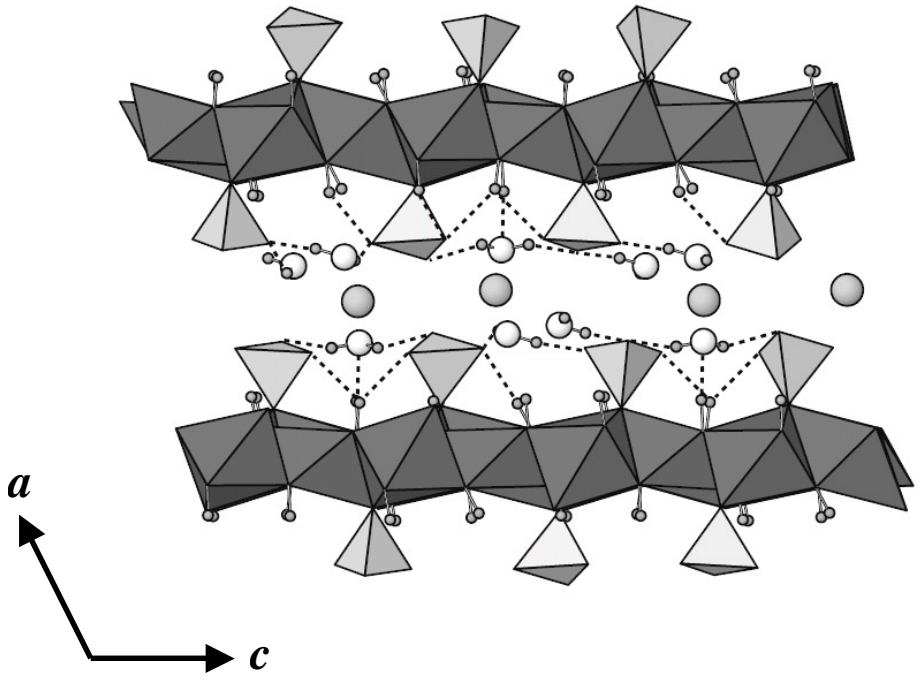

Figure 8. The crystal structure of cadmian serpierite projected onto (100); (Ca,Cd)ϕ_6 octahedra are dark grey; SO_4 tetrahedra are pale grey; hydrogen atoms are small grey spheres. Hydrogen bonds are shown as dotted lines.

Bond lengths and angles for the hydrogen bonds (except those involving H1 and H2) are given in Table 10 and the hydrogen bond arrangement is shown in Figures 8 and 9. All H...O distance are 1.823 to 2.282 Å indicate moderate to weak H-bonding.

Table 9. Bond-valence analysis for cadmian serpierite.

	*X*1	Cu1	Cu2	Cu3	Cu4	Cu5	S1	S2	H1	H2	H3	H4	H5	H6	H7	H8	H9	H10	H11	H12	Sum (excluding H)	Sum (including H)
O1	0.17						1.48							0.20					0.12		1.65	1.97
O2	0.34						1.54								0.10		0.10				1.88	2.08
O3			0.11	0.11		0.12	1.52														1.86	1.86
						0.12															0.12	
O4	0.22						1.56			0.20											1.78	1.98
O5		0.22	0.15	0.12				1.46													1.95	1.95
O6	0.34							1.51							0.15						1.85	2.00
O7								1.68	0.21			0.20									1.68	2.09
O8								1.48			0.19		0.21								1.48	1.88
H2O(9)	0.34								0.79	0.80						0.16					0.34	2.09
H2O(10)	0.34										0.81	0.80									0.34	1.95
H2O(11)	0.39												0.79	0.80							0.39	1.98
OH12		0.41	0.47												0.75						1.25	2.00
		0.37																				
OH13		0.42		0.46												0.84					1.23	2.07
		0.35																				
OH14			0.46	0.47	0.29												0.90				1.22	2.12
					0.29																	
OH15		0.22	0.47	0.49														1.00			1.18	2.18
OH16			0.46		0.32	0.45													0.88		1.23	2.11
					0.32	0.45																
OH17				0.45	0.32	0.44														1.00	1.21	2.21
					0.32	0.44																
Sum	2.14	1.99	2.12	2.10	1.86	2.02	6.10	6.13	1.00	1.00	1.00	1.00	1.00	1.00	1.00	1.00	1.00	1.00	1.00	1.00		

Bond-valence calculations show that O1, O4, O7, O8 in particular are weakly bonded acceptor anions that require the hydrogen bond to satisfy their bond-valence requirements.

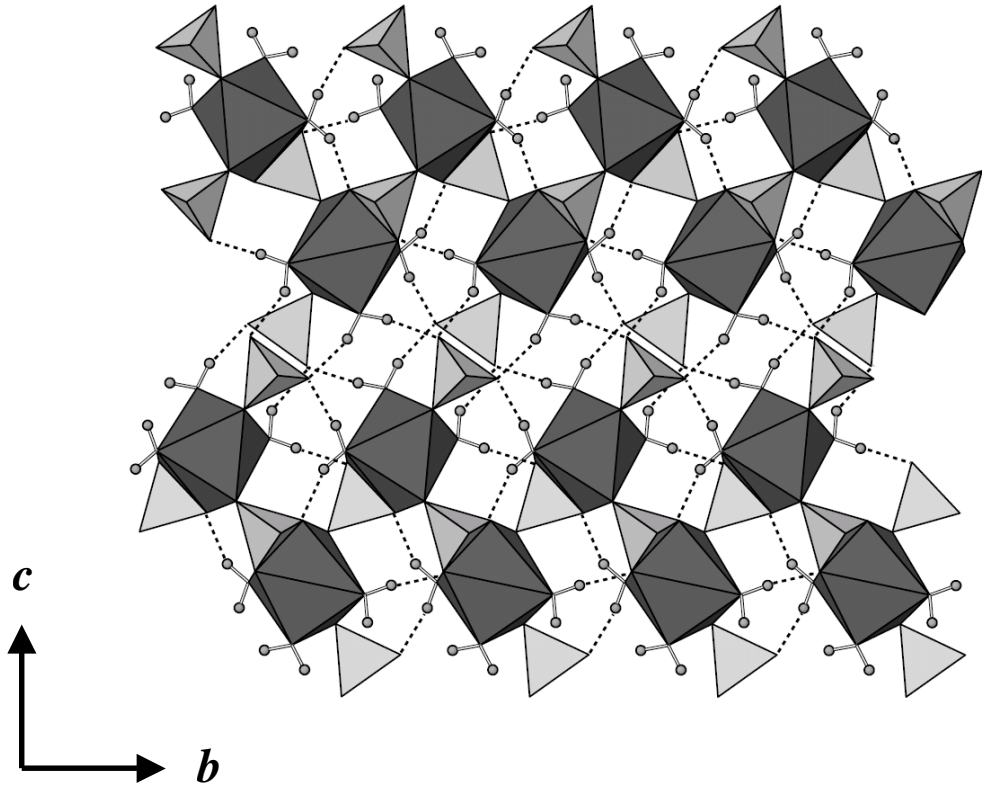

Figure 9. The crystal structure of cadmian serpierite viewed along [010]; (Ca,Cd)ϕ_6 octahedra are dark grey; SO_4 tetrahedra are pale grey; H_2O molecules are white spheres; (Ca,Cd) cations are pale grey spheres; hydrogen atoms are small grey spheres. Hydrogen bonds are shown as dotted lines.

Each of H8, H9 and H11 of the OH(13), OH(14) and OH(16) groups provide a single H bond to the $H_2O(9)$, O2 and O atoms respectively. The H7 atom forms a multiple H-bond with O2 and O6. Such bonds, which have comparable strength, can be considered to be bifurcated hydrogen bonds (Chiari and Ferraris 1982).

The OH(15) and OH(17) anions also have the potential to donate H bonds, but all suitable acceptor anions that are less than ~3.12 Å from the donor anion are contained within the same polyhedron as the donor. It is unlikely that an H bond will form along

the edge of a coordination polyhedron, except where the coordination polyhedron involves a monovalent cation of high coordination number (Baur 1972, 1973).

The $H_2O(10)$ and $H_2O(11)$ groups each donate two H bonds accepted by the O1, O7 and O8 atoms coordinated to S1 and S2. Although H1 and H2 associated with $H_2O(9)$ were not located, stereochemical considerations suggest that $H_2O(9)$ likely donates two H bonds accepted by O4 and O7, with O...O distances of 2.669 and 2.710 Å respectively.

Table 9. Details of hydrogen bonding in cadmian serpierite (Å, °).

D-H	d(D-H)	d(H..A)	<DHA	d(D..A)
$H_2O(10)$-H3…O8	0.952	1.972	138.84	2.761
$H_2O(10)$-H4…O7	0.937	1.823	161.82	2.730
$H_2O(11)$-H5…O8	0.939	1.879	145.62	2.706
$H_2O(11)$-H6…O1	0.924	1.848	157.45	2.724
OH(12)-H7…O2	0.936	2.205	140.76	2.989
OH(12)-H7…O6	0.936	2.214	126.86	2.875
OH(13)-H8… $H_2O(9)$	0.973	1.872	170.00	2.835
OH(14)-H9…O2	0.939	2.282	140.07	3.062
OH(16)-H11…O1	0.942	2.111	147.02	2.946

RELATIONSHIPS TO OTHER MINERALS

Serpierite is dimorphous with orthoserpierite (Sarp 1985) the structure of which is not known. It is closely related to devilline, $Ca(Cu,Zn)_4(SO_4)_2(OH)_6{\cdot}3H_2O$, which is monoclinic, $P2_1/c$, with a = 20.870, b = 6.135, c = 22.191, β = 102.73°, V = 2771.4 and Z = 8 (Sabelli and Zanazzi 1972).

Brucite-like sheets, decorated by SO_4 tetrahedra, are the basis for the structures of many Cu^{2+} and Zn sulphate minerals (Hawthorne *et al*. 2000). Two sided tetrahedral decorated sheets are found in the structures of ktenasite, $Zn_2(Cu,Zn)_8(OH)_{12}(SO_4)_4{\cdot}12H_2O$, (Mellini and Merlino 1978), devilline ($Ca(Cu,Zn)_4(OH)_6(SO_4)_2{\cdot}3H_2O$) (Sabelli and Zanazzi 1972), schulenbergite $(Cu,Zn)_7(OH)_{10}(SO_4)_2(H_2O)_2{\cdot}H_2O$ (Mumme *et al*. 1994), christelite, $Zn_3Cu_2(SO_4)_2(OH)_6{\cdot}4H_2O$, (Adiwidjaja *et al*., 1996), niedermayrite, $Cu(4)Cd(SO_4)_2(OH)_6{\cdot}4H_2O$, (Giester *et al*. 1998). Of these, linkage between the sheets is also provided by intersheet cations (Ca^{2+}, Zn, Pb^{2+}, Cd^{2+}) in, devilline,

christelite and niedermayrite. In schulenbergite, intersheet linkage is provided by hydrogens bonds only, and in ktenasite linkage is provided via an isolated $Zn\phi_6$ octahedron which links to the sheets by hydrogen bonding only between H_2O molecules coordinated to the $Zn\phi_6$ octahedron and O atoms of SO_4 tetrahedra.

Hawthorne and Schindler (2000) examined the principles involved in the structures of hydroxy-hydrated copper (and zinc) minerals based on substituted and decorated $[Cu^{2+}\phi_2]_N$ sheets. These authors noted that "there are currently 20 minerals known that correspond to this structural theme, and it is almost certain that many others await discovery". Given that the formula of cadmian serpierite is $(Ca,Cd)(Cu,Zn)_4(SO_4)_2(OH)_6{\cdot}3H_2O$, then the structural unit is $[(Cu,Zn)_{16}(SO_4)_8(OH)_{24}]$ which can be written $[M_{16}\, X_8\, \phi_{24}] = [M_{16}\phi_{32}] = [M\phi_2]_{16}$. Hence the structure of cadmian serpierite is based on a decorated $[M\phi_2]_N$ sheet and fits into the classification scheme of Hawthorne and Schindler (2000) who found that topological enumeration of $[Cu^{2+}\phi_2]_N$ ($\phi = O^{2-}$, OH, Cl, H_2O) sheets for $3 < N < 9$ results in 17 distinct coloured graphs, some of which occur as homeomorphisms in the structures of copper-oxysalt sheet minerals. The sheet in the structure of cadmian serpierite is homeomorphic to graph 4a. Serpierite and devilline are the only two structures that are homeomorphic to graph 4a.

The sheet, which also also occurs in the structure of devilline, is an example of an "interrupted" $[Cu^{2+}\phi_2]_N$ sheet in which the arrangement of [4 + 2]-distorted octahedra in the sheet is interrupted by regular non-Jahn–Teller distorted octahedra. Sheets interrupted by regular $Cd\phi_6$ octahedra is found in the structure of the synthetic compound $CdCu(3)(OH)_6(NO_3)_2{\cdot}H_2O$ (Oswald, 1969). Sheets interrupted by vacancies are found in the structures of spangolite, sabelliite, gordaite, bechererite, namuwite, osakaite and in the synthetic compound $Zn_4SO_4(OH)_6{\cdot}3H_2O$.

ACKNOWLEDGEMENTS

We thank Angus Netting and John Terlet of Adelaide Microscopy, The University of Adelaide for their assistance with the microprobe analysis and Hayley Brown and Paul Pigou for assistance with collection of the infrared spectrum.

REFERENCES

Adiwidjaja, G., Friese, K. Klaska, K.-H. and Schlüter, J. (1996) The crystal structure of christelite $Zn_3Cu_2(SO_4)_2(OH)_6 \cdot 4H_2O$. Zeitschrift für Kristallographie, 211, 518–521.

Altomare, A., Burla, M.C., Camalli, M., Cascarano, G., Giacovazzo, C., Guagliardi, A. and Polidori, G. (1994) SIR92-A program for automatic solution of crystal structures by direct methods. Journal of Applied Crystallography, 27, 435.

Baur, W.H. (1972) Prediction of hydrogen bonds and hydrogen atom positions in crystalline solids. Acta Crystallographica, B28, 1456–1465.

Baur, W.H. (1973) Criteria for hydrogen bonding. II. A hydrogen bond in the edge of a coordination polyhedron around a cation. Acta Crystallographica, B29, 139–140.

Baur, W.H. (1981) Interatomic distance predictions for computer simulation of crystal structures. In M. O'Keeffe and A. Navrotsky, Eds., Structure and Bonding in Crystals Vol. II, p. 31–52. Academic Press, New York.

Bertrand E (1881) Étude optique de différents minéraux: Nouveau minéral du Laurium, Bulletin de la Société Minéralogique de France 4, 87–93.

Birch, W.D. (1999) The Minerals. In Minerals of Broken Hill. W.D. Birch, ed., Broken Hill Council, Broken Hill, p. 88–256.

Blessing, R.H. (1995) An Empirical Correction for Absorption Anisotropy. Acta Crystallographica, A51, 33–38.

Brese, N.E. and O'Keeffe, M. (1991) Bond-valence parameters for solids. Acta Crystallographica, B47, 192–197.

Brown, I.D. (1996) VALENCE: a program for calculating bond-valences. Journal of Applied Crystallography, 29, 479–480.

Brown, I.D. and Altermatt, D. (1985) Bond-valence parameters obtained from a systematic analysis of the inorganic crystal structure database. Acta Crystallographica, B41, 244–247.

Burns, P.C. and Hawthorne, F.C. (1996) Static and dynamic Jahn-Teller effects in Cu^{2+} oxysalts. Canadian Mineralogist, 34, 1089–1105.

Chiari, G. and Fenaris, G. (1982) The water molecule in crystalline hydrates studied by neutron diftaction. Acta Crystallographica, B38, 2331–2341.

Cooper, R.I., Gould, R.O., Parsons, S. and Watkin, D.J. (2002) The derivation of non-merohedral twin laws during refinement by analysis of poorly fitting intensity data and the refinement of non-merohedrally twinned crystal structures in the program CRYSTALS. Journal of Applied Crystallography, 35, 168–174.

Des Cloizeaux (1881) Bulletin de la Société française de Minéralogie, 4, 89.

Eby, R.K. and Hawthorne, F.C. (1993) Structural relationships in copper oxysalt minerals. I. Structural hierarchy. Acta Crystallographica, B49, 28–56.

Faraone, D., Sabelli, C. and Zanazzi, P. F. (1967) Su di solfatibasici idrati: serpierite e devillite. Rendiconti della Accademia Nazionale dei Lincei, Classe di Scienze Fisiche, Matematiche e Naturali, 43, 369–382.

Giester, G., Rieck, B. and Brandstätter, F. (1998) Niedermayrite, $Cu_4Cd(SO_4)_2(OH)_6 \cdot 4H_2O$, a new mineral from the Lavrion District, Greece. Mineralogy and Petrology, 63, 9–34.

Hawthorne , F.C. and Schindler, M.S. (2000) Topological enumeration of decorated $[Cu^{2+}\phi_2]^N$ sheets in hydroxy-hydrated copper-oxysalt minerals. Canadian Mineralogist, 38, 751–761.

Hawthorne, F.C., Krivovichev, S.V. and Burns, P.C. (2000) Crystal chemistry of sulfate minerals. In C.N. Alpers, J.L. Jambor, and D.K. Nordstrom, Eds., Sulfate Minerals, Crystallography, Geochemistry, and Environmental Significance, 40, p.

1–112. Reviews in Mineralogy and Geochemistry, Mineralogical Society of America, Chantilly, Virginia.

Herbst-Irmer, R. and Sheldrick, G.M. (1998) Refinement of twinned structures with SHELXL97. Acta Crystallographica, B54, 443–449.

Jahn, H.A., and Teller, E. (1937) Stability of polyatomic molecules in degenerate electronic states. Proceedings of the Royal Society, Series A, 161, 220–236.

Mellini, M. and Merlino, S. (1978) Ktenasite, another mineral with $[(Cu,Zn)_2(OH)_3O]^-$ octahedral sheets. Zeitschrift für Kristallographie, 147, 129–140.

Milman, V. and Winkler, B. (2001) Prediction of hydrogen positions in complex structures. Zeitschrift für Kristallographie, 216, 99–104.

Mumme, W.G., Sarp, H. and Chiappero. P.J. (1994) A note on the crystal structure of schulenbergite, Archives des Sciences, Genève, 47, 117–124.

Otwinowski, Z. and Minor, W. (1997) Processing X-ray diffraction data collected in oscillation mode. In Macromolecular Crystallography, C.W. Carter Jr. and R.M. Sweet, Eds., Vol. 276, p. 307–326. Academic Press, New York.

Otwinowski, Z., Borek, D., Majewski, W. and Minor, W. (2003) Multiparametric scaling of diffraction intensities. Acta Crystallographica, **A59**, 228–234.

Pouchou, J.L. and Pichoir, F. (1985) "PAP" $\phi(\rho Z)$ procedure for improved quantitative microanalysis. In J.T. Armstrong, Ed., Microbeam Analysis, 104–106.

Renner, B., and Lehmann, G. (1986) Correlation of angular and bond length distortions in TO_4 units in crystals. Zeitschrift für Kristallographie, 175, 43–59.

Robinson, K., Gibbs, G.V. and Ribbe, P.H. (1971) Quadratic elongation; a quantitative measure of distortion in coordination polyhedra. Science, 172, 567–570.

Sabelli C. and Zanazzi, P.F. (1968) The crystal structure of serpierite. Acta Crystallographica, B24, 1214–1221.

Sabelli, C. and Zanazzi, P.F. (1972) The crystal structure of devillite [devilline]. Acta Crystallographica, 28, 1182–1189.

Sarp, H. (1985) Orthoserpiérite $Ca(CuZn)_4(SO_4)_2(OH)_6 \cdot 3H_2O$, un nouveau minéral de la Mine de Chessy, France, polymorphe de la serpiérite, Schweizerische Mineralogische und Petrographische Mitteilungen, 65, 1–7.

Shannon, R.D. (1976) Revised effective ionic radii and systematic studies of interatomic distances in halides and chalcogenides. Acta Crystallographica, A32, 751–767.

Shape Software (1997) ATOMS for Windows and Macintosh V 4.0, Kingsport, Tennessee, U.S.A.

Sheldrick, G.M. 1997a. SHELXS–97, a Program for the Solution of Crystal Structures. University of Göttingen, Göttingen, Germany.

Sheldrick, G.M. 1997b. SHELXL–97, a Program for Crystal Structure Refinement. University of Göttingen, Göttingen, Germany.

Spek, A.L. (2003) Single-crystal structure validation with the program PLATON. Journal of Applied Crystallography, 36, 7–13.

Wilson, A.J.C., Ed. (1992) International Tables for Crystallography, vol. C, 883 p. Kluwer Academic, Dordrecht, The Netherlands.

CHAPTER 6

The crystal chemistry of gartrellite group minerals from the Kintore Opencut, Broken Hill, New South Wales

Peter Elliott[1,2] and Anthony C. Willis[3]

[1]School of Earth and Environmental Sciences, The University of Adelaide, Adelaide, South Australia 5005, Australia.

[2]South Australian Museum, North Terrace, Adelaide, South Australia 5000, Australia.

[3]Research School of Chemistry, The Australian National University, Australian Capital Territory 0200, Australia.

STATEMENT OF AUTHORSHIP

The crystal chemistry of gartrellite group minerals from the Kintore Opencut, Broken Hill, New South Wales

Peter Elliott (Candidate)

Performed analysis on all samples, interpreted data and wrote manuscript. I hereby certify that the statement of contribution is accurate.

Signed .....*Date*.....23/8/2010

Anthony Willis

Single-crystal X-ray data collection and data reduction.

I hereby certify that the statement of contribution is accurate and I give permission for the inclusion of the paper in the thesis.

Signed .....*Date*.....12/7/2010

The crystal chemistry of gartrellite group minerals from the Kintore Opencut, Broken Hill, New South Wales

Peter Elliott[1,2] and Anthony C. Willis[3]

[1]School of Earth and Environmental Sciences, The University of Adelaide, Adelaide, South Australia 5005, Australia

[2]South Australian Museum, North Terrace, Adelaide, South Australia 5000, Australia

[3]Research School of Chemistry, The Australian National University, Australian Capital Territory 0200, Australia

ABSTRACT

Extensive solid solution is observed between gartrellite, zincgartrellite and yancowinnaite from the Kintore Opencut, Broken Hill, New South Wales. Compositions in the gartrellite-zincgartrellite series range from $Pb(Fe^{3+},Al)Cu(AsO_4)(OH)(H_2O)$ to $Pb(Fe^{3+},Al)(Cu_{0.29}Zn_{0.71})(AsO_4)(OH)(H_2O)$. Compositions in the gartrellite- aluminium gartrellite series range from $Pb(Fe^{3+}_{0.97}Al_{0.03})(Cu,Zn)(AsO_4)(OH)(H_2O)$ to $Pb(Fe^{3+}_{0.18}Al_{0.82})(Cu,Zn)(AsO_4)(OH)(H_2O)$. Positive correlations between Cu and Al *pfu* and between Fe and Zn *pfu* indicate a replacement of Zn by Cu in conjunction with replacement of Fe by Al. The crystal structure of gartrellite has been refined using single-crystal X-ray data to $R1 = 9.29\%$ for 832 observed reflections. The structure is $P\bar{1}$, Z = 1, with refined unit cell parameters $a = 5.5502(5)$, $b = 5.5413(5)$, $c = 7.5727(7)$ Å, $\alpha = 69.131(6)$, $\beta = 69.059(5)$, $\gamma = 69.669(6)°$, $V = 196.68(3)$. The structure contains three *Me* sites, with Pb located in the *Me*1 site, Fe^{3+}, Al minor Zn and very minor Cu in the *Me*2A site and Cu, Zn and very minor Fe^{3+} in the *Me*2B site. *Me*2A and *Me*2B octahedra alternate and share *trans* edges to form a $[M\phi_4]$ chain that extends along [110]. Chains link by sharing (AsO_4) tetrahedron vertices to form a sheet of the form $[(Me2(OH)_2(AsO_4)_2]$ in the (001) plane. The sheets are linked in the *c*-direction by PbO_8 square-antiprisms and by hydrogen bonds.

INTRODUCTION

The tsumcorite group of minerals, general formula $Me(1)Me(2)_2(XO_4)_2(H_2O,OH)_2$, have a highly flexible crystal chemistry which facilitates the incorporation of various cations, and greater than 30 natural and synthetic representatives of the group are known (*cf.* Tillmanns and Gebert, 1973; Giester and Zemann, 1987; Beran *et al*., 1997; Krause *et al*., 1998a, 2002; Effenberger *et al*., 2000; Brugger *et al*., 2000, Brugger *et al*., 2002). Natural endmembers have been described with Pb, Bi, Ca, and Na dominating on the *Me*(1) site, Zn, Fe^{3+}, Cu^{2+}, Mn^{3+}, Mg and Co on the *Me*(2) site, and As^{5+}, P^{5+}, V^{5+}, and S^{6+} on the *X*-site. Extensive solid solution is known at the *Me*(2) site, especially for (Fe,Co,Ni), (Fe,Zn), (Zn,Cu) and (Mg,Al,Fe). Synthetic members of the group can also contain *Me*(1) = K, Rb, Ag, NH_4, Bi and Tl, *Me*(2) = Al, Ni, Zn and *X* = Se and Mo (cf. Mihajlovic and Effenberger 2004 and references therein). Charge balance is maintained by the coupled exchange of cations of different valences in the *Me*(1), *Me*(2) and *X* sites and by adjustment of the $OH:H_2O$ ratio.

Tsumcorite was first found at the Tsumeb mine, Namibia (Geier *et al*. 1971). The mineral is monoclinic, space group *C*2/*m* with Z = 2. The crystal structure was determined by Tillmanns and Gebert (1973). The majority of the 19 natural tsumcorite group minerals since discovered also crystallize in space group *C*2/*m* (tsumcorite type). Only gartrellite, zincgartrellite, phosphogartrellite, lukrahnite, rappoldite and helmutwinklerite are triclinic, space group $P\bar{1}$ and Z = 1. The reduction in symmetry from monoclinic to triclinic is due either to an ordering of cations on two *Me*(2) sites in the structure (gartrellite type) or to an ordering of the hydrogen bonds (helmutwinklerite type). A monoclinic structural variant is known in the synthetic compound $SrCo_2(AsO_4)(AsO_3OH)(OH)(H_2O)$, in which the unit cell volume is doubled and symmetry is lowered to $P2_1/a$ (Mihajlovic and Effenberger 2004).

Gartrellite was originally described from Ashburton Downs, WA, where it formed fine-grained, powdery encrustations and cavity fillings associated with a variety of secondary Pb and Cu minerals, and from the Kintore Opencut, Broken Hill, NSW, where it formed powdery encrustations and possible pseudomorphs after a hexagonal mineral (Nickel *et al*. 1989). The chemical formula, derived from electron

microprobe and CHN analyses and calculated on the basis of Pb+Cu+Fe = 3, was given as $Pb_{1.04}Cu_{1.22}Fe_{0.74}(AsO_4)_{1.88}(SO_4)_{0.10}(CO_3)_{0.54}(H_2O)_{0.18}$. Because of the very small size of available crystals no single-crystal X-ray study could be performed. A study of the tsumcorite-group minerals, using microprobe analysis, powder X-ray diffraction, infrared spectroscopy and Mössbauer spectroscopy was completed by Krause *et al*. (1998a). On the basis of their reinvestigation of gartrellite, using holotype material, Krause *et al*., (1998a), redefined the mineral as ideally $PbCu(Fe,Cu)(AsO_4)_2(OH,H_2O)_2$. No evidence for the presence of carbonate was found using microchemical tests and infrared spectroscopy. Due to their small size and twinning, no suitable crystals could be found suitable for a single-crystal X-ray study. Rietveld refinement of the structure using powder X-ray diffraction data was completed. The details of the refinement and structure were not published; they are however available from the Inorganic Crystal Structure Database (Belsky *et al*. 2002)

Subsequent to the original description of gartrellite, specimens containing gartrellite group minerals with much larger crystals than those previously known were collected from the Kintore Opencut, Broken Hill in the late 1980s. The crystals are overgrown by yellow-orange crystals of beudantite-segnitite and are also associated with adamite, agardite-Y, carminite, mimetite and chlorargyrite. Although all crystals from Broken Hill examined are either twinned or intergrowths of two or more individuals, a crystal was located that proved suitable for structure determination. This study reports the results of the single crystal X-ray diffraction and electron microprobe study of gartrellite using these samples.

CHEMICAL ANALYSIS

Seven crystal aggregates of gartrellite were embedded in epoxy resin, polished and analyzed using a Cameca SX51 electron microprobe, with an acceleration voltage of 20 kV, a beam current of 20 nA, peak count-time 20 s, background count-time 10 s and a beam diameter of 5 mm. Data were reduced using the $\phi(\rho Z)$ method of Pouchou and Pichoir (1985). The following standards and X-ray lines were used for calibration: galena (Pb*M*α), chalcopyrite (Cu*K*α), sphalerite (Zn*K*α), almandine (Fe*K*α, Al*K*α), rhodonite (Mn*K*α), GaAs (As*L*α), and hydroxylapatite (P*K*α). Elements present in

minor amounts (>0.05 wt% oxide) were Ca, Ba and Si. No additional element with atomic number ≥9 was detected in amounts >0.05 wt% oxide.

The microprobe analyses indicate that gartrellite crystals from the Kintore Opencut show a wide range in chemical composition. The chemical variabliliy is apparent in the range in colour shown by the crystals, from yellow to orange-yellow, yellow-brown, yellow-green and bright green. The chemical variability in gartrellite occurs in both the *Me*2A site in the structure, involving Fe^{3+}, Al, Zn and very minor Cu^{2+} and Mn^{3+}, and the *Me*2B site, involving Cu^{2+}, Zn and minor Fe^{3+}. Each of Fe^{3+}, Al, Cu^{2+} and Zn shown wide compositional ranges: Fe_2O_3 2.05–13.13, Al_2O_3 0.24–6.67, CuO 3.15–14.08 and ZnO 0.17–12.08 Wt.% (Table 1).

A plot of atoms of Cu vs. atoms of Zn *pfu* (per formula unit) (Figure 2a) for all analyses of gartrellite shows a strong negative linear correlation, with $R^2 = 0.935$ and a slope close to –1 indicating a simple replacement of Cu by Zn in the *Me*2B site. Occupancy the site varies from 100% occupancy by Cu to a Cu:Zn ratio of 0.29:0.71. The most Cu rich analyses, with greater than ~12.50 Wt.% CuO, result in greater than 1.0 *apfu* (atoms per formula unit) Cu, indicating minor Cu^{2+} for Fe^{3+} substitution (up to 0.13 *apfu*) in the *Me*2A site. Gartrellite from Ashburton Downs, Western Australia, contains up to ~14.0 Wt.% CuO (Krause *et al*. 1998a) also indicating a degree of Cu^{2+} for Fe^{3+} substitution in the *Me*2A site.

Krause *et al*., (1998a) suggested that the series gartrellite–zincgartrellite is likely to be complete, based on a correlation between unit cell parameters and Zn content. Effenberger *et al*. (2000) proposed that the gartrellite–zincgartrellite series is complete, based on experimentally verified substitution of 2Zn ⇆ Fe+Cu. Based on the formula of zincgartrellite, $Pb(Zn_xFe^{3+}_{1-x})(Zn_xCu_{1-x})(AsO_4)(OH)_{1-x}(H_2O)_{1+x}$ with $0.4 < x < \sim 0.8$, as proposed by Effenberger *et al*. (2000), the compositions of samples 5, 6 and zone 1 of sample 1 fall within the gartrellite field and the compositions of samples 3 and 4 fall within the zincgartrellite field. Gartrellite–zincgartrellite from Broken Hill shows a continuous series between $Pb(Fe^{3+}Al,Zn)Cu(AsO_4)(OH)(H_2O)$ and $Pb(Fe^{3+}Al,Zn)(Cu_{0.29}Zn_{0.71})(AsO_4)(OH)(H_2O)$, which supports the proposition of Effenberger *et al*. (2000). Compositions with *x* close to 1.0 are helmutwinklerite, $PbZn_2(AsO_4)_2{\cdot}2H_2O$, (Süsse and Schnorrer 1980) and Effenberger *et al*. (2000) noted

Table 1. Chemical analyses of gartrellite.

Sample number	1		2	3	4	5	6	7	Min.	Max.
	Zone1	Zone 2								
No. of analyses	60	20	11	13	18	18	15	13		
As_2O_5	35.90	36.08	36.05	37.40	36.41	36.39	35.69	36.74	33.68	38.54
SiO_2	0.07	0.04	0.02	0.44	0.11	0.12	0.00	0.00	0.00	1.02
PbO	36.44	36.36	35.98	36.78	36.40	37.24	36.36	36.48	34.15	38.27
CaO	0.03	0.06	0.02	0.02	0.02	0.03	0.03	0.03	0.00	0.12
CuO	9.68	12.94	13.56	5.47	4.65	10.90	11.66	13.30	3.51	14.08
ZnO	3.38	0.80	0.68	8.97	9.33	2.89	1.76	0.58	0.17	12.08
Fe_2O_3	9.61	4.24	5.09	9.29	9.19	8.59	9.42	4.15	2.05	13.13
Al_2O_3	1.65	5.06	4.38	1.01	0.85	2.14	1.47	5.24	0.24	6.67
MnO	0.03	0.06	0.02	0.01	0.18	0.02	0.02	0.01	0.00	0.46
H_2O (calc)*	4.28	4.34	4.34	4.38	4.26	4.36	4.27	4.39	4.10	4.51
Sum	101.07	99.98	100.14	103.77	101.40	102.68	100.68	100.92	97.08	106.19
As	1.97	1.96	1.95	2.01	2.01	1.96	1.97	1.97	1.87	2.06
Si	0.00	0.00	0.00	0.03	0.01	0.01	0.00	0.00	0.00	0.07
Sum	1.97	1.96	1.95	2.04	2.02	1.97	1.97	1.97	1.92	2.06
Pb	1.03	1.01	1.00	1.02	1.03	1.03	1.03	1.01	0.98	1.09
Fe^{3+}	0.76	0.33	0.40	0.72	0.73	0.67	0.75	0.32	0.16	0.97
Al	0.20	0.62	0.53	0.12	0.11	0.26	0.18	0.63	0.03	0.82
Zn	0.03	0.06	0.05	0.10	0.10	0.07	0.07	0.04	0.00	0.29
Mn^{3+}	0.00	0.00	0.00	0.00	0.02	0.00	0.00	0.00	0.00	0.04
Cu^{2+}	0.00	0.00	0.06	0.00	0.00	0.00	0.00	0.03	0.00	0.10
$\sum Me2A$	1.00	1.00	1.04	0.94	0.95	1.00	1.00	1.02	0.92	1.08
Cu^{2+}	0.77	1.01	1.00	0.42	0.37	0.85	0.93	1.00	0.29	1.00
Zn	0.23	0.00	0.00	0.58	0.63	0.15	0.07	0.00	0.00	0.71
Fe^{3+}	0.00	0.00	0.00	0.00	0.00	0.00	0.00	0.00	0.00	0.10
$\sum Me2B$	1.00	1.01	1.00	1.00	1.00	1.00	1.00	1.00	0.95	1.01
OH	1.09	1.16	1.16	0.62	0.74	1.07	1.09	1.12	0.37	1.53
H_2O	0.91	0.84	0.84	1.38	1.26	0.93	0.91	0.88	0.47	1.63

The analyses are normalized on the basis of five cations.
*The H_2O content is calculated to obtain (OH + H_2O) = 2.

a

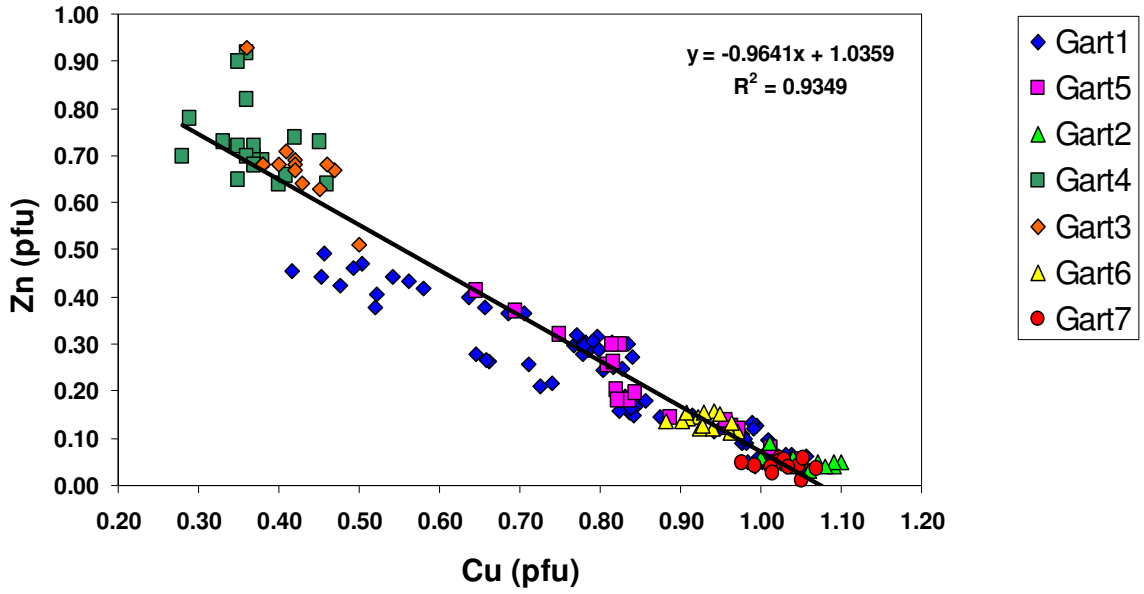

b

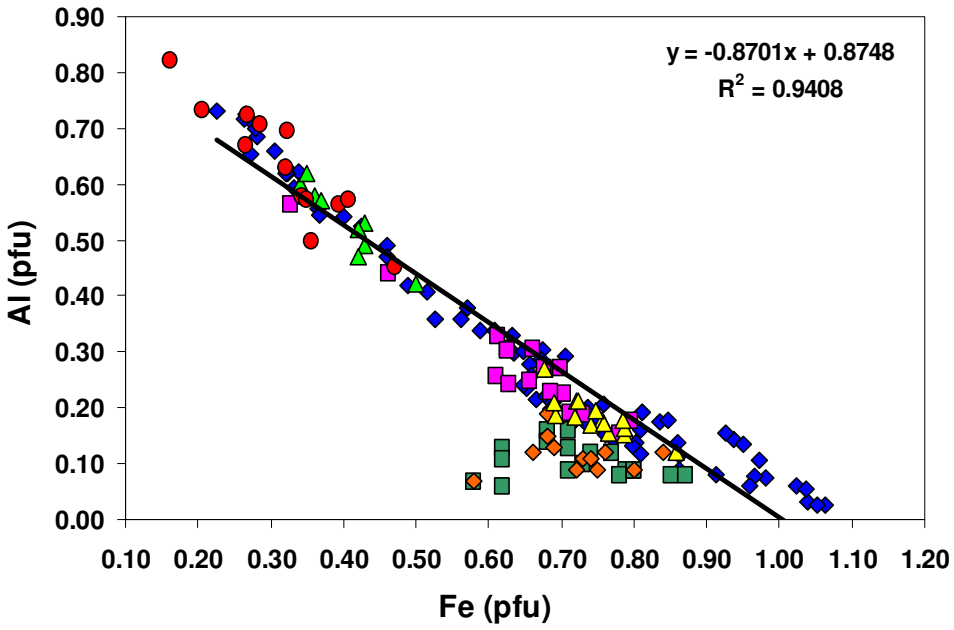

Figure 2. Bivariate plots illustrating the chemical composition of gartrellite. (a) Negative correlation between Cu and Zn. (b) Negative correlation between Fe and Al.

that the transition between zincgartrellite towards a pure Zn end-member is not proved. Like gartrellite, helmutwinklerite is triclinic, space group $P\bar{1}$, however, the two minerals are not isotypic and helmutwinklerite is not the end member of the gartrellite–zincgartrellite series. The reduction of the symmetry from monoclinic to triclinic in gartrellite is due to the ordering of cations on two *Me*(2) sites, and in helmutwinklerite is due to the presence of two H_2O molecules *pfu* and the ordering of the hydrogen bonds (Krause *et al*., 1998a; Effenberger *et al*. 2000).

A negative correlation between atoms of Fe^{3+} and atoms of Al *pfu* ($R^2 = 0.826$) (Figure 2b) shows that the major chemical variability in the *Me*2A site involves the $Fe^{3+}{}_x\ Al^{3+}{}_{x-1}$ exchange vector. The strong negative correlation however is less apparent for those analyses that correspond to zincgartrellite, due to the replacement of Fe^{3+} and Al in the *Me*2A site by Zn, up to a maximum of 0.29 *apfu*. Analyses with the highest Fe content result in > 1.00 (Fe^{3+}+Al) *apfu*, suggesting minor presence of Fe^{3+} in the *Me*2B site. $Cu^{2+} \leftrightarrow Fe^{3+}$ substitution is very rare in minerals. It is known in the plumbojarosite-beaverite solid solution, in which Cu can replace Fe^{3+} up to a ratio of Cu:Fe ~ 0.40:0.60, with Cu and Fe^{3+} occupying a single octahedrally coordinated site in the structure (Jambor and Dutrizac 1983; Breidenstein *et al*. 1992). Analyses of gartrellite from Tsumeb, Namibia; Reichenbach, Germany and Ashburton Downs (Krause *et al*. 1998a) found that Fe contents varied from ~7.8 to ~12.8 Wt.% Fe_2O_3. Up to 25 mol.% of Fe in type gartrellite can be replaced by Cu (Nickel *et al*. 1989), however, most gartrellite analyses show Cu:Fe ratios near 1:1. Mössbauer spectroscopy of ferrilotharmeyerite, tsumcorite, gartrellite and zincian gartrellite indicates that all Fe in the tsumcorite group minerals is present as Fe^{3+} (Krause *et al*., 1998a).

Al-dominant gartrellite was approved as a new mineral species, yancowinnaite, by the IMA Commission on New Minerals, Nomenclature and Classification (IMA 2010-030) in July 2010. The highest Al concentrations are associated with higher Cu content (and lower Zn content). The positive correlation between atoms of Cu and atoms of Al *pfu* has a correlation coefficient, R^2, of 0.846 based on a fit of a power law curve to the data (Figure 3a).

a

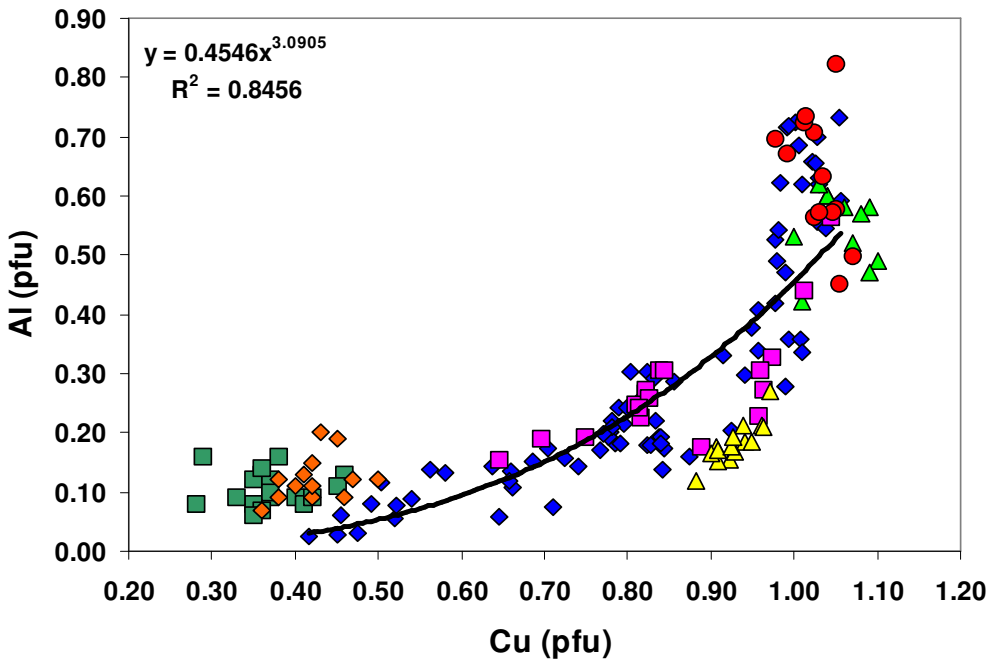

b

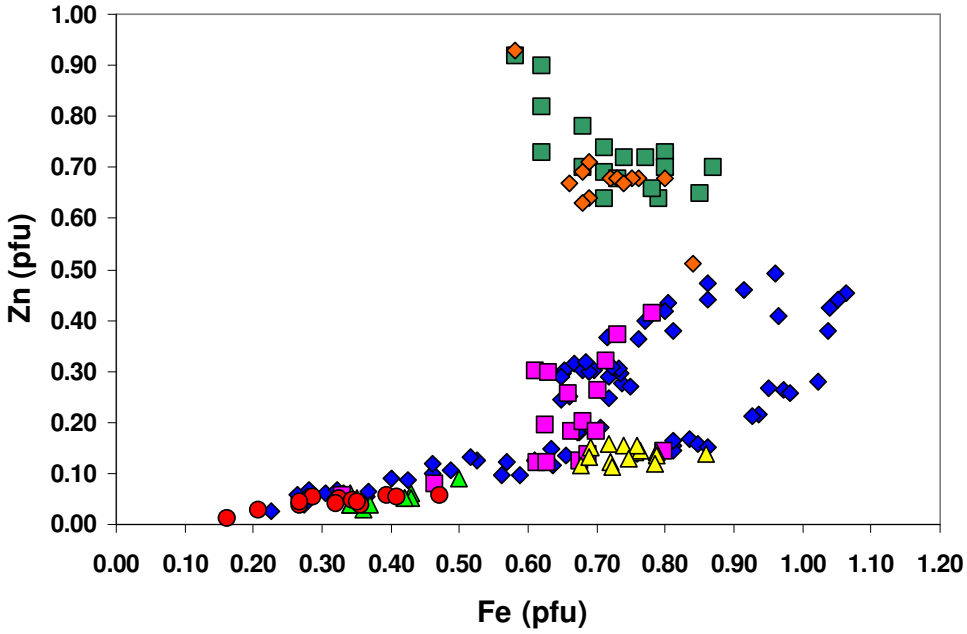

Figure 3. Bivariate plots illustrating the chemical composition of gartrellite. (a) Positive correlation between Cu and Al. (b) Positive correlation between Fe and Zn. Legend as in Figure 2.

The lowest Zn concentrations are associated with lower Fe content, and higher Al content (Figure 3b). Levels of Al higher than 0.50 *apfu* occur only for compositions containing <0.09 atoms of Zn *pfu*. At the highest Al atomic concentration of 0.82 *apfu*, the Zn content is reduced to ~0.01 atoms Zn. For Zn in amounts up to 0.50 *apfu*, there is a positive correlation between atoms of Zn and atoms of Fe *pfu*. For compositions corresponding to zincgartrellite, Zn replaces each of Cu, Fe and Al in roughly equal amounts, and Zn-rich gartrellite may be distinguished from a Zn-poor population.

The replacement of Zn by Cu in conjunction with replacement of Fe by Al is shown by the significant negative correlation between Cu+Al atoms and Zn+Fe atoms *pfu* (Figure 4) with $R^2 = 0.996$ and a slope close to –1. The following coupled substitution is suggested:

$$Cu^{2+} + Al = Zn + Fe^{3+}$$

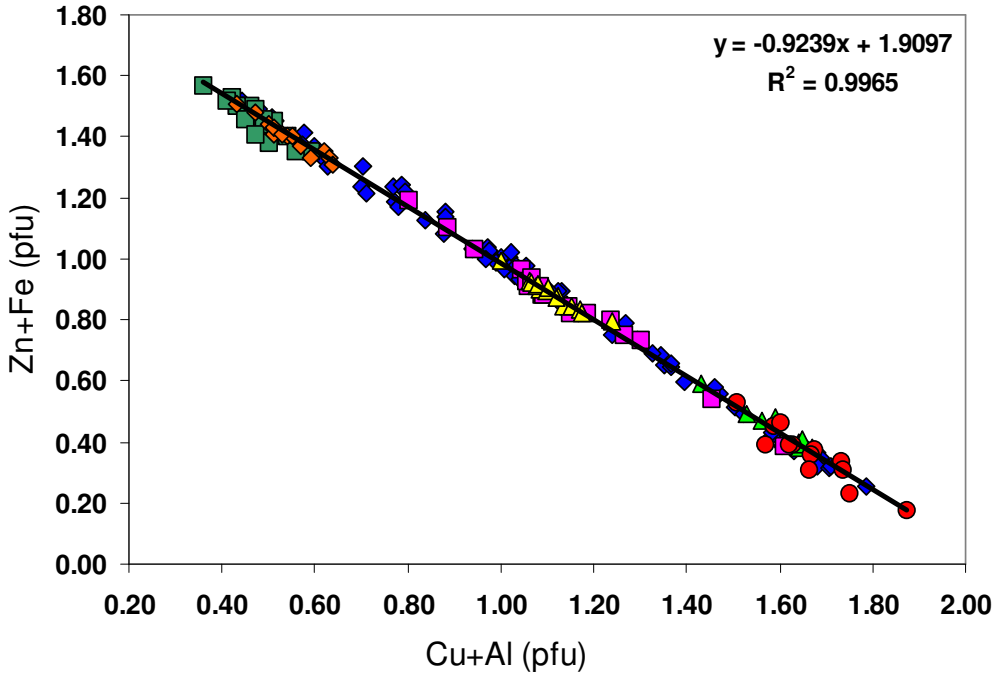

Figure 4. Bivariate plot illustrating the negative correlation between Fe+Zn and Cu+Al in gartrellite. Legend as in Figure 2.

In a Fe^{3+}–Al–(Zn+Cu) triangular projection for occupation of the *Me*2A site, all analyses are distributed the Fe^{3+} and Al fields (Figure 5). The (Zn+Cu) content for the site reaches a maximum of 0.29 *apfu*.

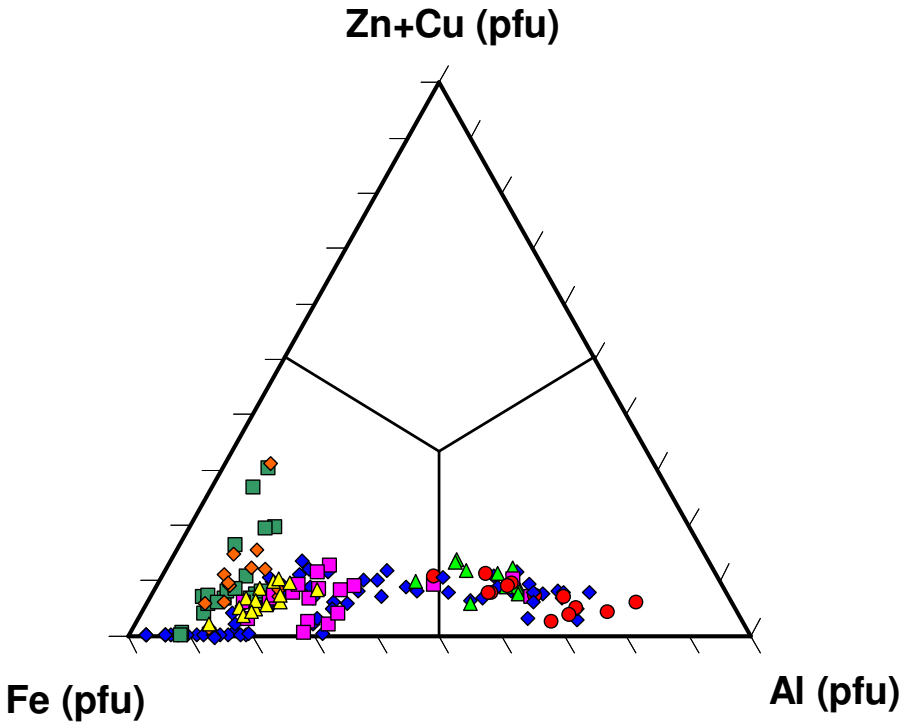

Figure 5. Ternary Fe–Al–(Zn+Cu) diagram showing the occupancy of the *Me*2A position for gartrellite as determined from electron-microprobe analysis. Additional minor Mn^{3+} is assigned to Fe. Legend as in Figure 2.

According to the chemical and structural data of Krause *et al*., (1998a) and Effenberger *et al*., (2000), Zn in gartrellite-zincgartrellite substitutes for Fe and Cu in nearly equal amounts. In gartrellite-zincgartrellite-yancowinnaite from Broken Hill, Zn in amounts up to ~2.6 Wt.% ZnO, which corresponds to 0.20 *apfu*, replaces Cu and Fe in equal amounts (Figure 6). For increasing amounts of Zn, the amount of Zn replacing Fe in the *Me*2A site remains consistent at > 0.20 *apfu*, and Zn increasingly replaces Cu in the *Me*2B site. The amount of Zn in the *Me*2A site does not exceed 0.20 *apfu* until the total Zn reaches ~11.0 Wt.% ZnO.

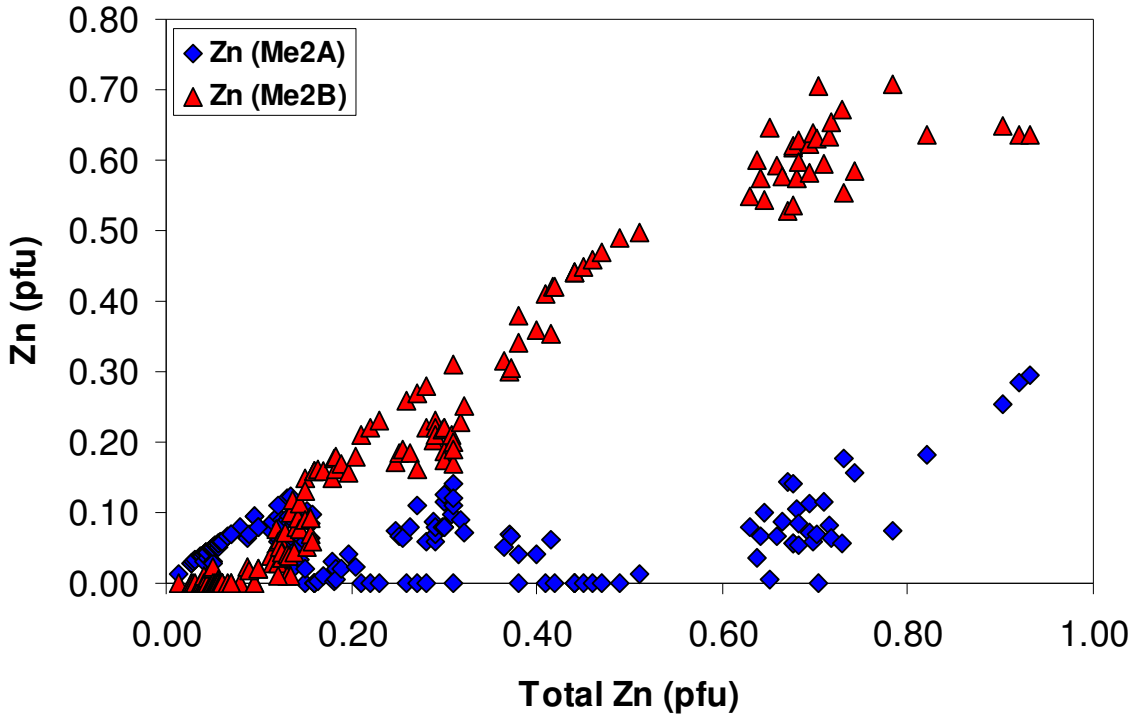

Figure 6. Bivariate plot illustrating the Zn occupancies of the *Me*2A and *Me*2B sites.

Many gartrellite crystal aggregates from the Kintore Opencut are colour-zoned, showing two distinct regions; yellow to yellow-brown cores with a bright green overgrowth. A zoned crystal aggregate is shown in Figure 7 and is designated sample Gart1 in Table 1. The results of the microprobe analyses show two chemically distinct regions.

(1) A zone rich in Zn and Fe. Electron-microprobe analyses gave: CuO 9.68 (range: 5.10–13.11), ZnO 3.38 (range: 1.27–6.12), Fe_2O_3 9.61 (range: 6.12–13.13), Al_2O_3 1.65 (range: 0.21–3.36). The composition plots in the gartrellite field, and gives a formula of $Pb_{1.03}(Fe^{3+}_{0.76}Al_{0.20},Zn_{0.03})(Cu_{0.77}Zn_{0.23})(AsO_4)_{1.97}[(OH)_{1.09}(H_2O)_{0.91}]$.

(2) A zone rich in Cu and Al. Electron-microprobe analyses gave: CuO 12.94 (range: 12.45–13.89), ZnO 0.80 (range: 0.37–1.18), Fe_2O_3 4.24 (range: 2.99–5.58), Al_2O_3 5.06 (range: 4.35–6.17). This composition represents the Al analogue of gartrellite, and gives a formula of $Pb_{1.01}(Al_{0.63},Fe^{3+}_{0.32},Zn_{0.06})Cu_{1.02}(AsO_4)_{1.96}[(OH)_{1.16}(H_2O)_{0.84}]$. This represents the first triclinic tsumcorite group mineral (gartrellite type) in which

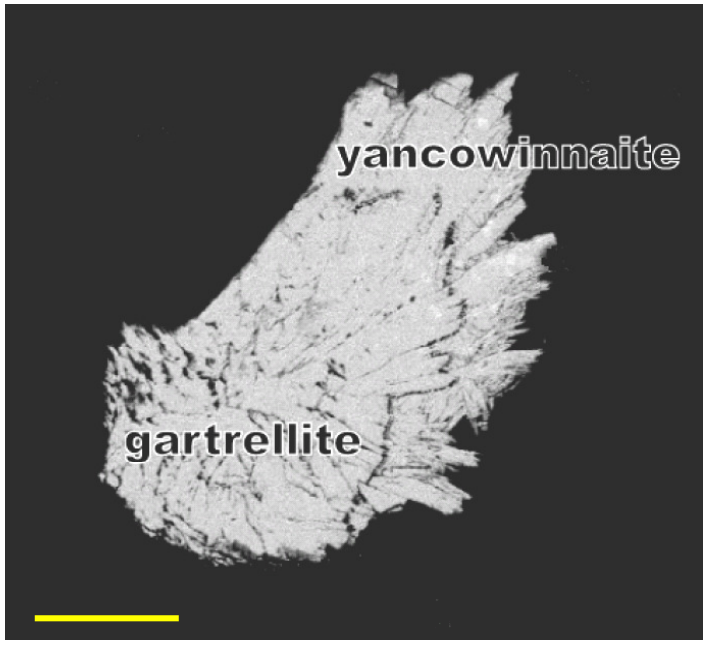

Figure 7. SEM photomicrograph showing a polished crystal aggregate of overgrowth of green yancowinnaite (top and right hand side) over yellow gartrellite (bottom and left hand side). The boundary between the two is clearly visible. The scale bar is 80 μm in length.

Al is the dominant cation in the *Me*(2)A site. The only other tsumcorite group mineral containing significant Al is cabalzarite, $Ca(Mg,Al,Fe,Mn)_2(AsO_4)_2(H_2O,OH)_2$ which lies in the middle of a solid solution series, with compositions in which either Mg^{2+} and Al^{3+} can dominate the *Me*(2) site (Brugger *et al*. 2000).

The chemical analyses show that gartrellite from Broken Hill contains only very minor Ca replacing Pb; up to 0.12 Wt%. CaO. Analyses by Krause *et al*. (1998a) and Effenberger *et al*., (2000) showed only traces of Ca in the Pb bearing tsumcorite group species ferrilotharmeyerite, gartrellite, helmutwinklerite, mounanaite, thometzekite and tsumcorite. Also, none of the Ca-dominant tsumcorite group minerals contain any appreciable Pb replacing Ca, despite their common close association with Pb minerals. The coordination environments of the Pb^{2+} and Ca cations in the tsumcorite group minerals is very similar and does not show the asymmetric coordination associated with a stereoactive $6s^2$ electron lone pair on the Pb^{2+} cation. It would thus be expected that solid solution between Pb and Ca is, at least to some extent, likely.

Gartrellite from Ashburton Downs contains up to 1.68 Wt.% SO_3 (Krause *et al*. 1998a) indicating substitution involving *di*- and *tr*ivalent anions. Substantial S (up to 11.0 Wt.%) replacing As in thometzekite was noted by Krause *et al*. (1998a), with likely charge balance mechanism $[(AsO_4)^{3-}(H_2O)]^{3-} \leftrightarrows [(SO_4)^{2-}(OH^-)]^{3-}$. Coupled substitution involving *di*- and *tr*ivalent cations was also observed in thometzekite; $[(Zn,Cu,Co,Ni)^{2+}(H_2O)]^{2+} \leftrightarrows [(Fe,Al,Mn)^{3+}(OH^-)]^2$. A correlation exists between the $Me(2)^{2+}$:$Me(2)^{3+}$ and $(AsO_4)^{3-}$:$(SO_4)^{2-}$ratios, with $(OH)^-$:(H_2O) showing very little variation, and charge balance being maintained by adjusting the $Me(2)^{3+}$:$(SO_4)^{2-}$ ratio. The analyses of gartrellite in this study did not show the presence of any S, however, the analysis of gartrellite from the Kintore Opencut, Broken Hill by Nickel *et al*., (1989) did show 0.74 Wt.% SO_3.

Although a continuous series from gartrellite to phosphogartrellite would be expected, samples of gartrellite from Tsumeb, Namibia; Reichenbach, Germany and Ashburton Downs were found to contain only very minor P replacing As (Krause *et al*. 1998a). Phosphogartrellite from the type locality, Hohenstein, Germany, contains up to 4.58 Wt.% As_2O_5 (Krause *et al*. 1998b). The analyses of gartrellite from Broken Hill in this study indicated only very minor P replacing As; only two points analysed showed the presence of P in an amount greater than 0.1 Wt.% P_2O_5.

INFRARED SPECTROSCOPY

The infrared absorption spectrum of yancowinnaite (Figure 1) was measured between 4000 and 650 cm^{-1} using a Nicolet 5700 FTIR spectrometer equipped with a Nicolet Continuum IR microscope and a diamond-anvil cell. A strong broad absorption band between 3570 and 2208 cm^{-1}, centred on about 2915 cm^{-1}, with peaks at 3198, 2362 cm^{-1} and shoulders at 2940, 2495 and 2335 cm^{-1} is attributed to OH stretching vibrations and the antisymmetric stretching mode of H_2O. The band at 1590 cm^{-1} is the H–O–H bending vibration. A strong band at 808 cm^{-1}, with a shoulder at 882 cm^{-1}, is attributed to AsO_4^{3-} stretching. The band at 1025 cm^{-1} may be the SiO_4 stretching mode, due to very minor Si for As substitution. Effenberger *et al*., (2000) noted differences in the IR spectra of the tsumcorite group minerals, with that of the helmutwinklerite type being distictive from those of the tsumcorite or gartrellite type. The spectrum of yancowinnaite from Broken Hill shows similar features to those of

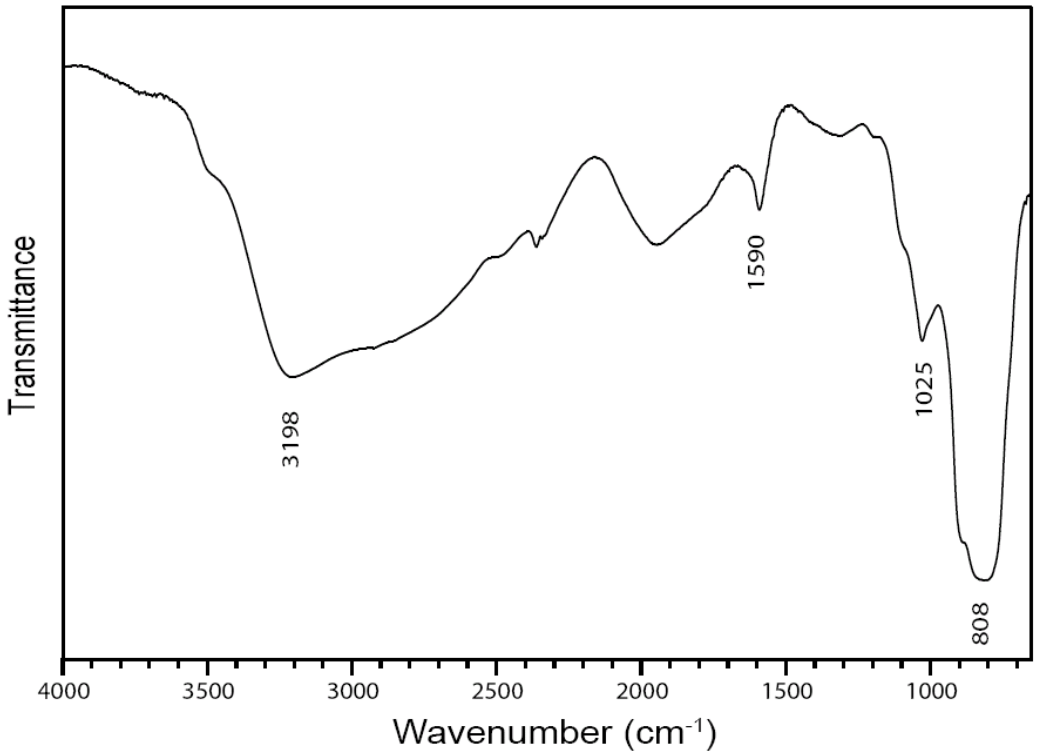

Figure 1. FT-IR spectrum of powdered yancowinnaite.

gartrellite and zincgartrellite, a broad OH stretching band and a relatively weak H_2O bending band.

STRUCTURE SOLUTION AND REFINEMENT

A platy crystal of gartrellite from the Kintore Opencut was selected by optical examination, mounted on a glass fibre and X-ray data was obtained using a Nonius KappaCCD diffractometer at the Research School of Chemistry, The Australian National University. A total of 4105 reflections were collected from $2\theta = 5.96 – 55.8°$, of which 914 were unique, with 832 classified as observed, ($|F_0| > 4\sigma_F$). The measured intensities were corrected for Lorentz and polarization effects and a Gaussian integration absorption correction, based on the crystal size and indexing of faces, was applied (Coppens 1970). Details of the data collection can be found in Table 2.

The lattice metric indicated either a C-centred monoclinic unit cell [a = 9.1059(8), b = 6.3359(5), c = 7.5742(7) Å, β = 115.768(5)°, , V = 393.53(6) or a

triclinic unit cell [a = 5.5502(5), b = 5.5413(5), c = 7.5727(7) Å, α = 69.131(6), β = 69.059(5), γ = 69.669(6)°, V = 196.68(3)]. The data were reduced in both monoclinic and triclinic symmetry and both unit cells were refined using the program HKL SCALEPACK (Otwinowski and Minor, 1997; Otwinowski *et al*. 2003). The monoclinic unit cell transforms to the triclinic cell according to the transformation matrix (½ ½ 0, ½ -½ 0, 0 0 1). The refined triclinic unit cell has the same volume as that of Krause *et al*., (1998a) for gartrellite (Table 3), which was refined from powder X-ray data, but the cell parameters of each show small differences.

Scattering curves for neutral atoms, together with anomalous-dispersion corrections, were taken from International Tables for X-Ray Crystallography (Wilson 1992). An initial attempt to solve the structure was made using the monoclinic unit cell. Intensity statistics did not provide a conclusive indication of the presence of a centre of symmetry ($|E^2-1| = 0.868$). The highest Laue symmetry indicated from the intensities of symmetry equivalent data was 2/m and the systematic absences of h00: h=2n+1, 0k0: k=2n+1, 0kl: k=2n+1, h0l: h=2n+1, hk0: h+k=2n+1, hkl: h+k=2n+1 indicated space group C2/m. An initial solution of the structure using direct methods (SHELXS-97, Sheldrick 1997a) found the positions of three heavy atoms, as would be expected in the structure, but refinement by full-matrix least-squares techniques (SHELXL-97, Sheldrick 1997b) resulted in positions of O atoms with unrealistic cation–oxygen distances and the refinement would not progress beyond R1 ~ 18%.

A refinement was then initiated in space group $P\bar{1}$, using SHELXL-97 (Sheldrick 1997b), and starting with the atom coordinates of Krause *et al*., (1998a) for gartrelltite. The structure refined to an R1 index of 15.5% for an isotropic displacement model. Conversion to anisotropic displacement factors for all of the atoms in the structure resulted in convergence to an agreement index (R1) of 9.29% calculated for 832 observed reflections $F_o^2 > 4\sigma(F_o^2)$. The addition of an isotropic-extinction factor did not improve the results. Hydrogen atoms were not able to be located in the difference Fourier map. The final atomic coordinates and anisotropic-displacement parameters are given in Table 4 and selected interatomic distances in Table 5.

Table 2. Crystal data, data collection and refinement details.

Crystal data	
Formula (ideal)	$Pb(Cu,Zn)(Fe,Al,Zn)(AsO_4)_2(OH,H_2O)_2$
Space group	$P\bar{1}$
a,*b*,*c* (Å)	5.550(5), 5.541(5), 7.573(7)
α, β, γ (°)	69.131(6), 69.059(5), 69.669(6)
V (Å^3), Z	196.83(3), 1
F(000)	284
μ (mm^{-1})	34.457
Absorption correction	Gaussian integration
Crystal dimensions (mm)	0.10 x 0.08 x 0.03
Data collection	
Diffractometer	Nonius KappaCCD
Temperature (K)	293
Radiation	Mo$K\alpha$, λ = 0.71073 Å
Crystal detector distance (mm)	40
Rotation axis, width (°)	ϕ, ω 2.0
Total number of frames	281
Collection time per degree (s)	20
θ range (°)	3.01 to 28.21 deg.
h,k,l ranges	-7 → 7, -7 → 7, -9 → 9
Total reflections measured	4105
Data completeness (%)	94.4
Unique reflections	914 (R_{int} = 0.2946)
Refinement	
Refinement on	F^2
$R1^*$ for $F_0 > 4\sigma(F_0)$	9.29%
w$R2^\dagger$ for all F_0^2	21.95%
Reflections used $F_o^2 > 4\sigma(F_o^2)$	832
Number of parameters refined	77
Extinction coefficient	none
GooF	1.120
$(\Delta/\sigma)_{max}$	0.0001
$\Delta\rho_{max}$, $\Delta\rho_{min}$ (e/Å)	8.036, -5.721

$^*R1 = \Sigma||F_O|-|F_C|| / \Sigma|F_O|$

$^\dagger wR2 = \Sigma w(|F_O|^2-|F_C|^2)^2 / \Sigma w|F_O|^2)^{1/2}$; $w = 1/[\sigma^2(F_o^2) + (0.042\ P)^2 + 12.60\ P]$;
$P = ([\text{max of } (0 \text{ or } F_0^2)] + 2F_C^2)/ 3$

Table 3. Comparison of gartrellite and zincgartrellite.

	Gartrellite	Gartrellite	Zincgartrellite
Locality	Broken Hill, NSW, Australia	Ashburton Downs, WA, Australia	Tsumeb mine, Namibia
Reference	this work	Krause *et al*. (1998a)	Effenberger *et al*. (2000)
Formula	$Pb_{1.02}(Cu_{0.65}Zn_{0.47}Fe^{3+}_{0.80}Al_{0.08})_{2.01}(AsO_4)_{2.00}(OH)_{1.03}(H_2O)_{0.97}$	$Pb_{1.04}(Cu_{1.12}Fe^{3+}_{0.82}Zn_{0.02}Al_{0.01})_{1.97}[(AsO_4)_{1.83}(SO_4)_{0.13}]_{1.96}(OH)_{1.10}(H_2O)_{1.03}$	$(Pb_{0.97}Ca_{0.04})_{1.01}(Zn_{0.91}Cu_{0.51}Fe^{3+}_{0.59}Al_{0.03})_{2.04}[(AsO_4)_{1.96}(SO_4)_{0.01}]_{1.97}(OH)_{0.81}(H_2O)_{1.31}$
Symmetry	triclinic	triclinic	triclinic
Space group	$P\bar{1}$	$P\bar{1}$	$P\bar{1}$
a (Å)	5.550(5)	5.460(1)	5.550(1)
b (Å)	5.541(5)	5.653(1)	5.620(1)
c (Å)	7.573(7)	7.589(1)	7.621(1)
α	69.059(5)	67.68(1)	68.59(1)
β	69.131(6)	69.27(1)	69.17(1)
γ	69.669(6)	70.04(1)	69.51(1)
V (Å^3),	196.68(3)	196.8(1)	200.1
Z	1	1	1

Table 4. Fractional coordinates and displacement parameters (Å^2) for atoms for gartrellite.

	x	y	z	U_{eq}
Me(1)	0	0	0	0.0337(5)
Me(2a)	0	0.5	0.5	0.0253(11)
Me(2b)	0.5	0	0.5	0.0231(11)
As	0.4180(3)	0.4171(3)	0.7866(2)	0.0217(7)
O(1)	0.158(2)	0.159(2)	0.4115(17)	0.027(2)
O(2)	0.308(2)	0.308(2)	0.6500(18)	0.033(3)
O(3a)	0.2472(19)	0.685(2)	0.2668(15)	0.029(2)
O(3b)	0.6840(19)	0.247(2)	0.2676(16)	0.030(2)
O(4)	0.278(2)	0.280(3)	0.0200(16)	0.037(3)

	U_{11}	U_{22}	U_{33}	U_{12}	U_{13}	U_{23}
Me(1)	0.0306(6)	0.0321(7)	0.0265(7)	-0.0028(5)	-0.0035(4)	-0.0036(4)
Me(2a)	0.0187(13)	0.0224(16)	0.0209(15)	-0.0003(10)	-0.0006(9)	0.0003(9)
Me(2b)	0.0175(14)	0.0204(16)	0.0179(15)	-0.0003(10)	-0.0008(9)	0.0017(9)
As	0.0194(9)	0.0195(11)	0.0175(10)	-0.0010(7)	-0.0025(6)	-0.0015(6)
O(1)	0.021(4)	0.019(5)	0.028(5)	-0.004(4)	0.000(4)	0.001(4)
O(2)	0.036(5)	0.032(6)	0.032(5)	-0.003(5)	-0.008(4)	-0.017(4)
O(3a)	0.023(4)	0.027(6)	0.025(5)	0.000(4)	-0.005(4)	-0.002(3)
O(3b)	0.029(4)	0.016(5)	0.030(5)	0.002(4)	-0.004(4)	-0.002(3)
O(4)	0.033(5)	0.048(7)	0.020(4)	-0.004(5)	0.001(4)	-0.012(5)

Note: The anisotropic displacement factors (U_{ij}) are defined as $\exp[-2\pi^2\Sigma^3_{i=1}\Sigma^3_{\varphi=1}3jU_{ij}\mathbf{a_i}^*\ \mathbf{a_j}^*\ h_ih_j]$.

Table 5. Selected interatomic distances (Å), angles (°) for gartrellite.

Me(1)	O3A	2.569(10)	Me(2b)	O3B	1.971(11)
	O3A	2.569(10)		O3B	1.971(11)
	O4	2.601(12)		O1	1.999(11)
	O4	2.601(12)		O1	1.999(11)
	O3B	2.667(10)		O2	2.204(12)
	O3B	2.667(10)		O2	2.204(12)
	O2	2.863(10)	<Me-O>		2.058
	O2	2.863(10)			
<Me-O>		2.675			
Me(2a)	O3A	1.973(10)	As	O4	1.647(11)
	O3A	1.973(10)		O3A	1.661(9)
	O1	2.089(11)		O3B	1.709(11)
	O1	2.089(11)		O2	1.724(11)
	O2	2.103(12)	<As-O>		1.685
	O2	2.103(12)			
<Me-O>		2.055			
O3A–*Me*2A–O1		90.8(5)	O3B–*Me*2B–O1		90.7(5)
O3A–*Me*2A–O1		89.2(5)	O3B–*Me*2B–O1		89.3(5)
O3A–*Me*2A–O1		89.2(5)	O3B–*Me*2B–O1		89.3(5)
O3A–*Me*2A–O1		90.8(5)	O3B–*Me*2B–O1		90.7(5)
O3A–*Me*2A–O2		91.6(4)	O3B–*Me*2B–O2		89.4(4)
O3A–*Me*2A–O2		88.4(4)	O3B–*Me*2B–O2		90.6(4)
O1–*Me*2A–O2		80.2(4)	O1–*Me*2B–O2		100.2(4)
O1–*Me*2A–O2		99.8(4)	O1–*Me*2B–O2		79.8(4)
O3A–*Me*2A–O2		88.4(4)	O3B–*Me*2B–O2		90.6(4)
O3A–*Me*2A–O2		91.6(4)	O3B–*Me*2B–O2		89.4(4)
O1–*Me*2A–O2		99.8(4)	O1–*Me*2B–O2		79.8(4)
O1–*Me*2A–O2		80.2(4)	O1–*Me*2B–O2		100.2(4)
<O-Me-O>		90.0	<O-Me-O>		90.0
O4–As–O3A		111.8(6)			
O4–As–O3B		109.6(6)			
O3A–As–O3B		111.6(5)			
O4–As–O2		106.2(6)			
O3A–As–O2		106.9(5)			
O3B–As–O2		110.6(6)			
<O-As-O>		109.5			

DESCRIPTION OF THE STRUCTURE

The structure of gartrellite is topologically identical to that of other tsumcorite-group minerals. The Pb atom at the *Me*(1) site [special position *e* (0, 0, 0)] is coordinated by eight O atoms to form distorted square-antiprism (Figure 8). The site occupancy refinement and electron-microprobe results indicate that the site is completely occupied by Pb^{2+}.

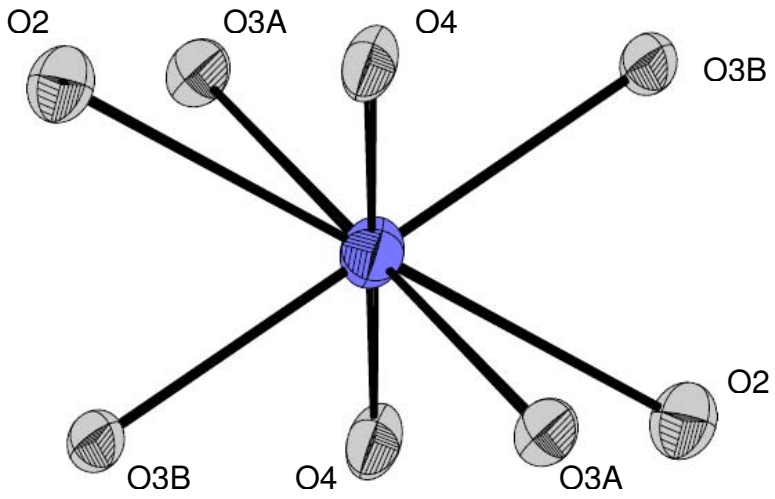

Figure 8. Coordination of the *Me*(1) site in the structure of gartrellite. All structure drawings were completed using ATOMS (Shape Software 1997).

Pb^{2+} is commonly lone-pair stereoactive, which typically results in a very asymmetrical coordination, with the lone pair of electrons positioned on the opposite side of the atom to the coordinating anions. However, the coordination of the Pb^{2+} cation *Me*1 site in gartrellite is relatively symmetrical, and does not show the one-sided coordination typical of a Pb^{2+} cation that is lone-pair stereoactive. The bond-valence sum for the Pb site, calculated using the parameters of Brown and Altermatt (1985), is 1.83 *vu*. Recalculation using the bond-valence parameters of Krivovichev and Brown (2001) gave a sum of 1.92 *vu*.

The *Me*2A site, at (1/2, 0, 1/2), and the *Me*2B site, at (0, 1/2, 1/2), are both located on special positions (Wyckoff positions *f* and *g* respectively with site symmetry $\bar{1}$). Each site is coordinated by six oxygen atoms in a distorted octahedral arrangement. Due to variations in *d*-electron configuration of the transition element

cations occupying the *Me*2A and *Me*2B sites, differences are observed between their coordination polyhedra. The *Me*2A site shows a distinct [4+2]-coordination with *Me*–O distances of 2 × 1.965, 2 × 2.001 and 2 × 2.200 Å, while the *Me*2A site shows a more regular coordination with *Me*–O distances of 2 × 1.975, 2 × 2.092 and 2 × 2.103 Å.

The polyhedral distortion can be evaluated in terms of bond length distortion (BLD) (Renner and Lehmann 1986), edge length distortion (ELD) (Renner and Lehmann, 1986) and octahedral angle variance (OAV) (Robinson *et al*., 1971). The greater bond-length distortion exhibited by the *Me*2B octahedron compared to the *Me*2A octahedron (Table 5) is consistent with the occupancy of the site by Cu^{2+} ($3d^9$ configuration). Virtually all $Cu^{2+}\phi_6$ octahedra in mineral structures are distorted (Burns and Hawthorne, 1996) owing to the Jahn-Teller effect (Jahn and Teller, 1937) that is associated with the electronic energy-degeneracy of a d^9 cation in an octahedral ligand-field.

Table 6. Comparison of polyhedral distortion parameters for the *Me*2B site in gartrellite and zincgartrellite.

	gartrellite	gartrellite	zincgartrellite
Reference	this work	Krause *et al*. (1998a)	Effenberger *et al*. (2000)
<*Me*–O>	2.057	2.079	2.099
<O–O>	2.908	2.939	2.947
BLD* (%)	4.73	6.80	4.13
ELD** (%)	4.82	7.46	5.60
OAV§	38.14	80.25	59.21

* Bond length distortion (BLD) = $(100/n)\sum^{n}_{i=1}\{[(X–O)_i – (<X –O>)]/(<X –O>)\}$, with n = number of bonds, $(X–O)_i$ = central cation±oxygen bond length and (<*X* –O>) = average cation-oxygen bond length (Renner and Lehmann, 1986). ** Edge length distortion (ELD) = $(100/n)\sum^{n}_{i=1}\{[(O–O)_i – (<O–O>)]/(< O–O>)\}$, with n = number of edges, $(O–O)_i$ = polyhedron edge length and <O–O> = average polyhedron edge length (Renner and Lehmann, 1986). § Octahedral angle variance (OAV) = $\sum^{n}_{i=1}(\theta_i – 90)^2/11$ (Robinson *et al*., 1971).

Eby and Hawthorne (1993) have shown that there is a very strong bimodal distribution of Cu–ϕ (ϕ: O^{2-}, OH, H_2O) distances in Cu^{2+} oxysalt minerals, with

maxima at 1.97 and 2.44 Å. The apical Cu–O bond distance for the *Me*2B site (2.200 Å) is considerably less than 2.44 Å and is at the lower end of the range of apical Cu–O distances (2.20–2.80 Å) quoted by Eby and Hawthorne (1993), which is consistent with replacement of some Cu by Zn.

Site refinement of the Cu:Zn content of the *Me*2B site was not possible because of the similar scattering factors for Cu and Zn. Similarly, the ionic radii of Cu^{2+} (0.73 Å) and Zn (0.74 Å) (Shannon 1976) preclude calculation of their relative occupancies from differences in ionic radii. The lower bond-length distortion for the *Me*2B site compared to that in gartrellite (Krause *et al*. (1998a) and the higher bond-length distortion compared to that in zincgartrellite (Effenberger *et al*. 2000) are consistent with the presence of lower and greater relative occupancy of the site by Cu.

The *Me*2A site has a refined site-scattering value of 26.19 *epfu*. The crystal that was used for structure determination was not analysed, however, taking into consideration the range of Fe, Al and Zn content from the microprobe analysis (Table 1), an occupancy of the site near $Fe^{3+}_{0.80}Al_{0.08}Zn_{0.12}$, which gives a calculated site-scattering of 25.44 *epfu*, is suggested. The calculated mean bond-length for this occupancy, using the hard-sphere model, where each ion is considered to be a sphere of a specific size, and the ionic radii of Shannon (1976), is equal to 1.347 + 0.648 = 1.994 Å which compares to the observed value of 2.057 Å (Table 5).

The bond-valence sum for the *Me*2A site, calculated using the parameters of Brown and Altermatt (1985) is 2.62 *vu* (Table 7) suggesting occupancy by both *di*- and *tr*ivalent cations. The bond-valence sum for *Me*2B site, 2.27 *vu*, is higher than the ideal of 2.00 *vu* expected for full occupancy by divalent cations. Bond-valence sums for *Me*2B site in gartrellite (Krause *et al*., 1998a) and zincgartrellite (Effenberger *et al*., 2000) are also higher than expected (2.22 and 2.15 *vu* respectively). These values are however, within the range of about ±20% of the mean value for bond valences found for cations in a wide range of crystal structures by Brown (1981).

The structure of gartrellite contains one As site which is coordinated by four O atoms in a tetrahedral arrangement. The electron-microprobe data, refined site-occupancy and bond-valence analysis confirm that the site is completely occupied by

As^{5+} plus very minor Si. Individual bond lengths range from 1.647(11) to 1.724(11), with an <As–O> distance of 1.685 Å which is in good agreement with the value of 1.69 Å expected from the sums of effective ion radii for $^{[4]}As^{5+}$ and $^{[3]}O^{2-}$ (Shannon 1976), and with the reported grand mean <As–O> value of 1.682 Å (Baur, 1981). The O–As–O angles range from 106.2(6) to 111.8(6)°. The AsO_4 tetrahedron in gartrellite (this study) shows a marked decrease in bond length distortion, edge length distortion and tetahedral angle variance with respect to the corresponding parameters observed for gartrellite (Krause *et al*., 1998a) and a small decrease with respect to those for zincgartrellite (Effenberger *et al*. 2000) (Table 6).

*Me*2A and *Me*2B octahedra alternate and share *trans* edges to form a [$M\phi_4$] chain that extends along [110] (Figure 9). Chains link by sharing (AsO_4) tetrahedron vertices to form a sheet of the form [$(Me2(OH)_2(AsO_4)_2]$] in the (001) plane (Figure 10).

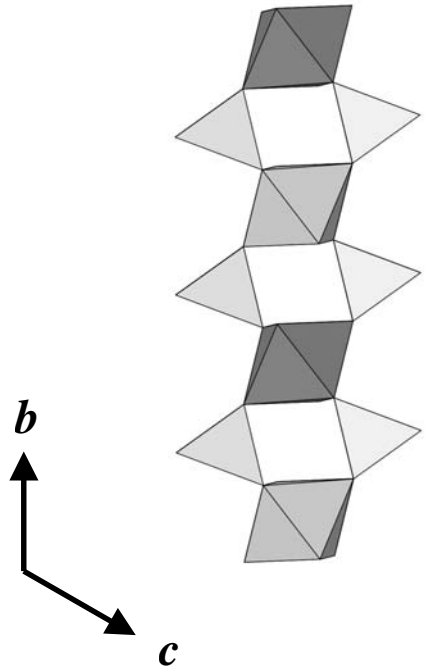

Figure 9. The [$(M_2(OH)_2(AsO_4)_2]$] sheet in gartrellite projected onto the (1-10) plane. *Me*2Aϕ_6 octahedra are dark grey; *Me*2Bϕ_6 octahedra are pale grey Asϕ_4 tetrahedra are pale grey.

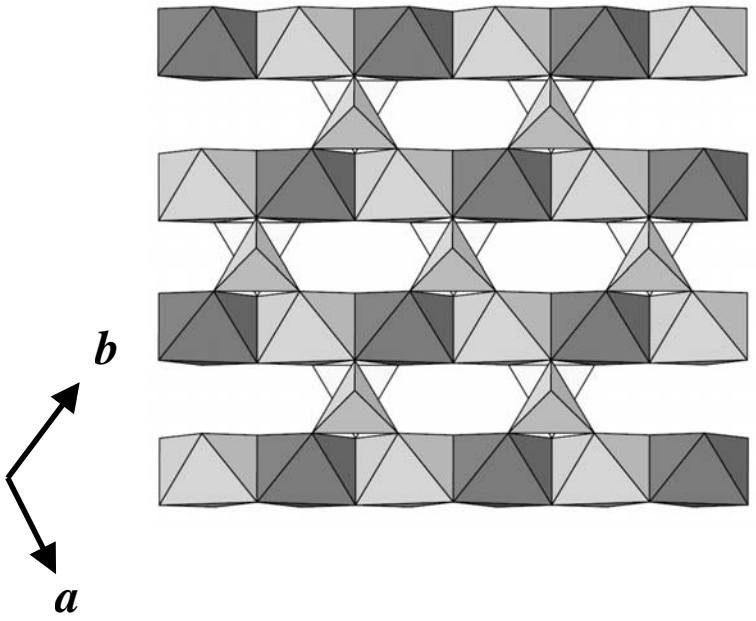

Figure 10. The $[(M_2(OH)_2(AsO_4)_2]$ sheet in gartrellite projected onto the (1-10) plane. *Me*2Aϕ_6 octahedra are dark grey; *Me*2Bϕ_6 octahedra are pale grey Asϕ_4 tetrahedra are pale grey.

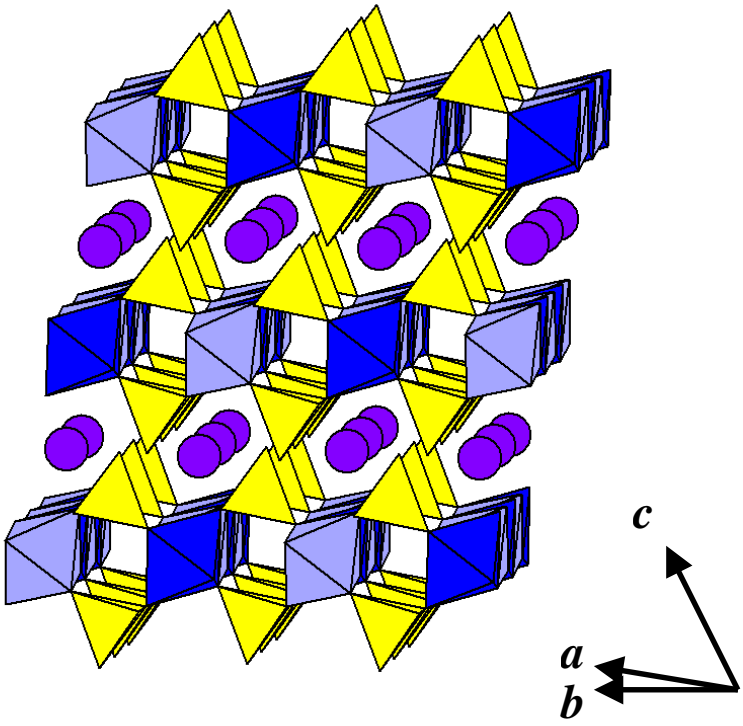

Figure 11. The crystal structure of gartrellite projected onto a plane close to (10-1). *Me*2Aϕ_6 octahedra are dark blue; *Me*2Bϕ_6 octahedra are pale blue Asϕ_4 yellow.

The sheets are linked in the *c*-direction by PbO_8 square-antiprisms and by hydrogen bonds (Figure 11).

HYDROGEN BONDING

The positions of the hydrogen atoms in the structure were not able to be located in difference Fourier maps. Peaks in the electron density map reasonable for H atoms were located at (0.3720, 0.8233, 0.21073) and (0.3956, 0.9924, 0.0032). These positions have the expected O1–H distances and O1–H…*A* angles and correspond to the H atom positions in the structures of other tsumcorite group minerals (eg. cabalzarite, Brugger *et al*. 2000). However these peaks would not refine reliably as H atoms were not included in the final refinement.. Inferred positions of the H atoms are shown in Figure 12. The H2–H2 distance is ~1.1 Å so the site would not be expected to be 100% occupied.

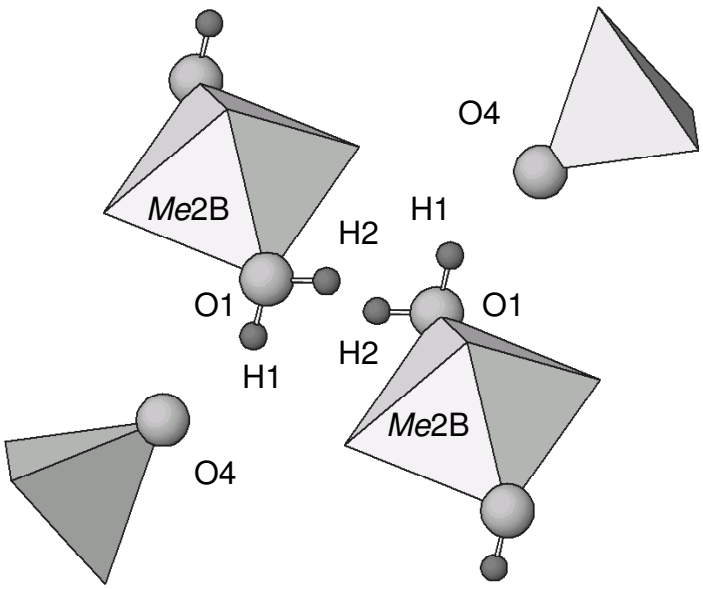

Figure 12. Details of the hydrogen bonding in gartrellite.

The bond valence sum around the O1 anion (0.82 *vu*) (Table 7) lies between the values expected for donor atoms of OH^- groups (~ 1.0 *vu*) and H_2O molecules (~0.5 *vu*) indicating a mixed occupancy of the site.

Table 7. Bond valence table for gartrellite.

	Me(1)	Me(2a)	Me(2b)	As	Sum
O(1)		0.40 ↓→	0.43 ↓→		0.83
		0.40 ↓	0.43 ↓		
O(2)	0.16 ↓→	0.38 ↓→	0.25 ↓→	1.12	1.91
	0.16 ↓	0.38 ↓	0.25 ↓		
O(3a)	0.29 ↓→	0.54 ↓→		1.33	2.16
	0.29 ↓	0.54 ↓			
O(3b)	0.24 ↓→		0.46 ↓→	1.16	1.86
	0.24 ↓		0.46 ↓		
O(4)	0.27 ↓→			1.38	1.65
	0.27 ↓				
Sum	1.92	2.64	2.28	4.99	

Note: Bond-valences for the *Me*(2a) site are based on an occupancy of $Cu_{0.80}Zn_{0.20}$ and for the *Me*(2b) site an occupancy of $Fe^{3+}_{0.80}Al_{0.08}Zn_{0.12}$.

In the natural and synthetic compounds of the tsumcorite group, the *Me*(1) site can be occupied by by *mono*-, *di*- or *tri*-valent cations, the *Me*(2) site can be occupied by by two- or three-valent cations and the *X* site can be occupied by *penta*- or *hexa*-valent cations. Charge balance is maintained by adjusting the ratio $OH:H_2O$ with the coupled substitution:

$$Me2^+ + H_2O = Me^{3+} + OH^-$$

The bond valence analysis shows that O4 (*vu* = 1.65) would be expected to be an acceptor of a hydrogen bond with an O1…O4 distance of 2.66 Å, characteristic of strong hydrogen bonding. The O2 anion, with a bond valence sum of 1.90 *vu* and on O1–O2 distance of 2.698 A forms a shared edge of the *Me*2A and *Me*2B octahedra,

and thus is a highly improbable receptor for a hydrogen bond (Baur 1972, 1973). The O3A and O3B anions are probable acceptors of weak hydrogen bonds with O…O1 distances of 2.957 and 3.093 Å respectively.

The O1 anion is adjacent to an inversion centre at (0, 0, 0.5), resulting in a quite short O1…O1 distance of 2.569 Å. A strong, symmetry restricted hydrogen bond is formed between the two adjacent O1–H groups. The hydrogen-bonding scheme is:

O(4)–H(2)…O(1)…H(1)–O(1)…H(2)–O(4)
↑↓
O(4)–H(2)…O(1)–H(1)…O(1)…H(2)–O(4)

As a consequence, as observed by Krause *et al*., (1998a), H_3O^+ groups are formed in the tsumcorite type structures. H_3O^+ groups had previously been noted in natrochalcite type structures as well as a number of other compounds (Clearfield *et al*., 1976; Chevrier *et al*. 1990; Chevrier *et al*. 1993 and references therein).

Kampf *et al*. (1984) proposed an acid arsenate group for lotharmeyerite based on a broad absorption centered on 2800 cm^{-1} in the IR spectrum, similar to the absorptions for strongly bonded OH in PO_3OH (Ross 1974), AsO_3OH (Sumin de Portialla 1981) and VO_3OH (Harlow *et al* 1984). Non-acid arsenate groups have expected sharper absorption at ~3580 cm^{-1}. Even though the X-O2 distance is the longest in the XO_4 groups, Krause *et al*. (1998a) considered that the XO_4 groups in the tsumcorite group minerals are not protonated, based on crystal-chemical reasons and IR spectra.

STRUCTURAL RELATIONS

[$MT\phi_4$] chains of edge-sharing octahedra are found as a fundamntal building block in a wide variety of oxysalt mineral structures. Chains are usually decorated by tetrahedral oxyanions in a staggered arrangement on either side of the chain along its length. Isolated [$MT\phi_4$] chains occur in the structures of the linarite, $PbCu(OH)_2SO_4$, (Bachmann and Zemann, 1961; Araki, 1962; Effenberger 1987) brackebuschite, $PbMn^{2+}(VO_4)_2H_2O$, (Foley and Hughes 1997), fornacite, $PbCu^{2+}(AsO_4)(CrO_4)OH$, Cocco *et al*. 1967 and vauquelinite, $PbCu^{2+}(PO_4)(CrO_4)OH$, (Fanfani and Zanazzi 1968) group minerals.

Decorated chains can polymerize to form octahedron-tetrahedron linked sheets of general form $[M(TO_4)\phi]$ in the monoclinic tsumcorite-group minerals, the bermanite-group minerals (e.g., bermanite, $Mn^{2+}Mn^{3+}(PO_4)(OH)_2{\cdot}4H_2O$, Kampf and Moore 1976) and in ercitite, $NaMn^{3+}{}_2(PO_4)(OH){\cdot}2H_2O$, (Cooper *et al*., 2009), and sheets of general form $[(M_2(OH)_2(TO_4)_2]$ in the triclinic tsumcorite-group minerals. Sheets with identical topology are found in the structure of natrochalcite and are linked via 8-coordinated Na atoms (Chevrier *et al*., 1993). Many synthetic natrochalcite-type compounds are also known (eg. Chevrier *et al*., 1993; Krickl and Wildner, 2007 and references therein).

Octahedron-tetrahedron linked $[(M_2(OH)_2(TO_4)_2]$ sheets are also found in the structures of medenbachite, neustädtelite and cobaltneustädtelite, however, in these structures the tetrahedra which link the chains adopt a different arrangement along the length of the chain (Figure 13).

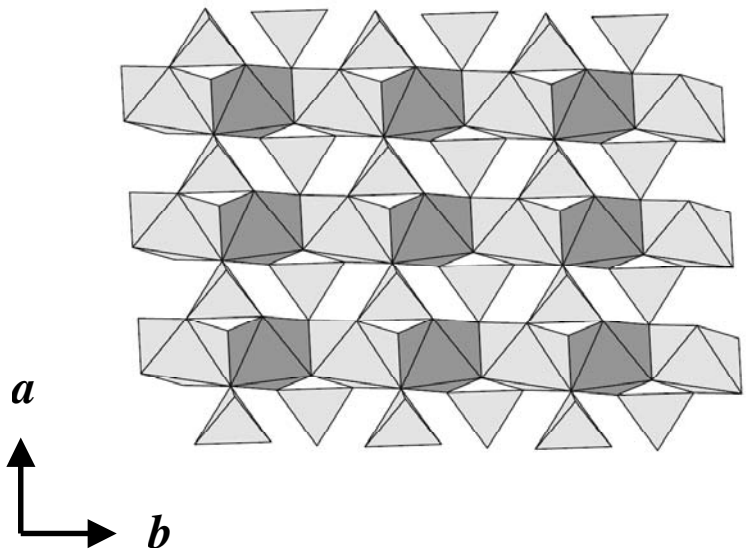

Figure 13. The $[(M_2(OH)_2(AsO_4)_2]$ sheet in medenbachite projected onto a plane close to (001) with the sheet tilted 5° about a horizontal axis to give a clearer view of the polyhedron linkage.

$[MT\phi_4]$ chains can also polymerize to form octahedron-tetrahedron linked heteropolyhedral frameworks as in the descloizite-group minerals, the conichalcite-group minerals and in numerous silicate minerals.

ACKNOWLEDGEMENTS

We thank Angus Netting and John Terlet of Adelaide Microscopy, The University of Adelaide for their assistance with the microprobe analysis. Hayley Brown provided assistance with collecting the infrared spectrum of yancowinnaite.

REFERENCES

Araki, T. (1962) The crystal structure of linarite, reexamined. Mineralogical Journal, 3, 282–295.

Bachmann, H.G. and Zemann, J. (1961) Die Kristallstruktur von Linarit, $PbCuSO_4(OH)_2$. Acta Crystallographica, 14, 747–753.

Baur, W.H. (1972) Prediction of hydrogen bonds and hydrogen atom positions in crystalline solids. Acta Crystallographica, B28, 1456–1465.

Baur, W.H. (1973) Criteria for hydrogen bonding. II. A hydrogen bond in the edge of a coordination polyhedron around a cation. Acta Crystallographica, B29, 139–140.

Beran, A., Giester, G. and Libowitzky, E. (1997) The hydrogen bond system in natrochalcite-type compounds - an FTIR spectroscopic study of the $H_3O_2^-$ unit. Mineralogy and Petrology, 61, 22–235.

Breidenstein, B., Schlüter, J. and Gebhard, G. (1992) On beaverite: new occurrence, chemical data and crystal structure. Neues Jahrbuch für Mineralogie, Monatshefte 213–220.

Brown, I.D. (1981) The bond-valence method: an empirical approach to chemical structure and bonding. In M. O'Keefe and A. Navrotsky, Eds., Structure and Bonding in Crystals. Academic Press, London.

Brown, I.D. and Altermatt, D. (1985) Bond-valence parameters obtained from a systematic analysis of the inorganic crystal structure database. Acta Crystallographica, B41, 244–247.

Brugger, J, Meisser, N., Schenk, K., Berlepsch, P., Bonin, M., Armbruster, T., Nyfeler, D. and Schmidt, S. (2000) Description and crystal structure of cabalzarite $Ca(Mg,Al, Fe)_2(AsO_4)_2(H_2O,OH)_2$, a new mineral of the tsumcorite group. American Mineralogist, 85, 1307–1314.

Brugger, J., Krivovichev, S., Kolitsch, U., Meisser, N., Andrut, M., Ansermet, S. and Burns, P.C. (2002) Description and crystal structure of manganlotharmeyerite, $Ca(Mn_{3+},\square,Mg)_2\{AsO_4,[AsO_2(OH)_2]\}_2(OH,H_2O)_2$, from the Starlera Mn deposit, Swiss Alps, and a redefinition of lotharmeyerite. Canadian Mineralogist, 40, 1597–1608.

Burns, P.C., and Hawthorne, F.C. (1996) Static and dynamic Jahn-Teller effects in Cu^{2+} oxysalts. Canadian Mineralogist, 34, 1089–1105.

Chevrier, G., Giester, G., Jarosch, D. and Zemann, J. (1990) Neutron diffraction study of the hydrogen-bond system in $Cu_2K(H_3O_2)(SO_4)_2$. Acta Crystallographica, C46, 175–177.

Chevrier, G., Giester, G. and Zemann, J. (1993) Neutron refinements of $NaCu_2(H_3O_2)(SO_4)_2$ and $RbCu_2(H_3O_2)(SeO_4)_2$: variation of the hydrogen bond system in the natrochalcite-type series. Zeitschrift für Kristallographie, 206, 7–14.

Clearfield, A., Sims, M.J. and Gopal, R. (1976) Studies in heavy-metal molybdates. 1. Crystal structure of a basic zinc molybdate, $NaZn_2OH(H_2O)(MoO_4)_2$. Inorganic Chemistry, 15, 335–338.

Cocco, G., Fanfani, L. and Zanazzi, P.F. (1967) The crystal structure of fornacite. Zeitschrift für Kristallographie, 124, 385–397.

Cooper, M.A., Hawthorne, F.C., and Černý, P. (2009) The crystal structure of ercitite, $Na_2(H_2O)_4[Mn^{3+}{}_2(OH)_2(PO_4)_2]$, and its relation to bermanite, $Mn^{2+}(H_2O)_4[Mn^{3+}{}_2(OH)_2(PO_4)_2]$. Canadian Mineralogist, 33, 889–905.

Coppens, P. (1970) Crystallographic Computing. F.R. Ahmed, S.R. Hall and C.P. Huber, Eds., p. 255–270. Munksgaard, Copenhagen.

Eby, R.K. and Hawthorne, F.C. (1993) Structural relationships in copper oxysalt minerals. I. Structural hierarchy. Acta Crystallographica, B49, 28–56.

Effenberger, H. (1987) Crystal structure and chemical formula of schmiederite, $Pb_2Cu_2(OH)_4(SeO_3)(SeO_4)$, with a comparison to linarite, PbCu(OH)2(SO4). Mineralogy and Petrology, 36, 3–12.

Effenberger, H., Krause, W., Bernhardt, H.-J. and Martin, M. (2000) On the symmetry of tsumcorite-group minerals based on the new species rappoldite and zincgartrellite. Mineralogical Magazine, 64, 1109–1126.

Fanfani, L. and Zanazzi, P.F. (1968) The crystal structure of vauquelinite and the relationship to fornacite. Zeitschrift für Kristallographie, 126, 433–443.

Foley, J.A., Hughes, J.M. and Lange, D. (1997) The atomic arrangement of brackebuschite, redefined as $Pb_2(Mn^{3+},Fe^{3+})(VO_4)_2(OH)$, and comments on Mn^{3+} octahedra. Canadian Mineralogist, 35, 1027–1033.

Geier, B.H., Kautz, K. and Mtiiler, G. (1971) Tsumcorit(e) [$PbZnFe(AsO_4)_2H_2O$, ein neues Mineral aus den Oxidationszonen der Tsumeb-Mine, Südwestafrika. Neues Jahrbuch für Mineralogie, Monatshefte, 305–309.

Giester, G. and Zemann, J. (1987) The crystal structure of the natrochalcite type compounds $Me^+Cu_2(OH)(zO_4)_2.2H_2O$ [Me^+ = Na, K, Rb; z = S, Se], with a special reference to the hydrogen bonds. Zeitschrift für Kristallographie, 179, 431–442.

Harlow, G.E., Dunn, P.J. and Rossman, G.R. (1984) Gamagarite: a re-examination and comparison with brackebushite-like minerals. American Mineralogist, 69, 803–806.

Jahn, H.A. and Teller, E. (1937) Stability of polyatomic molecules in degenerate electronic states. Proceedings of the Royal Society, Series A, 161, 220–236.

Jambor, J.L. and Dutrizac, J.E. (1983) Beaverite-plumbojarosite solid solutions. The Canadian Mineralogist, 21, 101–113.

Kampf, A.R. and Moore, P.B. (1976) The crystal structure of bermanite, a hydrated manganese phosphate. American Mineralogist, 61, 1241–1248.

Kampf, A.R., Shigley, J.E. and Rossman, G.R. (1984) New data on lotharmeyerite. Mineralogical Record, 15, 223–226.

Krause, W., Belendorff, K., Bernhardt, H.-J., McCammon, C., Effenberger, H. and Mikenda, W. (1998a) Crystal chemistry on the tsumcorite-group minerals. New data on ferrilotharmeyerite, tsumcorite, thometzekite, mounanaite, helmutwinklerite, and a redefinition of gartrellite. European Journal of Mineralogy, 10, 179–206.

Krause, W., Belendorff, K. and Bernhardt, H.-J. (1998b) Phosphogartrellite, $PbCuFe(PO_4)_2(OH,H_2O)$, a new member of the tsumcorite group. Neues Jahrbuch für Mineralogie, Monatshefte, 111–118.

Krause, W., Bernhardt, H.J., Effenberger, H., and Witzke, T. (2002) Schneebergite and nickelschneebergite from Schneeberg, Saxony, Germany: the first Bi-bearing members of the tsumcorite group. European Journal of Mineralgy, 14, 115–126.

Krickl, R. and Wildner, M. (2007) Crystal chemistry of synthetic Co- and Ni-analogues of natrochalcite – the shortest known hydrogen bonds among mineral-type compounds Part I: single-crystal X-ray structures. European Journal of Mineralogy, 19, 805–816.

Krivovichev, S.V. and Brown, I.D. (2001) Are the compressive effects of encapsulation an artifact of bond valence parameters? Zeitschrift für Kristallographie, 216, 245–247.

Mihajlovic, T., and Effenberger, H. (2004) The first proof of protonated anion tetrahedra in the tsumcorite-type compounds. Mineralogical Magazine, 68, 757–767.

Nickel, E.H., Robinson, B.W., Fitzgerald, O. and Birch, W.D. (1989) Gartrellite, a new secondary arsenate mineral from Ashburton Downs, W.A. and Broken Hill, N.S.W. Australian Mineralogist, 4, 83–89.

Otwinowski, Z. and Minor, W. (1997) Processing X-ray diffraction data collected in oscillation mode. In Macromolecular Crystallography, C.W. Carter Jr. and R.M. Sweet, Eds., Vol. 276, p. 307–326. Academic Press, New York.

Otwinowski, Z., Borek, D., Majewski, W. and Minor, W. (2003) Multiparametric scaling of diffraction intensities. Acta Crystallographica, A59, 228–234.

Pouchou, J.L. and Pichoir, F. (1985) "PAP" ϕ (ρZ) procedure for improved quantitative microanalysis. In J.T. Armstrong, Ed., Microbeam Analysis, 104–106.

Renner, B. and Lehmann, G. (1986) Correlation of angular and bond length distortions in TO_4 units in crystals. Zeitschrift für Kristallographie, 175, 43–59.

Robinson, K., Gibbs, G.V. and Ribbe, P.H. (1971) Quadratic elongation; a quantitative measure of distortion in coordination polyhedra. Science, 172, 567–570.

Ross, S.D. (1984) Phosphates and other oxy-anions of group V; in The Infrared Spectra of Minerals, V.C Farmer ed. Mineralogical Society Monograph 4, London, 539 p.

Shannon, R.D. (1976) Revised effective ionic radii and systematic studies of interatomic distances in halides and chalcogenides. Acta Crystallographica, A32, 751–767.

Shape Software (1997) ATOMS for Windows and Macintosh V 4.0, Kingsport, Tennessee, U.S.A.

Sheldrick, G.M. 1997a. SHELXS–97, a Program for the Solution of Crystal Structures. University of Göttingen, Göttingen, Germany.

Sheldrick, G.M. 1997b. SHELXL–97, a Program for Crystal Structure Refinement. University of Göttingen, Göttingen, Germany.

Sumin de Portilla, V.I., Quevedo, M.P. and Stepanov, V.I. (1981) The structure of bayldonite: chemical analysis, differential thermal analysis and IR spectroscopy. American Mineralogist, 66, 148–153.

Süsse, P. and Schnorrer, G. (1980) Helmutwinklerite, a new arsenate mineral from Tsumeb, S.W. Africa. Neues Jahrbuch für Mineralogie, Monatshefte, 1980, 118–124.

Tillmanns, E. and Gebert, W. (1973) The crystal structure of tsumcorite, a new mineral from the Tsuemb mine, S.W. Africa. Acta Crystallographica, B29, 2789–2794.

Wilson, A.J.C., Ed. (1992) International Tables for Crystallography, vol. C, 883 p. Kluwer Academic, Dordrecht, The Netherlands.

CHAPTER 7

The crystal structure of osakaite, $Zn_4SO_4(OH)_6 \cdot 5H_2O$

Peter Elliott[1,2], Joël Brugger[1,2], Eugen Libowitzky

[1]School of Earth and Environmental Sciences, The University of Adelaide, Adelaide, South Australia 5005, Australia.

[2]South Australian Museum, North Terrace, Adelaide, South Australia 5000, Australia.

[3]Institut für Mineralogie und Kristallographie, Geozentrum, Universität Wien, Althanstrasse 14, A-1090 Wien, Austria

STATEMENT OF AUTHORSHIP

The crystal structure of osakaite, $Zn_4SO_4(OH)_6 \cdot 5H_2O$

Peter Elliott (Candidate)

Obtained X-ray data, performed analysis on all samples, interpreted data, wrote manuscript and acted as corresponding author. I hereby certify that the statement of contribution is accurate

Signed .....*Date*.....23/8/2010

Joël Brugger

Assistance with X-ray data collection, manuscript evaluation

I hereby certify that the statement of contribution is accurate and I give permission for the inclusion of the paper in the thesis

Signed .....*Date*.....24/8/10

Eugen Libowitzky

Raman data collection, manuscript evaluation

I hereby certify that the statement of contribution is accurate and I give permission for the inclusion of the paper in the thesis

Signed .....*Date*.....06.08.2010

The crystal structure of osakaite, $Zn_4SO_4(OH)_6 \cdot 5H_2O$

Peter Elliott[1,2], Joël Brugger[1,2] and Eugen Libowitzky[3]

[1]School of Earth and Environmental Sciences, The University of Adelaide, Adelaide, South Australia 5005, Australia.

[2]South Australian Museum, North Terrace, Adelaide, South Australia 5000, Australia.

[3]Institut für Mineralogie und Kristallographie, Geozentrum, Universität Wien, Althanstrasse 14, A-1090 Wien, Austria

ABSTRACT

The crystal structure of osakaite, triclinic, a = 8.3390(17), b = 8.3440(17), c = 10.901(2) Å, α = 87.77(3), β = 83.42(3), γ = 60.05(3)º, V = 652.8(2) Å^3, space group $P\bar{1}$, Z = 1, has been solved by direct methods and refined by least-squares techniques to an agreement index ($R1$) of 10.55% and a for 1662 unique observed reflections, with $F_o > 4\sigma(F_o)$, collected using synchrotron X-ray radiation (λ = 0.773418 Å) and a CCD area detector. The structure contains four distinct Zn positions, three are coordinated by six anions in octahedral arrangements and one is coordinated by four anions in tetrahedral arrangement. One distinct S position is coordinated by four anions in a tetrahedral arrangement. The $Zn\phi_6$ octahedra (ϕ: O, OH) form an edge-sharing sheet with every seventh octahedral position vacant. On each side of the vacant octahedral site, a $Zn\phi_4$ tetrahedron is attached to three anions of the sheet and points away from the sheet. Sulphate groups are connected to the sheets on both sides by corner sharing. The sheets are held together by hydrogen bonding only. Osakaite can be considered as a decorated sheet structure of the form $[^{[6]}M\phi_2]_4$ with an interrupted sheet, and is isomorphous to that of the synthetic basic zinc sulphate pentahydrate, $Zn_4SO_4(OH)_6 \cdot 5H_2O$.

INTRODUCTION

In 2001, specimens of a Zn sulphate mineral were collected from recently mined ore stockpiles from the Block 14 Opencut, Broken Hill, New South Wales, Australia.

The mineral occurs as crusts of colourless to white, thin bladed to tabular, six-sided crystals in thin seams in a sphalerite-galena-quartz matrix (Figure 1). Associated minerals are crystals of cerussite, anglesite and pyromorphite and thin crusts of yellow greenockite.

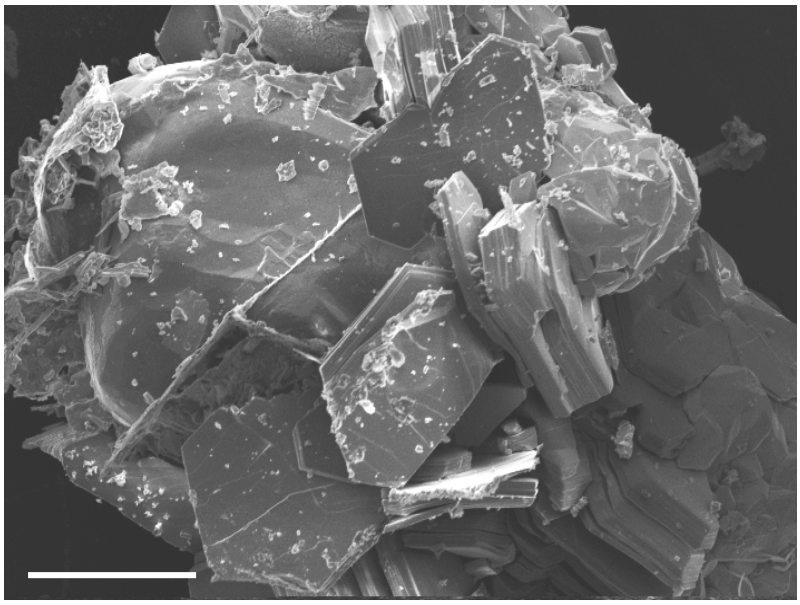

Figure 1. SEM photomicrograph showing platy crystals of osakaite on quartz. The crystals are flattened on (001). The scale bar is 100 μm long.

An X-ray powder diffraction pattern, obtained under vacuum using a 100 mm Guinier-Hägg camera, was identical to that of the synthetic, basic zinc sulphate trihydrate, $Zn_4SO_4(OH)_6{\cdot}3H_2O$ (Bear *et al*. 1986, 1987). Bear *et al*. (1986) reported that the lower hydrates $Zn_4SO_4(OH)_6{\cdot}mH_2O$ with m = 4, 3 and 1 will form by dehydration of the basic zinc sulphate pentahydrate $Zn_4SO_4(OH)_6{\cdot}5H_2O$. Subsaquently, it was shown that the Broken Hill mineral dehydrates under vaccum and that the powder X-ray diffraction pattern matches that of the basic zinc sulphate pentahydrate, $Zn_4SO_4(OH)_6{\cdot}5H_2O$. Naturally occuing $Zn_4SO_4(OH)_6{\cdot}5H_2O$ has recently been described as the mineral osakaite (Ohnishi *et al*. 2007) from the Hirao mine, Osaka Prefecture, Japan where it occurs as stalactitic aggregates of pale blue to colourless or white, hexagonal platy crystals up to 0.5 mm across and 0.01 mm in

thickness in cracks in altered shale. No single-crystal X-ray study was carried out due to the lack of suitable crystals.

POWDER X-RAY DATA

The X-ray powder-diffraction pattern for osakaite (Table 1) was recorded on a 100 mm Guinier-Hägg camera using monochromatic Cr*K*α radiation (λ 2.28970 Å) and calibrated using an internal standard of silicon powder (NBS SRM 640a). The intensities were visually estimated and the calculated intensities were obtained from the structural model (Yvon *et al*., 1977). A line in the powder X-ray diffraction pattern, at d = 10.519 Å, could not be indexed using the unit cell of osakaite. This line is close to the strongest line of the basic zinc sulphate tetrahydrate, $Zn_4SO_4(OH)_6{\cdot}4H_2O$, at d =10.34 Å, and also the strongest line of namuwite, $(Zn,Cu^{2+})_4SO_4(OH)_6{\cdot}4H_2O$, at d =10.59 Å, suggesting that a minor amount of one of these phases may also be present. Bear *et al*. (1986) found that, during controlled dehydration of $Zn_4SO_4(OH)_6{\cdot}5H_2O$, the tetrahydrate forms as an intermediate phase between the penta- and trihydrates, although it occupies only a very narrow stability region. Namuwite is isomorphous with $Zn_4SO_4(OH)_6{\cdot}4H_2O$ (Groat 1996). Unit cell refinement using the Le Bail profile-fitting method (Le Bail *et al*. 1988; Hunter 1998), starting from the unit-cell parameters determined using single-crystal methods, gave the following parameters: a = 8.338(2), b = 8.346(1), c = 10.945(1) Å, α = 87.76, β = 83.40(1)°, γ = 60.05(1), V = 655.39(2) Å^3.

Table 1. X-ray powder diffraction data for osakaite.

I_{obs}	d_{obs}	I_{calc}	d_{calc}	h	k	l	I_{obs}	d_{obs}	I_{calc}	d_{calc}	h	k	l
100	10.902	100	10.869	0	0	1			3	2.584	2	1	-3
25	10.519								8	2.567	3	2	-1
		5	7.230	0	1	0		2.563 {	9	2.561	3	1	-1
5	7.235 {	1	7.194	1	1	0			7	2.562	0	1	-4
		2	7.181	1	0	0			5	2.548	3	1	2
5	6.343 {	5	6.320	1	0	1			5	2.541	3	2	2
		0	6.262	1	1	1	20	2.532	15	2.532	0	2	3
5	6.071	1	6.080	0	1	-1			8	2.526	0	1	4
5	5.935	10	5.961	0	1	1	10	2.505 {	2	2.497	2	3	2
10	5.449	15	5.435	0	0	2			2	2.497	1	-2	2
		2	4.584	1	0	2	15	2.469	9	2.470	1	1	-4
		3	4.536	1	1	2			6	2.459	1	3	2
5	4.261	4	4.301	0	1	2			5	2.420	2	0	-3
35	4.17 {	20	4.170	1	2	0	25	2.411	24	2.410	0	3	0
		3	4.162	1	-1	0	10	2.398	9	2.398	3	3	0
		5	4.162	1	1	-2			4	2.394	3	0	1
5	3.806 {	3	3.843	1	2	-1	5	2.321 {	4	2.328	3	2	-2
		3	3.792	1	-1	-1			6	2.320	3	1	-2
		0	3.730	2	1	-1			3	2.319	1	2	4
5	3.624	2	3.623	0	0	3			3	2.304	3	1	3
		8	3.615	0	2	0	5	2.281	4	2.285	3	0	2
5		2	3.527	2	0	1			8	2.278	2	-1	3
5	3.508 {	5	3.510	2	2	1	5	2.235	2	2.237	1	2	-4
		4	3.493	2	1	2			3	2.221	0	3	-2
5	3.478	4	3.452	0	2	-1	5	2.209	4	2.200	1	3	3
		5	3.409	0	2	1	5	2.183	5	2.186	0	3	2
15	3.339	11	3.327	2	2	-1			3	2.163	1	3	-3
20	3.242	17	3.247	1	2	-2			2	2.147	1	0	5
15	3.218	14	3.212	0	1	3			2	2.134	1	1	5
5	3.197	2	3.189	1	-1	-2	5	2.125	2	2.125	3	3	-2
5	3.134	9	3.131	2	2	2	5	2.084	2	2.086	2	-1	-3
5	3.005	3	3.040	0	2	-2			2	2.071	4	2	0
5	2.964	2	2.883	2	2	-2	10	2.066	5	2.066	3	2	-3
		3	2.854	2	0	-2			6	2.063	2	4	1
5	2.765	0	2.790	1	2	3	5	2.028	5	2.027	0	3	-3
		36	2.732	1	3	0	5	2.00	4	2.003	1	-3	0
100	2.733 {	27	2.726	2	3	0			2	1.999	3	4	0
		10	2.721	2	-1	0			2	1.997	4	3	1
20	2.713 {	7	2.717	0	0	4	5	1.978	1	1.973	2	4	2
		12	2.713	3	2	0	5	1.970	2	1.970	1	4	-1
		11	2.706	3	1	1	5	1.919 {	5	1.919	3	4	2
		10	2.702	3	2	1			19	1.918	4	1	-1
		12	2.698	2	-1	1			2	1.865	4	2	-2
		10	2.675	2	2	3	5	1.817	5	1.816	3	-1	-2
20	2.666	25	2.661	1	3	1	5	1.79	2	1.791	2	2	-5
40	2.642	34	2.639	1	3	-1							

RAMAN AND INFRARED SPECTROSCOPY

A Raman spectrum of crystals of osakaite (Figure 2) was recorded in the range from 4000 to 200 cm^{-1} with a Renishaw M1000 confocal micro-Raman Imaging System using a 17 mW He Ne-laser at 632.8 nm and excitation through a Leica DMLM optical microscope (50x/0.75 N.A. objective, 180° backscatter geometry, 1200 lines/mm grating, spectral resolution (apparatus function) 4 cm^{-1}, minimum lateral resolution ~2 μm, thermo-electrically-cooled CCD detector, random sample orientation). The Raman spectrum shows an intense group of bands in the O-H stretching region, from 3650 to 3080 cm^{-1}, with seven distinct peaks at 3633, 3550, 3510, 3455, 3330, 3257sh, 3243 and 3175 cm^{-1}. These strong bands are most likely stretching vibrations of the six (OH^-) groups in the zinc hydroxide layer. Using the correlation of O–H stretching frequencies and O…O hydrogen bond lengths in minerals by Libowitzky (1999), the observed O–H stretching frequencies in osakaite would correspond to approximate O…O distances ranging from 2.67 and 3.30 Å. Values very close to these can all be found around the six OH sites in the osakaite structure. Interlayer H_2O molecules could produce a broad underlying band. Despite the high water content of osakaite, only a low intensity band at 1666 cm^{-1} corresponds

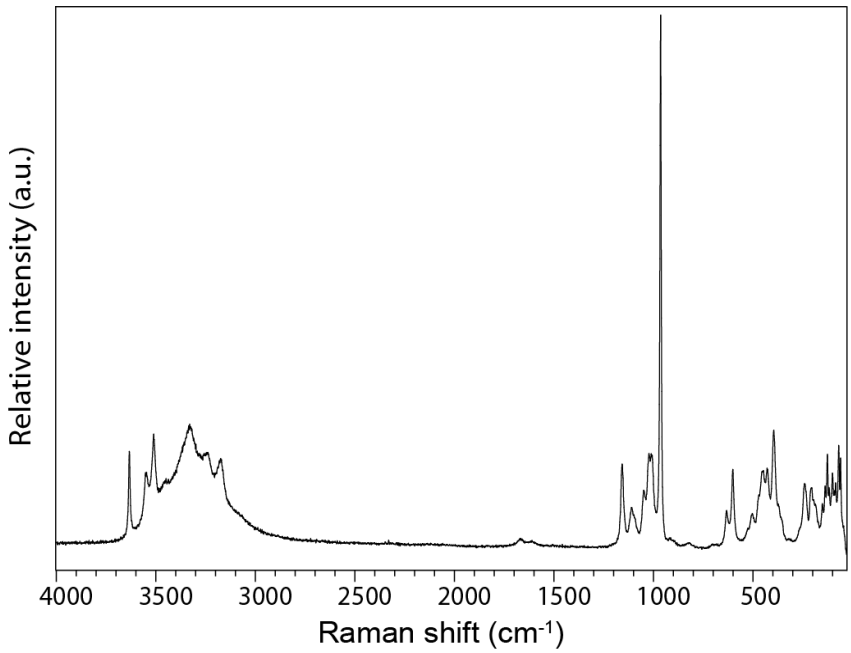

Figure 2. Single-crystal Raman spectrum of osakaite.

to an H–O–H bending vibration of water molecules. However, Raman spectroscopy is not very sensitive for the detection of water-bending modes. The strong absorption band at 964 cm^{-1} is attributed to the ν1 symmetric stretching vibration of the SO_4 tetrahedra. The bands at 1160, 1112, 1051, 1024 and 1011 cm^{-1} are due to ν3 antisymmetric stretching modes of SO_4, the bands at 636 and 604 cm^{-1} are due to SO_4 tetrahedra ν4 antisymmetric bending and the bands at 508, 456, 430 and 398 cm^{-1} are ν2 bending modes of SO_4. Bands below 398 cm^{-1} are overlaping bands of the vibrations of the $Zn(O,OH)_6$ octahedra and lattice modes.

The infrared absorption spectrum of osakaite (Figure 3) was measured between 4000 and 400 cm^{-1} using a Nicolet Avatar 370Dtgs spectrometer and the CsI pressed-disk technique. A strong broad absorption band between 3720 and 2910 cm^{-1} (centered at about 3430 cm^{-1}) is attributed to OH stretching vibrations and the antisymmetric stretching mode of H_2O and the band at 1620 cm^{-1} is the H–O–H bending vibration. Medium to strong bands at 1120, 1070 and 960 cm^{-1} are attributed to ν3 and ν1 SO_4^{2-} stretching vibrations and 602 and 440 cm^{-1} to ν4 and ν2 SO_4^{2-} bending vibrations, respectively. Bands at 790, 705, 595 and 511 cm^{-1} can likely be attributed to overlaping bands of OH bending vibrations and Zn-O vibrations and lattice modes.

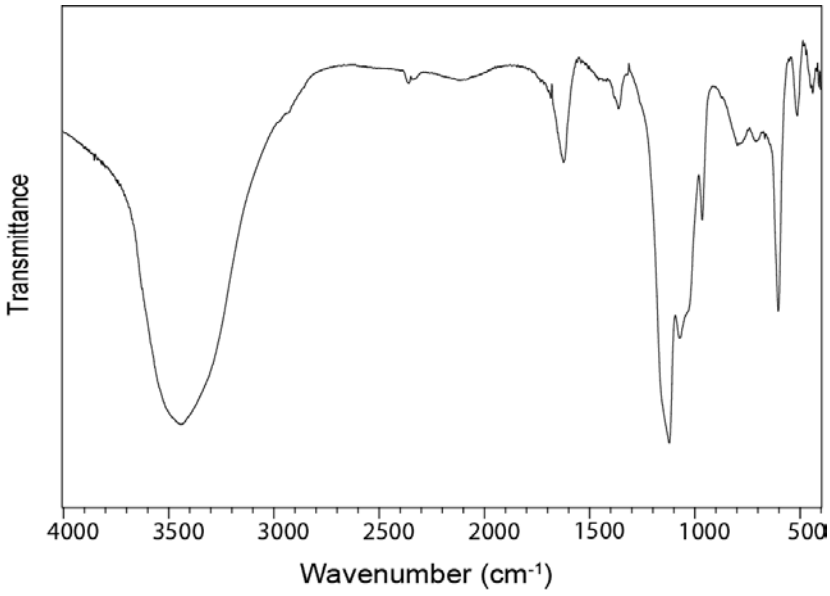

Figure 3. FT-IR spectrum of powdered osakaite.

CHEMICAL ANALYSIS

Chemical analyses were carried out with a Cameca SX51 electron microprobe using the following probe standards: sphalerite (Zn *K*α), chalcopyrite (S *K*α), tugtupite (Cl *K*α). No additional element with atomic number ≥ 9 was detected (detection limit approximately 0.05 wt%). The electron microprobe was operated at an acceleration voltage of 15 kV, a beam current of 10 nA, peak count-time 20 s, background count-time 10 s and a beam diameter of 20 μm. Data were reduced using the φ(ρZ) method of Pouchou and Pichoir (1985). The mineral was extremely unstable under the electron beam due to H_2O loss, which has resulted in a large spread in the analytical totals. Table 2 summarizes the analytical data.

Table 2. Chemical composition (Wt.%) and unit formula† (*apfu*) of osakaite.

	Mean	Range	Number of ions	
SO_3	13.81	10.83–16.10	S	0.96
ZnO	59.14	55.05–61.56	Zn	4.03
Cl	0.06	0.00–0.10	Cl	0.01
H_2O (calc)*	26.23		OH**	6.14
O≡Cl	-0.01		H_2O	5.01
Total	99.23			

Number of analysis = 7
† number of ions based on 15 anions
* calculated from structure determination
**OH calculated to obtain charge balance

CRYSTAL STRUCTURE

X-ray data collection

A crystal, 0.07 x 0.06 x 0.005 mm in size, was attached to a glass fibre and mounted on a ADSC Q210r diffractometer equiped with a CCD-detector and intensity data collected at 100 K using synchrotron X-radiation (λ = 0.773418 Å). A total of 6641 reflections were collected to 48.64° 2θ, of which there are 1824 unique reflections, with 1663 classed as observed, $F_o > 4\sigma(F_o)$. Data were indexed, integrated and scaled using the program XDS (Kabsch 1993, 2010) and were corrected for

Table 3. Crystal data, data collection and refinement details for osakaite.

Crystal data	
Formula (ideal)	$Zn_4SO_4(OH)_6{\cdot}5H_2O$
Space group	$P\,\overline{1}$
a,*b*,*c* (Å)	8.3390(17), 8.3440(17), 10.901(2)
α, β, γ (°)	87.77(3), 83.42(3), 60.05(3)
V (Å^3), Z	652.8(2), 2
F(000)	324.0
μ (mm^{-1})	4.14
Absorption correction	none
Crystal dimensions (mm)	0.07 x 0.06 x 0.005
Data collection	
Diffractometer	ADSC Quantum 210r
Temperature (K)	100
λ (Å)	0.773418
θ range (°)	2.82-24.32
Detector distance (mm)	83.97
Rotation axes	ϕ, ω
Rotation width	2.0
Total no. of frames	180
Collection time per frame (s)	10
h,k,l ranges	$-9 \rightarrow 9,\ -9 \rightarrow 9,\ -11 \rightarrow 11$
Total reflections measured	6727
Unique reflections	1824 (R_{int} = 0.0646)
Refinement	
Refinement on	F^2
$R1^*$ for $F_o > 4\sigma(F_o)$	10.55%
w$R2^\dagger$ for all F_0^2	28.75%
Reflections used $F_o > 4\sigma(F_o)$	1663
Number of parameters refined	97
(Δ/σ)max	0.0001
Δρmin, Δρmax (e/Å3)	3.889, -2.332
GooF	1.135

$^*R1 = \Sigma||F_O|-|F_C|| \,/\, \Sigma|F_O|$

$^\dagger wR2 = \Sigma w(|F_O|^2-|F_C|^2)^2 \,/\, \Sigma w|F_O|^2)^{1/2}$; $w = 1/[\sigma^2(F_o^2) + (0.042\ P)^2 + 12.60\ P]$;
$P = ([\text{max of } (0 \text{ or } F_0^2)] + 2F_c^2)/\ 3$

Lorentz, polarization and background effects. The refined unit-cell parameters of a = 8.3390(17), b = 8.3440(17), c = 10.901(2) Å, α = 87.77(3), β = 83.42(3), γ = 60.05(3)°, V = 652.8(2) Å^3 are close to the reduced unit cell of Bear *et al*. (1986) for $Zn_4SO_4(OH)_6 \cdot 5H_2O$: a = 8.350(2), b = 8.354(2), c = 11.001(2) Å, α = 82.95(2), β = 85.58(2), γ = 60.0(2)°, V = 659.9(2) Å^3. Conditions for the data collection and subsequent refinement are summarized in Table 3.

Structure solution and refinement

Scattering curves for neutral atoms, together with anomalous dispersion corrections, were taken from the International Tables For Crystalography (Wilson 1992). The lack of systematic absences of reflections was consistent with space groups $P1$ and $P\bar{1}$, and assigning phases to sets of normalized structure-factors gave mean value $|E^2-1|$ of 0.976, indicating the centrosymmetric space group $P\bar{1}$. Four Zn sites and one S site were located by direct methods (SHELXS-97, Sheldrick, 1997a) and the O sites were located by successive cycles of least-squares refinement and difference-Fourier refinement (SHELXL-97, Sheldrick, 1997b).

High isotropic displacement parameters indicated that two of the O sites (O14 and O15), which are not linked to any cation, were positionally disordered (split). The O14A and O14B positions refined to a separation of 1.064 Å and site occupancy refinement indicated occupancies of 0.63 and 0.37 respectively for these sites. The O15A and O15B positions refined to a separation 1.463 Å with refined site occupancies of 0.54 and 0.46 respectively. No hydrogen atoms could be located in difference-Fourier maps.

Anisotropic refinement resulted in non-positive definite temperature factors for more than half of of the atoms (ie. one of the axes defining the thermal ellipsoid for the atom had a negative or near zero value). Such a result could be due to a combination of several factors. All of the CCD frames showed pronounced streaking of reflections indicating that the crystal quality was very poor, resulting in poor quality X-ray data, which are not good enough to refine the atoms anisotropically. The data may also be affected by absorption. Due to the minute size of crystals generally used for collection of synchrotron X-ray data, absorption effects might be expected to be minimal. However, absorption correction to overcome negative or near zero anisotropic displacement parameters in structures refined from synchrotron data

is often required (e.g. Bonaccorsi and Pasero 2003). Also, Giester *et al*. (2007) has noted that problems in the anisotropic refinement of displacement parameters using low-temperature synchroton data are quite common.

The most commonly methods of absorption correction are analytical (de Meulenaer and Tompa, 1965) and Gaussian quadrature absorption corrections (Coppens 1970), based on the crystal size and faces, and semi-empirical absorption correction (Blessing 1995). To apply these absorption correction methods requires the so-called directional cosines of each measured reflection, which provides information about the relative orientation of the crystal relative to the primary X-ray beam and to the detector. Direction cosines are generally provided by the integration software associated with most single-crystal X-ray diffractometers. However, the data for osakaite were processed using the XDS program, which only provides ψ (the azimuthal angle corresponding to rotation of the crystal about its diffraction vector) for each reflection, but not the direction cosines. Attempts to convert the ψ values to direction cosines were not successful, so no absorption correction was applied to the data.

Recently it has become apparent that problems with small refined anisotropic displacement parameters from X-ray data collected at the Australian Synchrotron may be due to incomplete absorption in the CCD phosphor of high-energy photons, which leads to a variation in the measured signal depending on the path-length of the diffracted photon through the phosphor (Hester and Edwards 2010). Possible correction routines are currently being investigated.

The isotropic refinement model for the structure of osakaite was retained. The atomic coordinates and displacement parameters are listed in Table 4, selected interatomic distances and angles are compiled in Table 5.

STRUCTURE DESCRIPTION

Cation coordination

The structure contains four Zn sites. The Zn(1), Zn(2) and Zn(3) cations are each coordinated by five OH groups and one O^{2-} anion in an octahedral arrangement with <Zn–O> distances of 2.116, 2.128 and 2.131 Å respectively. Each site has a distorted [5+1]-coordination, with five short Zn–O distances to OH groups (range: 2.024(14)–

2.122(16) Å) and one long Zn–O distance to the O(7) anion [2.335(14), 2.374(14) and 2.418(14) Å], which coordinates to the S atom. The Zn(4) site is coordinated by three OH groups and one H_2O group in a distorted tetrahedral arrangement, with bond lengths of 1.959(16), 1.964(16), 1.965(15) and 1.992(16) Å. The mean Zn-O distance of 1.970 Å is equal to the $^{[4]}$Zn–O distance (1.97 Å) calculated using ionic radii from Shannon (1976). The O–Zn–O angles range between 103.1(5) and 113.4(5)°.

Table 4. Fractional coordinates and displacement parameters (Å^2) for atoms for osakaite.

	x	y	z	U_{eq}
Zn(1)	0.2132(3)	0.9175(3)	0.50011(18)	0.0075(11)
Zn(2)	0.6285(3)	0.7856(3)	0.50756(19)	0.0080(11)
Zn(3)	0.0831(3)	0.6308(3)	0.50859(19)	0.0076(11)
Zn(4)	0.5232(3)	0.4974(3)	0.33705(19)	0.0091(10)
S	-0.1232(7)	0.8209(7)	0.2376(4)	0.0093(15)
OH(1)	0.706(2)	0.556(2)	0.3900(13)	0.016(4)
OH(2)	0.267(2)	0.690(2)	0.3914(13)	0.016(3)
OH(3)	0.579(2)	0.248(2)	0.3852(13)	0.013(3)
OH(4)	0.5916(19)	1.026(2)	0.5841(12)	0.010(3)
OH(5)	0.005(2)	0.879(2)	0.5879(13)	0.014(3)
OH(6)	0.859(2)	0.602(2)	0.5885(12)	0.011(3)
O(7)	-0.1500(19)	0.831(2)	0.3766(12)	0.009(3)
OW(8)	0.538(2)	0.519(2)	0.1540(14)	0.025(4)
O(9)	-0.278(2)	0.986(2)	0.1895(14)	0.021(4)
O(10)	0.059(2)	0.810(2)	0.1961(13)	0.017(3)
O(11)	-0.121(2)	0.654(2)	0.1978(14)	0.023(4)
OW(12)	0.815(3)	0.214(3)	0.0458(18)	0.042(5)
OW(13)	-0.124(4)	0.850(4)	0.843(3)	0.076(8)
OW(14A)	0.439(4)	0.896(4)	0.152(3)	0.019(12)
OW(14B)	0.522(7)	0.824(7)	0.069(5)	0.06(2)
OW(15A)	0.270(4)	0.384(4)	0.151(3)	0.035(11)
OW(15B)	0.180(8)	0.388(9)	0.042(5)	0.05(2)

Table 5. Selected interatomic distances (Å) and angles (°) for osakaite.

Zn(1)	OH(4)	2.024(14)	Zn(2)	OH(6)	2.039(14)
	OH(5)	2.050(15)		OH(4)	2.062(14)
	OH(5)	2.074(15)		OH(4)	2.068(15)
	OH(2)	2.104(16)		OH(3)	2.104(15)
	OH(3)	2.108(15)		OH(1)	2.122(16)
	O(7)	2.335(14)		O(7)	2.374(14)
<Zn–O>		2.116	<Zn–O>		2.128
Zn(3)	OH(5)	2.028(15)	Zn(4)	OH(3)	1.959(16)
	OH(6)	2.056(15)		OH(2)	1.964(16)
	OH(1)	2.076(15)		OH(1)	1.965(15)
	OH(6)	2.092(15)		OW(8)	1.992(16)
	OH(2)	2.114(16)	<Zn–O>		1.970
	O(7)	2.418(14)			
<Zn–O>		2.131	S	O(11)	1.465(18)
				O(9)	1.468(17)
				O(10)	1.489(16)
				O(7)	1.505(14)
			<S–O>		1.482
OH(4)–Zn(1)–OH(5)		95.3(6)	OH(6)–Zn(2)–OH(4)		98.2(6)
OH(5)–Zn(1)–OH(5)		82.2(6)	OH(4)–Zn(2)–OH(4)		81.4(6)
OH(4)–Zn(1)–OH(2)		100.0(6)	OH(6)–Zn(2)–OH(3)		100.8(6)
OH(5)–Zn(1)–OH(2)		83.2(6)	OH(4)–Zn(2)–OH(3)		83.3(6)
OH(5)–Zn(1)–OH(2)		98.1(6)	OH(4)–Zn(2)–OH(3)		101.5(6)
OH(4)–Zn(1)–OH(3)		84.1(6)	OH(6)–Zn(2)–OH(1)		83.2(6)
OH(5)–Zn(1)–OH(3)		97.7(6)	OH(4)–Zn(2)–OH(1)		96.1(6)
OH(2)–Zn(1)–OH(3)		93.1(6)	OH(3)–Zn(2)–OH(1)		93.3(6)
OH(4)–Zn(1)–O(7)		81.1(5)	OH(6)–Zn(2)–O(7)		82.5(5)
OH(5)–Zn(1)–O(7)		95.8(5)	OH(4)–Zn(2)–O(7)		93.3(5)
OH(5)–Zn(1)–O(7)		82.0(5)	OH(4)–Zn(2)–O(7)		79.2(5)
OH(3)–Zn(1)–O(7)		86.8(5)	OH(1)–Zn(2)–O(7)		85.8(5)
<O–Zn(1) –O>		90.0	<O–Zn(2) –O>		89.9
OH(5)–Zn(3)–OH(1)		103.2(6)	O(9)–S–O(7)		109.4(8)
OH(6)–Zn(3)–OH(1)		83.9(6)	O(9)–S–O(10)		111.1(9)
OH(5)–Zn(3)–OH(6)		97.6(6)	O(10)–S–O(7)		108.0(8)
OH(6)–Zn(3)–OH(6)		81.8(6)	O(11)–S–O(7)		108.2(9)
OH(1)–Zn(3)–OH(6)		101.0(6)	O(11)–S–O(9)		110.1(9)
OH(5)–Zn(3)–OH(2)		83.4(6)	O(11)–S–O(10)		110.1(9)
OH(6)–Zn(3)–OH(2)		95.3(6)	<O–S–O>		109.5
OH(1)–Zn(3)–OH(2)		92.7(6)			
OH(5)–Zn(3)–O(7)		80.9(5)	OH(2)–Zn(4)–OH(3)		113.6(6)
OH(6)–Zn(3)–O(7)		92.0(5)	OH(2)–Zn(4)–OH(1)		111.7(7)
OH(6)–Zn(3)–O(7)		80.4(5)	OH(3)–Zn(4)–OH(1)		111.2(6)
OH(2)–Zn(3)–O(7)		85.5(5)	OH(2)–Zn(4)–OW(8)		103.0(7)
<O–Zn(3) –O>		89.8	OH(3)–Zn(4)–OW(8)		110.8(7)
			OH(1)–Zn(4)–OW(8)		106.0(7)

The mean Zn–O bond lengths for the Zn(1)ϕ_6, Zn(2)ϕ_6 and Zn(3)ϕ_6 octahedra and the Zn(4)ϕ_4 tetrahedron are comparable with values for other basic Zn salts that contain both [6]- and [4]-coordinated Zn (Bear *et al*. 1986 and references therein)

The structure contains one S site, which is tetrahedrally coordinated by two O^{2-} anions and two OH groups, with S–O distances of 1.462(13), 1.466(14), 1.490(12) and 1.503(11). The O–S–O angles are in the range 107.8(6) to 110.9(7)°. The <S–O> distance of 1.480 Å is consistent with the average <S–O> length of 1.473 Å typical for a sulphate ion (Hawthorne *et al*. 2000).

Structure connectivity

The structure of osakaite is based on a sheet of edge-sharing Zn(1)ϕ_6, Zn(2)ϕ_6 and Zn(3)ϕ_6 octahedra, which can be derived from a brucite-like sheet, but with every seventh octahedral site vacant (Figure 4). The vacant site is replaced by two ZnO_4

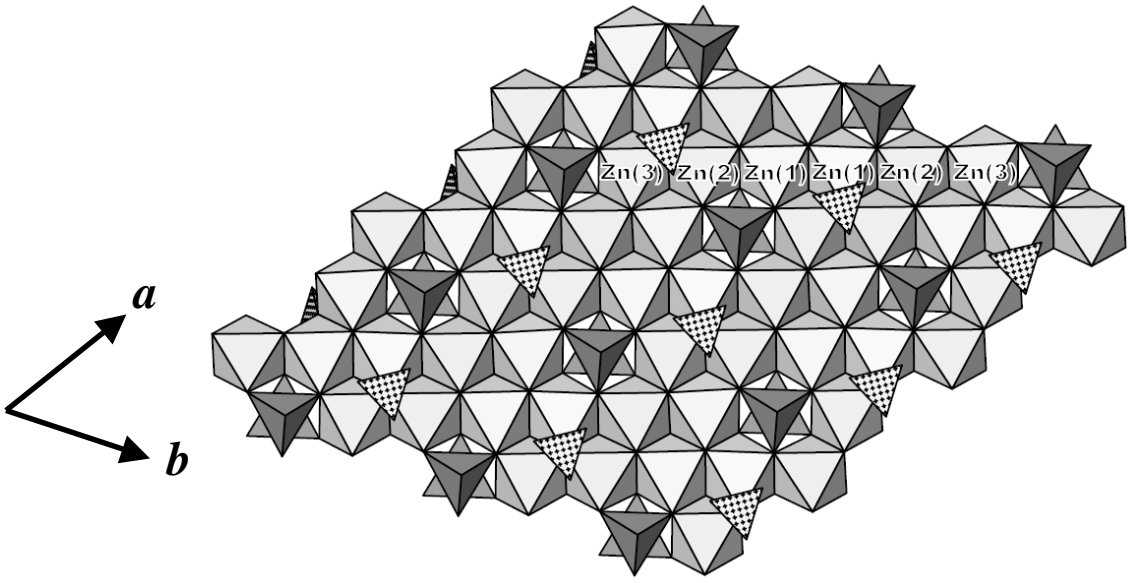

Figure 4. The [(Zn$_6$ □){Zn(OH)$_4$}$_2$(SO$_4$)$_2$(OH)$_6$] sheet in osakaite projected onto a plane close to (001), with the sheet tilted 5° about a horizontal axis to give a clearer view of the polyhedron linkage. Znϕ_6 octahedra are pale grey; Znϕ_4 tetrahedra are dark grey; SO_4 tetrahedra are cross-shaded.

that are attached to the sheet above and below this position with their apices pointing away from the sheet (Figure 2). The sheets are decorated on both sides by corner-sharing (SO_4) tetrahedra. The result is a sheet of the form $[(Zn_6\square)\{Zn(OH)_4\}_2(SO_4)_2(OH)_6]$.

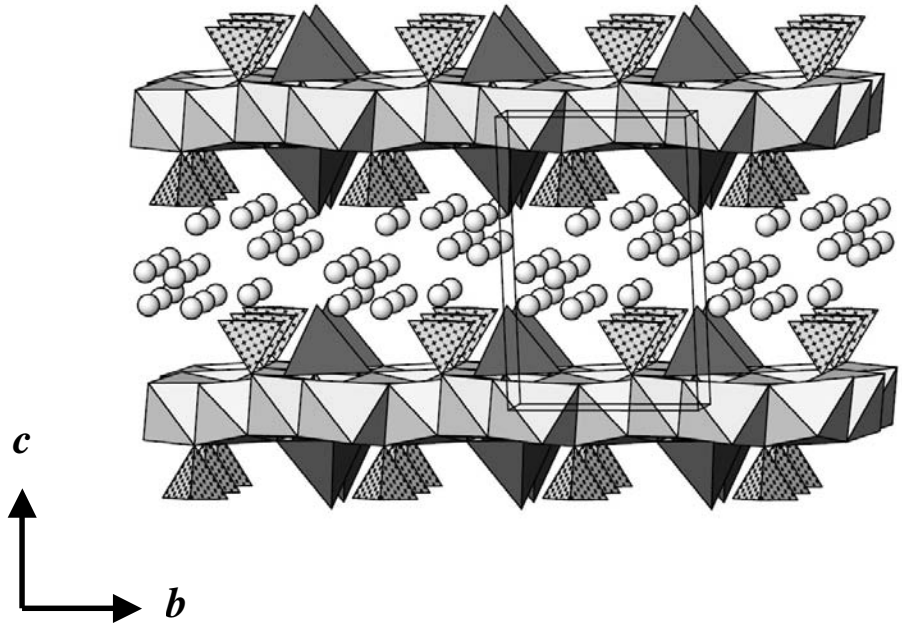

Figure 5. The structure of osakaite viewed along a direction close to [100]; legend as in Figure 4.

Interstitial H_2O molecules occupy the space between the sheets (Figure 5). The only linkage between adjacent sheets is provided by very weak to strong hydrogen bonding between OH and OW(8) groups of the basal oxygens of the sulphate groups and interstitial H_2O groups. This weak linkage between sheets accounts for the platy habit of osakaite and the perfect cleavage on {001}.

TABLE 6. Bond-valence analysis for osakaite.

	Zn(1)	Zn(2)	Zn(3)	Zn(4)	S1	Sum
OH(1)		0.32	0.36	0.49		1.17
OH(2)	0.34		0.33	0.50		1.17
OH(3)	0.34	0.34		0.51		1.19
OH(4)	0.42	0.38↓→				0.80
		0.38↓→				
OH(5)	0.40↓→		0.41			0.81
	0.37↓→					
OH(6)		0.40	0.39↓→			0.79
			0.35↓→			
O(7)	0.18	0.16	0.14		1.38	1.86
OW(8)				0.46		0.46
O(9)					1.52	1.52
O(10)					1.42	1.42
O(11)					1.54	1.54
OW(12)						0.00
OW(13)						0.00
OW(14A)						0.00
OW(14B)						0.00
OW(15A)						0.00
OW(15B)						0.00
Sum	2.05	1.98	1.98	1.96	5.86	

Hydrogen bonding

The hydrogen atoms were not located in electron density maps, however, the bond valence calculations (Table 6) indicate that there are six OH groups and five H_2O groups in the structure. The crystal-structure refinement indicates that all OH and H_2O sites, apart from the split sites OW(14) and OW(15), are fully occupied, even those that are only hydrogen-bonded within the structure.

Table 7. Atomic separations corresponding to possible hydrogen-bonds.

OH(1)–O(11)	2.737	OW(13)–OW(14B)	2.516
OH(2)–O(10)	2.737	OW(13)–OW(15A)	2.411
OH(3)–O(9)	2.816	OW(13)–OW(15B)	3.130
OH(4)–OW(15A)	2.929	OW(14A)–O(10)	3.109
OH(5)–OW(13)	2.910	OW(14A)–O(11)	2.888
OH(6)–OW(14A)	2.904	OW(14A)–OW(15B)	2.853
OW(12)–O(9)	2.764	OW(14B)–O(11)	2.804
OW(12)–O(10)	2.701	OW(14B)–OW(15B)	2.420
OW(13)–OW(12)	2.772	OW(15A)–O(9)	2.884
OW(8)–OW(12)	2.635	OW(15A)–OW(13)	2.411
OW(8)–OW(14A)	2.966	OW(15B)–O(9)	3.037
OW(8)–OW(15A)	2.825	OW(15B)–O(11)	3.071
OW(8)–OW(15B)	2.619		

The proposed hydrogen-bonding scheme (Table 7) is essentially identical to that of Bear *et al*. (1986) for $Zn_4SO_4(OH)_6{\cdot}5H_2O$, who during their refinement, located all H atoms except those associated with the disordered atom component OW(14B). All six OH groups are hydrogen-bond donors. The OH(1), OH(2) and OH(3) groups provide hydrogen-bonds to the O(11), O(10) and O(9) anions coordinated to S1. The OH(4), OH(5) and OH(6) groups provide hydrogen-bonds to OW(15A), OW(13) and OW(14A) respectively. The OW(8) group, at the apex of the $Zn4O_4$ tetrahedron, is a hydrogen-bond donor to OW(12), OW(14A), OW(15A) and OW(15B). The remaining H_2O groups are held in the structure by hydrogen bonds only and are both hydrogen-bond donors and acceptors. The OW(12), OW(14A), OW(14B), OW(15A) and OW(15B) groups are hydrogen-bond donors to the O(9), O(10) and O(11) anions coordinated to S1. The OW(13) OW(14A) and OW(15A) groups accept hydrogen-bonds from OH groups. There is a complex network of hydrogen bonding between the interlayer H_2O groups, with each being a hydrogen bond donor and acceptor.

Structural relations

The basic zinc sulphates have the general formula $Zn_n(OH)_2SO_4{\cdot}mH_2O$, with $1 \leq n \leq 7$ and $0 \leq m \leq 5$, and have been known since the early 19th century [(Kuhn, 1830;

Pascal (1962) cited by Bear *et al*. (1986)]. The structures of three basic zinc sulphates, $Zn_2SO_4(OH)_2$ (Iitaka *et al*. 1962), $Zn_4SO_4(OH)_6{\cdot}3H_2O$ (Bear *et al*. 1986) and $Zn_4SO_4(OH)_6{\cdot}5H_2O$ (Bear *et al*. 1986) have been solved by single-crystal X-ray diffraction. The structures of $Zn_4SO_4(OH)_6{\cdot}3H_2O$ and $Zn_4SO_4(OH)_6{\cdot}5H_2O$ are based on sheets of edge-sharing $Zn\phi_6$ octahedra with tetrahedrally coordinated zinc atoms located above and below empty octahedral positions. Three other basic Zn salts also have structures that are based on similar sheets. e.g. $Zn_5(OH)_8(NO_3)_2.2H_2O$ (Stahlin and Oswald, 1970), $Zn_5(OH)_8Cl_2.H_2O$ (Allmann, 1968) and $Ca[Zn_8(SO_4)_2(OH)_{12}Cl_2](H_2O)_9$ (Burns *et al*. 1998) as are the minerals hydrozincite, $Zn_5(OH)_2CO_3$, (Ghose, 1964) and namuwite, $(Zn,Cu^{2+})_4SO_4(OH)_6{\cdot}4H_2O$, (Groat 1996). The compounds, $Zn_4SO_4(OH)_6{\cdot}5H_2O$ and $Zn_5(OH)_8Cl_2.H_2O$ have mineral analogues; osakaite and simonkolleite (Hawthorne and Sokolova 2002) respectively.

Namuwite is isomorphous with synthetic $Zn_4SO_4(OH)_6{\cdot}4H_2O$, the structure of which has not been described. The compound is very difficult to prepare as it forms as an intermediate phase during the dehydration of $Zn_4SO_4(OH)_2{\cdot}5H_2O$ (osakaite) to $Zn_4SO_4(OH)_2{\cdot}3H_2O$ and occupies only a very narrow stability region (Bear *et al*. 1986). Groat (1996) suggested that the stability of the namuwite structure relative to that of $Zn_4SO_4(OH)_2{\cdot}4H_2O$ may be due to the presence of up to 20% of Cu in the octahedral Zn sites.

There are many minerals with structures based on brucite-like ($[M\phi_2]_N$) sheets of edge sharing octahedra. This includes many hydroxy-(hydrated) Cu^{2+} and Zn oxysalt minerals, particularly sulphates (Hawthorne and Schindler 2000). The sheet in osakaite has composition $[Zn_7\ X_2\ \phi_{12}]$ and is an interrupted $[M\phi_2]_N$ sheet in which the arrangement of octahedra in the sheet is interrupted by a vacant octahedral position, with two ZnO_4 tetrahedra attached to the sheet above and below the position The sheet is identical to that in the basic zinc sulphate trihydrate, $Zn_4SO_4(OH)_6{\cdot}3H_2O$ (Bear *et al*. 1986). The relative stacking of the sheets is however different in osakaite and the trihydrate (Figure 2). In osakaite, successive octahedral sheets are aligned vertically along the c axis such that the Zn tetrahedra are almost above and below each other in adjacent sheets, whereas in $Zn_4SO_4(OH)_6{\cdot}3H_2O$, adjacent sheets are displaced by ½ [a + b].

In the osakaite structure, three Zn cations are octahedrally coordinated, one Zn cation is tetrahedrally coordinated and there is one octahedrally coordinated vacancy

thus, the structural unit formula can be written $[Zn_8 (SO_4)_2 (OH)_{12}] (H_2O)_{10} \rightarrow [\{Zn_6 \square\} (Zn\phi_4)_2 (SO_4)_2 (OH)_6] (H_2O)_5$. The octahedrally coordinated cations sum to seven; the SO_4 groups link to two sheet anions, each $\{Zn (OH)_4\}$ tetrahedron bonds to three sheet anions, and there are an additional six (OH) groups, resulting in fourteen sheet anions. Thus the sheet can be written $[M_7 X_8 \phi_6] = [M_7\phi_{14}] = [M\phi_2]_7$. Hence the structure of osakaite is based on a decorated $[M\phi_2]_N$ sheet and fits into the classification scheme of Hawthorne and Schindler (2000) who found that topological enumeration of $[Cu^{2+}\phi_2]_N$ ($\phi = O^{2-}$, OH, Cl, H_2O) sheets for $3 < N < 9$ results in 17 distinct coloured graphs, some of which occur as homeomorphisms in the structures of copper-oxysalt sheet minerals. The sheet in the structure of osakaite is homeomorphic to graph 4b of Hawthorne and Schindler (2000).

Sheets homeomorphic to graph 4b of Hawthorne and Schindler (2000) are also found in the structures of spangolite (Merlino *et al*. 1992), sabelliite (Olmi *et al*. 1995), gordaite, $NaZn_4(SO_4)(OH)_6Cl{\cdot}6H_2O$ (Adiwidjaja *et al*. 1997), bechererite, $Zn_7Cu^{2+}(OH)_{13}SiO(OH)_3(SO_4)$ (Giester and Rieck 1996; Hoffmann *et al*. 1997), and namuwite, $(Zn,Cu^{2+})_4SO_4(OH)_6{\cdot}4H_2O$ (Groat 1996), and in the synthetic compounds $Zn_4(SO_4)(OH)_6{\cdot}3H_2O$ (Bear *et al*. 1986), and $CaZn_8(SO_4)_2(OH)_{12}Cl_{12}{\cdot}9H_2O$ (Burns *et al*. 1998). Sheets in gordaite and namuwite also have every seventh octahedral site vacant and replaced by (ZnO_4) tetrahedra that are attached to the sheet above and below this position. In spangolite, every seventh octahedron position is occupied by a regular ($Al\phi_6$) octahedron and in bechererite every seventh octahedron position is vacant.

ACKNOWLEDGEMENTS

We thank Angus Netting of Adelaide Microscopy, The University of Adelaide for assistance with the microprobe analysis. Trevor Huyton provided assistance with collecting the synchrotron data for osakaite and Christine Ta provided assistance with collecting the infrared spectrum.

REFERENCES

Adiwidjaja, G., Friese, K., Klaska, K.-H., and Schlüter, J. (1997) The crystal structure of gordaite $NaZn_4(SO_4)(OH)_6Cl{\cdot}6H_2O$. Zeitschrift für Kristallographie, 212, 704–707.

Allmann, R. (1968) Verfeinerung der Struktur des Zinkhydroxidchlorids. II. $Zn_5(OH)_8Cl_2 \cdot 1H_2O$. Zeitschrift für Kristallographie, 126, 417–426.

Bear, I.J., Grey, I.E., Madsen, I.C., Newnham, I.E. and Rogers, L.J. (1986) Structures of the basic zinc sulfates $3Zn(OH)_2 \cdot ZnSO_4 \cdot mH_2O$, m = 3 and 5. Acta Crystallographica, B42, 32–39.

Bear, I.J., Grey, I.E., Newnham, I.E. and Rogers, L.J. (1987) The $ZnSO_4 \cdot 3Zn(OH)_2 \cdot H_2O$ system. I. Phase formation. Australian Journal of Chemistry, 40, 539–556.

Blessing, R.H. (1995) An Empirical Correction for Absorption Anisotropy. Acta Crystallographica, A51, 33–38.

Bonaccorsi, E. and Pasero, M. (2003) Crystal structure refinement of sahlinite, $Pb_{14}(AsO_4)_2O_9Cl_4$. Mineralogical Magazine, 67, 15–21.

Burns, P.C., Roberts, A.C., and Nikischer, A.J. (1998) The crystal structure of $Ca[Zn_8(SO_4)_2(OH)_{12}Cl_2](H_2O)_9$, a new phase from slag dumps at Val Varenna, Italy European Journal of Mineralogy, 10, 923–930.

Coppens, P. (1970) Crystallographic Computing. F.R. Ahmed, S.R. Hall and C.P. Huber, Eds., p. 255–270. Munksgaard, Copenhagen.

de Meulenaer, J. and Tompa, H. (1965) The absorption correction in crystal structure analysis. Acta Crystallographica, 19, 1014–1018.

Ghose, S. (1964) The crystal structure of hydrozincite, $Zn_5(OH)_6(CO_3)_2$. Acta Crystallographica, 17, 1051–1057.

Giester, G. and Rieck, B. (1996) Bechererite, $(Zn,Cu)_6Zn_2(OH)_{13}[(S,Si)(O,OH)_4]_2$, a novel mineral species from the Tonopah-Belmont mine, Arizona. American Mineralogist, 81, 244–248

Giester, G., Kolitsch, U., Leverett, P., Turner, P. and Williams, P.A. (2007) The crystal structures of lavendulan, sampleite, and a new polymorph of sampleite. European Journal of Mineralogy, 19, 75–93.

Groat L.A. (1996) The crystal structure of namuwite, a mineral with Zn in tetrahedral and octahedral coordination, and its relationship to the synthetic basic zinc sulfates. American Mineralogist, 81, 238–243.

Hawthorne , F.C. and Schindler, M.S. (2000) Topological enumeration of decorated $[Cu^{2+}\phi_2]_N$ sheets in hydroxy-hydrated copper-oxysalt minerals. Canadian Mineralogist, 38, 751–761.

Hawthorne, F.C. and Sokolova, E.S. (2002) Simonkolleite, $Zn_5(OH)_8Cl_2(H_2O)$, a decorated interrupted-sheet structure of the form $(M\phi_2)_4$. Canadian Mineralogist, 40, 939–946.

Hawthorne, F.C., Krivovichev, S.V. and Burns, P.C. (2000) Crystal chemistry of sulfate minerals. In C.N. Alpers, J.L. Jambor, and D.K. Nordstrom, Eds., Sulfate Minerals, Crystallography, Geochemistry, and Environmental Significance, 40, p. 1–112. Reviews in Mineralogy and Geochemistry, Mineralogical Society of America, Chantilly, Virginia.

Hester, J. and Edwards, A. (2010) Unusually small atomic displacement parameters from Australian Synchrotron MX1 and MX2 beamlines (unpublished note).

Hoffmann, Ch., Armbruster, Th., and Giester, G (1997) Acentric structure (*P*3) of bechererite, $Zn_7Cu(OH)_{13}[SiO(OH)_3SO_4]$. American Mineralogist 82, 1014–1018.

Hunter, B.A. (1998) Rietica - A Visual Rietveld Program. Commission on Powder Diffraction Newsletter, 20, 21.

Iitaka, V., Oswald, H. R. and Locchi S. (1962) Die Kristallstruktur von Zink-hydroxidsulfat I, $Zn(OH)_2{\cdot}ZnSO_4$. Acta Crystallographica, 15, 559–563.

Kabsch, W. (1993) Automatic Processing of Rotation Diffraction Data from Crystals of Initially Unknown Symmetry and Cell Constants. Journal of Applied Crystallography, 26, 795–800.

Kabsch, W. (2010) XDS. Acta Crystallographica, D66, 125–132.

Libowitzky, E. (1999) Correlation of O-H stretching frequencies and O-H···O hydrogen bond lengths in minerals. Monatshefte für Chemie, 130, 1047–1059.

Merlino S., Pasero M., Sabelli C., Trosti-Ferroni R. (1992) Crystal structure refinements of spangolite, a hydrated basic sulphate of copper and aluminum, from three different occurrences. Neues Jahrbuch für Mineralogie, Monatshefte 1992, 349–357.

Ohnishi, M., Kusachi, I., Kobayashi, S. (2007) Osakaite, $Zn_4SO_4(OH)_6{\cdot}5H_2O$, a new mineral species from the Hirao mine, Osaka, Japan. Canadian Mineralogist, 45, 1511–1517.

Olmi, F., Sabelli, C., Trosti-Ferroni, R. (1995) The crystal structure of sabelliite. European Journal of Mineralogy, 7, 1331–1337.

Pouchou, J.L. and Pichoir, F. (1985) "PAP" ϕ (ρZ) procedure for improved quantitative microanalysis. In J.T. Armstrong, Ed., Microbeam Analysis, 104–106. San Francisco Press, California.

Shannon, R.D. (1976) Revised effective ionic radii and systematic studies of interatomic distances in halides and chalcogenides. Acta Crystallographica, A32, 751–767.

Sheldrick, G.M. 1997a. SHELXS–97, a Program for the Solution of Crystal Structures. University of Göttingen, Göttingen, Germany.

Sheldrick, G.M. 1997b. SHELXL–97, a Program for Crystal Structure Refinement. University of Göttingen, Göttingen, Germany.

Stählin, W., and Oswald, H.R. (1970) The crystal structure of zinc hydroxide nitrate, $Zn_5(OH)_8(NO_3)_2 \cdot 2H_2O$. Acta Crystallographica, B26, 860–863.

Wilson, A.J.C., Ed. (1992) International Tables for Crystallography, vol. C, 883 p. Kluwer Academic, Dordrecht, The Netherlands.

Yvon, K., Jeitschko, W., and Parthé, E. (1977) LAZY PULVERIX, a computer program, for calculating X-ray and neutron diffraction powder patterns. Journal of Applied Crystallography, 10, 73–74.

CHAPTER 8

Description and crystal structure of plimerite, $ZnFe^{3+}_4(PO_4)_3(OH)_5$, the Zn-analogue of rockbridgeite and frondelite, from Broken Hill, New South Wales, Australia

Peter Elliott[1,5], Uwe Kolitsch[2], Gerald Giester[3], Eugen Libowitzky[3], Catherine McCammon[4], Allan Pring[5], William D. Birch[6], Joël Brugger[1,5]

[1]School of Earth and Environmental Sciences, The University of Adelaide, Adelaide, South Australia 5005, Australia

[2]Mineralogisch-Petrographische Abt., Naturhistorisches Museum, A-1010 Wien, Austria

[3]Institut für Mineralogie und Kristallographie, Geozentrum, Universität Wien, Althanstrasse 14, A-1090 Wien, Austria

[4]Bayerisches Geoinstitut, Universität Bayreuth, D-95440 Bayreuth, Germany

[5]South Australian Museum, North Terrace, Adelaide, South Australia 5000, Australia

[6]Geosciences, Museum Victoria, GPO Box 666, Melbourne 3001, Victoria, Australia

Mineralogical Magazine, 2009, 73(1), 131–148

STATEMENT OF AUTHORSHIP

Description and crystal structure of plimerite, $ZnFe^{3+}_4(PO_4)_3(OH)_5$, the Zn-analogue of rockbridgeite and frondelite, from Broken Hill, New South Wales, Australia.
Mineralogical Magazine, 2009, 73(1), 131–148

Peter Elliott (Candidate)

Conducted chemical analyses and powder x-ray diffraction on all samples, interpreted data, wrote manuscript and acted as corresponding author. I hereby certify that the statement of contribution is accurate

Signed *Date*.23/8/2010

Uwe Kolitsch

Single-crystal X-ray data collection and data reduction. Assistance with interpretion of data, manuscript evaluation.

I hereby certify that the statement of contribution is accurate and I give permission for the inclusion of the paper in the thesis

Signed .....*Date*.....9 July 2010

Gerald Giester

Single-crystal X-ray data collection and data reduction, manuscript evaluation.

I hereby certify that the statement of contribution is accurate and I give permission for the inclusion of the paper in the thesis

Signed .....*Date*.....14.7.2010

Eugen Libowitzky

Raman data collection. Assistance with interpretion of data, manuscript evaluation.

I hereby certify that the statement of contribution is accurate and I give permission for the inclusion of the paper in the thesis

Signed *Date*.06.08.2010

Catherine McCammon

Mössbauer data collection, manuscript evaluation.

I hereby certify that the statement of contribution is accurate and I give permission for the inclusion of the paper in the thesis

Signed .....*Date*.....29.06.10.....

Allan Pring

Manuscript evaluation.

I hereby certify that the statement of contribution is accurate and I give permission for the inclusion of the paper in the thesis

Signed .....*Date*.....23/8/2010.....

William D. Birch

Manuscript evaluation.

I hereby certify that the statement of contribution is accurate and I give permission for the inclusion of the paper in the thesis

Signed .....*Date*.....17/8/10.....

Joël Brugger

Manuscript evaluation.

I hereby certify that the statement of contribution is accurate and I give permission for the inclusion of the paper in the thesis

Signed .....*Date*.....26/8/10.....

Elliott, P., Kolitsch, U., Giester, G., Libowitzky, E., McCammon, C., Pring, A. Birch, W.D. & Brugger, J. (2009) Description and crystal structure of a new mineral - plimerite, $ZnFe_4^{3+}(PO_4)_3(OH)_5$ - the Zn-analogue of rockbridgeite and frondelite, from Broken Hill, New South Wales, Australia. *Mineralogical Magazine, v. 73(1), pp. 131 -148.*

CHAPTER 9

Description and crystal structure of nyholmite, a mineral related to hureaulite, from Broken Hill, New South Wales, Australia

Peter Elliott[1,4], Peter Turner[2], Paul Jensen[2], Uwe Kolitsch[3], Allan Pring[4]

[1]School of Earth and Environmental Sciences, The University of Adelaide, Adelaide, South Australia 5005, Australia

[2]School of Chemistry, The University of Sydney, Sydney 2006, New South Wales, Australia

[3]Mineralogisch-Petrographische Abt., Naturhistorisches Museum, A-1010 Wien, Austria

[4]South Australian Museum, North Terrace, Adelaide, South Australia 5000, Australia

Mineralogical Magazine, 2009, 73(5), 521–533

STATEMENT OF AUTHORSHIP

Description and crystal structure of nyholmite, a new mineral related to hureaulite, from Broken Hill, New South Wales, Australia. *Mineralogical Magazine*, 2009, 73(5), 723–735

Peter Elliott (Candidate)

Performed analysis on all samples, interpreted data, wrote manuscript and acted as corresponding author. I hereby certify that the statement of contribution is accurate

Signed ....*Date*.....23/8/2010

Peter Turner

Single-crystal X-ray data collection and data reduction, manuscript evaluation.

I hereby certify that the statement of contribution is accurate and I give permission for the inclusion of the paper in the thesis

Signed .....*Date…13 July 2010*

Paul Jensen

Single-crystal X-ray data collection and data reduction, manuscript evaluation.

I hereby certify that the statement of contribution is accurate and I give permission for the inclusion of the paper in the thesis

Signed .....*Date*.....3/8/2010

Uwe Kolitsch

Assistance with interpretion of data, manuscript evaluation

I hereby certify that the statement of contribution is accurate and I give permission for the inclusion of the paper in the thesis

Signed .....*Date*.....9 July 2010

Allan Pring

Manuscript evaluation

I hereby certify that the statement of contribution is accurate and I give permission for the inclusion of the paper in the thesis

Signed .....*Date*.....23/8/2010

Elliott, P., Turner, P., Jensen, P., Kolitsch, U., & Pring, A. (2009) Description and crystal structure of nyholmite, a new mineral related to hureaulite, from Broken Hill, New South Wales, Australia, *Mineralogical Magazine, v. 73(5), pp. 521 -533.*

CHAPTER 10

Description and crystal structure of liversidgeite, $Zn_6(PO_4)_4 \cdot 7H_2O$, a new mineral from Broken Hill, New South Wales, Australia

Peter Elliott[1,4], Gerald Giester[2], Eugen Libowitzky[2], Uwe Kolitsch[3]

[1]School of Earth and Environmental Sciences, The University of Adelaide, Adelaide, South Australia 5005, Australia

[2]Institut für Mineralogie und Kristallographie, Geozentrum, Universität Wien, Althanstrasse 14, A-1090 Wien, Austria

[3]Mineralogisch-Petrographische Abt., Naturhistorisches Museum, A-1010 Wien, Austria

[4]South Australian Museum, North Terrace, Adelaide, South Australia 5000, Australia

American Mineralogist, 2010, 95, 397–404

STATEMENT OF AUTHORSHIP

Description and crystal structure of liversidgeite, $Zn_6(PO_4)_4 \cdot 7H_2O$, a new mineral from Broken Hill, New South Wales, Australia. *American Mineralogist*, 2010, 95, 397–404.

Peter Elliott (Candidate)

Performed analysis on all samples, interpreted data, wrote manuscript and acted as corresponding author. I hereby certify that the statement of contribution is accurate

Signed .....*Date*.....23./.8./2010

Gerald Giester

Single-crystal X-ray data collection and data reduction, manuscript evaluation

I hereby certify that the statement of contribution is accurate and I give permission for the inclusion of the paper in the thesis

Signed .....*Date*.....14. 7. 2010

Eugen Libowitzky

Raman data collection, manuscript evaluation

I hereby certify that the statement of contribution is accurate and I give permission for the inclusion of the paper in the thesis

Signed .....*Date*.....06. 08. 2010

Uwe Kolitsch

Assistance with interpretion of data, manuscript evaluation

I hereby certify that the statement of contribution is accurate and I give permission for the inclusion of the paper in the thesis

Signed .....*Date*.....9. July 2010

Elliott, P., Giester, G., Libowitzky, E. & Kolitsch, U. (2010) Description and crystal structure of liversidgeite, $Zn_6(PO_4)_4 \cdot 7H_2O$, a new mineral from Broken Hill, New South Wales, Australia. *American Mineralogist, v. 95(2-3), pp. 397 -404.*

Chapter 11. Discussion

11.1 Relation between stability and structure

Oxysalt minerals in geological environments such as the Broken Hill oxidized zone form a wealth of different and complex structural arangements. This together with the complexity of their growth conditions, make it difficult if not impossible to predict which structures will be formed.

The crystal structures examined in this study can be classified using the structural hierarchy of Hawthorne (1983, 1985), which is based on the polymerization of the strongly bonded coordination polyhedra. Munakataite is an infinite chain structure, edwardsite, cadmian serpierite, gartrellite and osakaite are infinite sheet structures and plimerite, nyholmite and liversidgeite are infinite framework structures.

The chemistry and stabilities of the structures can be examined in terms of structural Lewis acidity/basicity relations (Hawthorne 1985; Schindler and Hawthorne 2001a; Hawthorne and Schindler 2008). A structure is considered to be binary entity, a strongly bonded structural unit or (usually) complex oxyanion and a weakly bonded interstitial species or complex (generally hydrated) cation (Hawthorne 1985, 1990 1992; Schindler and Hawthhorne 2001a). The interstitial complex can be characterized by its Lewis acidity; a measure of the electrophilic (electron-accepting) character of the complex and the structural unit can be characterized by its Lewis basicity. The interaction between these two components can be examined using the valence-matching principle (Brown 1981):

Stable structures will form when the Lewis-acid strength of the cation closely matches the Lewis-base strength of the anion.

This approach gives an insight into mineral stability, as it is the weak interstitial bonds that will control the breakdown of the structure. The valence-matching principle can also be used to explain what controls the nature of interstitial cation chemistry in minerals. Minerals with different structural units often have contrasting interstitial-cation chemistry, a result of the matching of the acid and base strengths of the interstitial cations and the structural unit.

Following the form of Hawthorne (1985), munakataite, $Pb_2Cu_2(Se^{4+}O_3)(SO_4)(OH)_4$, has structural unit $[Cu_2(Se^{4+}O_3)(SO_4)(OH)_4]^{4-}$ interacting with interstial cation Pb^{2+}.

Number of bonds in the structural unit = 2 x [6] + 1 x [3] + 1 x [4] + 4 x [1] = 23

Number of bonds needed for [4]-coordination of all simple anions = 7 x 4 = 28

Number of bonds needed for [4]-coordination of (OH) = 4 x 4 = 16

Number of additional bonds required by the structural unit to achive this coordination = 44 – 23 = 21

Number of hydrogen bonds to the structural unit = 3

Number of bonds required from interstitial cations = 21 – 4 = 17

The Lewis basicity of a structural unit is its charge divided by the number of bonds required by the structural unit to achieve its ideal coordination of O = 4/17 = 0.22

This matches closely with the Lewis acidity of Pb^{2+} at 0.20 *vu* and hence the valence-matching principle is satisfied and a stable structure will form.

The infinite chain of edge-sharing octahedra in the structure of munakataite has general stoichiometry $[M(TO_4)\phi]$ and is the basis of many mineral structures. (e.g. the linarite-group, brackebuschite-group, fornacite-group and vauquelinite-group minerals). These minerals show a wide range in chemistry and are not restricted to any particular paragenesis. The interstitial cations in these structures are however restricted to Pb^{2+}, Ba and Sr but not Ca, a much more common cation. The Ca cation satisfies the electroneutrality requirement, however, its Lewis acidity (0.29 *vu*) does not match the Lewis basicity of the $[M(TO_4)\phi]$ structural unit and stable structures do not form.

Cadmian serpierite, $(Cd,Ca)(Cu,Zn)_4(SO_4)_2(OH)_6{\cdot}3H_2O$, contains the structural unit $[(Cu,Zn)_4(SO_4)_2(OH)_6]^{2-}$ and with interstial cation (Cd^{2+},Ca). The Lewis basicity of the structural unit is defined as its charge divided by the number of bonds required by the structural unit to achieve its ideal coordination of O. There are eight O^{2-} anions and six OH^- groups in the structural unit. The number of bonds implicit in the coordination polyhedra of the structural unit is 38; 4 x 6 (Cu,Zn)–O bonds, 2 x 4 S–O bonds and 6 x 1 H–O bonds. For an anion coordination number of four for O and four for (OH) (Hawthorne 1994), the anions of the structural unit require 8 x 4 + 6 x 4 = 56 bonds. It will receive six hydrogen bonds from the interstitial cation so the bonds

required to fulfil the anion-coordination requirements of the structural unit = 56 – 18 – 6 = 12. The Lewis basicity is the charge/number of required bonds = 4/12 = 0.17 *vu*.

By the valence-matching principle, for a stable structure to form, the Lewis basicity of the interstitial cation would be expected to be ~0.17 *vu*. This is the case for Pb^{2+}, with a Lewis acidity of 0.20 *vu*, but is not so for Ca, with a Lewis acidity of 0.29 *vu*, and Cd^{2+}, with a Lewis acidity of 0.326 *vu*) (Brown 1981). However the coordination of the interstitial cation is actually $M^{2+}(H_2O)_3(O,_t)_4$, where O_t represents an O atom linked to the tetrahedrally coordinated cation. Thus the $M^{2+}(H_2O)_3(O,_t)_4$ group is a complex cation. The H_2O groups are bond-valence transformers, which take one bond and transform it into two bonds of half the valence (Hawthorne 1985). Thus the number of bonds between the M^{2+} cation and the structural unit is increased, effectively increasing the large cation coordination number, decreasing the Lewis acidity of these bonds and decreasing the effective Lewis acidity of the large cation. So the effective Lewis acidity of the complex cation $M^{2+}(H_2O)_3(O,_t)_4$ becomes the charge divided by the number of bonds: 2/(3 x 2 + 4) = 0.20 *vu* which matches the Lewis basicity of the structural unit. Transformer H_2O groups moderate the Lewis acidity of the interstitial cation, and match it with the Lewis basicity of the structural unit. In this case, the effective Lewis acidity of the complex $Ca^{2+}(H_2O)_3(O,_t)_4$ cation is 2/(4 x 1 + 3 x 2) = 0.20 *vu*, and therefore it can function as the interstitial (complex) cation for the structural unit of cadmian serpierite.

Edwardsite, $Cu_3Cd(SO_4)_2(OH)_6{\cdot}4H_2O$, contains the structural unit $[Cu_3Cd(SO_4)_2(OH)_6(H_2O)]^{2-}$. There are eight O^{2-} anions, six OH groups and one H_2O group in the structural unit. The number of bonds implicit in the coordination polyhedra of the structural unit is 41; 3 x 6 (Cu,Zn)–O bonds 1 x 7 Cd–O bonds, 2 x 4 S–O bonds, 6 x 1 H–O and 1 x 1 H–O bonds. For an anion coordination number of four for O, four for (OH) and three for H_2O the anions of the structural unit require 8 x [4] + 6 x [4] + 1 x [3] = 59 bonds. It will receive eight hydrogen bonds from interstitial cations so the bonds required to fulfil the anion-coordination requirements of the structural unit = 59 – 41 – 8 = 10. The Lewis basicity is the charge/number of required bonds = 2/10 = 0.20 *vu*.

The Lewis basicity of the structural unit does not match the Lewis acidity of the interstitial Cd^{2+} cation (0.326 *vu*). The interstitial Cd^{2+} is however a complex cation, $Cd^{2+}(H_2O)_3(O,_t)_3$, and the transformer action of H_2O (Hawthorne 1985) will

considerably modify the actual cation acidity. The actual Lewis acidity of Cd thus becomes 2/(3 x 2 + 3 x 1) = 0.22 *vu*, which matches the structural unit basicity.

Osakaite contains the structural unit $[Zn_4(SO_4)(OH)_6]^0$. There are four O-anions and six OH groups in the structural unit. The number of bonds implicit in the coordination polyhedra of the structural unit is 34; 4 x 6 Zn–O bonds 1 x 4 S–O bonds, 6 x 1 H–O. For an anion coordination number of four for O, four for (OH) and three for H_2O the anions of the structural unit require 4 x 4 + 6 x 4 = 40 bonds. It will receive six hydrogen bonds from the interstitial cation so the bonds required to fulfil the anion-coordination requirements of the structural unit = 40 – 34 – 6 = 0. The Lewis basicity is the charge/number of required bonds = 0/0 = 0.00 *vu*.

Osakaite is an example of a non-framework structure with structural units of neutral charge, which have no formal interaction, and hence would not be expected to hold together. Thus the binary representation approach to crystal structure stability of Hawthorne (1994, 1997) does not provide a satisfactory indication of the stability of the structure. The structural unit has a polar nature and can be divided into an acidic component, comprising ($Zn^{2+}O_6$) and ($Zn^{2+}O_4$) polyhedra, and a basic component comprising SO_4 groups (Schindler *et al*. 2006). In such structures, adjacent structural units must arrange such that their acidic and basic parts are spatially adjacent to each other in order to allow linkage via hydrogen bonds or if not, interstitial H_2O groups must be available in order to link the acidic and basic part of adjacent structural units. Adjacent structural units in osakaite are separated by ~11 Å, which prevents direct hydrogen bonding, so the distance between hydrogen-bond acceptors and hydrogen-bond donors is bridged by interstitial H_2O groups. The acidic part of the structural unit (OH groups and OW8) hydrogen bonds to interstitial H_2O groups which hydrogen bond to the basic part of an adjacent structural unit (O7, O9, O10, O11), either directly of via other interstitial H_2O groups. Thus in order to promote intersheet linkage the osakaite structure contains many interstitial H_2O groups compared to a structure such as schulenbergite, a similar infinite sheet structure which also has no intersheet cations and has only one interstitial H_2O group, and in which the distance between sheets allows intersheet linkage via H bonding between the acidic and basic parts.

Gartrellite, $PbCu(Fe,Cu)(AsO_4)_2(OH,H_2O)_2$, has structural unit $[Cu(Fe,Cu)(AsO_4)_2(OH,H_2O)_2]^{2-}$.

Number of bonds in the structural unit: 1 x [6] + 1 x [6] + 2 x [4] + 3 = 23

Number of bonds needed for [4]-coordination of all simple anions: 8 x 4 = 32

Number of bonds needed for [4]-coordination of (OH): 2 x 4 = 8

Number of additional bonds required by the structural unit to achive this coordination: 40 – 23 = 17.

Number of hydrogen bonds to the structural unit = 6

Number of bonds required from interstitial cations: 17 – 6 = 11

The Lewis basicity of a structural unit is its charge divided by the number of bonds required by the structural unit to achieve its ideal coordination of O = 2/11 = 0.18 *vu*. The Lewis basicity of the structural unit is a close match to the Lewis acidity of Pb^{2+} (0.20 *vu*) (Brown 1981).

The ligands of the coordination sphere of the interstitial cation in gartrellite and other minerals of the tsumcorite group do not include any transformer H_2O groups to modify the Lewis acidity of the interstitial cation. Hence only interstitial cations with a Lewis acidity of ~0.18 *vu* (e.g. Pb^{2+}, Ba, Sr) would be expected in these minerals. Other minerals of the tsumcorite group such as cabalzarite, lotharmeyerite, ferrilotharmeyerite, cobaltlotharmeyerite, and manganlotharmeyerite do contain Ca as an interstitial cation (Lewis acidity 0.29 *vu*) which, by to the valence-matching principle, is not a good fit for a structural unit with a Lewis basicity of 0.18 *vu*. Hawthorne (1998) observed that a number of sheet structures that did not follow the valence-matching rule particularly well, including bermanite, which like the tsumcorite group minerals has a structure that is based on a $[M(TO_4)\phi]$ sheet, and noted that the significance of this is not clear as yet.

Infinite framework structures frequently contain cations located within interstices, usually alkali and alkaline-earth cations, but also smaller cations such as Mg, Mn or Fe (e.g. Hawthorne 1998). Plimerite, $[ZnFe^{3+}_4(PO_4)_3(OH)_5]$, and nyholmite, $[Cd_3Zn_2(AsO_3\{OH\})_2(AsO_4)_2{\cdot}4H_2O]$, are, however, are infinite framework structures which have no formal charge and contain no interstitial cations. Such structures are very strongly bound and hence would be expected to have high stability.

Based on further developments on the bond-valence approach to the structure, chemistry and paragenesis of hydroxy-hydrated oxysalt minerals, Schindler and Hawthhorne (2001a) defined the interstitial species as a single component or complex which, can be expressed as:

$$\{^{[m]}M^{+}_{a}\ ^{[n]}M^{2+}_{b}\ ^{[l]}M^{3+}_{c}\ (H_2O)_d(H_2O)_e\ ^{[q]}(OH)_f\ ^{[r]}Cl\ (H_2O)_g\}^{(a+2b+3c-f)+}$$

where M is any type of interstitial monovalent, divalent and trivalent cation, [m], [n], [l] and [q] denote coordination numbers, d denotes the number of transformer H_2O groups, e denotes the number of non-transformer H_2O groups bonded to two interstitial cations or bonded to one interstitial cation and receiving one hydrogen bond from another interstitial H_2O group, f denotes the number of interstitial OH groups and g denotes the number of H_2O groups not bonded to any interstitial cations.

Schindler and Hawthhorne (2001a) introduced a more flexible definition of the structural unit. As a crystal structure tends to break down by breaking the weaker chemical, only bonds of higher bond-valence should be considered to be part of the structural unit (Schindler *et al*. 2006). In sulphate minerals, the average bond-valences in the polyhedra of $^{[6]}M^{3+}$ and $^{[6]}M^{2+}$cations are between 0.50 and 0.33 *vu*, which are lower than the maximum bond-valence for interstitial cations. As weaker chemical bonds in the structure should not be considered to be the structural unit, Schindler and Hawthhorne (2001a) defined the structural unit for sulphate minerals as being formed by polymerization of (SO_4) tetrahedra with ($M\phi_n$) polyhedra involving the M cations of higher valence. In particular in sulphate minerals structural units should be defined as polymerized anion complexes of (SO_4) and ($M\phi_n$) polyhedra, with the minimum average bond-valence between a linking O atom of a sulphate tetrahedron and a ($M\phi_n$) polyhedron equal to 0.30 *vu*.

The structures of edwardsite, cadmian serpierite and osakaite, are based on sheets of edge-sharing (Cu^{2+},$Zn\phi_6$) octahedra The O-atom of the (SO_4) group, which links to the sheet, receives ~1.50 *vu* from the S–O bond and, on average, 0.167 *vu* from three apical Cu^{2+}–O bonds. Hence the structural unit in these minerals is an isolated (SO_4) group. These structures are strongly polar, consisting of an acidic component and a basic component. In edwardsite the acidic component, $[Cu_3Cd_2(OH)_6(H_2O)_4(H_2O)_0]^{4+}$,

has an effective positive charge and contains OH and H_2O groups which are bond-valence donors. The basic component, $(SO_4)^{2-}$, has an effective negative charge and and the O atoms of the (SO_4) groups are bond-valence acceptors.

Using the definition of the structural unit and interstitial complex of Schindler and Hawthhorne (2001a) and Schindler *et al*. (2006), edwardsite has interstitial complex $\{Cu_3Cd_2(OH)_6(H_2O)_4(H_2O)_0\}^{4+}$, interacting with a structural unit $[(SO_4)^{2-}]_2$. The O atoms of the $(S1O_4)$ group accept one hydrogen bond from OH groups, five hydrogen bonds from H_2O groups, two bonds to Cd1 and three apical Cu–O bonds. The Lewis basicity of the (SO_4) group is its charge divided by the number of bonds accepted by the (SO_4) group: 2 / 11 = 0.18 *vu*. The O atoms of the $(S2O_4)$ group accept two hydrogen bonds from OH groups, six hydrogen bonds from H_2O groups, one bond to Cd1 and three apical Cu–O bonds. The Lewis basicity of the SO_4 group is its charge divided by the number of bonds accepted by the (SO_4) group: 2 / 12 = 0.17 *vu*.

The general expression for the interstitial complex is:

$$\{^{[m]}M^{+}_{a}\ ^{[n]}M^{2+}_{b}\ ^{[l]}M^{3+}_{c}\ (H_2O)_d(H_2O)_e\ ^{[q]}(OH)_f\ ^{[r]}Cl\ (H_2O)_g\}^{(a+2b+3c-f)+}$$

The Lewis acidity of the interstitial complex is its effective charge divided by the number of bonds from the interstitial complex to the structural unit:

$$(a + 2b + 3c - f + h \times s) / [m \times a + n \times b + l \times c + d - f \times (q - 1) + s]$$

where h is the average bond-valence of the hydrogen bonds emanating from the structural unit (=0.20 *vu*) and s is the number of hydrogen bonds emanating from the structural unit that link to the interstitial complex.

There are no hydrogen bonds emanating from the structural unit hence $s = 0$. The interstitial complex has four transformer H_2O groups, no non-transformer H_2O groups, no H_2O groups not bonded to any cation and six OH groups. The effective charge of the interstitial complex is its formal charge plus the charge of hydrogen bonds transferred to the interstitial complex = 4 + 0 = 4. The number of bonds from the interstitial complex to the structural unit is 6 x 4 (from Cu_4+Cd1) + 7 x 1 (from Cd2) + 4 [from transformer H_2O groups] – 6 x 2 (the number of interstitial OH groups × the coordination of (OH) – 1) + 0 = 23. The Lewis acidity of the interstitial complex is 4 / 23 = 0.17 *vu*.

Cadmian serpierite has interstitial complex $\{(Ca,Cd)Cu_4(OH)_6(H_2O)_1(H_2O)_2\}^{4+}$ interacting with a structural unit $[SO_4]_2^{2-}$. The O atoms of the ($S1O_4$) group accept three hydrogen bond from OH groups, two hydrogen bonds from H_2O groups, three bonds to the (Ca,Cd) cation and three apical Cu–O bonds. The Lewis basicity of the ($S1O_4$) group is its charge divided by the number of bonds accepted by the (SO_4) group: 2 / 11 = 0.18 *vu*. The O atoms of the ($S2O_4$) group accept two hydrogen bonds from OH groups, three hydrogen bonds from H_2O groups, one bond to the (Ca,Cd) cation and three apical Cu–O bonds. The Lewis basicity of the SO_4 group is its charge divided by the number of bonds accepted by the SO_4 group: 2 / 9 = 0.22 *vu*.
There are no hydrogen bonds emanating from the structural unit hence $t = 0$ and $s = 0$. The interstitial complex has two transformer H_2O groups, one non-transformer H_2O group, no H_2O groups not bonded to any cation and six OH groups. The effective charge of the interstitial complex is its formal charge plus the charge of hydrogen bonds transferred to the interstitial complex = 4 + 0 = 4. The number of bonds from the interstitial complex to the structural unit is 7 x 1 (from Ca,Cd) + 6 x 4 (from Cu) + 2 [from transformer H_2O groups] – 6 x 2 (the number of interstitial OH groups × the coordination of (OH) – 1) + 0 = 21. The Lewis acidity of the interstitial complex is 4 / 21 = 0.19 *vu*.

Osakaite has interstitial complex $[^{[6]}Zn_3{}^{[4]}Zn\,{}^{[3]}(OH)_6(H_2O)(H_2O)_4]^{2+}$ interacting with a structural unit $(SO_4)^{2-}$. The O atoms of the (SO_4) group accept three hydrogen bond from OH groups, two hydrogen bonds from H_2O groups, three bonds to the Zn cations, and three apical Cu–O bonds. The Lewis basicity of the ($S1O_4$) group is its charge divided by the number of bonds accepted by the (SO_4) group: 2 / 11 = 0.18 *vu*. The O atoms of the ($S2O_4$) group accept two hydrogen bonds from OH groups, three hydrogen bonds from H_2O groups, one bond to the (Ca,Cd) cation and three apical Cu–O bonds. The Lewis basicity of the SO_4 group is its charge divided by the number of bonds accepted by the SO_4 group: 2 / 9 = 0.22 *vu*. There are no hydrogen bonds emanating from the structural unit hence $t = 0$ and $s = 0$. The interstitial complex has two transformer H_2O groups, one non-transformer H_2O group, no H_2O groups not bonded to any cation and six OH groups. The effective charge of the interstitial complex is its formal charge plus the charge of hydrogen bonds transferred to the

interstitial complex = 4 + 0 = 4. The number of bonds from the interstitial complex to the structural unit is 7 x 1 (from Ca,Cd) + 6 x 4 (from Cu) + 2 [from transformer H_2O groups] – 6 x 2 (the number of interstitial OH groups × the coordination of (OH) – 1) + 0 = 21. The Lewis acidity of the interstitial complex is 4 / 21 = 0.19 *vu*.

Munakataite has interstitial complex $\{^{[6]}Pb^{2+}\,^{[9]}Pb^{2+}Cu^{2+}{}_2\,^{[2]}(OH)_2\,^{[3]}(OH)_2\}^{4+}$ interacting with a structural unit $[(SO_4)^{2-},(SeO_3)^{2-}]$. The O atoms of the (SO_4) group accept one hydrogen bond from OH groups, six bonds to the Pb cation and two bonds to the Cu cation bonds. The Lewis basicity of the (SO_4) group is its charge divided by the number of bonds accepted by the (SO_4) group: 2 / 9 = 0.22 *vu*. The O atoms of the (SeO_3) group accept no hydrogen bonds, seven bonds to the Pb cation and two bonds to the Cu cation bonds. The Lewis basicity of the (SO_4) group is its charge divided by the number of bonds accepted by the (SO_4) group: 2 / 9 = 0.22 *vu*. There are no hydrogen bonds emanating from the structural unit hence $t = 0$ and $s = 0$. The interstitial complex has no H_2O groups and six OH groups. The effective charge of the interstitial complex is its formal charge plus the charge of hydrogen bonds transferred to the interstitial complex = 4 + 0 = 4. The number of bonds from the interstitial complex to the structural unit is 6 x 1 (from Pb2) + 9 x 1 (from Pb2) + + 6 x 2 (from Cu) – (2 x 2) – (2 x 1) (the number of interstitial OH groups × the coordination of (OH) – 1) + 0 = 21. The Lewis acidity of the interstitial complex is 4 / 21 = 0.19 *vu*.

Serpierite, linarite and gartrellite are common secondary minerals in the oxidized zone of many sulphide orebodies, and hureaulite and rockbridgeite are common pegmatitic phosphate minerals. This reflects the high thermodynamically stability of these phases (e.g. Ropp and Mooney 1960; Nriagu and Dell 1974; Abdul-Samad et al. 1982). That Cd analogues of serpierite and hureaulite as well as a range of other Cd secondary minerals are found at Broken Hill reflects the geochemical conditions that were dominant during their formation, in particular the ready availability of Cd in the solutions from which the minerals were precipitating. Similarly, the occurrence of munakataite, plimerite and Al dominant gartrellite is the result of the availability of Se, Zn and Al from solution.

The calculations above show that, in these minerals, the Lewis basicity of the structural unit matches the Lewis acidity of the interstitial complex. Hence, during crystallization, cooperative interaction between the formation of the structural unit and the interstitial complex has resulted in stable structural arangements. The calculations also show that, in cadmian serpierite and edwardsite, water plays a role in stabilizing the structures. Water molecules coordinated to the interstitial cations act as bond valence transformers, thereby reducing the cation's bonding strength to match the Lewis basicity of the structural unit.

11.2 Paragenetic and structural relations

Hawthorne (1998) has noted that complex geological environments, such as oxidized zones over sulphide orebodies, which contain a large number of complicated minerals of several different chemical types, present a challenge to our understanding of the geochemical processes responsible for their formation. These deposits form by nonequilibrium processes. As ambient conditions change, the minerals adjust their structure; i.e. break down to form new minerals. Thus the paragenetic sequences of minerals in such environments should be related to the crystal structures of the constituent minerals. Hawthorne (1998) has suggested that such an evolving system can be monitored through the progressive change in the crystal structures of the constituent phases.

Hawthorne (1992) in an examination of the paragenesis of magnesium sulphate minerals found that with progressive crystallization, there is a gradual depolymerization of the structural unit, accompanied by decrease in basicity of the structural unit. This is affected by the incorporation of increasing amounts of H_2O into the structural unit, blocking further polymerization. By using a pH–log[H_2O] activity–activity diagram, Schindler and Hawthorne (2001b) have shown that, for borate minerals, with increasing activity of [H_2O], there is a trend in structural units from frameworks to sheets to chains to clusters and isolated polyhedron structures.

The Broken Hill oxidized zone has had a long and complex history. Constructing a simple paragenetic model has presented difficulties, with many variables needing to be taken into consideration. Birch and van der Heyden (1997) identified four broad mineral associations in the oxidized zone, as revealed by the Kintore and Block 14 Opencuts: (1) a series rich in zinc; (2) an arsenate rich assemblage; (3) an iron and phosphate-rich assemblage; (4) a suite of zinc and copper sulphates.

The mineral species from the phosphate and arsenate assemblages, in particular, show a complex chemistry, with a wide variety of different cations being present and the minerals showing a wide range of crystal structure types.

Birch and van der Heyden (1997) noted that, in the complex mineral assemblages from the Broken Hill oxidized zone, there is little evidence for multiple stages of

dissolution and reprecipitation, and individual minerals crystallized in quite rapid succession in response to changes in solution chemistry. Textural features of the oxidized zone assemblages suggest that the overall sequence of crystallization likely represents a change from acid to more alkaline conditions.

Examination of specimens containing the minerals investigated in this study has identified a general sequence of crystallization for the plimerite, nyholmite, edwardsite and gartellite bearing parageneses.

In the plimerite bearing paragenesis, pyromorphite is the earliest formed mineral and is partially replaced by corkite/kintoreite, which is overgrown by the later minerals.

pyromorphite → corkite/kintoreite → strengite → rockbridgeite/plimerite → libethenite → corkite/kintoreite → tsumebite

Pyromorphite, strengite, rockbridgeite/plimerite and libethenite are infinite framework structures, corkite/kintoreite is an infinite sheet structure and tsumebite is an infinite chain structure. The general trend is for a depolymerization of the structural unit through the paragenetic sequence. No trend for a decrease or increase in basicity of the structural unit is however apparent.

In the gartrellite bearing paragenesis, mimetite is the earliest formed mineral, followed by agardite-Y. Gartrellite overgrows agardite-Y and carminite and is sprinkled with crystals of beudantite/segnitite.

mimetite → agardite-Y → carminite → gartrellite → beudantite/segnitite

Mimetite and agardite-Y are infinite framework structures and carminite, gartrellite and beudantite/segnitite are infinite sheet structures. Again the trend is for for a depolymerization of the structural unit through the paragenetic sequence.

In the nyholmite bearing parageneses the crystallization sequence is:

strengite → sampleite → goldquarryite → nyholmite

No trend towards depolymerization is apparent as each of these minerals has an infinite framework structure.

This is only a tiny sample of the many Broken Hill secondary mineral assemblages, and it is not clear if the minerals in these parageneses have precipitated progressively during the same episode of crystallization or if there were multiple stages of crystallization. However these parageneses do appear to give some (small) support for the concept that in complex parageneses, with progressive crystallization, framework structures should be replaced by sheet structures, chain structures, etc.

11.3 Crystal chemical behaviour of Cd^{2+} in oxysalt minerals

The Cd^{2+} cation typically occurs in sulphide and selenide mineral structures in sites that are [4]- or [6]-coordinated. Edwardsite is the first oxysalt mineral in which Cd^{2+} is [7]-coordinated. In all other Cd oxysalt mineral structures, the Cd^{2+} cation is in octahedral coordination, with an <Cd-ϕ>, (ϕ: O^{2-}, H_2O, Cl), bond length of 2.295 Å [range: 2.169–2.549 Å] (Cooper and Hawthorne 1996; Giester *et al.* 1998; Cooper and Hawthorne 2000; Cooper and Hawthorne 2004; Elliott *et al*. 2008; Elliott *et al*. 2009a; Elliott *et al*. 2009b).

Many Cd compounds have been synthesized, including sulphides, tellurides, selenides, halenogides, oxides, sulphates, phosphates, arsenates, chromates, molybdates, borates, silicates, arsenides and phosphides [Inorganic Crystal Structure Database (ICSD) (Belsky *et al*. 2002)]. The observed coordination number of Cd^{2+} in synthetic compounds is principally 6, 8, and 12, with rare examples of 4, 5, 7 and 9 (Brehler 1972).

There are eleven oxysalt minerals that contain essential cadmium (Table 1) and the crystal structure of each of these is known. As noted above, Cd^{2+} is in octahedral coordination in each structure (except edwardsite), however the connectivity of $Cd\phi_6$ (ϕ: unspecified anion) octahedra is very different in each. The structures of andyrobertsite, birchite, burnsite, goldquarryite and keyite have all proved to be new structure types.

Table 1. Oxysalt minerals containing essential cadmium.

Name	Formula	Reference
Andyrobertsite	$KCdCu_5(AsO_4)_4[As(OH)_2O_2]\cdot 2H_2O$	Cooper *et al*. (1999)
Birchite	$Cd_2Cu_2(PO_4)_2(SO_4)\cdot 5H_2O$	Elliott *et al*. (2007)
Burnsite	$KCdCu_7O_2(SeO_3)_2Cl_9$	Krivovichev *et al*. (2002)
Edwardsite	$Cu_3Cd_2(SO_4)_2(OH)_6\cdot 4H_2O$	this thesis
Goldquarryite	$CuCd_2Al_3(PO_4)_4F_2(H_2O)_{10}\cdot 2H_2O$	Roberts *et al*. 2003
dobrecite	$CdSO_4\cdot 4H_2O$	Giester (2010)
Keyite	$Cu_3(Zn,Cu)_4Cd_2(As)_6\cdot 2H_2O$	Embrey *et al*. (1977)
Monteponite	CdO	Anthony *et al*. (1990)
Niedermayrite	$Cu_4Cd(SO_4)_2(OH)_6\cdot 4H_2O$	Geister *et al*. (1998)
Nyholmite	$Cd_3Zn_2(AsO_3OH)_2(AsO_4)_2\cdot 4H_2O$	this thesis
Otavite	$CdCO_3$	Pinch and Wilson (1977)

The Broken Hill oxidized zone has proved to be an important source of Cd secondary minerals. These have resulted from the weathering of sphalerite, which contains small concentrations of Cd (up to 3000 ppm in the No. 3 lens), principally as an isomorphic replacement for zinc (Edwards 1955; Both 1973). Three of the eleven known Cd oxysalt minerals have been described from Broken Hill (birchite, nyholmite and edwardsite). In addition, otavite, $CdCO_3$, goldquarryite, $CuCd_2Al_3(PO_4)_4F_2(H_2O)_{10}(H_2O)_2$, and niedermayrite, $Cu_4Cd(SO_4)_2(OH)_6\cdot 4H_2O$, have been identified from the oxidized zone, as have cadmian varieties of conichalcite-duftite, sampleite-lavendulan, zdenekite, christelite and serpierite (see below).

A notable feature of the Cd bearing secondary minerals from Broken Hill is that, in most, Cd is in solid solution with another cation; Ca, Pb or Zn. Very little is known about solid solution involving Cd in minerals. The only published analysis of an oxysalt mineral from another locality which shows any solid solution involving Cd is that of cadmian smithsonite from Laurium, Greece, which has a CdO content of 2.70 wt.% [analysis of Christomanos (1896) cited by Palache *et al*., (1951)].

The extent to which atomic substitution takes place in minerals is determined by the nature of the structure, the relative sizes of the ionic radii and the temperature of formation of the mineral. There are four solid solution possibilities: (l) no solid

solution, (2) complete solid solution without structural ordering, (3) solid solution with structural ordering at some intermediate composition or (4) partial solid solution (Nickel 1992). Generally, if the size difference of substituting ions and the ions substituted for do not differ by more that 15%, then extensive solid solution can be expectecd at room temperature. Atomic substitution increases as temperature increases.

Otavite, $CdCO_3$, a member of the calcite group (as is smithsonite), from the Kintore Opencut, Broken Hill is close to pure end-member composition, containing only minor amounts of Pb (0.06 *apfu*), Zn (0.03 *apfu*) and Ca (0.02 *apfu*) (Birch 1990). The calcite-otavite solid solution has been shown to be complete using synthetic material (Chang and Brice 1971; Borodin *et al*. 1979), as would be expected based on the similarities in ionic radii of $^{[6]}Ca^{2+}$ (1.00 Å) and $^{[6]}Cd^{2+}$ (0.95 Å) and their similar electronic configuration (Ca [Ar]$4s^2$; Cd [Kr]$4d^{10}5s^2$).

Nyholmite, $Cd_3Zn_2(AsO_3OH)_2(AsO_4)_2{\cdot}4H_2O$, is the first natural Cd-bearing (and Zn-bearing) member of the hureaulite group. The synthetic compound $Cd_5(AsO_4)_2(AsO_3OH)_2{\cdot}4H_2O$ (Johnson *et al*. 2003) and its phosphate analogue $Cd_5(PO_4)_2(PO_3OH)_2{\cdot}4H_2O$ (Hideki *et al*. 1976), which have hureaulite-type structures, have both been prepared by hydrothermal methods. The discovery of nyholmite leads to the question of the extent of possible solid solution involving Cd (ionic radius 0.95 Å; Shannon 1976) and Zn (ionic radius 0.74 Å) in hureaulite group minerals, as well as in other oxysalt minerals.

Nyholmite was the first natural mineral with a hureaulite-type structure that showed structural evidence for ordering of cations in the three *M* sites in the structure. Although containing significant Ca (Mn:Ca = 2.69:2.07), type villyaellenite from the Sainte-Maie aux Mines, France was defined as ideally $Mn_5(AsO_3OH)_2(AsO_4)_2{\cdot}4H_2O$ (Sarp 1984). Kampf and Ross (1988) refined the structure of villyaellenite using a Zn-bearing crystal from the Ojuela Mine, Mapimi, Mexico and suggested that, although no structural information was available as to the extent of ordering of Ca and Mn in type villyaellenite, bond distances and refined site occupancies suggest that Zn is preferentially contained in the *M*2 site in the structure and Ca in the *M*3 site. The authors also cited paragenetic evidence, which supports some degree of ordering of Mn and Ca in type villyaellenite, but suggested that a complete solid solution may not

exist. Based on a single-crystal structure refinements, Kampf (2009) renamed endmember $Mn_5(AsO_3OH)_2(AsO_4)_2{\cdot}4H_2O$ miguelromeroite and, using type material, villyaellenite was redefined as an ordered species, $(Mn,Ca)Mn_2Ca_2(AsO_3OH)_2(AsO_4)_2{\cdot}4H_2O$, in the sainfeldite-miguelromeroite series, with the *M*1 site occupied by Mn plus Ca, the *M*2 site occupied by Mn and the *M*3 site dominated by Ca.

Moore and Araki (1973) noted that natural hureaulites in the series $Mn_{5-x}Fe_x(H_2O)_4(PO_4H)_2(PO_4)_2$, $0 < x < 5$, are limited to a Fe:Mn ratio of ~1:3. Von Klement *et al*. (1970) prepared synthetic hureaulites containing Mn^{2+}, Fe^{2+}, Co^{2+}, Zn, Cd^{2+}, and Cu^{2+} and concluded that experimental evidence suggests that Fe content appears to be limited to 35% of Mn^{2+} being replaced by Fe^{2+}. However Moreira *et al*. (1994) showed that there is a continuous solid solution between $Mn_5(H_2O)_4(PO_4H)_2(PO_4)_2$ and $Fe_5(H_2O)_4(PO_4H)_2(PO_4)_2$ and that Fe^{2+} is preferentially substituted into the *M*2 and *M*3 sites in the structure.

The refinement of the nyholmite structure also shows that ordering of cations occurs in the *M* sites and strongly suggests that there is at least a partial ordering of Cd+Zn in the *M*1 site, Zn+Cu+Cd+Mn and minor Al in the *M*2 site and Cd with minor Zn, Ca and Pb in the *M*3 site.

Evidence from the chemistry and structure refinements of nyholmite, sainfeldite, villyaellenite, miguelromeroite, synthetic hureaulites and an unnamed mineral from the Gozaisho mine, Honshu Island, Japan (Matsubara *et al*. 1996) suggests that the *M*1 site is capable of accepting a full range of large (e.g. Ca, Cd) and small (e.g. Mn, Fe, Zn) cation occupancies. Thus it might be expected that a continuous solid solution series, $(Cd_{1-x},Zn_x)M2_2M3_2(AsO_3OH)_2(AsO_4)_2{\cdot}4H_2O$, exists for Cd and Zn bearing hureaulites. The degree of solid solution between large and small cations on the *M*2 the *M*3 sites appears to be limited in the hureaulite type compounds.

Although, apart from nyholmite (and smithsonite containing minor Cd), there are no oxysalt minerals known with Cd<=>Zn substitution, a number of synthetic compounds are listed in the Inorganic Crystal Structure Database (ICSD) (Belsky *et al*. 2002) that show significant solid solution involving Cd and Zn, including oxides, phosphates, tungstates and nitrides, including both continuous solid solutions and partial solid solutions with miscibility gaps and phase transitions.

Synthetic analogues of spinel show a solid solution series between Zn–Ni and Cd–Ni ferrites, with composition $Cd_{0.5-\alpha}Zn_{\alpha}Ni_{0.5}Fe_2O_4$, and with Cd and Zn in tetrahedral coordination. The octahedral site in the structure is occupied by Ni and Fe.

Cd for Zn substitution occurs, in an octahedrally coordinated site, in the solid solution system $Zn_{1-x}Cd_xWO_4$ from x = 0.0~1.0 (Dahlborg *et al*. 1999). $ZnWO_4$ has a wolframite structure type and as x increases, the structure distorts towards a scheelite type structure. The series is continuous with no miscibility gap.

Six solid solution phases, which are structurally closely related to graftonite, $(Fe^{2+},Mn^{2+},Ca)_3(PO_4)_2$, occur in the β-$Zn_3(PO_4)_2$ – $Cd_3(PO_4)_2$ system,. Two of the phases, $CdZn_2(PO_4)_2$ and $Cd_2Zn(PO_4)_2$, crystallize in space group $P2_1/c$ with closely related structures and a miscibility gap between the two. Cd has a preference for the 7-coordinate M1 site in the structures rather than the 5 coordinate M2 and M3 sites (Calvo and Stevens 1968).

Several synthetic Cd-bearing compounds have structures that are analogues of those of natural minerals. These include analogues of halite (Kusigerski *et al*. 1996), alluaudite (Hatert 2008) and langbeinite (Magome *et al*. 2002), which each show solid solutions of Cd and Mn^{2+} (ionic radius 0.83 Å).

Chemical analyses of serpierite, sampleite-lavendulan, zdenekite, conichalcite-duftite and christelite from Broken Hill show solid solutions involving Ca, Pb^{2+} (ionic radius 1.23 Å) and Cd^{2+}.

Serpierite from the Block 14 Opencut, Broken Hill contains up to 12.18 wt% CdO, equivalent to ~0.64 atoms per formula unit (*apfu*), which is high enough to warrant separate species status. Results from electron microprobe analysis show that there is a strong negative linear correlation between Ca atoms and Cd atoms *pfu* indicating that Cd subsitutes for Ca in the crystal stucture. The crystal structure of cadmian serpierite has been refined using single-crystal X-ray data. Full details of the chemistry and crystal structure are provided in Chapter 9 of this thesis. Refinement of the occupancy of the [7]-coodinated Ca site in the structure, using the Ca scattering factor, resulted in a value of 1.20, which shows partial occupancy by a heavier atom and refinement of the Ca:Cd ratio gave 0.659(7):0.341(7). Occupancy refinement of the five Cu sites did not give any indication of the presence of any atoms heavier than Cu or Zn (e.g. Cd).

As would be expected, considering the similar ionic radii of $^{[7]}Ca^{2+}$ (1.06 Å) and $^{[7]}Cd^{2+}$ (1.03 Å), there is little variation between the (Ca,Cd)–O bond lengths in the structure of cadmian serpierite and the Ca–O bond lengths in serpierite (Sabelli and Zanazzi 1968), with mean distances of 2.399 and 2.41 Å respectively). Similarly, the sites in both structures have an augmented octahedral coordination and show only a small variation in O–(Ca,Cd)–O angles. The analyses of cadmian serpierite show only very low Pb contents (<0.5 Wt.% PbO). Based on the valence-matching principal (Brown 1981), Pb would however be expected as an interstitial cation in the cadmian serpierite structure.

The lavendulan group of minerals comprises lavendulan, $NaCaCu_5(AsO_4)_4Cl{\cdot}5H_2O$, zdenekite, $NaPbCu_5(AsO_4)_4Cl{\cdot}5H_2O$, and sampleite, $NaCaCu_5(PO_4)_4Cl{\cdot}5H_2O$. The crystal structure of the lavendulan group minerals comprises sheets of $Cu(O,H_2O,Cl)_5$ tetragonal pyramids and XO_4 (X=As,P) tetrahedra which link via NaO_6 and CaO_7 (sampleite, lavendulan) or PbO_7 (zdenekite) polyhedra as well as by weak hydrogen bonding into a loose framework (Zubkova *et al*. 2003; Giester *et al*. 2007). Solid solubility among the members of the lavendulan group has been noted from several occurrences. These mostly involve As<=>P substitution. Phosphatian lavendulan with an As:P ratio of 79:21 has been described from the Dome Rock Mine, South Australia (Kleeman and Milnes 1973). Members of the solid solution series lavendulan-sampleite with variable As:P ratios are also known from the Santa Catalina Mine, Sierra Gorda, Antofogasta Province, Chile (Giester *et al*. 2007). Zincian lavendulan has been reported from Tsumeb, Namibia (Strunz 1959). Calcian zdenekite, with Pb:Ca ~88:12, has been recorded from the Cap Garonne deposit, Var, France and a probable restricted solid solution between zdenekite and lavendulan was postulated by Chiappero and Sarp (1995). Cadmian-plumboan and plumboan varieties of sampleite and calcian, calcian-phosphatian and cadmian varieties of zdenekite from Broken Hill have previously been noted (Birch and van der Heyden 1988 1997; Giester *et al*. 2007).

Microprobe analyses of cadmian-plumboan sampleite from the Block 14 Opencut, Broken Hill (Appendix A) shows solid solution series involving Ca, Pb and Ca, with wide compositional ranges: PbO 2.82–12.43, CdO 1.34–5.76, CaO 1.99–3.86 Wt.%.

Figure 1 shows a negative correlation (R^2 = 0.750) between Cd and Pb+Ca *pfu* consistent with the occurrence of these elements on a single crystallographic site. The analyses show only very minor As and S for P substitution (<0.15 Wt.% As_2O_5 and SO_3).

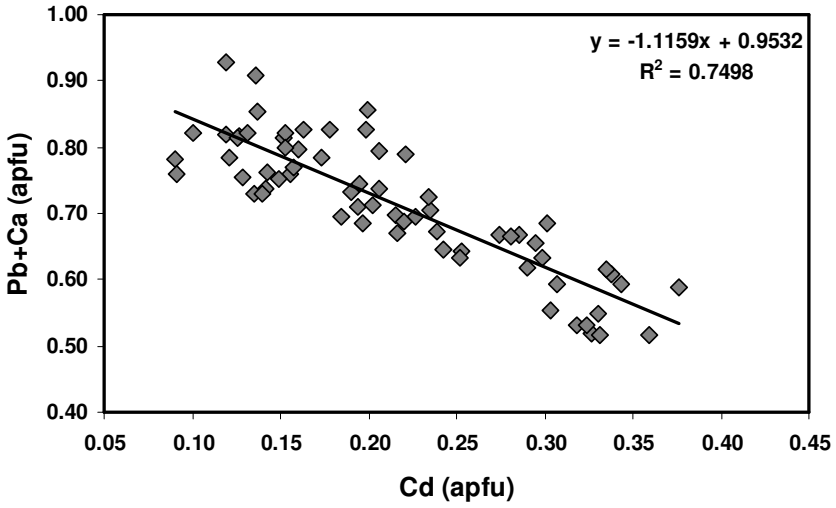

Figure 1. Bivariate plot illustrating the negative correlation between Cd and Pb+Ca in sampleite.

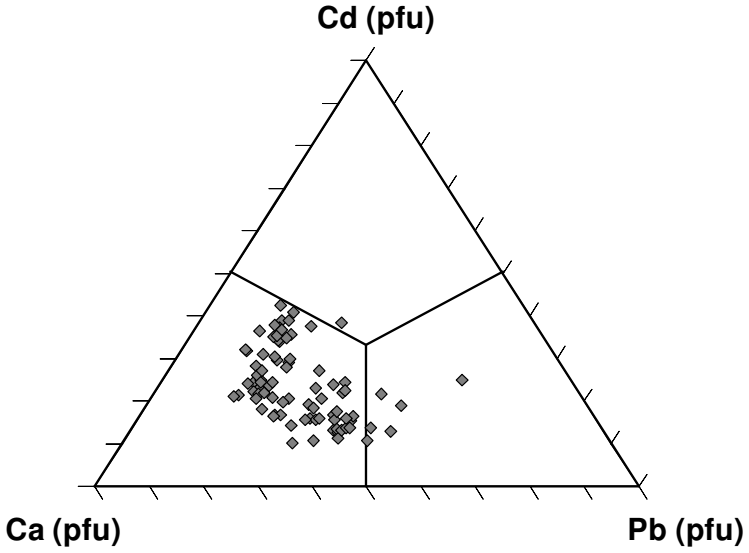

Figure 2. Ternary diagram showing the variation of Ca, Pb and Cd content in sampleite from Broken Hill as determined from electron-microprobe analysis.

In a Ca-Cd-Pb ternary diagram (Figure 2), most of the analyses are within the Ca field, with several analyses plotting in the Pb field and only one analysis plots within the Cd field.

Microprobe analyses of zdenekite from the Block 14 Opencut, Broken Hill (Appendix A) shows contents of up to 5.43 wt% CdO, equivalent to ~0.50 *apfu*, which is high enough to warrant separate species status. The analyses show only the presence of only a small amount of Ca (< 0.80 wt.% CaO) and minor P for As and S for As substitution (< 1.10 Wt.% P_2O_5 and < 0.50 Wt.% SO_3). A plot of Cd vs. Pb+Ca pfu (Figure 3) shows shows solid solution series of these elements. The fair correlation ($R^2 = 0.66$) is most likely a result of the variable analyses due to the deterioration of the mineral under the electron beam.

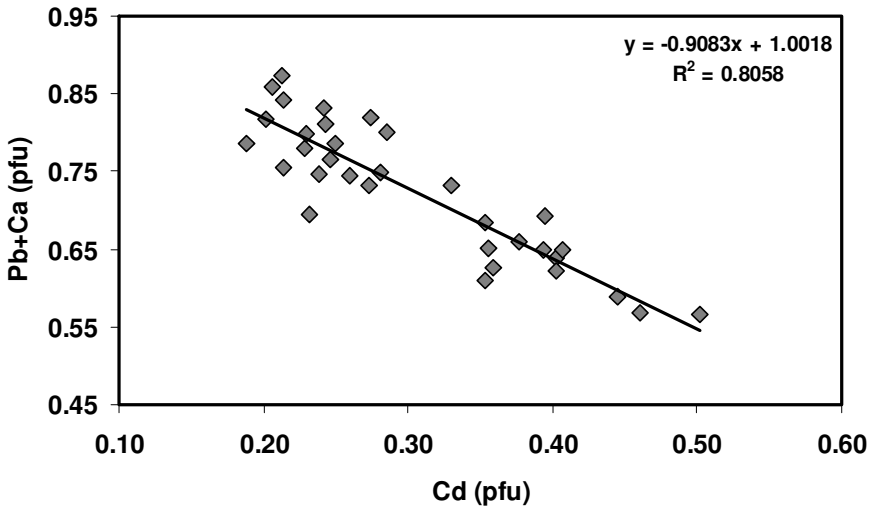

Figure 3. Bivariate plot illustrating the negative correlation between Cd and Pb+Ca in sampleite.

In a Pb-Ca-Cd ternary diagram (Figure 4), the majority of analyses are within the Pb field, with several analyses plotting in the Cd field. The Ca content reaches a maximum of only 0.14 *apfu*.

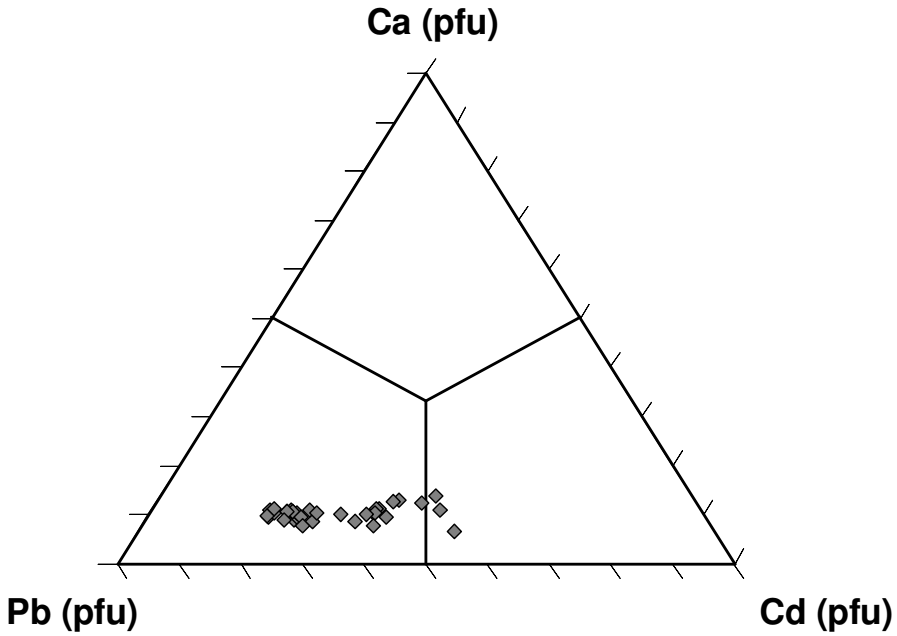

Figure 4. Ternary diagram showing the variation of Ca, Pb and Cd content in zdenekite from Broken Hill as determined from electron-microprobe analysis.

Qualitative Energy Dispersive X-ray analysis (EDS) using an XL20 scanning electron microscope at Adelaide Microscopy has shown that conichalcite-duftite from Broken Hill can contain significant Cd (Appendix A). Attempts to analysis the mineral by electron microprobe were not successful, as the tiny crystals proved to be very difficult to polish.

Conichalcite is a member of the adelite group of minerals which is characterized by the general formula $AB_2C(XO_4)(OH)$, where the A site can be Ca or Pb, the B site can be Co, Cu, Fe^{2+}, Mg, Ni, Zn and the X site can contain P^{5+}, As^{5+}, and V^{5+} (Krause *et al*. 1998, 2002; Brugger *et al*. 2000). The minerals are orthorhombic, space group $P2_12_12_1$. The crystal structure of conichalcite was first determined by Qurashi and Barnes (1963) and was later refined by Radcliffe and Simmons (1971). The structure is based of chains of edge-sharing MO_6 octahedra, parallel to *c*; which are linked via AsO_4 tetrahedra and Ca atoms, in distorted square antiprismatic co-ordination, to form a framework network. Substitution of cations is common in the minerals of the adelite group and complete solid solutions have been demonstrated between austinite, $CaZn(AsO_4)(OH)$, and conichalcite, $CaCu(AsO_4)(OH)$, (Taggart and Foord 1980; Jambor *et al*. 1980), and between duftite, $PbCu(AsO_4)(OH)$, and conichalcite,

(Jambor *et al*. 1980). The occurrence of cadmian conichalcite from Broken Hill suggests that continuous Cd↔Ca and Cd↔Pb solid solutions may also exist in the adelite group minerals.

The existance of solid solutions involving Ca, Pb^{2+} and Cd^{2+} in sampleite, zdenekite and conichalcite and involving Ca and Cd^{2+} in serpierite, as well as the possibility of Pb^{2+} substitution in serpierite can be examined in terms of the coordination environments of the sites occupied by these cations each crystal structure. Although distorted, the [7]-coordinated Ca site in sampleite (Giester *et al*. 2007), the [7]-coordinated Pb site in zdenekite (Zubkova *et al*. 2003), the [8]-coordinated (Ca,Pb) site in conichalcite-duftite and the [7]-coordinated (Ca,Cd) site in cadmian serpierite do not show an appreciable assymmetry. All (Ca,Pb)-O bond distances are in the range 2.297–2.811 Å and the sites do not show the a one-sided coordination characteristic of a Pb^{2+} cation in which the $6s^2$ lone-electron pair is stereoactive (ie. short Pb^{2+}–O bonds in one half of the coordination sphere and long Pb^{2+}–O bonds in the other). Hence it would be expected that there is no crystal chemical constraint on solid solutions between Pb^{2+} and Ca or Cd in these minerals. The presence of only a minor amount of Pb in cadmian serpierite and Ca in zdenekite is likely due to geochemical rather than crystal-chemical reasons.

Other mineral pairs in which the coordination environments of the Ca and Pb cations are very similar, and which raise the possibility of Ca<=>Pb solid solution are mottramite-tangeite and carminite-sewardite, although analyses of natural mineral specimens do not show any significant Pb<=>Ca substitution in these minerals.

Evidence that the existance of solid solution involving Pb and Ca in minerals may be governed by the crystal-chemical constraint of an asymmetric coordination due to the stereoactive $6s^2$ electron lone pair on the Pb^{2+} cation is provided by structures in which there is both distorted and undistorted Pb^{2+} sites. Compounds with the barysilite structure type have the structural formula $Pb1_6Pb2_2M^{2+}(T_2O_7)_3$, with M^{2+} = Be, Mg, Ca, Mn, Fe, Co, Ni, Cu, Zn, Sr, Ba, Cd or Pb, and T = Si or Ge (Schmidt *et al*. 1983). The [6]-coordinated Pb1 site has a highly irregular, one-sided coordination characteristic of stereoactive lone-pair behavior of Pb^{2+}, whereas the [6+3]-coordinated Pb2 site is fairly regular. Structure refinement of a Ca bearing barysilite has provided evidence of a preference of Ca for the Pb2 site, and not the more distorted Pb1 site or the Mn site (Kolitsch and Holtstam 2002).

11.4 References

Anthony, J.W., Bideaux, R.A., Bladh, K.W. and Nichols, M.C. (1990) Handbook of Mineralogy. Vol. III: Halides, Hydroxides, Oxides. Mineral Data Publishing, Tucson, Arizona, USA, 628 p.

Belsky, A., Hellenbrandt, M., Karen, V.L. and Luksch, P. (2002) New developments in the Inorganic Crystal Structure Database (ICSD): accessibility in support of materials research and design. Acta Crystallographica, B58, 364–369.

Birch, W.D. (1990) Minerals from the Kintore and Block 14 Opencuts, Broken Hill, N.S.W.; a review of recent discoveries, including tsumebite, kipushite and otavite. Australian Mineralogist, 5, 125–141.

Birch, W.D., and van der Heyden, A. (1988) Minerals of the Kintore Opencut, Broken Hill, New South Wales. Mineralogical Record, 19, 425–436.

Birch, W.D. and van der Heyden, A. (1997) Minerals from the Kintore and Block 14 Open cuts, Broken Hill, New South Wales. Australian Journal of Mineralogy, 3, 23–71.

Borodin V.L., Lyntin V.I., Ilyukhin V.V. and Belov N. V. (1979) Isomorphous calcite-otavite series. Soviet Physics, Doklady, 24, 226–227.

Both, R. A. (1973) Minor element geochemistry of sulphide minerals in the Broken Hill lode (N.S.W.) in relation to the origin of the ore. Mineralium Deposita, 8, 349–369.

Brehler, B. (1972) Cadmium crystal chemistry. In Handbook of Geochemistry, Vol. II. K.H. Wedepohl, Ed., Springer-Verlag, Berlin, Germany.

Brown, I.D. (1981) The bond-valence method: an empirical approach to chemical structure and bonding. In M. O'Keefe and A. Navrotsky, Eds., Structure and Bonding in Crystals. Academic Press, London, 1-30.

Calvo, C. and Stephens, J.S. (1968) Crystal Structure of $CdZn_2(PO_4)_2$ and $Cd_2Zn(PO_4)_2$. Canadian Journal of Chemistry, 46, 903–915.

Chang, L.L.Y. and Brice, W.R. (1971) Subsolidus phase relations in the system calcium carbonate-cadmium carbonate. American Mineralogist, 56, 338–341.

Chiappero, P.-J. and Sarp, H. (1995) Zdenekite, $NaPbCu_5(AsO_4)_4Cl{\cdot}5H_2O$, a new mineral from the Cap Garonne mine,Var, France. European Journal of Mineralogy, 7, 553–557.

Cooper, M.A., and Hawthorne, F.C. (1996) The crystal structure of keyite, $Cu_3(Zn,Cu)_4\ Cd_2(AsO_4)_6(H_2O)_2$, an oxysalt mineral with essential cadmium. Canadian Mineralogist, 34, 623–630.

——— (2000) Highly undersaturated anions in the crystal structure of andyrobertsite–calcio-andyrobertsite, a doubly acid arsenate of the form $K(Cd,Ca)[Cu^{2+}{}_5(AsO_4)_4\{As(OH)_2O_2\}](H_2O)_2$. Canadian Mineralogist 38, 817–830.

——— (2004) The crystal structure of goldquarryite, $(Cu^{2+},\square)(Cd,Ca)_2Al_3(PO_4)_4F_2(H_2O)_{10}\{(H_2O),F\}_2$, a secondary phosphate from the Gold Quarry mine, Eureka County, Nevada, U.S.A. Canadian Mineralogist, 42, 753–761.

Cooper, M.A., Hawthorne, F.C., Pinch, W.W. and Grice, J.D. (1999) Andyrobertsite and calcioandyrobertsite: two new minerals from the Tsumeb mine, Tsumeb, Namibia. Mineralogical Record, 30, 181–186.

Dahlborg, M.A., and Svensson, G. (1999) Structural changes in the system $Zn_{1-x}Cd_x\ WO_4$, determined from single crystal data. Acta Chemica Scandinavica, 53, 1103–1109.

Edwards, A.B. (1955) Cadmium in the Broken Hill lode. Proceedngs of the Australasian Institute of Mining and Mellallurgy, 176, 71–96.

Elliott, P., Brugger, J., Pring, A., Cole, M.L., Willis, A.C., and Kolitsch, U. (2008) Birchite, a new mineral from Broken Hill, New South Wales, Australia: description and structure refinement. American Mineralogist, 93, 910–917.

Embrey, P.G., Fejer, E.E., and Clark, A.M. (1977) Keyite: a new mineral from Tsumeb. Mineralogical Record, 8, 87-90.

Giester, G. (2010) Drobecite, a novel mineral from the Lavrion, Greece, deposit. 20th General Meeting of IMA (IMA2010) August 21 – 27, 2010, Budapest, Hungary (poster).

Giester, G., Kolitsch, U., Leverett, P., Turner, P. and Williams, P.A. (2007) The crystal structures of lavendulan, sampleite, and a new polymorph of sampleite. European Journal of Mineralogy, 19, 75–93.

Giester, G., Rieck, B., and Brandstätter, F. (1998) Niedermayrite, $Cu_4Cd(SO_4)_2(OH)_6{\cdot}4H_2O$, a new mineral from the Lavrion District, Greece. Mineralogy and Petrology, 63, 9–34.

Hatert, F. (2008) Crystal chemistry of the divalent cation in alluaudite-type phosphates: A structural and infrared spectral study of the $Na_{1.5}(Mn_{1-x}M^{2+}{}_x)_{1.5}Fe_{1.5}(PO_4)_3$ solid solutions (x = 0 to 1, M^{2+} = Cd^{2+}, Zn^{2+}). Journal of Solid State Chemistry, 181, 1258–1272.

Hawthorne, F. C. (1983) Graphical enumeration of polyhedral clusters. Acta Crystallographica, A39, 724–736.

Hawthorne, F. C. (1985) Towards a structural classification of minerals: The $^{(VI)}M^{(IV)}T_2O_n$ minerals. American Mineralogist, 70, 455–473.

Hawthorne, F. C. (1990) Structural hierarchy in $M^{[6]}T^{[4]}\phi_n$ minerals. Zeitschrift für Kristallographie, 192, 1–52.

Hawthorne, F.C. (1992) Bond topology, bond valence and structure stability. In G.D. Price and N.L. Ross, Eds., The Stability of Minerals. Chapman and Hall, London, pp. 25–87.

Hawthorne, F.C. (1994) Structural aspects of oxide and oxysalt crystals. Acta Crystalographica, B50, 481–510.

Hawthorne, F.C. (1998) Structure and chemistry of phosphate minerals. Mineralogical Magazine, 62, 141–164.

Hawthorne, F.C., and Schindler, M. (2008) Understanding the weakly bonded constituents in oxysalt minerals. Zeitschrift für Kristallographie, 223, 41–68.

Hideki, A., Masaru, A. and Iwai, S.I. (1976) Synthesis and crystal structure of cadmium hydrogen phosphate hydrate. Tokyo Ika Shika Daigaku Iyo Kizai Kenkyusho Hokoku, 10, 63–68 (in Japanese).

Jambor, J.L., Owens, D.R. and Dutrizac, J.E. (1980) Solid solution in the adelite group of arsenates. Canadian Mineralogist, 18, 191–195.

Johnson, C.D., Shakle, J.M.S., Johnston, M.G., Feldmann, J. and Macphee, D.E. (2003) Hydrothermal synthesis, crystal structure and aqueous stability of two cadmium arsenate phases, $CdNH_4(HAsO_4)OH$ and $Cd_5H_2(AsO_4)_4{\cdot}4H_2O$ Journal of Materials Chemistry, 13, 1429–1432.

Kampf, A.R. (2009) Miguelromeroite, the Mn analogue of sainfeldite, and redefinition of villyaellenite as an ordered intermediate in the sainfeldite-miguelromeroite series. American Mineralogist, 94, 1535–1540.

Kampf, A.R. and Ross, C.R. (1988) End-member villyaellenite from Mapimi, Durango, Mexico: Descriptive mineralogy, crystal structure, and implications for the ordering of Mn and Ca in type villyaellenite. American Mineralogist, 73, 1172–1178.

Kleeman, A.W. and Milnes, A.R. (1973) Phosphorian lavendulan from Dome Rock mine, South Australia. Transactions of the Royal Society of South Australia, 97, 135–137.

Kolitsch, U. and Holtstam, D. (2002) Barysilite from Garpenberg Norra, Dalarna, Sweden: occurrence and crystal structure refinement. Mineralogical Magazine, 66, 353–363.

Krivovichev, S.V., Vergasova, L.P., Starova, G.L., Filatov, S.K., Britvin, S.N., Roberts, A.C. and Steele, I.M. (2002) Burnsite, $KCdCu_7O_2(SeO_3)_2Cl_9$, a new mineral species from the Tolbachik volcano, Kamchatka Peninsula, Russia. Canadian Mineralogist, 40, 1171–1175.

Kusigerski, V., Spasojevic, V. and Mitric, M. (1996) Synthesis and some physical properties of the diluted magnetic semiconductor $Cd_{1-x}Mn_xO$. Journal of Physics: Condensed Matter, 8, 10581–10588.

Magome, E., Moriyoshi, C., Itoh, K. and Vlokh, R. (2002) X-ray structure analysis of $K_2Cd_{2x}Mn_{2(1-x)}(SO_4)_3$ mixed crystal in the high-temperature phase. Ferroelectrics, 269, 93–98.

Matsubara, S., Kato, A., Shimizu, M., Sekiuchi, K. and Suzuki, Y. (1996) Romeite from the Gozaisho mine, Iwaki, Japan. Mineralogical Journal, 18, 155–160.

Moore, P.B. and T. Araki (1973) Hureaulite, $Mn^{2+}_5(H_2O)_4[PO_4(OH)]_2[PO_4]_2$: its atomic arrangement. American Mineralogist, 58, 302–307.

Moreira, L.F., Domingues, P.H. and Mattievich, E. (1994) Mössbauer studies of the solid solutions of synthetic hureaulite, $[Fe_xMn_{5-x}]PO_4H]_2[PO_4]_2[H_2O]_4$. Journal of Magnetism and Magnetic Materials, 132, 191–196.

Nickel, E.H., (1992) Nomenclature for mineral solid solutions. American Mineralogist, 77, 660–462.

Nriagu, J.O. and Dell, C.I. (1974) Diagenetic Formation of lron Phosphates in Recent Lake Sediments. American Mineralogist, 59, 934–946.

Palache, C., Berman, C. and Frondel, C. (1951) Dana's System of Mineralogy. 7th ed., Vol. II. John Wiley and Sons, New York, 1124 p.

Pinch, W.W. and Wilson, W.E. (1977) Tsumeb minerals: A descriptive list. Mineralogical Record, 8, 5–111.

Roberts, A.C., Cooper, M.A., Hawthorne, F.C., Jensen, M.C. and Foord, E.E. (2003) Goldquarryite, a new Cd-bearing phosphate mineral from the Gold Quarry Mine, Eureka County, Nevada. Mineralogical Record, 34, 237–240.

Sabelli C. and Zanazzi, P.F. (1968) The crystal structure of serpierite. Acta Crystallographica B24, 1214–1221.

Sarp, H. (1984) Villyaellenite, $H_2(Mn,Ca)_5(AsO_4)_4{\cdot}4H_2O$ un nouveau mineral de Sainte-Marie aux Mines (France). Schweizerische Mineralogische und Petrographische Mitteilungen, 64, 323–328.

Schindler, M. and Hawthorne, F.C. (2001a) A bond-valence approach to the structure, chemistry and paragenesis of hydroxy-hydrated oxysalt minerals. I. Theory. Canadian Mineralogist, 39, 1225–1242.

Schindler, M., and Hawthorne, F.C. (2001b) A bond–valence approach to the structure, chemistry and paragenesis of hydroxyhydrated oxysalt minerals. II.

Crystal structure and chemical composition of borate minerals. Canadian Mineralogist, 39, 1243–1256.

Schindler, M., Huminicki, D.M.C. and Hawthorne, F.C. (2006) Sulfate Minerals. I. Bond Topology and Chemical Composition. Canadian Mineralogist, 44, 1403–1429.

Schmidt, U., Breuer, K.H. and Eysel, W. (1983) Crystal chemistry of barysilite-type compounds. Neues Jahrbuch für Mineralogie, Monatshefte, 227–235.

Shannon, R.D. (1976) Revised effective ionic radii and systematic studies of interatomic distances in halides and chalcogenides. Acta Crystallographica, A32, 751–767.

Strunz, H. (1959) Tsumeb, seine Erze und Sekundärminerale, insbesondere der neu aufgeschlossenen zweiten Oxydations-Zone. Fortschr. Mineral., 37, 87–90. (in German)

Taggart, J.E. and Foord, E.E. (1980) Conichalcite, cuprian austinite, and plumbian conichalcite from La Plata County, Colorado. Mineralogical Record, 11, 37–38.

Zubkova, N.V., Pushcharovsky, D.Yu., Sarp, H., Teat, S.J. and MacLean, E.J. (2003) Crystal structure of zdenekite $NaPbCu_5(AsO_4)_4Cl{\cdot}5H_2O$. Crystallography Reports, 48, 939–943.

Chapter 12. Conclusion and Future Work

12.1 Final summary

This thesis has concentrated on the crystal chemistry of eight heavy metal, oxysalt minerals from Broken Hill; plimerite, nyholmite, liversidgeite, edwardsite, gartrellite, munakataite, osakaite and cadmian serpierite. The principal techniques used have been single crystal X-ray diffraction and electron microprobe analysis, with additional data being supplied by powder X-ray diffraction, infrared absorption spectroscopy, Raman spectroscopy and Mössbauer spectroscopy. The minerals plimerite, nyholmite, liversidgeite and edwardsite are species new to science and have been fully characterized and their descriptions published. In addition, the Cd analogue of serpierite and the Al analogue of gartrellite have been identified and await full characterization and publication.

Zincian rockbridgeite has been known from several world localities for many years, however, previous attempts to characterize the mineral as a new species have not been successful. Refinement of the crystal structure using single-crystal x-ray data has confirmed that the mineral, which has been named plimerite, is a distinct species, the Zn analogue of rockbridgeite and frondelite. The structure is ordered, with Fe^{3+}, $Zn+Fe^{2+}$ and Fe^{3+}+Al located in the *M*1, *M*2 and *M*3 sites in the structure respectively. Compositions of rockbridgeite-plimerite from Broken Hill show a solid-solution series from near end member rockbridgeite to $Zn:(Fe^{2+}+Fe^{3+}) = 1:1.67$.

Although several synthetic cadmium compounds with a hureaulite like structure have been prepared, nyholmite is the first known naturally occuring Cd (and Zn) bearing member of the hureaulite group. The structure of nyholmite is ordered with Cd+Zn in the *M*1 site, Zn+Cu+Cd+Mn and minor Al in the *M*2 site and Cd with minor Zn, Ca and Pb in the *M*3 site.

Liversidgeite is the fifth known zinc phosphate mineral. It is structurally closely related to bakhchisaraitsevite, rimkorolgite and synthetic $Zn_2Co_4(PO_4)_4(H_2O)_5{\cdot}2H_2O$. The structure is based sheets parallel to the (011) plane comprising two distinct zig-zag chains of $Zn\phi_6$ edge-sharing octahedra which link to each other and to corner

sharing PO_4 tetrahedra. The sheets link via $[Zn_2\phi_8]$ clusters, comprising edge sharing $Zn\phi_5$ trigonal bipyramids and $Zn\phi_4$ tetrahedra, resulting an open framework. Large ellipsoid channels extend along the *a* direction and are occupied by interstitial H_2O groups. An extensive network of hydrogen bonds provides additional linkage between the sheets in the structure, via the interstitial H_2O groups.

The structure of gartrellite has been refined from single-crystal X-ray data. The structural model agrees with that refined from powder X-ray data by Krause *et al*., (1998). Although the lattice is metrically monoclinic, the structure is triclinic due to the ordering of (Cu+Zn) and (Fe^{3+}+Al) into distinct sites, *Me*2A and *Me*2B, in the structure. Gartrellite from Broken Hill shows considerable chemical variability with substitutions involving Fe^{3+}, Zn and Al and very minor Mn in the *Me*2A site, and Zn replacing Cu^{2+} in the *Me*2B site. Minor presence of Cu^{2+} in the *Me*2A site and Fe^{3+} in the *Me*2B site is indicated, however, the possible extent of these substitutions is not known.

The structure of edwardsite is based on a modified brucite-like $[M\phi_2]_N$ sheet of edge-sharing octahedra. Brucite like sheets are found in a wide variety of structures of both minerals and inorganic compounds. In brucite-like sheets in mineral structures, the octahedral sites are be occupied by medium sized cations like Cu^{2+}, Zn, Al, Mn, Mg, Fe^{3+} and Cr^{3+}, and a number of sheets also contain vacant octahedral sites. Edwardsite is the first mineral structure in which a brucite-like sheet contains both a large cation (ie. Cd) and a cation that is [7]-coordinated.

The structure refinement of munakataite has shown it to warrant separate species status, the SO_4^{2-} dominant analogue of schmiederite, with Se^{4+} and S^{6+} located in distinct sites in the structure with trigonal pyramidal and tetrahedral coordinations respectively.

Structural and chemical data for nyholmite and cadmian serpierite, and chemical data for cadmian varieties of sampleite, zdenekite and conichalcite has shown that Cd forms extensive solid solutions in these minerals. In nyholmite, solid solution occurs between Cd and Zn and in cadmian serpierite, sampleite, zdenekite and conichalcite,

solution occurs between Cd, Ca and Pb. The question of the extent of solid solution in these and other Cd bearing minerals will likely require laboratory preparation of synthetic material.

12.2 Possible areas for future study

Secondary minerals of Pb, Zn, Cd, As and other toxic metals play a critical role in governing mobility of heavy metals in natural systems and an understanding of the chemistry and crystal structures of these minerals is essential to accurately assessing their fate and transport in the environment and in designing chemical remediation strategies.

Hawthorne (1998) suggested the eventual possibility of predicting the stoichiometry and structural characteristics of oxysalt minerals in complex low-temperature geochemical environments. If the factors affecting the incorporation of toxic elements into the mineral structures can be understood sufficiently, this may then be able to be predicted. Hawthorne (1979) proposed that structural units in minerals form by condensation of fundamental building blocks that occur as complexes in hydrothermal or surficial aqueous solutions. If this is the case, there should be a connection between the structural arrangements of minerals and their conditions of crystallization from aqueous solution (e.g. pH) (Hawthorne and Schindler 2008).

Hawthorne (1985, 1986, 1990, 1992, 1994) and Schindler and Hawthorne (2001a) have used a combination of binary representation of structure and bond-valence theory in an attempt to understand the relations between the chemical composition, structure and stability of oxysalt minerals crystallizing from low-temperature aqueous solutions. Schindler and Hawthorne (2001a, b, c 2004, 2007) and Schindler *et al*. (2000a, b 2006) have applied various aspects of this approach to borate, vanadate, uranyl-oxide-hydroxy-hydrate and sulphate minerals. They have shown that Lewis acidity exerts significant restrictions on the chemical and structural details of the interstitial complexes and that the Lewis basicities of some structural units do not allow certain cations to occur as interstitial components (Hawthorne and Schindler 2008). Charge deficiency per anion of the structural unit correlates with the pH of the

environment of crystallization. Predictions of the chemical composition of interstitial complexes have also been fairly successful.

It would be interesting to apply these ideas to other complex parageneses of low-temperature minerals such as the oxidized zones of sulphide ore-bodies. The Broken Hill oxidized zone is one such complex parageneses, and the sulphate, phosphate, arsenate assemblages at Broken Hill, which comprise many minerals, that show wide chemical and structural variation, in close association, may offer an opportunity to study the relationship between the paragenetic sequences of these minerals and their crystal structures. The secondary mineral assemblages at Broken Hill also offer an opportunity for a wide-ranging study of solid solution series in these and many other oxysalt minerals.

This study has identified solid solution series involving Cd, Ca and Pb in serpierite, sampleite, zdenekite and conichalcite and between Cd and Zn in nyholmite. Minor substitutions of Cu and Fe^{3+} have been noted in gartrellite and the possibitity of solid solution between Pb and Ca also exits in gartrellite and other tsumcorite group minerals. In plimerite, Zn replaces both Fe^{2+} and Fe^{3+} in distinct sites in the structure.

At Broken Hill, extensive solid solutions occur in a number other of mineral groups including the olivenite group minerals (adamite, libethenite, olivenite, zincolibethenite) involving Cu, Zn, Fe, As and P, the alunite-jarosite group minerals (Fe, Al, Zn, Cu, P, As, S), turquoise-chalcosiderite (Cu, Zn, Fe, Al, P, As), the agardite group minerals (Y, Ce, Ca, Pb, Cu, Zn, As, P) as well as in many other carbonates, phosphates, arsenates and sulphates. In many instances, specimens are available that show continuous solid solution series in these mineral groups. In other minerals, in order to characterize fully the nature of solid solution series, the laboratory preparation of synthetic material will likely be required. Thermodynamic stability and solubilities could also be determined by synthesis of analogues of the minerals.

Several of the minerals in this study, or closely related minerals, have been identified as having implications for the mobility of heavy metals in the environmental and in the remediation of heavy metal contamination as well as having applications in material science. These possibilities could be explored further.

Serpierite, linarite and tsumcorite group minerals are among those identified as possible solubility controls on the release and mobility of toxic elements from contaminated soils and slags (e.g. Horckmans *et al*. 2005; Ettler *et al*. 2008). Rockbridgeite and zinc rockbridgeite are two of a number of highly insoluble Fe and Zn phosphate minerals that, along with phosphates of other metals such as Pb, Cd, Cr, Cu, have potential application in reactive barriers for remediation projects to remove heavy metal contaminants from groundwaters and sediments (Crannell *et al*. 2004).

Nyholmite is a Cd, Zn arsenate member of the hureaulite group of minerals. The hurealuite group mineral sainfeldite and the closly related minerals ferrarisite, guerinite, haidingerite and pharmacolite have been investigated as possible immobilization phases, both by precipitation as low-solubility phases by reaction with suitable compounds or sorption onto carbonate or sulphate mineral surfaces (Nishimura *et al*. 2000; Jiminez *et al*. 2004). Arsenic can be removed from solution by precipitation of sainfeldite and guerinite onto the surface of gypsum in aqueous arsenic-bearing solution of pH ~7.2–9 (Rodriguez *et al*. 2008). Potential may also exist for the use of Cd and Zn bearing hurealuites for the removal of these cations from solution. During a study into synthetic phases for the storage of arsenic and other hazardous by-products of non-ferrous metal extraction the hurealuite-type compound $Cd_5H_2(AsO_4)_4{\cdot}4H_2O$ was prepared by hydrothermal techniques and evaluated for the precipitation and immobilization of arsenic (Johnson *et al.* 2003). The compound is relatively stable and can be shown to continue to crystallize from amorphous material without substantial leaching of cadmium or arsenic. There is potential for the syntheses of other Cd compounds that are are highly insoluble and potentially suitable for the fixation and also their thermodynamic properties and long-term stabilities need to be determined.

The interaction of water with sulphide minerals in mine waste commonly results in the formation of sulphate minerals (e.g. Potter and Nordstrom 1978). These reactions produce acidic solutions that contain toxic metal ions that can be incorporated in the secondary sulfates (Dutrizac and Jambor 2000). $ZnSO_4^0$ and $Zn(OH)_2^0$ are the dominant complex ions of Zn in solutions containing sulphate, chloride, carbonate and hydroxyl anions and the solid phases which limit Zn solubility in most solutions are $Zn_4(SO_4)(OH)_6$, which is stable in acid solutions, $Zn(OH)_2$,

which is stable in neutral and alkaline solutions and $ZnCO_3$ (smithsonite) (Mann and Deutscher 1980). Thus zinc sulphate minerals such as osakaite and the related basic zinc sulphates, $Zn_4SO_4(OH)_6{\cdot}3H_2O$ and $Zn_4SO_4(OH)_6{\cdot}4H_2O$, may be important in the release of Zn from oxidizing sulphide ores and its subsequent migration and dispersion via groundwater systems.

New and novel mineral structures are also likely to be of potential interest from the viewpoint of material science (Pring 1995; Bulakh *et.al*. 2003). Structures with unique characteristics may open the way to the synthesis of new compounds. Open-framework materials including silicates, phosphates, arsenates, sulfates, selenates, selenites, germanates, phosphites and carboxylates have many potential applications in catalysis, separations, electronics and gas storage (e.g. Natarajan and Mandal 2008, and references therein). Open-framework compounds of the transition metals provide many variations, arising from their coordination preferences, ligand geometry, and the valence state (Cheetham *et al*. 1999). Synthetic analogues of hureaulite and alluaudite (Corbin *et al*. in 1986) were amoung the first open-framework iron phosphates described, and opened the way for the preparation of other open-framework phosphates. The structure of liversidgeite is an open framework containing large ellipsoid channels along [100]. Compounds isostructural to liversidgeite have been synthesized as part of research into the properties of open-framework materials (Whang 1995).

12.3 References

Bulakh, A.G., Zolotarev, A.A. and Britvin S.N. (2003) A Retrospect of Discovery of Minerals (1775-2000) and a look into the Future. Neues Jahrbuch für Mineralogie Montatscheft, 2003, 446–460.

Cheetham, A.K., Férey, G. and Loiseau, T. (1999) Open-framework inorganic materials. Angewandte Chemie International Edition, 38, 3268–3692.

Corbin, D.R., Whitney, J.F., Fultz, W.C., Stucky, G.D., Eddy, M.M. and Cheetham A.K. (1986) Synthesis of open-framework transition-metal phosphates using organometallic, precursors in acidic media. Preparation and structural characterization of $Fe_5P_4O_{20}H_{10}$ and $NaFe_3P_3O_{12}$. Inorganic Chemistry, 25, 2279–2280.

Crannell, B.S., Eighmy, T.T., Willson, C., Reible, D.D. and Yin, M. (2004) Pilot-scale reactive barrier technologies for containment of metalcontaminated sediments and dredged materials. A final report submitted to NOAA/UNH Cooperative Institute for Coastal and Estuarine Environmental Technology (CICEET).

Dutrizac, J.E. and Jambor, J.L. (2000) Jarosites and their application in hydrometallurgy. In C.N. Alpers, J.L. Jambor, and D.K. Nordstrom, Eds., Sulfate Minerals, Crystallography, Geochemistry, and Environmental Significance, 40, p. 405–452. Reviews in Mineralogy and Geochemistry, Mineralogical Society of America, Chantilly, Virginia.

Ettler V., Johan Z., Kříbek B., Šebek O. and Mihaljevič M. (2009) Mineralogy and environmental stability of slags from the Tsumeb smelter, Namibia. Applied Geochemistry 24, 1–15.

Hargreaves, A. (1955) Some observations on the probability distribution of X-ray intensities. Acta Crystallographica, 8, 12–14.

Hawthorne, F.C. (1979) The crystal structure of morinite. Canadian Mineralogist, 17, 93–102.

Hawthorne, F. C. (1985) Towards a structural classification of minerals: The $^{(VI)}M^{(IV)}T_2O_n$ minerals. American Mineralogist, 70, 455–473.

Hawthorne, F. C. (1986) Structural hierarchy in $^{VI}M_x{}^{III}T_y\phi_z$ minerals. Canadian Mineralogist, 24, 625–642.

Hawthorne (1990) Structural hierarchy in $M^{[6]}T^{[4]}\phi_n$ minerals. Zeitschrift für Kristallographie, 192, 1–52.

Hawthorne, F.C. (1992) The role of OH and H_2O in oxide and oxysalt minerals. Zeitschrift für Kristallographie, 201, 183–206.

Hawthorne, F.C. (1994) Structural aspects of oxide and oxysalt crystals. Acta Crystalographica, B50, 481–510.

Hawthorne, F.C. (1998) Structure and chemistry of phosphate minerals. Mineralogical Magazine, 62, 141–164.

Hawthorne, F.C. and Schindler, M. (2008) Understanding the weakly bonded constituents in oxysalt minerals. Zeitschrift für Kristallographie, 223, 41–68.

Horckmans L., Swennen R. and Deckers J. (2006) Geochemical and mineralogical study of a site severely polluted with heavy metals (Maatheide, Lommel, Belgium). Environmental Geology, 50, 725–742.

Jiménez, A., Prieto, M., Salvadó, M.A. and Gracía-Granda, S. (2004) Structure and crystallization behavior of the $(Ba,Sr)HAsO_4{\cdot}H_2O$ solid-solution in aqueous environments. American Mineralogist, 89, 601–609.

Johnson, C.D., Shakle, J.M.S., Johnston, M.G., Feldmann, J., and Macphee, D.E. (2003) Hydrothermal synthesis, crystal structure and aqueous stability of two cadmium arsenate phases, $CdNH_4(HAsO_4)OH$ and $Cd_5H_2(AsO_4)_4\,4H_2O$. Journal of Materials Chemistry, 13, 1429–1432.

Mann, A.W. and Deutscher, R.L. (1980) Solution geochemistry of lead and zinc in water containing carbonate, sulphate and chloride ions. Chemical Geology, 29, 293–311.

Natarajan, S. and Mandal, S. (2008) Open-Framework Structures of Transition-Metal Compounds. Angewandte Chemie International Edition, 47, 4798–4828.

Nishimura, T., Robins, R.G. and Twidwell, L.G. (2000) The removal of arsenic from hydrometallurgical processes and effluent streams. In M.A. Sánchez, F. Vergara, and S.H. Castro, Eds., Waste treatment and Environmental Impact in the Mining Industry Proceedings of the 5th International Conference on Clean Technologies for the Mining Industry, vol. I, p. 131–141. Santiago, Chile.

Potter, R.W. and Nordstrom, D.K., (1978) The weathering of sulfide ores in Shasta County, California, U.S.A. Proceedings 2nd International Symposium on Water-Rock Interaction, Sect. I, pp. I42–I46.

Pring, A. (1995) The place of descriptive mineralogy in modern science. The Australian Mineralogist, 1, 3–7.

Rodriguez, J.D., Jimenez, A., Prieto, M., Torre, L. and Garcia-Granda S (2008) Interaction of gypsum with As(V)-bearing aqueous solutions: Surface precipitation of guerinite, sainfeldite, and $Ca_2NaH(AsO_4)_2{\cdot}6H_2O$, a synthetic arsenate. American Mineralogist, 93, 928–939.

Schindler, M. and Hawthorne, F.C. (2001a) A bond-valence approach to the structure, chemistry and paragenesis of hydroxy-hydrated oxysalt minerals. I. Theory. Canadian Mineralogist, 39, 1225–1242.

Schindler, M. and Hawthorne, F.C. (2001b) A bond-valence approach to the structure, chemistry and paragenesis of hydroxyhydrated oxysalt minerals. II. Crystal structure and chemical composition of borate minerals. Canadian Mineralogist, 39, 1243–1256.

Schindler, M. and Hawthorne, F.C. (2001c) A bond-valence approach to the structure, chemistry and paragenesis of hydroxy-hydrated oxysalt minerals. III. Paragenesis of borate minerals. Canadian Mineralogist, 39, 1257–1274.

Schindler, M. and Hawthorne, F.C. (2004) A bond-valence approach to the uranyl-oxide hydroxy-hydrate minerals: chemical composition and occurrence. Canadian Mineralogist, 42, 1601–1627.

Whang, D.M., Hur, N.H. and Kim, K. (1995) A Novel Microporous Mixed-Transition-Metal Phosphate: Hydrothermal Synthesis, Characterization, and Structure of $Zn_2Co_4(PO_4)_4(H_2O)_5 \cdot 2H_2O$. Inorganic Chemistry, 34, 3363–3366.

Appendix A

Chemical analyses for sampleite, zdenekite and conichalcite from Broken Hill.

Table 1. Chemical composition (Wt.%) and unit formula† (*apfu*) of sampleite.

	Average (66 points)	Minimum	Maximum	Probe Standard
As_2O_5	0.05	0.00	0.26	gallium arsenide
P_2O_6	32.86	29.50	34.55	hydroxylapatite
SO_3	0.13	0.00	1.36	chalcopyrite
Na_2O	2.93	2.27	3.39	albite
PbO	5.82	2.82	12.43	galena
CdO	3.34	1.34	5.76	Cd metal
CaO	3.08	1.99	3.86	hydroxylapatite
CuO	43.87	39.79	46.44	chalcopyrite
ZnO	0.11	0.00	0.50	sphalerite
Cl	3.50	3.07	3.87	tugtupite
H_2O (calc)*	11.17	9.35	12.23	
Sum	106.86	97.85	111.30	
Na	0.86	0.70	0.97	
Pb	0.22	0.11	0.50	
Cd	0.22	0.09	0.38	
Ca	0.47	0.30	0.58	
∑	0.92	0.85	1.06	
Cu	4.74	4.49	5.04	
Zn	0.01	0.00	0.05	
∑	4.76	4.52	5.09	
AsO_4	0.00	0.00	0.02	
PO_5	3.98	3.84	4.00	
SO_4	0.01	0.00	0.15	
∑	4.00	4.00	4.00	
Cl	0.85	0.73	0.97	
H_2O	5.59	4.98	5.60	

Table 2. Chemical composition (Wt.%) and unit formula† (*apfu*) of zdenekite.

	Average (33 points)	Minimum	Maximum	Probe Standard
As_2O_5	39.52	34.89	43.88	gallium arsenide
P_2O_6	0.65	0.26	1.04	hydroxylapatite
SO_3	0.10	0.00	0.41	chalcopyrite
Na_2O	2.36	1.97	2.92	albite
PbO	12.22	8.49	15.34	galena
CdO	3.53	2.12	5.43	Cd metal
CaO	0.53	0.41	0.71	hydroxylapatite
CuO	35.07	32.29	37.32	chalcopyrite
ZnO	0.07	0.00	0.02	sphalerite
Cl	2.97	2.55	3.23	tugtupite
H_2O (calc)*	8.01	6.82	9.50	
Sum	105.03	94.67	114.48	
Na	0.86	0.66	1.02	
Pb	0.62	0.43	0.77	
Cd	0.31	0.19	0.50	
Ca	0.11	0.08	0.14	
∑	1.04	0.93	1.09	
Cu	4.98	4.48	5.20	
Zn	0.01	0.00	0.04	
∑	4.99	4.67	5.20	
AsO_4	3.89	3.82	3.95	
PO_5	0.10	0.04	0.17	
SO_4	0.01	0.00	0.06	
∑	4.00	4.00	4.00	
Cl	0.95	0.81	1.08	
H_2O	5.02	4.83	5.39	

†The analyses are normalized on the basis of 4 (As+P+S).
*The H_2O content is calculated to obtain charge balance.

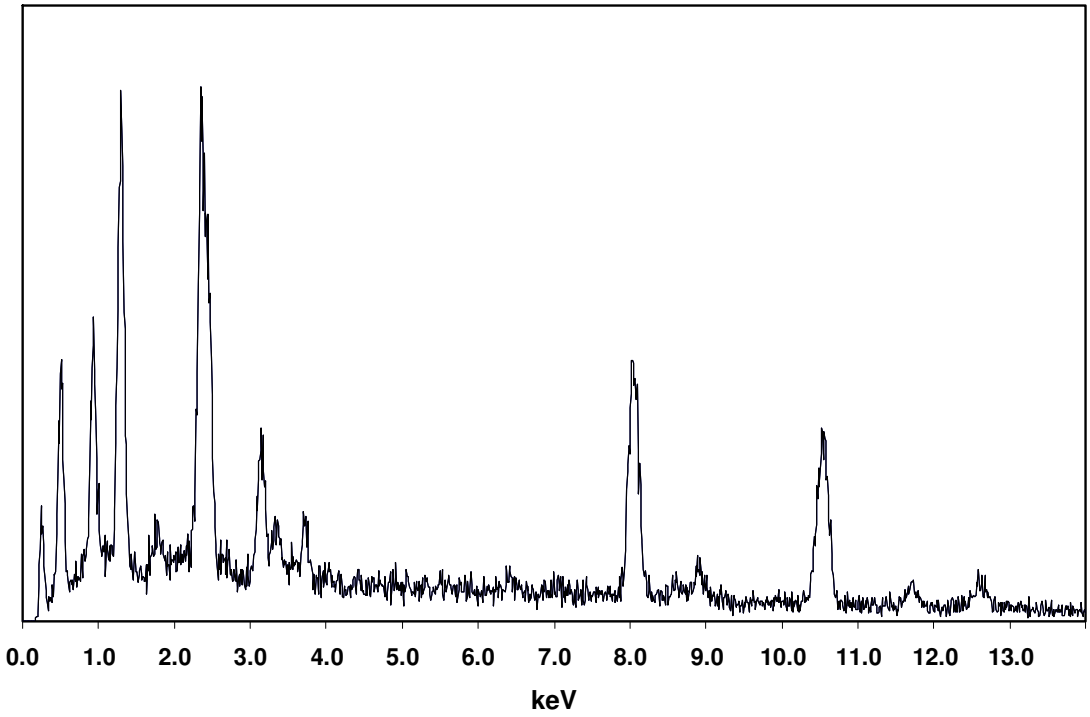

Element	Wt. %	At. %
O *K*	4.32	28.01
As *L*	7.79	10.77
Cd *L*	4.76	4.39
Ca *K*	0.79	2.04
Cu *K*	11.01	17.96
Zn *K*	1.05	1.66
Pb *L*	70.29	35.17

Figure 1. Qualitative Energy Dispersive X-ray analysis (EDS) of cadmian conichalcite from Broken Hill.